UNIVERSITÀ DELLA CALABRIA

UNIVERSITA' DELLA CALABRIA

Dipartimento di CHIMICA E TECNOLOGIE CHIMICHE

Dottorato di Ricerca in

MEDICINA TRASLAZIONALE

CICLO

XXIX

COMPUTATIONAL STUDY OF NEW DRUGS FOR PHOTODYNAMIC THERAPY

Settore Scientifico Disciplinare CHIM/03

Coordinatore: Ch.mo Prof. Sebastiano Andò

Firma _____

Supervisori: Ch.mo Prof. Nino Russo

Firma _____

Dott.ssa Gloria Mazzone

Firma _____

Dottoranda: Dott.ssa Jenny Pirillo

Firma

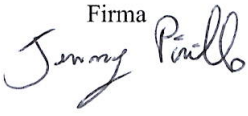

ABSTRACT

Photodynamic therapy (PDT) is a non-invasive therapeutic technique for the treatment of different kind of tumours through the production of reactive oxygen species (ROS) that act as cytotoxic agents.

PDT works through the associated events of three key components: photosensitizer (PS), visible or near-infrared region light, and molecular oxygen in tissues. In general, after the injection of a PS agent and subsequent accumulation in the target tissues, the agent is activated by a radiation with appropriate wavelength to give a photosensitization of the endogenous oxygen (photoreaction of type II) or the production of free radicals from the surrounding molecules (photoreaction of type I). In both cases, a cytotoxic species is generated, and destruction of the cancer cells occurs.

Success in PDT relies on the advantage that a non-invasive technique can selectively annihilate altered cells without undesirable side effects. Recent research in PDT has been focused on the development of more specific and powerful PSs.

In this thesis, the photophysical properties of different kinds of PSs, found to be good candidates for PDT, have been investigated. The PSs under study differ in the chemical nature and in the photosensitization mechanism: i) PSs based on the nucleobases analogue of DNA can be used as UVA chemotherapeutic agents, due to their absorption in the range 300−400 nm; ii) PSs based on the Ru(II) polypyridine complex, which are designed to give a long-lying excited state, can act as PSs through both type I and II reactions; iii) PSs based on aza-BODIPY core should be of interest for type II mechanism. Other BODIPY derivatives, linked to an antioxidant molecule (e.g. α-tocopherol) have been suggested to obtain a chemicontrolled $^1O_2$ photosensitization.

Density functional theory (DFT) and time-dependent DFT (TD-DFT) have been employed in all the computations.

ABSTRACT

La terapia fotodinamica (PDT) è una tecnica medica non-invasiva per il trattamento di varie forme tumorali mediante la produzione di specie altamente reattive dell'ossigeno (ROS) che agiscono da agenti citotossici. La PDT esplica la sua funzione attraverso l'azione combinata di tre componenti chiave: il fotosensibilizzatore (PS), la luce ad un'adeguata lunghezza d'onda (UV-vis), e l'ossigeno presente nei tessuti. Dopo la somministrazione dell'agente fotoreattivo, ed il successivo accumulo nei tessuti malati, il PS viene attivato mediante irraggiamento con luce di opportuna lunghezza d'onda, che provoca la fotosensibilizzazione dell'ossigeno endogeno (fotoreazioni di tipo II) oppure la formazione di specie radicaliche a partire dai substrati biologici presenti nell'ambiente di reazione (fotoreazioni di tipo II). Entrambi i casi comportano la generazione di specie citotossiche che portano alla morte delle cellule tumorali.

La capacità di causare la distruzione selettiva delle cellule tumorali e l'assenza di effetti collaterali, rappresentano i maggiori vantaggi della PDT. La moderna ricerca in PDT è finalizzata soprattutto allo sviluppo di nuovi fotosensibilizzatori sempre più selettivi ed efficaci.

Nella seguente tesi sono state studiate le proprietà fotofisiche di una serie di promettenti fotosensibilizzatori che differiscono nella natura chimica e nel meccanismo di azione: i) Fotosensibilizzatori derivati delle basi azotate del DNA, che possono essere usati come agenti chemioterapeutici UVA (assorbono nell'intervallo 300-400 nm); ii) Fotosensibilizzatori basati sui complessi polipiridinici di Ru(II) che, opportunamente sostituiti, possono accedere ad uno stato eccitato con lungo tempo di vita innescando fotoreazioni di tipo I e II; iii) Fotosensibilizzatori derivati dell'aza-BODIPY che favoriscono fotoreazioni di tipo II. Fotosensibilizzatori derivati del BODIPY funzionalizzati con degli antiossidanti (es. α-tocoferolo) che sono in grado di controllare a livello chimico l'azione citotossica dei ROS nell'ambiente cellulare.

CONTENTS

INTRODUCTION

In this thesis, we reported a theoretical investigation performed at density functional theory (DFT) and time-dependent DFT (TD-DFT) levels of theory, aimed to shed light on the photophysical properties of a series of promising photosensitizers (PSs) for Photodynamic Therapy (PDT).

PDT is known as one of the non-invasive therapeutic techniques to treat different kinds of tumors through the production of reactive species (ROS) which act as cytotoxic agents. Today research in PDT field is focused on the design of new PSs, more efficient, selective and with multiple therapeutic actions.

Chapter 1 introduces the subject of the thesis, giving the main background aspects of PDT, a brief history, and mechanisms of photoreactions characterizing PDT. A detailed description of the three key PDT components—light, oxygen and photosensitizers—is also reported, together with a brief outline of photophysical and photochemical PDT processes.

Chapter 2 illustrates the computational approaches selected to study the photophysical properties of investigated PSs. In particular, the quantum mechanical methods that allow to predict and understand molecular excited states, will be presented. The simulations of the absorption and emission spectra are helpful to better understand the experimental adsorption spectra and to characterize the electronic transitions. In this report, TD-DFT represent a good compromise between accuracy and computational efforts, especially for large systems that often contain heavy atoms.

Chapter 3 is devoted to the obtained results. The PSs studied differ in the chemical nature, in the possible applications, and in the photosensitization mechanism: i) PSs based on nucleobases analogue of DNA can be used as UVA chemotherapeutic agents, since they absorb in the range 300－400 nm; ii) PSs based on the Ru(II) polypyridine complex, designated to give a long-lying excited state, can act as PSs in both type I and II mechanisms, depending on the oxygen concentration in target tissue. iii) PSs characterized by aza-

BODIPY core, properly substituted to give a control over-light toxicity, are proposed as excellent type II PSs. Other PSs composed combining a BODIPY dye with an antioxidant (e.g. α-tocopherol), are suggested to give a chemicontrolled photosensitization.

LIST OF PAPERS INCLUDED IN THIS THESIS

1. Photophysical Properties Prediction of Selenium- and Tellurium-Substituted Thymidine as Potential UVA Chemotherapeutic Agents.
   Jenny Pirillo; Bruna Clara De Simone; Nino Russo.
   Theor Chem Acc **2016**, *135*, 8.

2. Photophysical Properties of S, Se, Te-Substituted Deoxyguanosine: Insight into Their Ability to Act as Chemotherapeutic Agents.
   Jenny Pirillo; Gloria Mazzone; Nino Russo; Luca Bertini.
   J Chem Inf Model **2016**. DOI: 10.1021/acs.jcim.6b00486

3. Theoretical Exploration of Type I/Type II Dual Photoreactivity of Promising Ru(II) Dyads for PDT Approach.
   Marta Erminia Alberto; Jenny Pirillo; Nino Russo; Carlo Adamo.
   Inorg Chem **2016**, *55*, 11185-11192.

4. Halogen Atom Effect on the Photophysical Properties of Substituted Aza-BODIPY Derivatives.
   Bruna Clara De Simone; Gloria Mazzone; Jenny Pirillo; Nino Russo; Emilia Sicilia.
   Phys Chem Chem Phys **2016**, *19*, 2530–2536.

5. Theoretical Insights on the Switch on/off Photosensitization in Chemicontrolled Photodynamic Therapy.
   Jenny Pirillo; Gloria Mazzone; Nino Russo.
   (MANUSCRIPT).

1. PDT - PHOTODYNAMIC THERAPY

1.1. PDT: DEFINITION AND BRIEF HISTORY

PDT is known as a non-invasive therapeutic technique for the treatment of different kinds of cancers through the production of reactive oxygen species (ROS) that act as cytotoxic agents. Therefore, the molecular oxygen naturally present in biological tissues is an essential player in PDT. The molecular oxygen can be activated to the lowest singlet excited oxygen species by irradiation, with lasers in either visible or near infrared region, of an administered photosensitizer (PS). The generated singlet oxygen is reactive enough to ablate cells, i.e. damaging cancer cells or tumour tissues.

The history of phototherapy dates back to around 2000 B.C. For instance, it was explored in China to cure smallpox and was also called heliotherapy in Greece. The discovery of phototherapy as a scientific method has been attributed to Niels Rydberg Finsen (Nobel Prize in Physiology or Medicine in 1903). Examining the effects caused by various kinds of radiation on animals, he realized that the red light possessed the best therapeutic effect, in particular, to cure smallpox. He became famous for the development of a phototherapeutic method to cure lupus vulgaris by 'filtered' sunlight (light from a carbon arc appropriately fitted to reduce IR intensity). Some researchers, however, believe that the real 'father' of phototherapy is Antonino Sciascia, who invented the system 'photocautery' (got the patent in 1894) by selective concentration of light with a specific wavelength. The invention was applied to the treatment of several diseases, and he introduced phototherapy as a scientific method for the first time in the XIII Ophthalmologic Congress of Palermo in 1892[1].

Since then, several milestones have been achieved. Raab[2] reported a photodynamic reaction for the first time in 1900. He studied the toxicity of several dye-drugs exposed to light with Herman von Tappeiner[3], who introduced the term 'photodynamic action' in 1904. He carried out a series of photodynamic experiments not only to reveal that topical application of eosin, in combination with sunlight exposure, can cure skin carcinoma, but also to study more sophisticated techniques of irradiating different kinds of sensitizers with two light sources, i.e. sunlight and arc lamp. Although this kind of PDT seemed to be very promising, the selectivity of the chromophore for the tumor tissue could not be proven.

The missing point was established by Lipson et al. [4,5] in 1960 when they developed a Hematoporphyrin derivative, HpD, that represents the basis of modern PS for PDT. Lipson and co-workers showed selective localization of HpD in the tumor tissue, hence it was considered a good diagnostic agent for cancer detection due to their fluorescent properties. Afterwards, several studies proved the cytotoxic action of HpD as a PS. For instance, one decade after the characterization of HpD, Diamond et al.[6] reported its use in the photodegradation of glioma cells implanted in rats, and in 1978, Dougherty and co-workers[7] clinically tested PDT in subcutaneous malignant tumours using HpD as a PS. HpD led to the rapid development of PDT, and the first PDT agent was approved for clinical use by Canadian authorities in 1993. The therapeutic success of PDT relies on the advantage that a non-invasive technique can selectively annihilate altered cells without incurring further risks. The recent increasing interest in PDT involves shifting focus onto the development of more specific and powerful sensitizers.

1.2. TWO TYPES OF PHOTODYNAMIC MECHANISMS

PDT works through the integration of three key components: PSs, the visible or near infrared region light, and molecular oxygen in tissues.

The PDT procedure can be summarized in four steps:

1. *Injection of PSs into the bodies;*
2. *Concentration of PSs at the tumour sites;*
3. *Activation of the PSs by visible light with suitable wavelength to generate reactive oxygen species (ROS) cytotoxic species;*
4. *Selective destruction of cancer cells.*

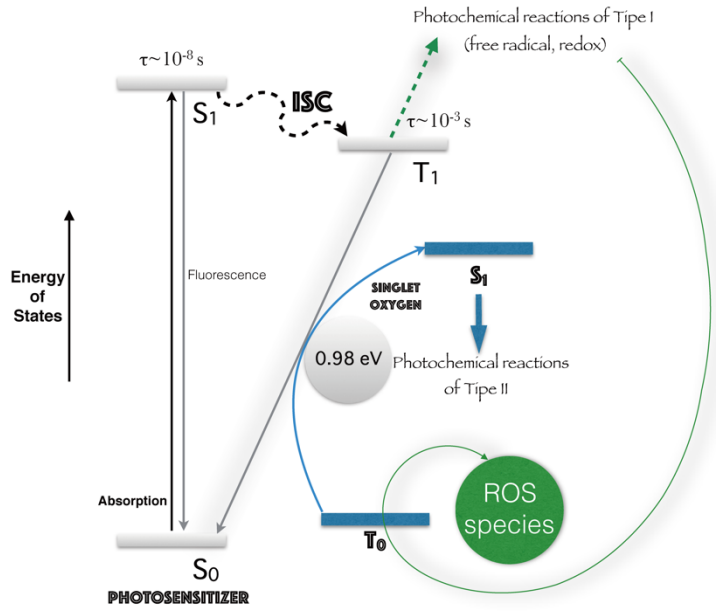

Figure 1. Schematic Jablonski's diagram showing the two photodynamic pathways for the different types of chemical reactions.

In the PS activation process by light (Figure 1), the PS will typically be excited from the ground state S_0 (usually closed-shell ground state: singlet spin multiplicity) to the singlet excited state S_1 within *ns* order lifetimes that is too short to interact with surrounding molecules. Energy releasing can take place during the return from the S_1 state to the S_0 ground state via either a radiative process, i.e. fluorescence, or a non-radiative process which can occur after an inter-system crossing (ISC) to the triplet excited state T_1 (forbidden by the selection rules in principle) allowed by spin-orbit couplings. Further deactivation from the T_1 state can be caused either by internal or external conversion or by phosphorescence. In order to reach the S_0 ground state from the T_1 one, a second spin forbidden process should be overcome. Since the transition probability and the lifetime of excited-states are inversely correlated, the lifetime of T_1 (*μs* to *ms* order) is usually longer than that of S_1.

The longer lifetime of the T_1 state is sufficient to allow energy or electron transfer to the surrounding molecules to generate cytotoxic species, which can take place through two different photoreactions to activate oxygen:

1. Photochemical reactions of type I
2. Photochemical reactions of type II

The ratio between type I and type II photoreactions depends on the PS and the local dioxygen concentration.

The *photochemical reactions of type I* produce free radicals through the interaction between the PS in the excited state (usually T_1) and surrounding molecules (e.g. lipids as biological molecules and molecular oxygen). The free radicals can be generated in different ways, for example via photo-electron transfer (PeT) or hydrogen atom abstraction (HAT) as shown in the following reaction schemes:

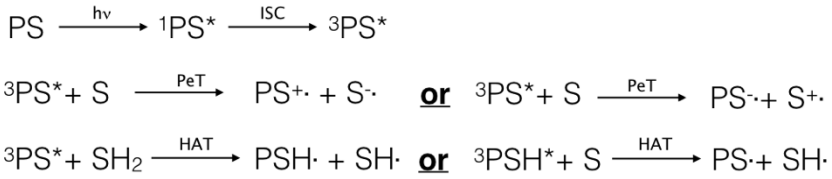

Scheme 1. Reaction schemes for the generation of free radicals via PeT or HAT.

The excited or radical PS reacts with the molecular oxygen present in the tissues to generate superoxide, $O_2^{-\cdot}$ as shown in Scheme 2 below:

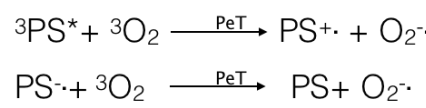

Scheme 2. Generation of superoxide.

The pH in cancer cells is usually less than 7.0 (acidic condition), where the superoxide can be protonated to be hydroperoxyl radical as shown in Scheme 3. The generation of hydroperoxyl radicals is not enough to ensure cell death due to the lower reactivity of these radicals compared to other active species such as HO^- and $HO^{\cdot}$. On the other hand, the hydroperoxyl radicals disproportionate to hydrogen peroxide and O_2, and they turn into mutagenic reactive oxygen species, hydroxyl radical ($HO^{\cdot}$) and hydroxide ion (HO^-). The last two processes are known as *Fenton reactions*, where ferrous iron (Fe^{2+}) or other transition metal ions present in the system reacts with the hydrogen peroxide to produce hydroxyl radical and ferric iron (Fe^{3+}). The Fe^{3+} is reduced to Fe^{2+} by superoxide. Thus, iron can work as a good catalyst even in trace amounts.

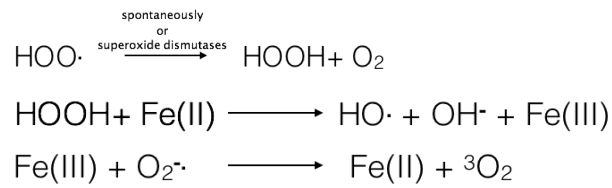

Scheme 3. Generation of reactive oxygen species.

The free radical generated in the photochemical reaction mentioned above will propagate sequential free radical reactions in the dark and generate highly reactive species as shown in Scheme 4. Therefore, exposing the cells to oxidative environments causes damage and ultimately leads to cell death.

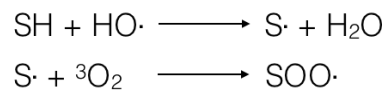

Scheme 4. Sequential reaction scheme mediated by free radicals.

In the *photochemical reaction of type II*, the excited state of the PS (usually $^3PS^*$) returns to the ground state via energy transfer to the triplet dioxygen, generating singlet oxygen (Scheme 5*)*. The singlet oxygen is the major reactive oxygen species and reacts readily with various biomolecules such cholesterol, amino acid derivates, nucleobases, and unsaturated lipids.

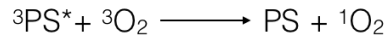

Scheme 5. Generation of singlet oxygen.

In order to produce singlet oxygen, the energy gap between S_0-T_1 of the PS must be larger than the energy gap required to generate excited oxygen ($^1\Delta_g$), i.e 0.98 eV[8].

The distinguishing tests for photoreactions of type II are based on singlet oxygen measured in different ways:

- Detecting the singlet oxygen by near-infrared luminescence at 1270 nm[9] in the reaction mixture. The luminescence of singlet oxygen gives two weak emissions:

$$^1O_2 \rightarrow {}^3O_2 + hv\ (1270\ nm)$$

$$2\,^1O_2 \rightarrow 2\,^3O_2 + hv\ (634, 704\ nm).$$

Detection of the second emission is complicated due to the luminescence of substrate molecules.

- Chemical trapping of singlet oxygen, which causes a decrease in reaction rate. The generated singlet oxygen species are quenched by 9,10-diphenilantracene in the

lowest excited singlet or triplet states, followed by the measure of its quantum yield for photo-peroxidation[10].

- Reaction with cholesterol, in which 5α-hydroperoxide is formed as a main product.

The tests to detect the photo-reaction of type I are based on the detection of free-radicals as follows:

- Reaction with cholesterol, in which a mixture of 7α- and 7β-hydroperoxides is formed;
- Addition of an antioxidant such as α-tocopherol to quench the autoxidation chain.

In principle, both photoreaction types can contribute to the final therapeutic process. The ratio of their contributions depends on the characteristic of the administered PS, e.g. the affinity for the substrates, and concentration of dioxygen in the target tissue.

1.3. THREE REQUIRED COMPONENTS FOR PDT

1.3.1 LIGHT

The electromagnetic spectrum can be divided into various regions, as shown in Figure 2.

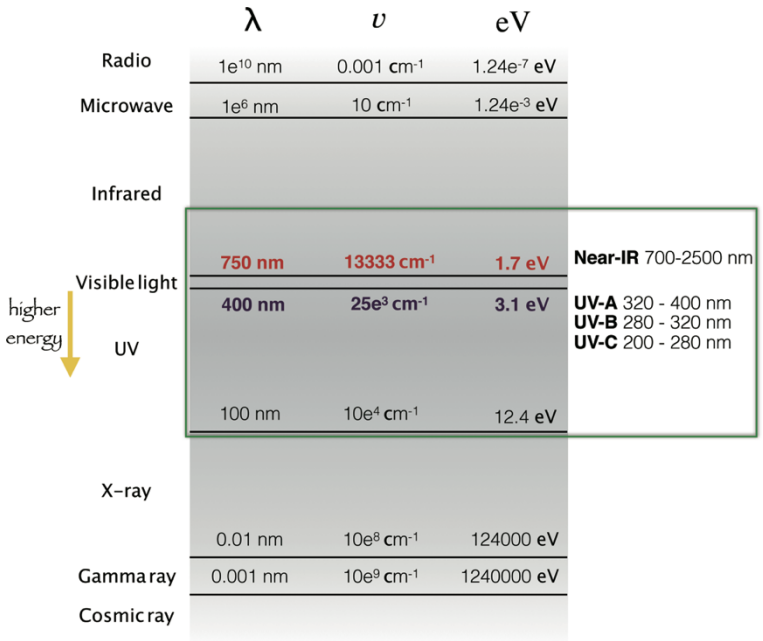

Figure 2. Classification of the electromagnetic spectrum. The green box emphasizes the UV region which is important for the photo-biological processes.

The visible light occupies a narrow range (from 400 to 750 nm) of the electromagnetic spectrum (Figure 2). The UV region is divided into three parts, UV-A,

UV-B and UV-C, and is very important in the photo-biological processes. A wavelength shorter than 300 nm (UV-B and UV-C) can damage the skin due to the absorption of radiation by specific nucleobases of DNA and specific α-amino acids. The used light sources in PDT are summarized below:

-**Sunlight**: Sunlight is neither convenient nor reliable enough to use routinely for the phototherapeutic purposes.

-Incandescent lamp: Incandescent lamps were the first light source used in PDT. They are composed of one metal filament (e.g. tungsten) in vacuum inside a glass bulb and the filament is heated by an electric current. This kind of light source was employed in the treatments of basal cell carcinoma, with **δ-**aminolevulinic acid as the precursor for PSs.

-Arc lamp[a]: The mercury arc lamp is widely used in the organic photochemistry and can be applied for photomedicine. These lamps can work by using different pressure loaded on mercury: low-pressure (10^{-3} mmHg), medium-pressure (1 atm) and high-pressure (100 atm). Only one line of emission at 253.7 nm (UV-C region) is obtained at low-pressure and is used as germicidal lamps. Medium-pressure ensures a greater number of emission lines and the principal lines are found at 366 and 546 nm. If the radiation is filtered with a Wood's glass, the emission in the UV-B region can be used to observe the fluorescence from the porphyrins or other pigments. The high-pressure working mode gives a continuum emission with a very short lifetime and needs a cooling system. The arc lamp with xenon or xenon-mercury gives more intense and economic light source under a pressure of 20 atm, and they do not need to be cooled.

-Light-emitting Diodes (LEDs): LEDs are devices based on semiconductors, which are able to emit non-coherent radiation with low-power. The wavelength can be modulated by changing the semiconductor. A useful advantage for PDT is the small size of these devices that assures the adaptability to the patient's diseased area.

-Lasers: Lasers (light amplification by stimulated emission of radiation) are the most used devices among the radiation source instruments and are based on the stimulated emission of one excited state.

The emitted radiation will be intense, coherent, and monochromatic. Among the different types of lasers in PDT, that based on organic pigments are the most suitable. For example, the rhodamine 6G gives fluorescence in the range between 570 and 620 nm, and the dye laser is tunable over this region as a function of the PS used

in PDT. Lasers allow for the control of several light parameters such as intensity, wavelength, direction, duration of pulse (flash), polarization and phase.

1.3.1.1 INTERACTION RADIATION-MATTER

The various outcomes of an interaction between electromagnetic radiation and a biological tissue[11] are shown in Figure 3. The light can be absorbed by chromophores, reflected or scattered, or further transmitted.

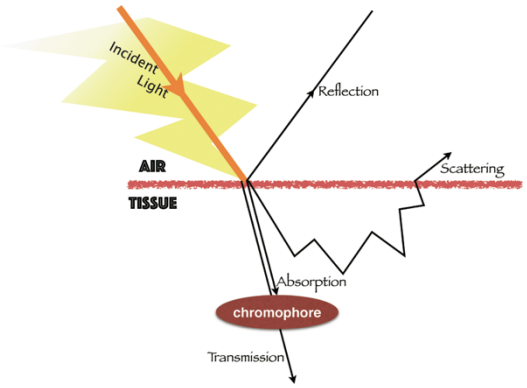

Figure 3. The phenomena that can occur in the interaction between light and biological tissue.

These phenomena take place to different extents depending on the optical properties of the tissue and the light (e.g. energy of the radiation, light exposure time, attenuation coefficient). The scattering phenomenon occurs inside the skin, and more precisely in the *stratum corneum* (the outmost layer of skin composed of dead keratinocytes, keratin, melanin, lipid), where different structures have different indices of refraction.

Absorption occurs due to the presence of endogenous chromophores (e.g. melanin, hemoglobin and their derivatives), therefore, it depends essentially on the skin type[12]. Melanin and hemoglobin strongly absorb at shorter wavelengths (~600 nm).

Svaasand[13], Wilson et al.[14]and Bolin et al.[15] demonstrated that radiation with wavelength of 800 nm can cross the epidermal layer and effectively reach the subcutaneous tissue (around 3.5 mm in depth). The use of wavelengths less than 800 nm increases the scattering phenomenon that is inversely proportional to the light wavelength[16].

Another important factor, attenuation coefficient, α (cm^{-1}), denotes the gradual intensity decay of an electromagnetic radiation through a tissue. According to the diffusion theory, it is possible to describe the attenuation of radiation using experimental data. The variation of the radiation flux (Ψ) into media, is defined by the following equation:

$$\psi = \psi_0 \frac{e^{-\alpha r}}{r},$$

where r is the distance from the radiation source. The radiation flux decreases exponentially with distance r, and small variation in the attenuation constant α leads to a large variation in the flux depending on the tissue depth. Thus, it is better to use PSs that absorb around 800 nm to maximize the depth of the PDT treatment in various tissues. The penetration depth, δ (cm), is the reverse of α, and refers to the depth at which the radiation is attenuated to 1/e (~37%) (e=2.72, called Euler's number).

A general scheme of the human skin structure is shown in Figure 4. The epidermis, from 0.0 to ~0.1 mm in depth, is composed primarily of keratinocytes and melanocytes. The latter is responsible for regenerating skin surfaces and producing melanin.

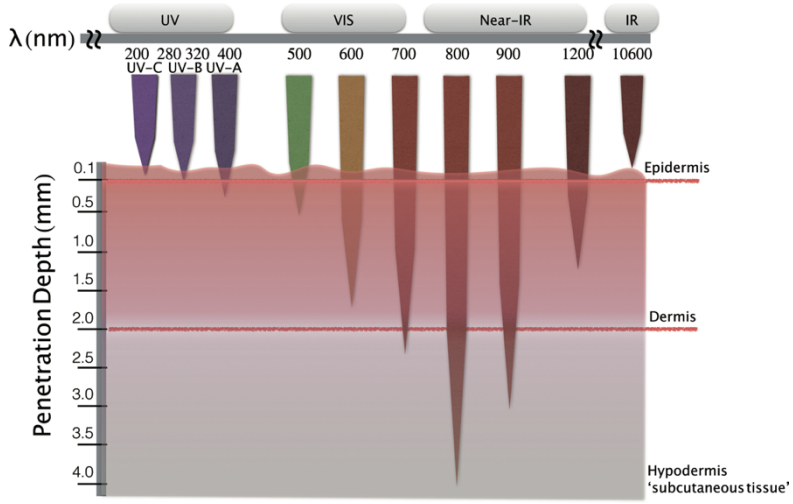

Figure 4. Schematic representation of the human skin structure, and dependency of the penetration depth on light wavelength.

The dermis layer, from ~0.1 to ~2.0 mm, contains connective tissues, fat, supportive tissues, blood and lymph vessels, sebaceous glands and sweat glands (these last three components mainly regulate body temperature). The subcutaneous tissue (or hypodermis) lies below the dermis at a depth of more than 4.0 mm, and consists primarily of adipocytes. Figure 4 shows the dependency of the penetration

depth into the human skin on light wavelength. A radiation ranging from 600 to 700 nm penetrates 50-200% more than that ranging between 400 and 500 nm. As mentioned before, the therapeutic window for PDT includes wavelength from 600 to 850 nm. The water molecules contained in the tissues absorb radiation with a wavelength over 850 nm and generate heat. Furthermore, administration of PSs with high molar attenuation coefficient in tissues containing high concentrations of endogenous chromophores attenuate the radiation penetration[17].

1.3.2 DIOXYGEN

The electron configuration of molecular oxygen in the ground state is $(1\sigma_g)^2(1\sigma_u^*)^2(2\sigma_g)^2(2\sigma_u^*)^2(3\sigma_g)^2(1\pi_u)^2(1\pi_g^*)^2$, where two electrons occupy the highest degenerate orbitals and configure in parallel spin. The ground-state is a triplet paramagnetic state as described by the spectroscopic notation ${}^3\sum_g^-$,. The dioxygen has two singlet excited states, ${}^1\Delta_g$ at 0.98 eV (1269 nm) and ${}^1\sum_g^+$ at 1.36 eV (762 nm). The electron configurations are shown in Figure 5.

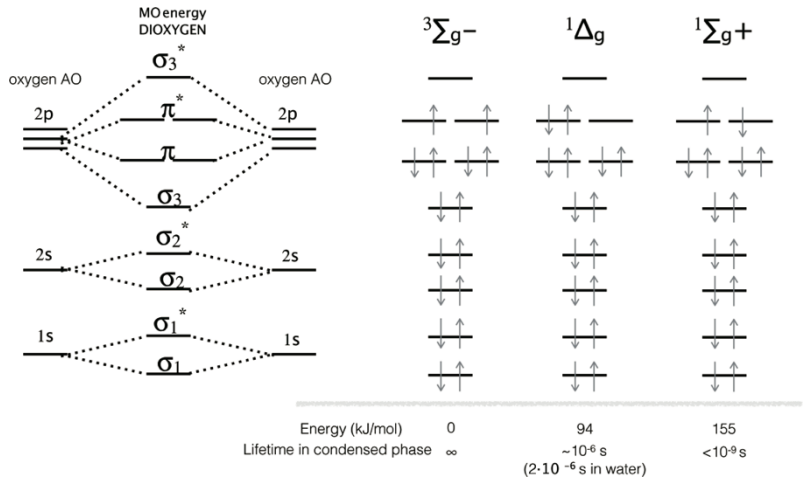

Figure 5. Molecular orbital diagram ground and low-lying excited states of dioxygen. The excitation energies are in kJ/mol and their lifetime are also shown.

The dioxygen in the ground state is not reactive towards organic compounds as the first excited state. The excitation converts the dioxygen to an electrophilic reagent, which reacts readily with electron-rich compounds.

Schweitzer and Schmidt evaluated the lifetime of the two excited states of dioxygen in vacuum: 72 min for the lowest excited state and 11 s for the second one. The lifetimes decrease in solution due to the intermolecular perturbations (solvation),

which favour the radiative processes[18,19]. The lifetime of the $^1\sum_g^+$ state is too short for practical use. Once formed in solution, it decays immediately to the $^1\Delta_g$ excited state. In PDT, even if the lifetime of singlet oxygen in solution is in the order of 10^{-6} s, generation of singlet oxygen ensures the production of reactive oxygen species in the reaction environment (tumour cells). The transition from $^1\Delta_g \rightarrow {}^3\sum_g^-$ has been experimentally observed by emission at 1268.7 nm, despite symmetry and spin forbidden transition.

In PDT, the formation of singlet oxygen is due to the photosensitization process of dioxygen by a suitable PS. The photosensitization of dioxygen is a widespread physical method in laboratories to efficiently produce singlet oxygen[20,21].

The first works of the photosensitization process using a PS, molecular oxygen and organic substrates were carried out by Schönberg (1935) and Kautsky (1937)[22] and resumed by Schenck (1964) and Foote (1968)[23]. They proposed two reaction mechanisms which share the first activation step by irradiation of the PS, and differ in the second one. Schönberg (1935) and Schenck (1964) proposed the 'sensitizer-oxygen complex theory', while Kautsky (1937) and Foote (1968) suggested the 'singlet oxygen theory'. The Sensitizer-oxygen complex theory suggested that the step after the excitation of the PS provides the formation of a complex between the PS and the ground state molecular oxygen. On the other hand, the singlet oxygen theory proposed the correct mechanism in which the second step of the reaction involves the photosensitization of the molecular oxygen to produce the reactive singlet oxygen responsible for the oxidation of organic substrates. In 1933, Kautsky demonstrated the generation of singlet oxygen experimentally. After three decades, the results obtained by Kautsky were confirmed by Foote (1968). In PDT, the reaction proposed by Kautsky is called the 'photochemical reaction of type II'. Today, due to the complexity of the dynamics in singlet oxygen formation (e.g. photobleaching processes and reactions with the produced singlet oxygen), the research interests in PDT have shifted to improving the properties of PSs.

1.3.3 PHOTOSENSITIZERS IN PDT

PSs are defined as molecules that are able to absorb a specific wavelength of light to activate surrounding molecules (e.g. O_2). An ideal PDT PS must possess the following chemical and photo-physical properties:

- Easily synthesizable and reproducible
- Chemical stability
- Water solubility
- No cytotoxicity in the dark
- Selective accumulation in target tissues
- Rapid clearance from patients
- High coefficient of molar extinction adsorption (or molar absorptivity)
- Strong absorption in the wavelength range from 650 to 850 nm (PDT's therapeutic window), in order to maximize the tissue penetration
- High triplet excited state quantum yields

The efficiency of the PSs in activating molecules depends on many factors. The most important factor is their *concentration*, because living systems contain PSs endogenously (e.g. porphyrins, melanin) in low concentration, which makes their potential photosensitizing effects negligible, or can induce different pathways preventing photosensitization reactions. Here, some of the basic properties mentioned above are discussed in detail.

- *Easily synthesizable and reproducible.* The first generation of PSs, the derivatives of HpD, are constituted of a mixture of monomers, dimers and oligomers, and the percentage of each fraction depends on the synthetic condition. The mixture of PSs makes the relationship between PS dose and their photodynamic action complicated. A number of hematoporphyrin are characterized by two chiral centres, therefore analysis of photodynamic effects is rather difficult due to the presence of stereoisomers. Therefore, it is necessary for an efficient PS to have a constant composition, preferably a single substance without chiral centres.

- *Chemical stability.* The synthesis of PSs, should be easy with high yield, and the product should be kinetically and thermodynamically stable.

- *Behaviour in solution.* An ideal PS should be localized selectively to the target tissue and at the same time should be easily excreted from the body at the end of the phototherapy in order to minimize the photosensitization in the body. Generally, PSs with these features are amphiphilic. Most PSs are based on porphyrinic macrocycles

(e.g. porphyrin, chlorin shown in Figure 6) or on porphyrazines (e.g. phthalocyanine, texaphyrin) that are hydrophobic, and need the introduction of hydrophilic substituents to achieve the correct amphiphilic balance. Since, biological tissues mainly contain water the PS should be soluble in aqueous media. The hydrophilic substituents usually employed are sulfonic acid, hydroxyl, and quaternary ammonium groups. The obtained PSs have amphiphilic characters, hence the micelle formation may play an important feature in their use.

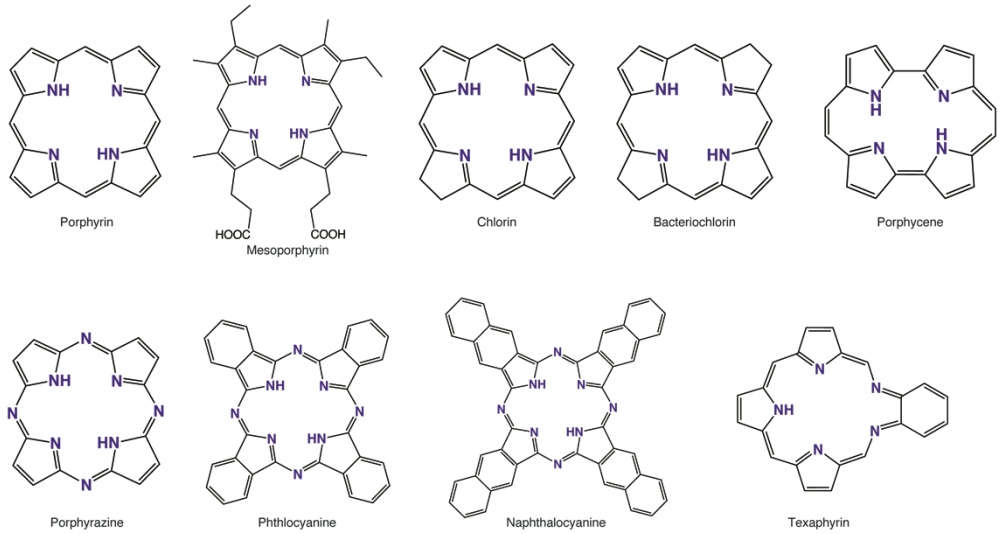

Figure 6. Examples of porphyrinic macrocycles and porphyrazine.

- *Selective accumulation in target tissue*. The delivery of the PSs to the target tissue is an important point to be considered. Generally, the PSs are solid and require a delivery system for intravenous injection. In order to transport the PSs, oil-based emulsions are commonly used. These emulsions are composed of cyclodextrin systems, detergents, liposomes and lipoproteins. In particular, efficient delivery of more hydrophobic PSs has been observed when using neutral detergents such as Tween 80 or Cremophor EL compared to simple ionic detergents. These neutral detergents are characterized by neutral polar groups and fatty acid chains, which lead to a stable emulsion of the hydrophobic PSs in aqueous solution.

- *High triplet excited state quantum yields.* PSs for PDT must have a high triplet quantum yield with energy higher than 0.98 eV (required energy to activate dioxygen) and long lifetime. These factors increase the probability of PSs to generate singlet

oxygen. The formation of singlet oxygen (type II photoreaction) is evaluated by the quantum yield of singlet oxygen Φ_{Δ}.

- *Strong absorption in the therapeutic window.* An ideal PS should absorb in the red region of the electromagnetic spectrum. The PSs for which the λ_{max} falls in the range between 600 and 850 nm, give a deep penetration in the biologic tissues. Higher values of wavelength do not lead to a greater penetration due to main three reasons: **i)** the absorption of the water that reduce the transmission of the radiation; **ii)** higher shift of the wavelength (i.e. λ_{max} move to lower energy) implies an increase of the charge conjugation, therefore an increase of the electron availability, and accordingly a decrease of the redox potential, due to the smaller HOMO-LUMO energy gap, hence the PS becomes more sensitive to oxidation. This photo-oxidation often leads to the 'photobleaching' phenomenon, i.e. irreversible chemical processes on the chromophore; **iii)** the last reason arises from consideration on the T_1 energy that should be lower than S_1, and similarly to type II reaction, should be higher than 0.98 eV (1270 nm).

PSs are classified into first, second and third generation PSs. The first-generation PSs include the hematoporphyrin derivatives 'HpD' and its commercially available derivatives -*Photofrin (USA), Photosan (Germany), Photogem (Russia), and Photocarcinorin (China), and Hematodrex (Bulgaria)*.

Since the pioneering work by Hausman[24,25] who noted the photodynamic properties of hematoporphyrin (Hp) (Figure 7) in 1908, many studies by various researchers up until the 1950s have contributed to further understanding the phenomenon[26-29]. The early studies have shown that Hp should be used in large quantities in order to be activated effectively in PDT[30,31]. This enhances the photosensitivity in patients and sometimes causes severe skin necrosis upon exposure to strong light.

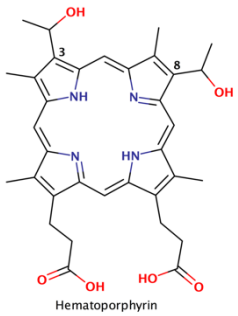

Figure 7. The hematoporphyrin (Hp).

Lipson et al.[32-33] introduced the use of HpD for the detection and treatment of tumours in humans in the 1960s. They demonstrated that HpD was more selective for the target tissue and has better fluorescent properties compared to Hp. The HpD was synthesized[34] by dissolving the hematoporphyrin in a mixture solution of glacial acetic acid/concentrated sulphuric acid with a ratio of 19:1, followed by filtering the resultant mixture and neutralizing the porphyrin solution with a 3% sodium acetate solution. The precipitate was washed several times with distilled water and dried in air at room temperature in the dark (HpD, Stage I). The obtained acetylated products (di- and mono-) of hematoporphyrin-IX was then dissolved in saline solution containing sodium hydroxide. The final pH was adjusted to pH 7.4 by the addiction of hydrochloric acid (HpD stage II). The basic hydrolysis gives a mixture containing monomers, dimers, and oligomers of the hematoporphyrin (hematoporphyrin derivatives 'HpD').

Photofrin is the most popular derivative of hematoporphyrin among the first generation PSs. Dougherty et al.[35-37] used gel exclusion chromatography to obtain a purified high-molecular weight aggregate of the HpD mixture in 1981. A reduced skin photosensitivity comparable to HpD was observed during the test on animals using the oligomers fraction mixture. Thus, an improvement in therapeutic ratio was achieved using this purified material known as Photofrin®. The definition is based on the ratio of mono-, di- and oligomeric hematoporphyrin in the mixture. The ratios in HpD and Photofrin® are 22:23:55 and14:19:67, respectively[38]. The Photofrin® has many advantages including low toxicity and little mutagenic effects, and was tested for different kinds of cancer. Disadvantages come from the usage of oligomers that can form aggregates in solution and decrease the quantum yield of singlet oxygen (Φ_Δ= 0.20 vs Φ_Δ=0.65 for the mono-hematoporphyrin). Other drawbacks of Photofrin® include the possibility that they contain a non-photoactive fraction, which make complex to find a relationship between clinical response and molecular structure. The photophysical properties of Photofrin® include (similar to HpD) absorption spectrum assigned to Soret's band at 400 nm (the most intense) and Q bands at 500, 540, 570 and 630 nm with decreasing intensities in that order. Although the band at 630 nm (ε=3000 M^{-1} cm^{-1}) has a low intensity, it is relatively important in PDT (penetrating more through tissue, ~5 mm); hence Photofrin® can be effectively activated in PDT only in high concentration, implying increased side effects and its ineffectiveness in

hypoxic environments. The advantages and disadvantages of the analogues of HpD PSs guided the development of a new class of PSs called *second-generation PSs* that are generally single substances.

The synthesis of second-generation PSs started in the early 1980s using a tetrapyrrole ring unit to intensify absorption in long-wavelength regions[39]. The most promising second generation compounds are the hydroporphyrins, chlorins and texaphyrin (Figure 6). Generally, the porphyrin is planar, which probably causes low solubility in organic solvents and insolubility in water. Substitution at the peripheral position increases the solubility, and in particular increasing side chain flexibility reduces crystal force and increases the solubility in organic solvents.

The design of the third-generation PSs is focused on improving their selective delivery to tumour tissues, and they are designated as antibody targeted photolysis (ATPL). This new approach combines the function of PSs with monoclonal antibodies that bind specifically to tumour cell surface antigens[40]. The tumour cells have different expression of cell surface antigens compared to the healthy cells. Consequently, it is possible to selectively deliver the PSs to the target cells avoiding side effects on the healthy tissue.

A new approach in the design of PSs involves coupling PSs with chemotherapeutic antitumor agents such as cisplatin and quantum dots. In the first case, the photodynamic reaction of PS enhances the antitumor activity of cisplatin that possesses a high affinity for the DNA. The solubility, reactivity, and selectivity of these combined PSs can be modulated by changing the functional groups on the first coordination sphere of the Pt(II) and/or on the porphyrin ring (Figure 8).

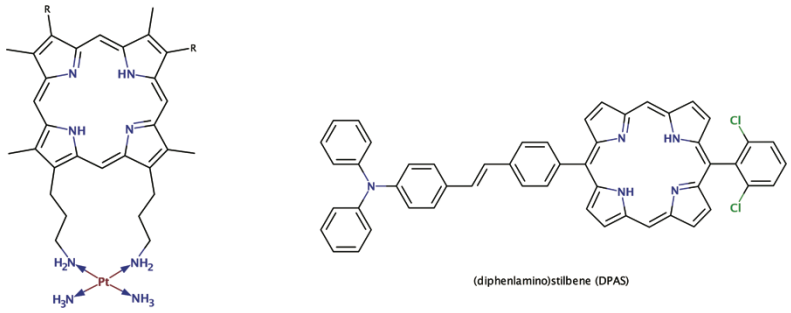

Figure 8. Examples of third generation of PSs.

Quantum dots that are CdSe-based semiconductor nanoparticles in nanometre scale can be axially linked to silicon(IV)- phthalocyanine through a

alkylamino bond[41]. Typical size ranges between 1 to 6 nm. Their dimension dictates the optical properties based on the quantum confinement effects, and can be modulated in the range between UV and IR by changing the size and the composition. Quantum dots have a lot of potential functions such as activating the PSs, generating singlet oxygen directly, and carrying the hydrophobic PSs into aqueous solution.

1.4 PHOTOPHYSICAL AND PHOTOCHEMICAL PROCESSES IN PDT

In Figure 9 are categorized the possible photo-physical and photo–chemical deactivation pathways of one excited molecule, after light-activation.

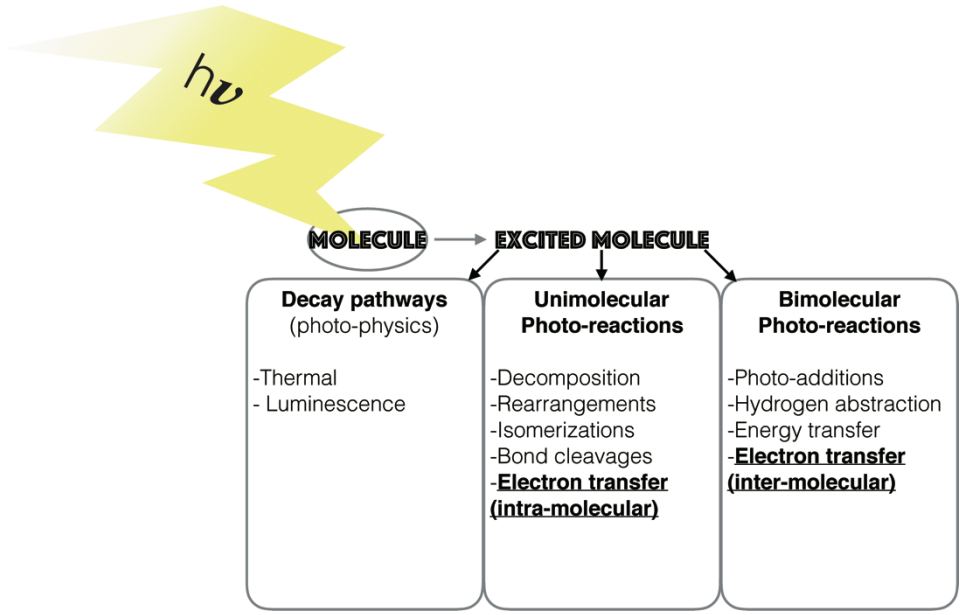

Figure 9. Category of photo-physical/-chemical pathways.

1.4.1 PHOTOPHYSICS OF EXCITED STATES

The photophysical processes involved in the absorption of light can be briefly summarized in a Jablonski diagram (Figure 10).

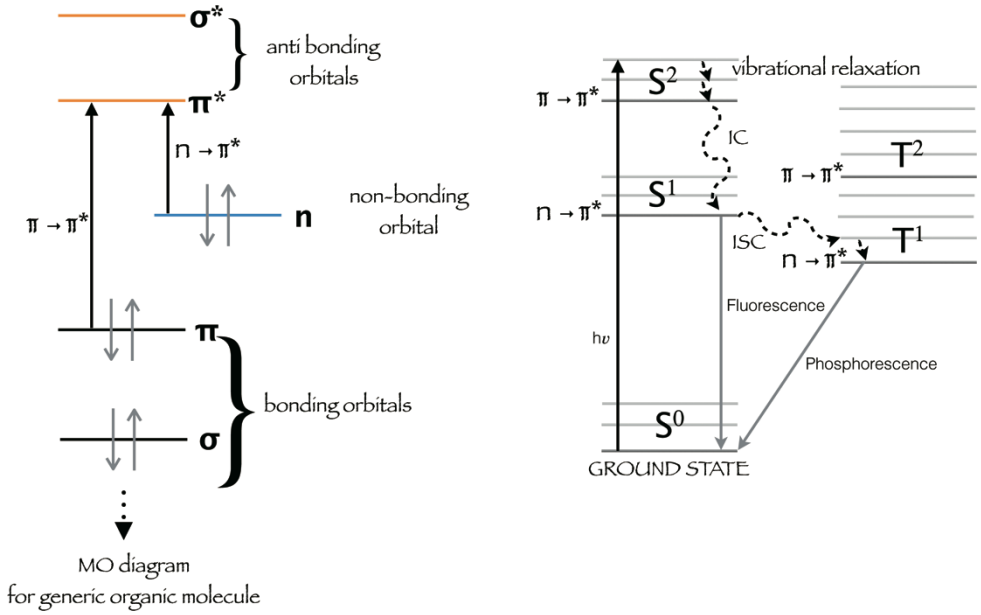

Figure 10. MO diagram and electron configuration (left) and Jablonski diagrams (right) for a compound possessing n and π electrons.

A state usually consists of closely spaced energy vibrational levels. The population of the vibrational levels follows a Boltzmann distribution. At room temperature, the lowest vibrational level, the zero-point level, is greater populated than the upper energy vibrational levels. The analysis of the deactivation pathway from one excited state after radiation absorption is made on the basis of some approximation and useful rules, such as El-Sayed rules, energy gap law, Kasha's rule and Fermi Golden rule [44]. During electronic transition, the nuclear position can be regarded as fixed (in general the electronic transition occurs within ~10^{-16} s, while the order of nuclear vibrational motion is 10^{-14} s). The transition is called 'vertical' and the resulting state is called the Franck-Condon state. The deactivation pathway proceeds through a vibrational relaxation that involves a molecular geometry change and a rearrangements of solvation structure in the excited state to an equilibrium geometry. The excess vibrational energy in an excited molecule is released by collision with neighboring molecules (the vibrational relaxation usually proceeds within ~10^{-14} to 10^{-12} s because it involves nuclear motions) and the molecule reach to the thermally equilibrated excited state. The energy of the equilibrated excited state is the zero-

spectroscopic energy (E_{00}) and represents the difference between the lowest vibrational levels of the ground and excited states. The excited state is energy-rich so a reactive species can undergo physical or chemical deactivation pathways to release its energy. In *section 1.4.2*, the chemical transformation of the excited states will be discussed.

A state energy diagram for a generic molecule shows the photophysical deactivation channels from the excited state that can occur through radiationless and radiative pathways. Two pathways are essentials for the non-radiative deactivation:

1. *Internal conversion* (IC): non-radiative transition between excited states with same multiplicity, where the energy of the upper excited states is dissipated as heat to the surrounding medium.
2. *Intersystem crossing* (ISC): non-radiative transition between excited states with different multiplicity, involving a spin flip of one orbital electron. Whereas the most typical ISC involves a transition from S_n to T_n, the triplet state has to lie below the singlet state energy.

The rate of ISC is essential for PDT, where an ideal PDT should have a high triplet quantum yield and slow ISC to the singlet electronic ground state. This state can serve as a long-lived intermediate for photochemical and photobiological transformations. The qualitative rules to evaluate the ISC rates are the El-Sayed rules and the energy gap law. The El-Sayed rules establish the rate of ISC from the lowest singlet excited state to the lowest triplet excited. The rate increases if orbitals type changes in the transition (e.g. $^1n,\pi^* \rightarrow {}^3\pi,\pi^*$ is faster than $^1n,\Pi^* \rightarrow {}^3n,\pi^*$).

Conversely, the radiative deactivation channels provide the light emission. For fluorescence, the emission accompanies the transition from the excited singlet to the ground state, which is defined by a rate constant (k_f), the energy of the released photon($h\nu_f$), or quantum yield (ϕ_f): the ratio of the number of emitted photons to the number of absorbed photons). The wavelength of fluorescence is usually longer than the absorption wavelength (Stokes shift). If the transition occurs from the excited triplet state to the ground state, the emission is called phosphorescence**.** Similar to fluorescence, it is described by $h\nu_p$, ϕp, or k_p. From the Jablonski diagram, the following consideration can be derived:

- The upper excited states can deactivate to the lowest excited state through intermolecular collision, and undergo vibrational relaxation until the zero-vibrational

level (v=0) is reached. The emission of radiation can take place only when it occurs from the lowest excited state, as explained by Kasha's rule. Consequently, the fluorescent energy will be less than the absorption energy since the excited state will be subjected to electronic and vibrational relaxations before giving off luminescence emission. The difference between absorption and emission is called Stokes shift and provides information of the structural distortion between the ground and excited states.

The lifetimes of excited states are very important in determining the deactivation pathways that will take place after photo-excitation of molecules. Considering a general molecule that has a singlet-ground state, it is known that a singlet excited state has a shorter lifetime ($<\mu s$) compared to a triplet state ($\sim ms$). This means that the triplet excited state is more reactive than the singlet excited one. Indeed, as described above, the achievement of the lowest excited state by ISC is the 'key step' for the molecular oxygen production (type II) as well as the radical chain reactions (type I) in PDT. The triplet excited state T_1 (Figure 10) can be populated by the radiationless ISC from S_1 to T_1^v (v: vibrational excited state) that leads to the T_1 state through a 'vibrational cascade'. Although the $S_1 \rightarrow T_1$ transition is spin-forbidden, it is energetically favored and an efficient ISC is fundamental in PDT.

The selection rules for transitions are briefly introduced:

The transitions between the excited states take place with different probabilities, depending on the 'allowed' or 'forbidden' decay pathways ('allowed' and 'forbidden' are quantum mechanical descriptions). Selection rules of a transition are summarized in the following points regarding orbital, momentum, spin, and symmetry:

- *Orbital overlapping*: Wavefunctions of the states involved in the transition must overlap, e.g. $n \rightarrow \pi^*$ is less energetic but forbidden.
- *Transition moment integral*: Transitions that lead to large changes in the linear or angular momentum of the molecule are forbidden.
- *Spin state*: The possible electronic transitions have same spin multiplicity (ex. $S_0 \rightarrow S_1$), except for molecules with effective SOCs values.
- *Symmetry*: When the sign of the wavefunction changes upon reflection through a center of symmetry, the symmetry is referred to as ungerade (denoted u). When it is

unchanged, it is termed gerade (denoted g). The transitions of u→g and g→u are allowed, while u→u and g→g transitions are forbidden.

A transition between excited states is mainly characterized by the energy (wavelength) and the molar absorption coefficient related to the probability of the transition (less probable, lower ε).

The probability of transition P^{if} from an initial state i to final state f is proportional to the square of module of transition moment Q, as follow:

$$P^{if} \propto |Q|^2 = \left|\langle\psi_f|er|\psi_i\rangle\langle\psi_f^{spin}|\psi_i^{spin}\rangle\right|^2,$$

where, following a Dirac notation, the ψ_i and ψ_f are the wavefunctions for the initial and final state, *er* is the dipole moment of the molecule (usually called μ), and ψ_f^{spin} and ψ_i^{spin} are the spin functions. A transition is possible ($P^{if} \neq 0$) if the spatial and spin terms are not equal to zero. In order for the spatial part to be different from zero, it is necessary that the initial and final wavefunction ψ_i and ψ_f have different symmetry under inversion operation. (i.e. electronic transition u→u and g→g 'centrosymmetric functions' are forbidden), due to the not-centrosymmetric 'or ungerade' character of the μ operator.

From an experimental point of view, the absorption phenomena are rationalized by Lambert law, which states that the fraction of radiation absorbed by molecules do not depend on the power of the incident radiation. Beer law suggests that the radiation is directly proportional to the solution concentrations. The combination of these two laws lead to the Beer-Lambert law as shown below, valid for diluted solutions,

$$\log_{10}\frac{I_0}{I} = A = \varepsilon \cdot c \cdot l,$$

where I_0 and I represent the intensity of the incident and diffuse radiations respectively, A is the absorbance, ε is the wavelength-dependent molar absorption (M^{-1} cm^{-1}), c is the molar concentration of the solution, and l is the path length of the sample (cm). The experimental electronic spectra in solution are characterized by the absorption band, where the width is due to the occurrence of vibrational and rotational relaxation from one excited state (different quantum numbers). Usually the molar absorption, ε, is expressed as a function of the wavenumber ($\bar{\nu} = \frac{1}{\lambda}$, cm^{-1}). When $\varepsilon=\varepsilon(\bar{\nu})$ implies $I = \int_0^\infty \varepsilon(\bar{\nu})\, d\bar{\nu}$, where the integral represents the area under the absorption band. The intensity often is defined using the dimensionless oscillator

strength f, ($f = 4.33 \cdot 10^{-9} \int_0^{\infty} \varepsilon\,(\overline{\boldsymbol{\nu}})\, d\overline{\boldsymbol{\nu}}$). The oscillator strength is a dimensionless quantity, defined as the ratio of strength of the absorption to the (hypothetical) strength of a single electron using a harmonic oscillator model. The f value is 1 in an allowed transition case, while $f \ll 1$ for forbidden transitions. The relationship between the ε and f values and the transition intensity are summarized in **Table 1**.

Table 1. Electronic transition condition

TRANSITION CONDITION	ε($M^{-1}cm^{-1}$)	f
Forbidden by spin rule	10^{-5}-10^{0}	10^{-5}
Allowed by spin rule, forbidden by Laporte rule	10^{0}-10^{3}	10^{-1}
Allowed by both rules	10^{3}-10^{5}	1

1.4.1.1 PHOTOPHYSICS OF PURE ORGANIC MOLECULES

The absorption of ultraviolet-visible (UV-Vis) radiation by molecules can promote the transition of valence electrons to higher energy levels. Generally, the photophysics of organic molecules differ from the photophysics of metal complexes.

All organic molecules are able to absorb UV-Vis radiation, promoting the valence electrons to higher energy levels. In organic molecules, there are four types of electron excitations shown below in energy decreasing order:

- $\sigma \rightarrow \sigma^*$ e.g. Alkanes
- $n \rightarrow \sigma^*$ e.g. Amines, Alcohols, Ethers
- $\pi \rightarrow \pi^*$ e.g. Alkenes, Aldehydes, Carboxylic acids, Esters
- $n \rightarrow \pi^*$ e.g. Aldehydes, Ketones, Esters

The last two electron excitations are predominant in organic photochemistry. The first two occur in the so-called vacuum ultraviolet region (<185 nm), while the experimental spectrophotometric investigation of organic molecules works in a range of wavelengths longer than 185 nm due to the capacity of molecules in atmosphere to absorb in this region.

In order to obtain the Jablonski diagram for a general organic molecule containing non-bonding and π electrons, it is common to start from a molecular

orbital diagram, where the lowest energetic electronic transition that brings to the excited states are reported. Different spin multiplicities (2S+1, where S is the total spin of the system $\sum \pm \frac{1}{2}$) can be taken for each electron configuration in excited states. As shown in Figure 10, the singlet states have higher energy than the corresponding triplet ones. The energy gap between the two excited states S_2 and T_2, derived from ⊓ →⊓* transition, is larger than the energy gap between S_1 and T_1, since the former has a higher inter-electronic repulsion due to the greater amount of spatial overlap between the molecular orbitals containing the two electrons.

1.4.1.2 PHOTOPHYSICS OF TRANSITION METAL COMPLEXES

The photophysics of transition metal complexes is more complicated than that of organic molecules, due to high symmetry and the number of degenerate orbitals, which creates the possibility of having more than two spin multiplicities for one electronic configuration in an excited state.

Figure 11 shows the main part of the MO diagram for a general complex of a transition metal in octahedral symmetry, including the main transition that can occur in visible and near UV range. The MOs are classified according to the contribution of their electronic density as: bonding, mainly ligand-centered π_L orbitals; non–bonding π_M metal-centered orbitals of t_{2g} symmetry; antibonding metal-centered σ_M^* orbitals of e_g symmetry and antibonding ligand-centered π_L^* orbitals. For simplicity's sake, the ligand-centered σ_L and σ_M* metal-centered orbitals are omitted in Figure 11. In a metal complex, the principal electronic transitions are: Metal-Centered (*MC*) $\pi_M \rightarrow \sigma_M^*$ transition from bonding to antibonding d-orbitals localized on the metal atom; ligand-centered (*LC*) $\pi_L \rightarrow \pi_L^*$ transition; Ligand-to-metal charge transfer (*LMCT*) $\pi_L \rightarrow \sigma_M^*$ transition and metal-to-ligand charge transfer (*MLCT*) $\pi_M \rightarrow \pi_L^*$. The associated energy ordering of the excited electronic configurations is determined by the nature of ligand and metal.

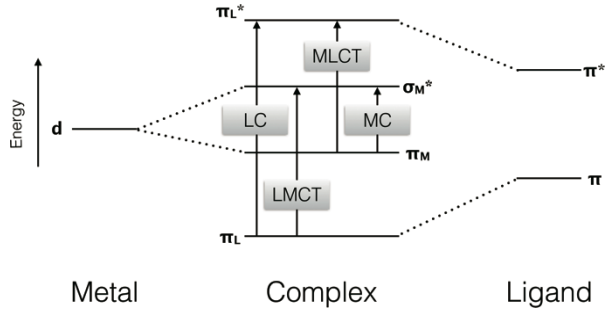

Figure 11. Simplified molecular orbital diagram for a metal complex in octahedral symmetry to show main contributions of electronic transitions such as LC, LMCT, MLCT, and MC.

A lower contribution of *MC* transition is expected for the first-row transition metals, while a low *LMCT* energy transition is expected in the case of complexes containing low ionization energy ligands and reductive metal and a high *MLCT* transition is predicted in opposite cases. Low ligand-centered (*LC*) transition can be predicted if the complex contains aromatic ligands with extended π and π* orbitals. In Figure 12**,** a simplified diagram for the octahedral complex $[Ru(bpy)_3]^{2+}$ is shown as an example. The metal with d^6 electrons (completely filled HOMO orbitals) has a closed-shell ground state configuration, therefore the S_0 state will be a singlet and the excited state can be either singlets or triplets as is with the case for organic molecules. The lowest excited state for complexes in an octahedral symmetry has a MLCT character since the Ru^{2+} is readily oxidized and the 2,2'-bipyridine ligands are easily reduced.

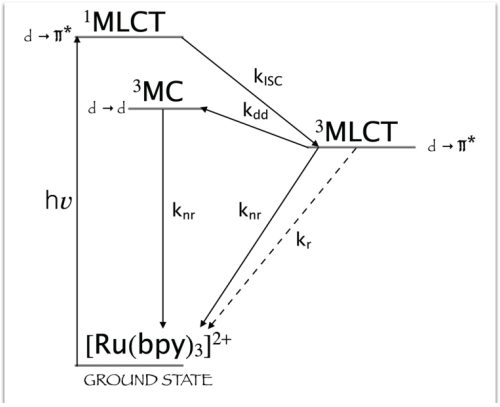

Figure 12. Schematic energy diagram for $[Ru(bpy)_3]^{2+}$ showing the lowest state that can be populated by photo-excitation. The possible photophysical deactivation pathways are also shown.

1.4.2 PHOTOCHEMISTRY OF EXCITED STATES

The excited state can undergo photochemical reactions such as photodissociation into radicals, photoionization, internal electron transfer, intramolecular rearrangement, photocyclization, and intramolecular cleavage.

In the contest of the photoreactivity, Kasha's rule states that the reaction starts from the minimum of the lowest excited state.

In bimolecular photoreactions, the energy and intermolecular electron transfer processes are quenching pathways**,** where the external component, called the quencher, deactivates an excited sensitizer. As show in Figure 5, in bimolecular processes, when the lifetime of the excited state in solution is long enough, chemical phenomena such as intermolecular interactions, photosensitization, photoaddiction, hydrogen atoms abstraction, external electron transfer, electron transfer to another molecule (oxidative or reductive electron transfer) or energy transfer can occur. The bimolecular processes of excited state deactivation follow a second-order kinetics. Bimolecular electron and energy transfers are very important processes in PDT since they allow the quenching of excited states (i.e. to prevent intramolecular reactivity and radiative emission), and luminescence from species which cannot absorb light.

The 'intermolecular energy transfer' was first demonstrated by Terenin and Ermolaev[42]. A solution of acetophenone (PhCOMe) in ethanol-ether at 90 K was irradiated at 366 nm, and phosphorescence emission was observed at 388 nm. When naphthalene was added to the solution, the luminescence occurred at 470 nm, which corresponds to the phosphorescence of naphthalene. It was deduced that naphthalene, which does not absorb the irradiated light at 366 nm, can be excited to the triplet state by energy transfer from acetophenone.

The process can be summarized as follow:

$$D \xrightarrow{h\nu} D^*$$

$$D^* (T_1) + A (S_0) \rightarrow D (S_0) + A^* (T_1)$$

Here, the donor D and the acceptor A are acetophenone and naphthalene, respectively. An important parameter in photochemical processes is the quantum yield, defined as the rate between the number of molecules formed in ml per second and the number of quanta absorbed in ml per second. The quantitative determination of the quantum yield is detected by an actinometer, which can measure the total incident energy. It is possible to determine the quantum yield of fluorescence,

phosphorescence, triplet, singlet, ISC, and IC, on the basis of the Stark-Einstein law $\sum \phi_x \leq 1$. (Stark-Einstein law states that the absorption of one photon excites only one molecule).

➢ BIBLIOGRAPHY

1. Duke-Elder, S. Ultra-Violet Light In The Treatment Of Ophthalmological Diseases Ii. Local Phototherapy. *Brit. J. Ophthalmol.* **1928**, *12*, 353–373.
2. Raab, 0. Uber die Wirkung fluorescierender Stoffe auf Infusoria, *Z. Biol.* **1900**, *39*, 524.
3. Tappeiner, H. V.; Jodlbauer, A. Uber die Wirkung der photodynamischen (fluoreszierenden) Stoffe auf Infusorien. *Dtsch. Arch. Klin. Med.* **1904**, *80*, 427-487.
4. Lipson, R.L. The Photodynamic and Fluorescent Properties of a Particular Hematoporphyrin Derivative and it's Use in Tumor Detection. **Masters Thesis**, University of Minnesota, Minneapolis. **1960**.
5. Lipson, R. L.; Baldes, E. J. The Photodynamic Properties of a Particular Hematoporphyrin Derivative. *Arch. Dermat.* **1960**, *82*, 508-516.
6. Diamond,I.; Granelli,S.G.; Mcdonagh,A.F.; Nielsen, S. L.; Wilson, C. B.; Jaenicke, R. Photodynamic therapy of malignant tumours. **1972**, *Lancet*, *2*,1175.
7. Dougherty, T.J.; Kaufman, J.E.; Goldfarb, A.; Weishaupt, K.R.; Boyle, D.; Mittleman, A. Photoradiation Therapy for the Treatment of Malignant Tumors. *Cancer Res.* **1978**, *38*, 2628–35.
8. Clark, W.D.K.; Steel, C. Photochemistry of 2,3-diazabicyclo[2.2.2]oct-2-Ene. *J. Am. Chem. Soc.* **1971**, *93*, 6347–6355.
9. Niedre, M; Patterson, M.; Wilson, B. Direct Near-infrared Luminescence Detection of Singlet Oxygen Generated by Photodynamic Therapy in Cell In Vitro and Tissues In Vivo. *Photochem. Photobiol.* **2002**, *75*, 382-391.
10. Drews, W.; Schmidt, R.; Brauer, H.D. Generation of 1O2 from O2 quenching of the lowest excited singlet and triplet states of 9,10-diphenylanthracene, *Chem. Phys. Let.* **1983**, *100*, 466-469.
11. Fodor, L.; Elman, M.; Ullmann, Y. Aesthetic Applications of intense Pulsed Light. (**2011**, *XI*, 133 p. 228. ISBN: 978-1-84996-455-5).
12. Everett, M.A.; Yeargers, E.; Sayre, R.M. et al. Penetration of epidermis by ultraviolet rays. *Photochem. Photobiol.* **1966**, *5*, 533–542.
13. Svaasand, L. O. In Porphyrin Localization and Treatment of Tumors. (*Doiron and Gomer editors*, New York, **1984**, 91-114).
14. Wilson, B. C.; Jeeves, W. P.; Lowe, D. M.; Adam G. Light Propagation in Animal Tissues in the Wavelength Range 375-825 Nanometers. *Prog. Clin. Biol. Res.* **1984**, *170*, 115-32.
15. Bolin, F.P.; Preuss, L.E.; Cain, B.W. A Comparison of Spectral Transmittance for Several Mammalian Tissues: Effects at PRT Frequencies., *Prog. Clin. Biol. Res.* **1984**, *170*, 211-25.
16. Herd, R.M.; Dover, J.S.; Arndt, K.A. Basic Laser Principles. *Dermatol. Clin.* **1997**, *15*, 355–372.
17. Dougherty, T.J.; Potter, W.R.; Of What Value is a Highly Absorbing Photosensitizer in PDT?. *Journal of Photochemistry and Photobiology B: Biology*. **1991**, *8*, 233-234.
18. Robinson, G. W. Intensity Enhancement of Forbidden Electronic Transitions by Weak Intermolecular Interactions. *J. Chem. Phys.* **1967**, *46*, 572–585.
19. Krishna, V. G. Simultaneous and Induced Electronic Transitions in Oxygen. I. *J. Chem. Phys.* **1969**, *50*, 792–799.
20. Schmidt, R.; Tanielian, C.; Dunsbach, R.; Wolff, C. Phenalenone, a Universal Reference Compound for the Determination of Quantum Yields of Singlet Oxygen Sensitization. *J. Photochem. Photobiol., A.* **1994**, *79*, 11–17.
21. Rosenthal, I. Phthalocyanines as Photodynamic Sensitizers. *Photochem. Photobiol.* **1991**, *53*, 859–870.
22. Kautsky, H.; de Bruijn, H.; Neuwirth, R.; Baumeister, W. Photo-sensibilisierte Oxydation als Wirkung eines aktiven, metastabilen Zustandes des Sauerstoff-Moleküls Energie-Umwandlung an Grenzflächen, VII. *Mitteil. Ber. Deutsch. Chem Gesell.* **1933**, *66*, 1588-1600.

23. Foote, C. S.; Valentine, J. S.; Greenberg, A.; Liebman, J. F. Active Oxygen in Chemistry. (Blackie Academic and Professional, London, **1995**).
24. Hausman, W. H. Uber die sensibilisierende Wirkung tierischer Farbstoffe und ihre physiologische, Anwendung. *Biochem. Z.* **1908**, 14, 275-283.
25. Hausman, W. H., Wien. Klin. Wchneschr. **1909**, 22, 1820.
26. Auler, H.; Banzer, G. Untersuchungen uber die Rolle der Porphine bei geschwulstkranken Mcnschen und Tieren. ***Z*** *Krebsforsch.* **1942**, *53*, 65-8.
27. Figge, F.H.J. Near ultraviolet rays and fluorescence phenomena as aids to discovery and diagnosis in medicine. *Univ. Maryland Med. Bull.* **1942**, *26*, 165-76.
28. Manganiello, L. O. J.; Figge; F. H. J. Cancer detection and therapy. II. Methods of preparation and biological effects of metalloporphyrins. *Bull. School Med. Univ. Maryland.* **1951**, *36*, 3.
29. Figge, F. H. J.; Peck, G. C. Cancer Detection and Therapy. Affinity of Lymphatic Tissue for Hematoporphyrin. *Anat. Rec.*, **1953**, *115*, 306.
30. Rassmussen-Taxdal, D. S.; Ward, G. E.; Figge, F. H. J. Fluorescence of human lymphatic and cancer tissues following high doses of intravenous hematoporphyrin. *Cancer.* **1955**, 8, 78.
31. Figge, F.H.J.; Diehl, W.K.; Peck, G.C. Evaluation of the use of intravenous hematoporphyrin injections to improve surgical and radiation therapy of cancer in human subjects, abstract. *Proc. Am. Assoc. Cancer Res.* **1956**, *2*, 105.
32. Lipson, R. L.; Baldes, E. J. Photosensitivity and Heat. *Arch. Dermat.* **1960**, *82*, 517-20.
33. Lipson, R. L.; Baldes, E. J.; Olsen, A.M. The Use of a Derivative of Hematoporhyrin in Tumor Detection. *J. Natl. Cancer Inst.* **1961**, *26*, 1-11.
34. Lipson, R. L.; Baldes, E. J.; Olsen, A.M. Hematoporphyrin Derivative: A New Aid for Endoscopic Detection of Malignant Disease. *J. Thorac. Cardiov. Surg.* **1961**,*42*,623-9.
35. Dougherty, T. J. Hematoporphyrin as a photosensitizer of tumors. *Photochem. Photobiol.* **1983**, *38*, 377-379.
36. Dougherty, T. J.; Boyle, D. G.; Weishaupt, K. R.; Henderson, B. A.; Potter, W. R.; Bellnier, D.A.; Wityk, K. E. In Porphyrin Photosensitization. (D. Kessel and T. J. Dougherty Eds.; Plenum Press: New York, **1983**, p. 3).
37. Mironov, A. F.; Nizhnik, A. N.; Nockel, A. Y. Hematoporphyrin derivatives: an oligomeric composition study. *J. Photochem. Photobiol., B: Biol.* **1990**, *3*, 297-306.
38. Smith, K. M. In Photodynamic Therapy of Neoplastic Disease, Volume II. (D. Kessel Ed.; CRC Press, Boca Raton, **1990**; pp 145-168).
39. Wohrle, D.; Weitemeyer, A.; Hirth, A.; Michelsen, U. In Photochemical Energy Conversion, Fundamentals and Applications. (M. Kaneko Ed.; Industrial Publishing & Consulting Inc.: Tokyo, **1996**, in press)
40. Samia, A.; Chen, X.; Burda, C. Semiconductor Quantum Dots for Photodynamic Therapy. *J. Am. Chem. Soc.* **2003**, *125*, 15736–15737.
41. Marian, C. Spin–orbit Coupling and Intersystem Crossing in Molecules. *Wiley Interdiscip. Rev. Comput. Mol. Sci.* **2012**, *2*, 187–203.
42. Terenin, A.; Ermolaev, V. Sensitized Phosphorescence in Organic Solutions at Low Temperature. Energy Transfer between Triplet States. *T Faraday Soc* **1956**,*52*, 1042–1052.

2.COMPUTATIONAL METHODS

Theoretical and Computational Chemistry provides an interface between chemistry, physics, mathematics and computational sciences. The growing of this field has been supported by the advancement in the computational technology as well as by the methodological developments.

The solution of the so-called *many-body problem,* that arises from *Schrödinger equation* for more than two-particle, requires very large computational efforts. The equation for many particle systems cannot be solved exactly by analytical mathematical methods. Computational methods can, however, provide approximated solutions to the many-body problem (which in principle may be refined to any desired degree of accuracy), based on the wave function methods such as Hartree-Fock (HF) and post-HF methods (e.g. perturbation theory (MPn, n = 2, 3, ...), configuration interaction (CI), and coupled cluster (CC)). An alternative way is given by density functional theory (DFT) originally developed for electron-gas systems by Thomas and Fermi in 1927[1,2].

The DFT overcomes the main problem in the wave function methods, i.e. the wave function complexities with the increasing of electrons, since DFT depends exclusively on three spatial coordinates. The computational cost is lower than post-HF methods and comparable to the HF one. DFT was developed by Hohenberg and Kohn who proved the one-to-one correspondence between the electron density of a system and the energy, therefore the ground state electronic energy is determined completely by the electron density. The main problem concerns the functional connecting electron density and state energy that is unknown, although it has been proven that each different density yields a different ground state energy. Indeed, a lot of functionals have been proposed.

In the work presented in this thesis DF based theory has been used and a brief introduction about these methods will be given in sections 2.1 and 2.2. A more comprehensive description is available in standard textbooks[3-6].

In section 2.3, the used approximation of SOC[7] operators is presented. Finally, in section 2.4, the derivation of the Gibbs energy of photoinduced electron transfer[8,9] equation is explained.

The computational details for the specific studies are reported in the papers collected in Chapter 3.

2.1. DENSITY FUNCTIONAL THEORY (DFT)

The DFT considers the energy of the system as functional of the electron density, as follow:

$$Energy = F[\rho(x,y,z)]. \qquad (2.1)$$

Hohenberg and Kohn[10] introduced, in 1964, the existence of a unique relationship between the electron density and all properties of a given system. The first Hohenberg-Kohn theorem states that every observable of a stationary quantum mechanical system can be calculated exactly from the ground state electron density, meaning that every observable can be written as a functional of the ground state electron density. Within the Born-Oppenheimer approximation, the total energy can be splitted into three terms, the kinetic energy term T[P], the electron-electron repulsion term E_{EE}[P] and the nuclei-electron attraction term V[P] as follows:

$$E[\rho] = T[\rho] + E_{ee}[\rho] + V[\rho], \qquad (2.2)$$

$$V[\rho] = \int \rho(r)v(r)dr. \qquad (2.3)$$

The terms of T[P] and E_{EE}[P] depend exclusively on the coordinates of the electrons and their formulation is the same for all systems, depending only on the number of electrons. They together form the universal Hohenberg-Kohn functional F^{HK}[ρ]:

$$F^{HK}[\rho] = T[\rho] + E_{ee}[\rho]. \qquad (2.4).$$

All efforts to improve the DFT are devoted to founding the explicit form of the Hohenberg-Kohn functional, because the exact form of the functional is unrevealed. However, at least the classical part, $J[\rho]$ namely the Coulomb electron-electron interaction, can be extracted from the $E_{ee}[\rho]$ described as follow:

$$E_{ee}[\rho] = J[\rho] + V_{ncl}[\rho], \qquad (2.5)$$

where the $V_{ncl}[\rho]$ is the non-classical contribution to the electron-electron interaction (self-interaction correction, exchange and Coulomb correlation). The main challenge in DFT is establishing an explicit functional form of $T[\rho]$ and $V_{ncl}[\rho]$. The second Hohenberg-Kohn theorem can be considered as the introduction of the variational principle into DFT. For a trial electron density $\tilde{\rho}$(r) which satisfies the necessary boundary conditions, such as $\tilde{\rho}(r) \geq 0$ and $\int \tilde{\rho}\,(r)dr = N$, the Hohenberg-Kohn variational methods states that:

$$E_0 \leq E[\tilde{\rho}] = T[\tilde{\rho}] + E_{ee}[\tilde{\rho}] + V[\tilde{\rho}], \quad (2.6)$$

where E_0 is the correct energy and $E[\tilde{\rho}]$ is the energy, written as functional of trial electron density of a system with an external potential. The variational principle can be applied only for the ground state. Unfortunately, it is difficult to obtain the density of an interacting system. The problem was overcome, in 1965, by Kohn-Sham[11] that introduced an auxiliary system of non-interacting particles. They proposed an approach to approximate the kinetic energy in the universal Hohenberg and Kohn functional, suggesting to calculate the exact kinetic energy of a reference system (ρ_s) with non-interacting electrons whose density is the same as the interacting real electron density, ρ as follows:

$$Ts[\rho] = \sum_i^N \left\langle \psi_i \middle| -\frac{1}{2}\nabla_i^2 \middle| \psi_i \right\rangle, \quad (2.7)$$

$$\rho_s(r) = \sum_i^N \sum_s |\psi_i(r,s)|^2 = \rho(r), \quad (2.8)$$

where ψ_i are referred to the orbitals of non-interacting system. The kinetic energy of the real system can be expressed as sum of two contributes: the kinetic energy of the reference system, $Ts[\rho]$ and the kinetic energy originated from the electron correlation $Tc[\rho]$, as follow:

$$T[\rho] = Ts[\rho] + Tc[\rho]. \quad (2.9)$$

Consequently, a new definition of the universal functional can be introduced as follow:

$$F[\rho] = Ts[\rho] + J[\rho] + E_{XC}[\rho], \quad (2.10)$$

where the exchange-correlation energy, $E_{XC}[\rho]$ contains an unknown analytically form, i.e. the difference between the exact kinetic energy and the kinetic energy of the reference system, and the non-classical contribution to the electron-electron interaction (self-interaction correction, exchange and Coulomb correlation as mentioned above). The $E_{XC}[\rho]$ functional can be defined as:

$$E_{XC}[\rho] = (T[\rho] - Ts[\rho]) + (E_{ee}[\rho] + J[\rho]). \quad (2.11)$$

The total-energy functional including all these considerations for the real interacting system is:

$$E[\rho] = Ts[\rho] + \frac{1}{2}\iint \frac{\rho(r)\rho(r\prime)}{|r-r\prime|} dr dr' + E_{XC}[\rho] + \int \rho(r)v(r)dr, \quad (2.12)$$

where the $E_{XC}[\rho]$ is the only term that has non-explicit form. Applying the variational method, imposing the wave function orthogonal condition ($\langle \psi_i | \psi_j \rangle = \delta_{ij}$) and using the Lagrange multipliers method, the Kohn-Sham results in the following equations:

$$\left(-\frac{1}{2}\nabla_i^2 + v_s[\rho](r)\right)\psi_i(r) = \varepsilon_i \psi_i(r). \quad (2.13)$$

The v_s stands for the local potential for the single particle and includes the exchange and correlation potential, v_{XC} as follows:

$$v_s[\rho](r) = v(r) + \int \frac{\rho(r')}{|r-r'|} dr' + v_{XC}[\rho](r), \qquad (2.14)$$

$$v_{XC}[\rho](r) = \frac{\delta E_{XC}[\rho]}{\delta \rho(r)}. \qquad (2.15)$$

The $v_s[\rho]$ term depends on the density and therefore the Kohn-Sham equations have to be solved iteratively.

2.1.1 THE EXCHANGE CORRELATION PART IN DFT

The major challenge in DFT is finding the appropriate form of the exchange-correlation energy, $E_{XC}[\rho]$, and the resulting $V_{XC}[P]$. Currently, although we do not know the exact form of this functional, there are a number of approximate form that are fairly good. These approximate models can roughly be divided into three classes:

i) Methods that use a local density approximation (LDA). LDA is based on assumption that the electron density varies very slowly and locally with position and can thus be treated as a homogeneous electron gas[4]. This is not the case for molecules, where the electron density is not uniform. Although LDA gives surprisingly accurate predictions for solid-state physics, it is not a useful model for chemistry due to its severe overestimation of chemical bond energies and underestimation of activation barriers.

ii) Methods that combine the electron density calculations with a gradient correction factor, namely Generalized Gradient Approximation (GGA). In order to account for the non-homogeneity of the real electron density, the information about the gradient of the charge density $\nabla P(R)$ was introduced. Although the GGA functionals have showed to give more accurate predictions for thermochemistry than the LDA ones, they still underestimate the activation barriers.

iii) Hybrid methods that are combination of HF exchange and DFT exchange correlation. They are more accurate than both GGA and LDA, especially for the main group thermochemistry. A hybrid exchange-correlation functional is usually constructed from a linear combination of HF exact exchange, E_x^{HF} and DFT exchange-correlation obtained via either GGA or LDA.

The HF exact exchange:

$$E_x^{HF} = -\frac{1}{2}\sum_{i,j} \iint \psi_i^*(r_1)\psi_j^*(r_1)\frac{1}{r_{12}}\psi_i(r_2)\psi_j(r_2)dr_1 dr_2, \qquad (2.16)$$

is referring to the exchange correlation between parallel spin electrons, not opposite spin ones. The inclusion of exact HF exchange often improves calculated results, although the optimum fraction to include the HF exchange depends on the specific property of interest. New functionals improved by including a suitable fraction of the exact exchange is nowadays a standard feature. At least, part of the improvement may arise from reducing the self-interaction error, since HF theory is completely self-interaction free.

A typical approach is proposed for a magic combination of exchange and correlation functionals by a few adjustable scaling parameters and a choice of basis set in order to reproduce a selected set of experimental data. This procedure is not theoretically justified, and should be merely considered as data fitting without much physical relevance. Therefore, this procedure can be taken as an experimental fitting to functions that can be useful to predict specific properties for a series of compounds. One may furthermore differentiate the functionals based on their use (or lack) of experimental data for the parameterization in the functional forms. The non-empirical ones such as PW86, PW91, PBE functionals use the free parameters to fulfill many requirements. Empirical ones as the BLYP, B3LYP were attempted to improve the performance by fitting the free parameters to give a good agreement with experimental data.

The main difference between the hybrid functionals is due to the different portion of the HF exact exchange functional, E_x^{HF}.

The composition of functionals B3LYP[12] (20% HF exchange), PBE0[13,14] (25% HF exchange) and M06[15] (27% HF exchange) are briefly reviewed:

B3LYP (Becke, three parameters, Lee-Yang-Parr) is the most used hybrid density functional and one of the most successful functional in term of overall performance. B3LYP incorporates a portion (20 %) of exact exchange functional from HF theory with exchange and correlation functional from other reference (ab-initio or semi-empirical methods). The B3LYP formula[12] is written as follow:

$$E_{xc}^{B3LYP} = E_x^{LDA} + a_0(E_x^{HF} - E_x^{LDA}) + a_x(E_x^{GGA} - E_x^{LDA}) + E_c^{LDA} + a_c(E_c^{GGA} - E_c^{LDA}) \quad , \quad (2.17)$$

where $a_0 = 0.20$, $a_x = 0.72$, $a_c = 0.81$ are the semi-empirical coefficients determined by an appropriate fitting to experimental data, E_x^{HF} is the HF exact exchange functional, E_x^{GGA} and E_c^{GGA} are the generalized gradient approximation given by combination of the Becke 88 exchange functional[15] and the correlation functional of

Lee, Yang and Parr[17], and E_x^{LDA} and E_c^{LDA} is the local density approximation to the exchange and correlation functional by Vosko, Wilk and Nusair[18], respectively.

Since the functional uses the three semi-empirical coefficients, it is referred as "B3LYP". The performance of B3LYP functional is usually better than pure-GGA functionals but the computational cost is more expensive.

PBE0[13,14] mixes the Perdew-Burke-Ernzerhof (PBE)[19] exchange and correlation functionals with the HF exchange functional, in different ratio:

$$E_{xc}^{PBE0} = \frac{1}{4}E_x^{HF} + \frac{3}{4}E_x^{PBE} + \frac{1}{4}E_c^{PBE}, \qquad (2.18)$$

where E_x^{HF} is the HF exact exchange functional, E_x^{PBE} and E_c^{PBE} indicates the PBE exchange and correlation functionals, respectively.

M06[15] is based on the meta-GGA approximation and 27% of HF exchange functional. It is designed for main-group thermochemistry and non-covalent interactions, transition metal thermochemistry and organometallics.

2.1.2 BASIS SETS AND EFFECTIVE CORE POTENTIAL (ECP)

Ab initio calculations are carried out using a basis set. It is important to point out that a basis set should be chosen enough large to get a good description of molecular wavefunctions. In real calculations, molecular orbitals are expressed as a linear combination of basis functions as follow:

$$\psi_i = \sum_{\mu=1}^{n} C_{\mu i}\phi_\mu, \qquad (2.19)$$

where, ψ_i is the i-th molecular orbital, ϕ_μ is the μ-th basis function which is usually atomic orbitals, $C_{\mu i}$ represents the coefficients of the linear combination for ϕ_μ, and n is the number of atomic orbitals. The basis sets can be divided in:

- Minimal basis sets: they often give inaccurate results, while they are helpful in understanding qualitatively and quickly thanks to low computational costs (e.g. STO-2G, STO-3G).
- Split-valence basis sets: A typical example are Pople type basis sets, X-YZG (double zeta basis). In this description, X indicates the number of primitive Gaussians comprising each core atomic orbital. Y and Z indicate that each valence orbital is composed of a linear combination of Y and Z primitive Gaussian functions, respectively. (e.g. 3-21G, 6-31G). In an analogous fashion, the split-valence triple zeta denoted as X-YZWG is also used (e.g 6-311G).

- Other typical functions are Dunning type basis sets. Double, triple and quadrupole zeta basis sets are multiple basis function corresponding to each atomic orbital, including both valence and core orbitals or just the valence orbitals (e.g. cc-pVDZ, cc-pVTZ, cc-pVQZ). cc-p stands for correlation consistent polarized basis sets and V stands for valence.

Examples of atomic basis sets are Slater-type orbitals (STO) of which all integral calculations can be performed analytically, and Gaussian-type orbitals (GTO) of which integral calculations are faster than those of STO. Therefore, the latter basis sets are widely used for molecular calculations in quantum chemistry while the former has been applied extensively for atomic and diatomic molecular systems.

Systems involving elements from the lower part of the periodic table have a large number of core electrons. These are unimportant in a chemical sense, but it is necessary to use a large number of basis functions to expand the corresponding orbitals, otherwise the valence orbitals will not be properly described, due to a poor description of the electron–electron repulsion. In the lower half of the periodic table relativistic effects further complicate matters. These two problems may be overcome by modeling the core electrons with a suitable function, and treating only the valence electrons explicitly.

The use of ECPs often gives quite good results at a fraction of the cost of a calculation involving all electrons, and part of the relativistic effects (especially the scalar effects) may also be taken care of, without having to perform the full relativistic calculation. The systems studied in this thesis are characterized by the presence of atoms with a large number of core electrons, therefore the Stuttgart-Dresden (SDD)[20] ECP basis sets was employed to describe Te, I, and Ru atoms.

2.2. TIME-DEPENDENT DENSITY-FUNCTIONAL THEORY (TD-DFT)

The basic ideas of DFT in the ground state are extended by means of time-dependent scheme to deal with the excitations or time-dependent phenomena. In TD-DFT, the standard way to obtain the electron density, $\rho(r,t)$, is helped by a fictitious system with non-interacting electrons, i.e. the Kohn-Sham system. The equations for the systems are numerically simple to be solved. The scheme is general and there are two regimes as explained below. When the time dependent potential is weak, it is sufficient to resort to linear response theory and for instance optical adsorption spectra can be calculated. The spectra calculated within this framework well agree with experimental results, although the potential is approximated simply. If the TD potential is strong, full description of the Kohn Sham equations is required. The treatment of atoms or molecules in strong laser field is a canonical example for this regime. In such case, TD-DFT can describe non-linear phenomena (e.g. high harmonic generation or multi-photon ionization)[4,10]. The TD-DFT formulation is analogous derivation of the Kohn-Sham equation from the Schrödinger equation with time-independent regime, except for consideration of time-dependency.

2.2.1 TIME DEPENDENT KOHN-SHAM EQUATIONS

The equations for a set of non-interacting electrons are described by single particle wavefunctions, $\{\phi_i(t)\}$ known as orbitals. The total electronic wavefunction in this context is taken to be a Slater determinant of the single particle orbitals as follow:

$$\psi(t) = \frac{1}{\sqrt{N!}}\begin{bmatrix} \phi_1(r_1,t) & \cdots & \phi_{1N}(r_1,t) \\ \vdots & \ddots & \vdots \\ \phi_1(r_N,t) & \cdots & \phi_N(r_N,t) \end{bmatrix}. \quad (2.20)$$

Herein, the time-dependent density of the interacting system can be computed from the following equation:

$$\rho(r,t) = \sum_{i=1}^{N} \phi_i^*(r,t)\phi_i(r,t). \quad (2.21)$$

The time-dependent Kohn-Sham orbitals are obtained by solving the time-dependent Schrödinger equation of the non-interacting particles system shown below:

$$\left[-\frac{1}{2}\nabla^2 + v_s[\rho](r,t)\right]\phi_j(r,t) = i\frac{\partial\phi_j(r,t)}{\partial t}. \quad (2.22)$$

The single particle on Kohn Sham potential is given by the following formula:

$$v_s[\rho](r,t) = \int dr' \frac{\rho(r',t)}{|r-r'|} + v_{ext}(r,t) + V_{XC}. \quad (2.23)$$

The first and second terms represent the Coulomb and the external potentials, respectively, while the third term means the exchange-correlation potential which is approximated by the same exchange-correlation potential as in the time-independent DFT. However, the time-dependent density at a particular time is used in TD-DFT, rather than the time-independent one.

2.3. SOLVATION AND DIELECTRIC EFFECTS

One important factor to be considered for reliable calculated results in quantum chemistry is the interaction between solute and solvent. The common approaches include the solvation effects by a continuum model with a dielectric permittivity constant, ε. In all continuum models, the basic concept is "cavity". The model is composed of a solute put into a void cavity surrounded by a continuous dielectric medium miming the solvent. As a general rule, a cavity should have a physical meaning and not be only a mathematical artifice. In particular, the cavity should exclude the solvent and contain the boundaries, where the solute charge can distribute most probably. The various shape and size of the cavity are defined differently as the continuum models[21]. A lot of attention has been paid to the interaction between the charge distribution of the solute in the outside of the cavity boundaries and the charge distribution of the solvent.

The Poisson equation written below can be used in order to describe the electrostatic interaction between an arbitrary charge density $\rho(r)$ and a continuum dielectric:

$$\nabla^2\phi(r) = \frac{-4\pi\rho(r)}{\varepsilon}, \quad (2.24)$$

where $\phi(r)$ is the electrostatic potential of charge density. During a quantum chemical calculation, Equation 2.24 is solved numerically. Consequently, the solvent charge distribution is returned to the SCF procedure which is performed accounting for the solvent charges. This process is called self-consistent reaction field (SCRF) method because it is repeated until the convergence of self-consistency. Continuum models, which are based on the assumption that the electrostatic interactions of the solute and the surrounding solvent do not depend on the molecular structure of the solvent, reveal their inadequacy when strong and specific interactions between a solute and one or more first-shell solvent molecules take place. The continuum solvation models used in this thesis are CPCM (Conductor Polarizable Continuum Model) and PCM. In

the CPCM, the cavities are defined as envelopes of spheres centered on atoms with radii approximately 20% larger than the Van der Waals radius. When the charge distribution of the solute polarizes the dielectric medium, the response of the medium is described by the generation of screening charges (q) on the cavity surface. The dielectric constant of the medium is changed from the specific finite value, ε, which is characteristic of each solvent, to infinite. The value of ε corresponds to a conductance of the solvent and this change strongly simplifies the electrostatic problem[21-24]. To take into account the finite permittivity of real solvents, the charges (q) are scaled by a factor $f(\varepsilon)$,

$$q^* = f(\varepsilon)q,\ f(\varepsilon) = \frac{\varepsilon-1}{\varepsilon+0.5}. \qquad (2.25)$$

2.4. SPIN-ORBIT COUPLING (SOC)

SOC is one of the relativistic effects that allow to change spin states, for example during a transition light-induced ISC, even though the spin state change is forbidden in the non-relativistic theory. The relativistic effects can be considered as perturbative corrections to the non-relativistic wavefunction. Differently approximated SOC operators (mixing different spin states) were employed to evaluate the SOC for the investigated systems, as intersystem crossing plays a key role in photochemistry. In particular, in reactions when heavy atoms are involved, the so-called *heavy atoms effect* largely increases the transition probability between different spin states. The transition can be efficiently induced when different spin states at similar energy levels are involved, even if the SOC matrix elements are small.

The SOC arises naturally from the Dirac theory which is a full relativistic one-particle theory, where the electron spin *s* couples with the orbital angular momentum *l*, and the resultant total electronic angular momentum, *j*, is only a 'good' quantum number. A one-electron theory should be extended to the many-body theory in order to address chemical phenomena. However, the contribution of three body potentials are small perturbations on the total results enough to be neglected[25]. The relativistic two-particle theory including the *Breit interaction* contains a retardation term to account for the speed of transmission[26] and a magnetic interaction term[27]. Approximated two-particle Hamiltonian is used to correct the relativistic transformation properties.

2.4.1 THE BREIT-PAULI SPIN-ORBIT HAMILTONIAN

The Breit-Pauli operator was originally established by Pauli[28] in 1927, and starts from the Schrödinger equation of a molecule in an external electric and magnetic field. The Breit-Pauli operator is obtained assuming that the scalar potential is purely Coulombic and the magnetic field arises from the intrinsic magnetic moment associated with the electronic spin. In atomic units (ħ=1, e=1), the Breit-Pauli spin operator is written as follow:

$$\hat{H}_{SO}^{BP} = \frac{1}{2\,m_e{}^2c^2}\sum_i\sum_I \frac{Z_I}{\hat{r}_{iI}^3}(\hat{r}_{iI} \times \hat{p}_i)\cdot\hat{s}_i - \frac{1}{2\,m_e{}^2c^2}\sum_i\sum_{j\neq i}\frac{1}{\hat{r}_{iI}^3}(\hat{r}_{iI} \times \hat{p}_i)\cdot\left(\hat{s}_i + 2s_j\right), \qquad (2.26)$$

where, i and j are labels of electrons, Z_I is the charge of the nucleus I, m_e is the electron mass, and c is the light speed. The first term is a one-electron operator describing the interaction of the spin magnetic moment of an electron i with the magnetic moment that arises from its orbiting in the field of the nucleus I. The second term represents a two-electron operator, which is a contraction of the two-electron spin-same-orbit describing the coupling between the spin magnetic moment of electron i and the orbital magnetic moment of electron j, and vice versa.

2.4.2 EFFECTIVE ONE-ELECTRON SPIN-ORBIT COUPLING OPERATORS

For systems containing heavy atoms, the one-electron terms of the spin-orbit Hamiltonians are the dominating part, and the screening effect of the two-electron contributions is taken into account by approximate ways discussed below.

One of the most rigorous approaches is a mean-field approximation. The spin-orbit mean-field operators constitute an extension of the frozen-core approximation to all-electron calculations in which the two-electron spin-orbit interaction of (partially filled) orbital k occupied by n_k electrons is averaged over α- and β-spin orientations before spin integration. A matrix element of effective one-electron Hamiltonian is given as below:

$$\left\langle i(1)\middle|\hat{H}_{SO}^{mf}\middle|j(1)\right\rangle = \left\langle i(1)\middle|\hat{h}_{SO}(1)\middle|j(1)\right\rangle + \frac{1}{2}\sum_k n_k\{2\left\langle i(1)k(2)\middle|\hat{H}_{SO}(1,2)\middle|j(1)k(2)\right\rangle -$$
$$3\left\langle k(1)i(2)\middle|\hat{H}_{SO}(1,2)\middle|j(1)k(2)\right\rangle - 3\left\langle i(1)k(2)\middle|\hat{H}_{SO}(1,2)\middle|k(1)j(2)\right\rangle\}, \qquad (2.27)$$

where the $\hat{h}_{SO}(1)$ and the $\hat{H}_{SO}(1,2)$ represent the one and two electron terms, respectively. The spin orbit mean field (SOMF) Hamiltonian is approximated effectively to correspond to full one- and two- particle operators, giving a good result even in the case of light molecules.

The spin-orbit coupling operator with effective nuclear charges is the less demanding approach as the two-electron contributions are taken into account through screening of the nuclear potential:

$$\widehat{H}_{SO}^{eff} = \frac{1}{2\, m_e{}^2 c^2} \sum_I \sum_i' \frac{Z_{I,l}^{eff}}{\hat{r}_{Ii_I}^3} \hat{l}_{Ii_I} \cdot \hat{s}_{i_I}, \quad (2.28)$$

In this one-electron one-center spin-orbit operator, I denotes an atom and i_I an electron occupying an orbital located at center I. The $\hat{l}_{Ii_I}$ indicates the angular momentum of electron i_I with respect to the orbital origin of atom I. The prime on the summation over electrons indicates that it includes only the open shell of an atom I with azimuthal quantum number.

When the spin-orbit Hamiltonian with effective nuclear charges is used in conjunction with pseudopotentials, the $Z_{I,l}^{eff}$ is a pure empirical parameter without any physical meaning.

2.5. FERMI-GOLDEN RULE

The rate of radiationless transition (e.g. electron-transfer process, ISC) between two states described by the potential energy surface is defined by the Fermi-Golden rule expression[9]. It is based on the electromagnetic interaction between states and is derived from perturbation theory.

The Fermi-Golden rule can be, thus, employed to determine ISC rate for the nonradiative transition between S_n and T_m:

$$k_{isc}^{nm} = \frac{2\pi}{\hbar} \left\langle S_n \middle| \widehat{H}_{SO} \middle| T_m \right\rangle^2 FCWD, \quad (2.30)$$

where the $\left\langle S_n \middle| \widehat{H}_{SO} \middle| T_m \right\rangle$ corresponds to the spin-orbit matrix elements and Franck-Condon weighted density of states (FCWD) representing the weighted density of final states at the initial energy, that ensures energy conservation. Assuming that the relaxation via internal conversion into the lowest excited singlet state S_1 is fast enough so that intersystem crossing essentially proceeds from S_1, in the framework of Marcus-Levich-Jortner theory [29,30] the FCWD:

$$FCWD = \frac{1}{\sqrt{4\pi\lambda k_B T}} \sum_{n=0}^{\infty} \exp(-S) \frac{S^n}{n!} \exp\left[-\frac{(\Delta E + n\hbar\omega + \lambda)^2}{4\lambda k_B T}\right], \quad (2.31)$$

Where λ is the Marcus reorganization energy, ΔE is the difference between the energies of S_1 and the triplet state at their equilibrium geometry, $\hbar\omega$ is the energy of an effective non-classical vibrational mode involved in the transition, and S is the

associated Huang-Rhys factor. From Equation 2.30, it appears that the rate of the ISC increases with the increasing of spin-orbit coupling between the two states involved in the transition and with the decreasing of the energy gap of the same states.

2.6. PHOTOINDUCED ELECTRON TRANSFER

The Electron Transfer process is viewed as a special nonradiative decay pathway, which quenches the excited state through electronic configuration relaxations in a thermally fluctuating environment.

Within the Marcus theory framework for the photoinduced ET reaction, the molecules are first excited to the Franck-Condon electronic states, which are characterized by nonzero vibrational populations[31-33]. In other words, it assumes that the electron transfer must take place from a transition state of this unstable molecule, and in low temperature conditions, it ignores the tunneling effects assisting the electron transfer. Actually, electronic excitation of a molecule populates a vibrationally hot intramolecular charge transfer (ICT) manifold in the high frequency regime ($\hbar\omega \gg k_B T$[34]. The excess vibrational energy is rapidly lost, following the excited state configuration relaxation and nuclear rearrangement, which further promotes ET proceeding from such nonthermalized states.

Complete understanding of the ET mechanism requires detailed vibrational charge-transfer motion information and electron-vibration constants, which is also cast into the contributions for driving the forward ET reactions. However, in the framework of Marcus-Levich-Jortner's, the rate of ET essentially depends on three key parameters: the free energy, ΔG, the reorganization energy, λ, and the charge-transfer integral.

To evaluate the driving force for electron transfer, a primary characterization can be made by calculating the Gibbs energy of photoinduced electron transfer, which is described in the next section.

It has been used in Paper II to evaluate the occurrence of electron transfer from $^3O_2$ to triplet excited states of deoxyguanosine derivatives. In such systems the photoelectron transfer (PeT) can occur leading to the quenching of the $^3PS^*$ with the formation of the charge-transfer intermediate. The initial step of the PeT leads to the formation of a charge-transfer complex in which charge and electronic excitation energy are shared by donor and acceptor molecules.

2.6.1 GIBBS ENERGY OF PHOTOINDUCED ELECTRON TRANSFER

Molecular properties in excited states are very different from the ground state, and molecules in excited states are stronger oxidant and reductant than those in the ground state (Figure 2.1.)

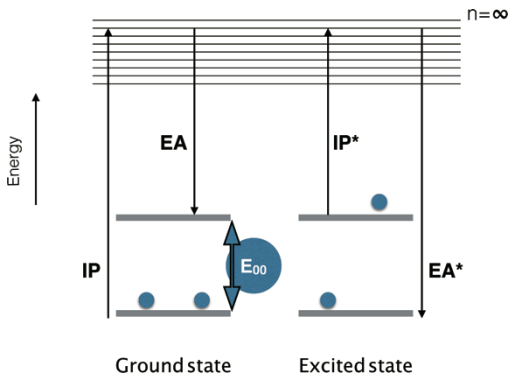

Figure 2.1. Comparison of the ionization potential (IP) and electronic affinity (EA) between ground and excited states.

The redox photo-reaction can lead to the excitation of donor (*D) as well as of acceptor (*A) that are schematically described below:

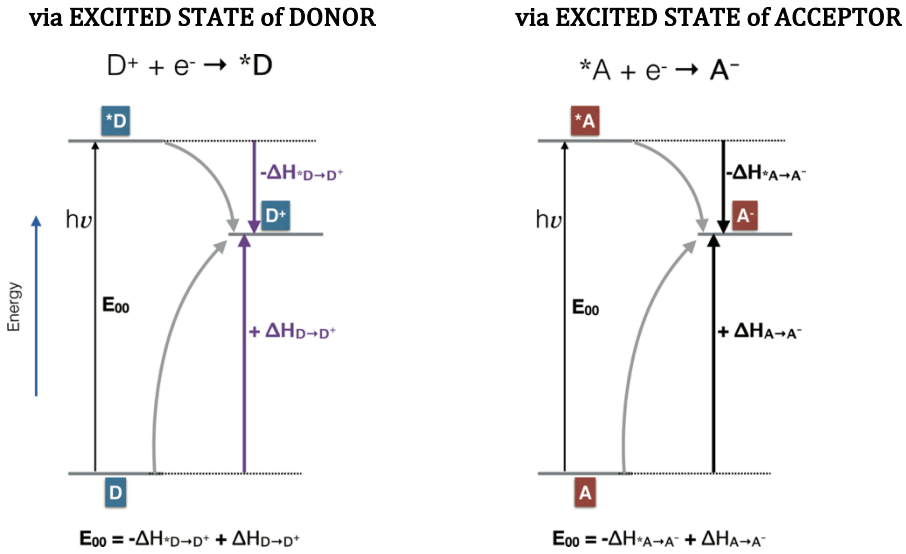

Figure 2.2. Enthalpy changes to form D^+ from D (endothermic) and *D (exothermic) and to form A- from A and *A.

From Figure 2.1 it appears clear that:

$$IP_{*D} = IP_D - E_{00} \qquad (2.32)$$

$$EA_{*A} = EA_A + E_{00} \quad (2.33)$$

According to reactions:

$D \xrightarrow{h\nu} \mathbf{*D}$ $\qquad$ $A \xrightarrow{h\nu} \mathbf{*A}$

$A + \mathbf{*D} \rightarrow D^+ + A^-$ $\qquad$ $D + \mathbf{*A} \rightarrow D^+ + A^-$

the energy change is:

$$\Delta E = IP_{*D} - IP_{A-} = IP_{*D} - EA_A =$$
$$= IP_D - E_{00} - EA_A \quad (2.34)$$

$$\Delta E = IP_D - IP_{A-} = IP_D - EA_{*A} =$$
$$= IP_D - E_{00} - EA_A \quad (2.35)$$

The IPs and EAs, that are one-electron properties obtained in gas phase, can be measured by photoelectron spectroscopy. The equations are useful only for comparison purpose: substituting IPs and EAs in the equations can give an indication whether an excited-state electron transfer is exothermic or endothermic, the estimated energies are not applicable to the solution phase due to lack of parameters which account for Coulombic and solvation effects.

Combining the free-energy difference between a reactant and a product, free-energy can be generally described as follow:

$$\Delta G = \Delta H - T\,\Delta S, \quad (2.36)$$

where ΔH and ΔS are enthalpy and entropy changes of a reaction, respectively, and T is the absolute temperature. E_{00}, which expression is reported in Figure 2.2, can be now written as follows:

$$E_{00} = -\Delta G_{*D\rightarrow D^+} - T\,\Delta S_{*D\rightarrow D^+} + \Delta G_{D\rightarrow D^+} + T\,\Delta S_{D\rightarrow D^+}, \quad (2.37)$$

$$E_{00} = -\Delta G_{*A\rightarrow A-} - T\,\Delta S_{*A\rightarrow A-} + \Delta G_{A\rightarrow A-} + T\,\Delta S_{A\rightarrow A-}. \quad (2.38)$$

Assuming that structural change and reorganization of solvation structure between initial and final states do not occur during electron transfer the free-energy is equal to the enthalpy ($\Delta G = \Delta H$).Therefore, the free-energy change in the oxidation of a donor and reduction of an acceptor are:

$$\Delta G_{*D\rightarrow D^+} = \Delta G_{D\rightarrow D^+} - E_{00}, \quad (2.39)$$

$$\Delta G_{*A\rightarrow A-} = \Delta G_{A\rightarrow A-} - E_{00}. \quad (2.40)$$

The free-energy change is correlated to the redox potential, E_{redox}, of the half-reaction, as follow:

$$\Delta G = -nFE_{redox}, \quad (2.41)$$

where n represents the number of transferred electrons and F is the Faraday constant ($9.6485309 \cdot 10^4$ C mol^{-1}). The redox potential is sign dependent, namely positive and negative signs mean exothermic and endothermic processes, respectively. The first approximation is the redox potential of the excited states couples which may be calculated from the redox potentials of the ground-state couples and the one-electron potential corresponding to the zero-zero excited-state energy:

$$E^0(D^+/{}^*D) \approx E^0(D^+/D) - E_{00} \qquad (2.42)$$

conventionally,

$$E^0(D^+/{}^*D) = - E_{{}^*D \rightarrow D^+}, \qquad (2.43)$$

$$E^0({}^*A/A^-) \approx E^0(A/A^-) + E_{00}, \qquad (2.44).$$

The Equations 2.43 and 2.44 imply that the excited state is a better electron donor and acceptor than the ground state, respectively.

The relationships among IP, EA, and E_{redox} for electron transfer at excited states in solution, the solvation terms are ΔG_{D+} and ΔG_{A-} for D^+ and A^-, respectively.

The following equations express the 'linear' relationships between the gas-phase energy terms and the redox potentials:

$$IP = E^0(D^+/D) - \Delta G_{D+} + \text{Constant}, \qquad (2.45)$$

$$EA = E^0(A/A^-) + \Delta G_{A-} + \text{Constant}. \qquad (2.46)$$

In order to evaluated the thermodynamics in the excited state, the redox potentials that are relevant to solution-phase reactions are used rather than IP and EA.

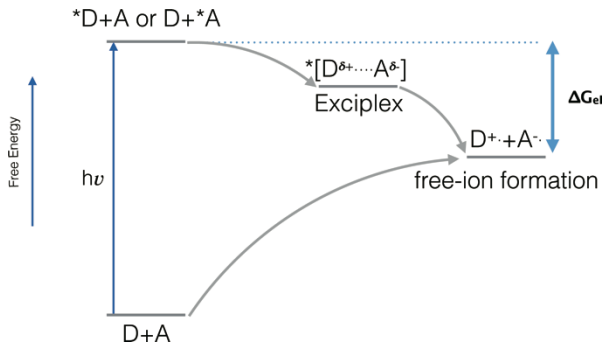

Figure 2.3. An archetypal energy diagram for photoinduced electron transfer processes, where the formation of the exciplex (a charge transfer complex) is shown as an intermediate in the photoelectron transfer reaction.

An important point of the process in photoelectron transfer from the exciplex is the total energy decreasing. The free-energy change for an electron transfer process

between a donor in excited state and an acceptor in ground state can be obtained according to the following scheme (same equation can be obtained for an acceptor in excited state and a donor in ground state):

$$\Delta G_{el}\ (eV)=nF[E^0\ (D^+/{}^*D)- E^0\ (A/A^-)], \qquad (2.47)$$

and substituting $E^0\ (D^+/{}^*D)$ as defined in *eq 2.43*,

$$\Delta G_{el}\ (eV)=nF[E^0\ (D^+/D)- \Delta G_{00} - E^0\ (A/A^-)], \qquad (2.48)$$

where ΔG_{00} is the free energy corresponding to the energy of equilibrated structure, E_{00}. For most one electron transfer, $nF \simeq 1$, ,therefore:

$$\Delta G_{el}\ (eV) = E^0\ (D^+/D)- \Delta G_{00} - E^0\ (A/A^-). \qquad (2.49)$$

The latter equation is applicable to an equilibrated excited state and not to a Frank-Condon state. It is assumed that photo-electron transfer (PeT) occurs after the relaxation of the Frank-Condon excited state.

An important refinement is introduced to obtain the Gibbs energy of photoinduced electron transfer, because two charged species are formed after PeT (here, supposed that the donor and acceptor are neutral species). When an ion pair is formed, attractive Coulombic force will draw the two ions closer together, resulting in a release of energy. This attraction is given by a work term, w_p, derived from a Coulomb's law shown below:

$$w_p = \frac{(z_{D^+} z_{A^-})e^2}{d_{cc}\varepsilon_s}, \qquad (2.50)$$

where z_{D^+} and z_{A^-} are the charges of donor and acceptor molecules, ε_s is the static dielectric constant of the solvent, and d_{cc} (in Å) is the distance between the two centers. Adding the w_p for one-electron transfer process to the previous equation, the *Gibbs energy of photoinduced electron transfer*[35,9] can be written as follow:

$$\Delta G_{el}\ (eV) = E^0\ (D^+/D) - E^0\ (A/A^-) - \frac{e^2}{d_{cc}\varepsilon_s} - \Delta G_{00}. \qquad (2.51)$$

The equation was applied to the X6-dGuo system in paper I, and to the BODIPY-dyes system in the manuscript.

➢ BIBLIOGRAPHY

1. Thomas, L. H. The calculation of atomic fields**.** *Proc. Cambridge Phil. Soc.* **1927**, *23*, 5, 542-548.
2. Fermi, E.: Un metodo statistico per la determinazione di alcune priorieta dell'atome. *Rend. Accad. Naz. Lincei.* **1927**, 6, 602-607.
3. Szabo, A.; Ostlund, N. S. Modern Quantum Chemistry: Introduction to Advanced Electronic Structure Theory. (Macmillan Publishing Co., Inc.: New York, **1982**).
4. Koch, W.; Holthausen, M. C.; (WILEY-VCH Verlag GmbH: Weinheim, **2001**).
5. Carsten A. Ullrich; Time-Dependent Density-Functional Theory Concepts and Applications. (Oxford Graduate Texts, **2012**).
6. Jensen, F; Introduction to Computational Chemistry. (John Wiley & Sons, Ltd.: England, **2007**).
7. Marian, C. Spin–orbit Coupling and Intersystem Crossing in Molecules. *Wiley Interdiscip. Rev. Comput. Mol. Sci.* **2012**, *2*, 187–203
8. Gilbert, A.; Specialist periodical reports PHOTOCHEMISTRY (volume 30); (Royal Society of Chemistry, **1999**).
9. Kavarnos, G. J.; Fundamentals of Photoinduced ElectronTransfer. (VCH,**1993**).
10. Hohenberg, P.; Kohn, Inhomogeneous Electron Gas. W. *Phys. Rev.* **1964**, *136*, B864-B871.
11. Kohn, W.; Sham, L. J. Self-Consistent Equations Including Exchange and Correlation Effects. *Phys. Rev.* **1965**, *140*, A1133-A1138.
12. Becke, D. Density-functional thermochemistry. III. The role of exact exchange *J. Chem. Phys.*, **1993,** *98*, 5648–5652.
13. Perdew, J. P.; Ernzerhof, M.; Burke, K. Rationale for Mixing Exact Exchange with Density Functional Approximations. *J. Chem. Phys.* **1996**, *105*, 9982–9985.
14. Adamo, C.; Barone V. Toward Reliable Density Functional Methods Without Adjustable Parameters: The PBE0 Model. *The Journal of Chemical Physics*. **1999**, *110*, 6158–6170.
15. Zhao, Y.; Truhlar, D. G. The M06 suite of density functionals for main group thermochemistry, thermochemical kinetics, noncovalent interactions, excited states, and transition elements: two new functionals and systematic testing of four M06-class functionals and 12 other functionals. *Theor. Chem. Acc.*, **2008**, *120,* 215-241.
16. Becke, A.D. Density-functional exchange-energy approximation with correct asymptotic behavior. *Phys. Rev. A*. **1988**, *38*, 3098–3100.
17. Lee C.; Yang, W.; Parr, R. G. Development of the Colle-Salvetti correlation-energy formula into a functional of the electron density. *Phys. Rev. B*. **1988**, *37*, 785–789.
18. Vosko, S. H.; Wilk, L.; Nusair, M. Accurate spin-dependent electron liquid correlation energies for local spin density calculations: a critical analysis. *Can. J. Phys.* **1980**, *58*, 1200–1211.
19. Perdew, J. P.; Burke, K.; Ernzerhof, M. Generalized Gradient Approximation Made Simple. *Physical Review Letters*. **1996**, *77*, 3865–3868.
20. Leininger, T.; Nicklass, A.; Stoll, H.; Dolg, M.; Schwerdtfeger, P. The Accuracy of the Pseudopotential Approximation. II. A Comparison of Various Core Sizes for Indium Pseudopotentials in Calculations for Spectroscopic Constants of InH, InF, and InCl. *J. Chem. Phys.* **1996**, *105*, 1052.
21. Tomasi,J.; Mennucci, B.; Cammi, R. Quantum Mechanical Continuum Solvation Models. *Chem. Rev.* **2005**, *105*, 2999-3094.
22. Barone, V.; Cossi, M. Quantum calculation of molecular energies and energy gradients in solution by a conductor solvent model. *J. Phys. Chem. A*, **1998**, *102*, 1995-2001.
23. Cossi, M.; Rega, N.; Scalmani, G.; Barone, V. Energies, Structures, and Electronic Properties of Molecules in Solution with the C-PCM Solvation Model *J. Comp. Chem.* **2003**, *24*, 669-681.

24. Takano, Y.; Houk K.N. Benchmarking the Conductor-like Polarizable Continuum Model (CPCM) for Aqueous Solvation Free Energies of Neutral and Ionic Organic Molecules. *J. Chem. Theory Comput.* **2005**, *1*, 70–7.
25. Mittleman, M.H. Structure of heavy atoms: three-body potentials. *Phys Rev A* **1971**, *4*, 893–900.
26. Breit, G. The effect of retardation on the interaction of two electrons. *Phys. Rev.* **1929**, *34*, 553–573.
27. Gaunt, A. IV. The triplets of helium. *Phil Trans R Soc A* **1929**, *228*, 151–196.
28. Pauli, W. Zur quantenmechanik des magnetischen elektrons. *Z. Phys.* **1927**, *43*, 601–623.
29. Marcus, R. A. On the Theory of Oxidation-Reduction Reactions Involving Electron Transfer.I* *J. Chem. Phys.* **1956**, *24*, 966–978.
30. Jortner, J. Temperature Dependent Activation Energy for Electron Transfer Between Biological Molecules. *J. Chem. Phys.* **1976**, *64*, 4860–4867.
31. Balzani, V. Electron Transfer in Chemistry, (Wiley-VCH,Weinheim, **2001**).
32. Marcus, R. A.; Sutin, N. *Biochim. Biophys. Acta* **1985**, *811*, 265.
33. Barbara, P. F.; Meyer, T. J.; Ratner, M. A. *J. Phys. Chem.* **1996**, *100*, 13148.
34. Delor, M.; Scattergood, P. A.; Sazanovich, I. V.; Parker, A. W.; Greetham, G. M.; Meijer, A. J. H. M.; Towrie, M.; Weinstein, J. A. *Science* **2014**, *346*, 1492.
35. Rehm, D.; Weller, A. H. Kinetics of Fluorescence Quenching by Electron and H-Atom Transfer. *Isr. J. Chem.* **1970**, *8*, 259−271.

3 RESULTS AND DISCUSSION

3.1. ANALOGUES OF NITROGENOUS BASES

Deoxyribonucleic acid (DNA), a basic molecule for life, dictates genetic information. DNA was discovered as an unknown substance with unexpected properties in 1869 by Miescher during his study on leukocytes[1]. Its properties during the isolation procedure and its resistance to protease digestion indicated that the novel substance was not a protein or lipid. Miescher was the first to obtain a crude precipitate of DNA which he coined 'nuclein', and Altmann later succeeded in separating the DNA from proteins[2]. Due to its acidic properties, Altmann named the substance nucleic acid, although little did he realize that it was the same substance as 'nuclein'. Kossel, who won the Nobel Prize in Physiology or Medicine in 1910[1], characterized the substances as purine and pyrimidine bases, one sugar, and phosphoric acid. He inferred that nucleic acids do not serve as a source of energy[3]. In 1994, Avery *et al.*[4] presented evidence that support the idea that DNA is not proteins as previously believed and instead is a carrier of genetic information. This discovery has been confirmed by Hershey and Chase[5] in 1952. Finally, Watson and Crick[6] structurally revealed that the secondary structure of DNA has the antiparallel double-helix formed by a pair of templates, which is complementary to each other. They also proposed a model for DNA replication that ensures genetic continuity[7].

The DNA is constituted by repeating units called nucleotides, which consists of three chemical components: nitrogenous base, deoxyribose and phosphate group. The primary structure of DNA consists of one filament of polynucleotides where the deoxyribose and phosphate group form a structural framework and the sequence of nitrogenous bases define the DNA function. There are five kinds of nitrogenous bases (four are for DNA) that can be categorized into two groups: purines and pyrimidines shown in Figure 3.1. Each of the polymer chains is formed by reactions between the 3' terminal hydroxyl group on the sugar of one nucleotide and the 5' terminal phosphate group of the next nucleotide. The secondary structure of DNA is organized in a complementary double strand that runs in opposite directions. The two DNA strands are paired via hydrogen-bridges between complementary base pairs: Adenine-Thymine and Guanine-Cytosine that stabilize the structure.

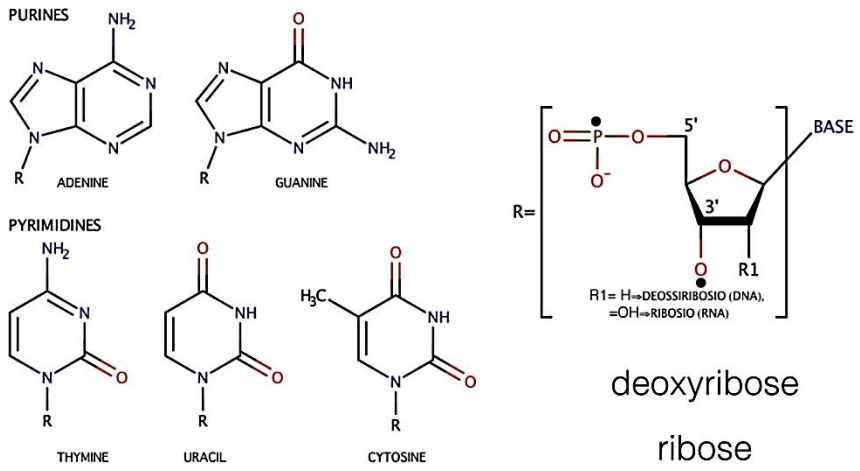

Figure 3.1. Natural nucleobases. The purine and pyridine bases are shown in the top and bottom rows, respectively.

The history of DNA is deeply linked to the interest in photoinduced phenomena in nucleic acids. Indeed, the bactericidal effect of UV radiation was discovered and became a fertile field of investigation within a decade of Miescher's isolating 'nuclein'. Here, brief historical backgrounds on the photoinduced processes in nucleic acids are introduced.

Downes and Blunt[8] proved the germicidal effects by sunlight in 1877, and Ward[9] revealed that these effects could be attributed to UV radiation. The relationship between skin cancer and UV radiation was also experimentally shown in 1928[10]. UV radiation was believed to be related to the mutagenic and carcinogenic phenomena, and a lot of effort has been devoted to the studies of photophysical properties of individual nucleobases and the double strands of DNA. Gates[11] found that the bactericidal effects of sunlight were caused by 'some single essential substance in the cell' and were due to the absorption of UV light between 260 and 270 nm. The absorption radiation was localized to the nucleus[12]. Swanson[13] defined a specific criterion to measure sensitivity of the chromosomes. The investigations of the interactions between DNA and UV radiation contributed to understanding the effect of radiation on nucleic acids and provided information about molecular events associated with DNA damage repair. Setlow et al.[14] found that intrastrand photoinduced thymine dimers were the major contributor to DNA damage. DNA can be damaged by exposure to UVB (280-320 nm) and UVC (<280 nm) radiation[15-19]. The photophysical properties of the building blocks of DNA are summarized in Table 3.1.

The work of Mouret and co-authors[20] showed that both UVA and UVB induce pyrimidine dimerization. The UVB induces formation of a number of dimers, mainly thymine-thymine and thymine-cytosine (6-4), while UVA almost exclusively induces the formation of thymine-thymine pyrimidine dimers.

Table 3.1. Summarized photophysical properties, such as maximum band λ_{max}, extinction coefficient ε, and quantum yield ϕ for absorption and fluorescence, of natural nucleobases in water.

	Absorption			***Fluorescence***		
Base	**λ_{max} (nm)**	**ε (10^3 M^{-1} cm^{-1})**	***Refs.***	**λ_{max} (nm)**	**ϕ (10^{-4})**	***Refs.***
Ade	260, 207	15	*21, 22*	321	2.6	*23*
Gua	252, 271	14, 10	*22*	328	3.0	*23*
Cyt	269, 230	10, 8	*22*	314	0.8	*23*
Thy	207, 269	10, 8	*22, 24*	338	1.0	*23*
Ura	258, 202	8, 9	*25*	309	0.5	*23*

As a powerful complement to experimental studies, computational investigations of DNA started in 1970, when a number of simulations of the absorption and emission spectra helped to assign measured absorption spectra[26]. On the basis of both experimental and computational photophysical data, it was deduced that the interaction between DNA and UV radiation can have some therapeutic application. Subsequent studies focused on thio-analogues of DNA building blocks. Even minor structural modifications showed alteration of photochemical properties of the natural DNA bases. Substitution of one or more molecular ring atoms with sulfur induced a significant red-shift in the absorption spectra, making thio-bases effective absorbers of UVB and UVA radiations with significant triplet quantum yield. Today, the thiopurine drugs are commonly used as cytotoxic agents[27,28]. Recently, the thio-analogues of nucleobases were proposed as good candidates for PSs in PDT because of their potential to generate singlet oxygen[29-31].

In the next sections (3.1.1 and 3.1.2) the studies on analogues of nitrogenous bases presented in this thesis will be briefly introduced: DFT and TD-DFT investigations for the photophysical properties of the S- Se- and Te- analogues of Thymidine and Guanosine.

3.1.1 **Photophysical Properties Prediction of Selenium and Tellurium Substituted Thymidine as Potential UVA Chemotherapeutic Agents** (PAPER I)

Purine, pyrimidines and their derivatives have been extensively studied due to their interesting pharmacological properties. Special emphasis has been reserved to thymidine since the substitution of oxygen in position 4 or both of 2 and 4 strongly enhances the production of the cytotoxic singlet excited oxygen. 4-Thiothymidine was found a promising photosensitizer for bladder cancer with a significant degree of selectivity[32,33]. Pollum et al.[34] studied the effect of oxygen substitution in the exocyclic carbonyl groups of the thymidine with sulfur atom by means of femto-second transient absorption spectroscopy. $S^{2,4}$-dTdR was selected as better PS due to the remarkable red-shift of the absorption spectrum (λ_{max} = 267 nm for thymidine to λ_{max} =363 nm for 2,4-dithiothymine) and a very fast ISC (180 ± 40 fs) that allows a high triplet quantum yield. The possibility that selenium and tellurium derivatives of thymidine work as PSs in PDT (as for thio-thymidine cases) has been theoretically explored employing DFT and TD-DFT. In order to set the best computational protocol, the photophysical properties of thio-thymidine derivatives (2-ThioT, 4-ThioT, and 2,4-DiThioT), for which a comparison between experimental data and previous theoretical results are possible, were investigated. On the basis of calculated absorption spectra, singlet and triplet excitation energies, spin-orbit matrix elements, and considering different deactivation pathways for the lowest triplet state, these systems were proposed as potential UVA chemo-theraupeutic agents.

3.1.2 **Photophysical Properties of S, Se and Te-Substituted Deoxyguanosines: Insight into Their Ability to Act as Chemotherapeutic Agents** (PAPER II)

Numerous studies at both, experimental and theoretical levels, have been performed on the photophysical and photochemical properties of 6-thioguanine and 6-thioguanosine. Selenium analogues of guanine and guanosine have also been synthetized and structurally characterized as potential chemotherapeutic agents, while the information for the tellurium derivatives is limited to some oligonucleotide derivatives.

In this paper, theoretical investigations of the photophysical properties regarding S, Se and Te-deoxyguanosine derivatives at DFT and TD-DFT levels of

theory were reported with the aim to gain more insights into the ability of these compounds to act as UVA chemotherapeutic agents and to rationalize the influence of the chalcogen atoms on the photophysical properties of deoxyguanosine. On the basis of the reported results, it was found that the substitution of oxygen with sulfur, selenium and tellurium atoms red-shifts the absorption spectrum, increases spin-orbit couplings, and decreases the energy gaps between the excited states. The possible pathways for the activation of the lowest triplet state was also discussed. These results show that the energy of the lowest triplet excited state was found sufficiently higher to excite the dioxygen, therefore all investigated systems in this work can act as type II PSs in PDT.

3.2. Ru(II)POLYPYRIDIL COMPLEXES

Ruthenium compounds, especially the Ru(II) polypyridinyl (bpy) complexes are among the most extensively studied compounds for the last 50 years. The original interest is essentially related to their potential applications for solar-energy conversion and memory storage because they can be triggered by photo- and redox-stimuli. The interests are also derived from the facility to manipulate the photophysical properties by synthetic chemical methods. The prototype compound $[Ru(bpy)_3]^{2+}$ (bpy=2,2'-bipyridine) complex attracts many researchers due to its chemical stability, redox properties, reactivity in the excited state, luminescence emission, and excited state lifetime. Starting from studies on these properties, researches have been extended to its derivatives.

The $[Ru(bpy)_3]^{2+}$ is a d^6 electron system with octahedral geometry, and exhibits electron transition from the d- metal orbital to one of π_L^* which is ligand-centered in polypyridyl complexes moiety, this process is known as metal-to-ligand charge transfer electronic transition (MLCT). Ruthenium tris-bpy has quasi D_3 symmetry[35], and the transferred electron is equally shared among the three bpy ligands[36]. Femtosecond transient-absorption studies showed that, after the ^{1}MLCT (absorption maximum at 450 nm) excitation, the triplet state ^{3}MLCT will be populated with a quantum yield near to the unity thanks to an ultrafast ISC that occurs within 100 fs[37,38]. The lifetime of the triplet excited state is ca. 600 ns in aqueous solution and at room temperature[39,40]**.** The absorption spectrum of $[Ru(bpy)_3]^{2+}$ is assigned to two peaks: the first one at 240 nm is originated from ligand centered transition (LC) and

the second one at 450 nm can be assigned to the MLCT transition. The shoulder peaks at 322 and 344 nm have been assigned to the metal centered transition (MC). The photophysical properties of $[Ru(bpy)_3]^{2+}$ have been extensively studied and can be explained using the Jablonski diagram (Figure 3.2)

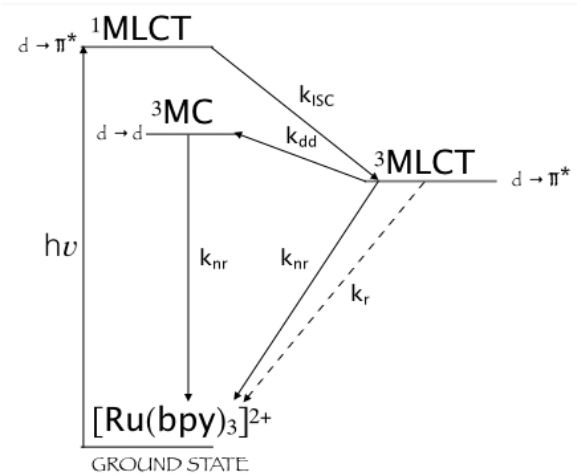

Figure 3.2. Jablonski diagram showing the lowest energy states of $[Ru(bpy)_3]^{2+}$.

The deactivation process from the MC excited state induces the photochemical loss of ligand, as discussed in the studies of Meyer and co-workers[41]. They also observed a strong dependency of the photolability on the used solvents. Acetonitrile solvent and coordinating counter ions increase the probability of the photolability process. The energy difference between the ^{3}MC and the ^{3}MLCT states is one of the important parameters to predict the deactivation pathway.

The quenching of the ^{3}MLCT lowest excited state of the $[Ru(bpy)_3]^{2+}$ to the ground state can be followed by energy or electron transfer processes. As shown in Figure 3.3, the lowest excited state lies at 2.12 eV, and its reduction and oxidation potentials are respectively +0.84 eV and -0.86 eV (aqueous solution, vs SCE). Therefore, the $*[Ru(bpy)_3]^{2+}$ is a good electron donor and acceptor at same time (i.e. oxidative and reductive quenching), and a good energy donor (energy transfer).

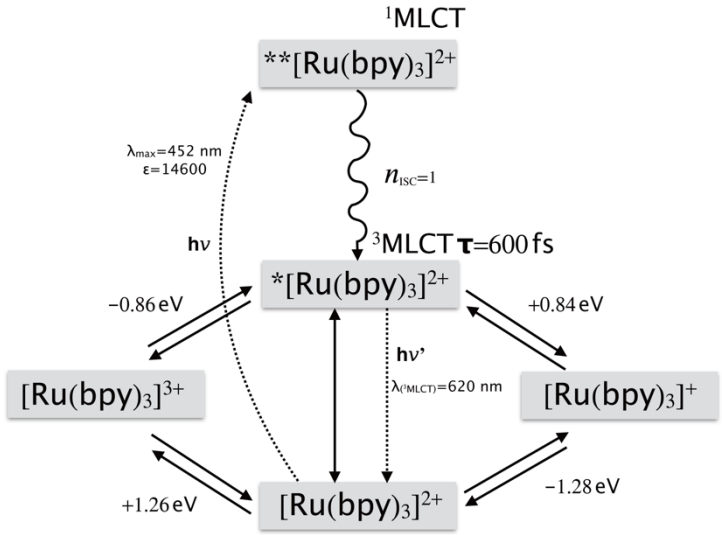

Figure 3.3. Molecular properties of $[Ru(bpy)_3]^{2+}$ relevant for energy and electron transfer processes. Reported potentials are in aqueous solution vs SCE.

The properties of the low-lying excited state are very important because they are closely connected to the photochemical reactions, as consequence of the Kasha's rule. The Ru(II)-polypiridyl complexes show very good physico-chemical properties that stimulate increasing interest in its biological behaviour.

The attractive features of the Ru complexes in biological environment are their rigid and well-defined spatial arrangement and highly potent and selective enzyme inhibitors[42-44] as well as the lower toxicity compared to platinum complexes and their higher cellular uptake, thanks to the specific transport of ruthenium inside cells by transferrin[45]. The application of ruthenium complexes as PSs in PDT is a promising approach, due to their tuneable photophysics and the aforementioned advantages for biological applications. The development of new photo-dynamic compounds (PDCs) based on Ru(II)-polypiridyl derivatives is focused, in particular, regarding the stability enhancement of the low-triplet excited state (i.e. increase τ_T).

3.2.1 Theoretical Exploration of Type I/Type II Dual Photoreactivity of Promising Ru(II) Dyads for PDT Approach (PAPER III)

New promising Ru(II)polypiridyl dyads[46] able to achieve dual type I/II photosensitization were focused on. The Ru polypiridyl complexes possess poly-thiophene chains with variable lengths and are able to access to a low-lying ^{3}IL excited state with longer lifetimes than traditional ^{3}MLCT states and to give non-covalent DNA

interaction[47]. These PSs, especially those containing three or more thiophene units, are remarkable DNA binders and photo-cleavers when exposed to light, while exhibit no interference with DNA structural integrity in the absence of light-trigger. The dual behavior was already observed for this class of compounds in the photo-inactivation of bacteria[48]. The in vitro effect of these compounds was found to be directly proportional to the poly-thiophene chain length. Among them, the complexes containing three thiophene units were also tested in vivo on mice, against colon carcinoma cells. In animals, the treatment with this compound and light irradiation at 525 nm, resulted in a complete tumor regression. These compounds are currently under optimization for clinical phase I trials[47].

The above-mentioned Ru(II)-polypiridyl dyads incorporating poly-thiophene chains with different lengths ($1 \leq n \leq 4$) were carefully performed by DFT and TD-DFT in order to explore the feasibility of Type I and Type II photoreactions.

3.3. BODIPY-DERIVATIVES

Due to the relative simple synthesis, high redox and thermodynamic stability and peculiar photophysical properties (large absorption extinction coefficients, sharp emissions and quantum fluorescence yields), the 4,4-difluoro-4-bora-3a,4a-diaza-s-indacene (BODIPY) and its aza (aza-BODIPY) derivatives have been proposed for a wide range of technological applications such as biological labelling, electroluminescent devices, tuneable laser dyes, solid-state solar concentrators, fluorescent switches, fluorophores in sensors, and in PDT.

The IUPAC numbering system for BODIPY dyes, are reported in Figure 3.4, the α- β- and meso- position are also shown.

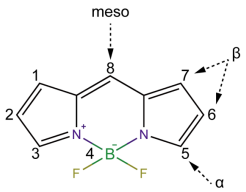

Figure 3.4. IUPAC labelling system for BODIPY dyes.

BODIPY without substituent groups has not been reported in the literature. This might be because the synthetic difficulties of this compound are related to the fact that none of the pyrrole-based carbons are blocked from electrophilic attack.

BODIPY dyes tend to be strong UV-absorbing molecules that emit relatively sharp fluorescence peaks with high quantum yields. Their photophysical properties are insensitive to the solvent polarity. Small modifications of their structures enable tuning of their fluorescence characteristics; for this reason they are widely used to label proteins and DNA. Furthermore, recently, they were also proposed as promising photosensitizers in PDT.

A number of illustrative examples, regarding the modulation of the photophysical properties of the BODIPY dyes by appropriate substitution, are given below. The photophysical properties of the dimethyl-substituted of BODIPY system (Figure 3.5) are characterized by minor differences in the reported UV-absorption maxima, fluorescence emission maxima, and quantum yields of these compounds.

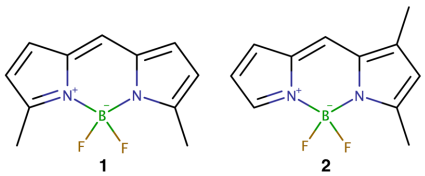

Figure 3.5. Dimethyl-substituted BODIPY.

Starting from the double substituted BODIPY, the increase of the methyl-substituents number symmetrically (Figure 3.6) results in a red-shifted absorption and emission maxima (compared **2** and **4** compounds).

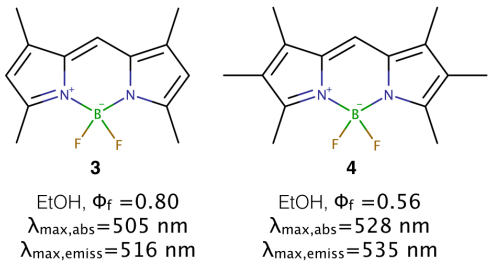

Figure 3.6. Symmetrically- tetra-, hexa- alkylated BODYPY systems.

Alkylation or arylation at the *meso* position has no special effect on the absorption and emission wavelengths (compare **1** with **6**, and **3** with **7**). However, the arylation of compound **1** in meso position leads to a significant decrease in the fluorescence quantum yield (**6** in Figure 3.7). Such differences are attributed to the

nature and conformational behavior of the 1,7-substituents. In addition, the introduction of ortho-substituents (**7**) on the phenyl ring increases the quantum yields, and similar explanations have been involved.

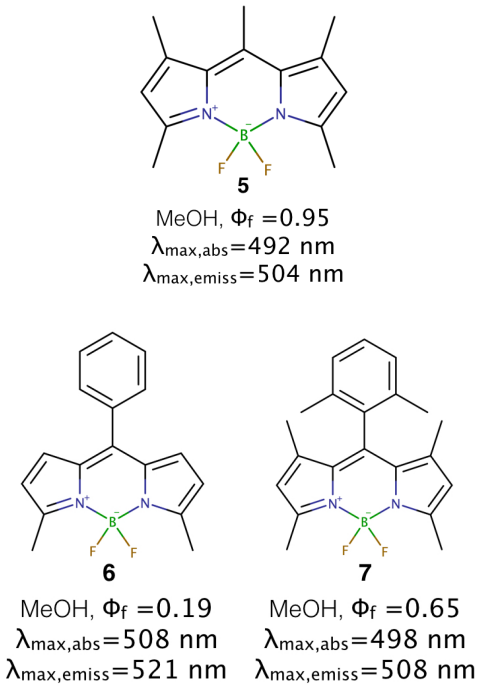

Figure 3.7. Alkylation or arylation at the *meso* position on the BODIPY system.

The introduction of heavy atoms substituent in the BODIPY core causes a significant red shift of both the UV-absorption and the emission maxima, and the quenching of the fluorescence quantum yield via the heavy atom effect (Figure 3.8).

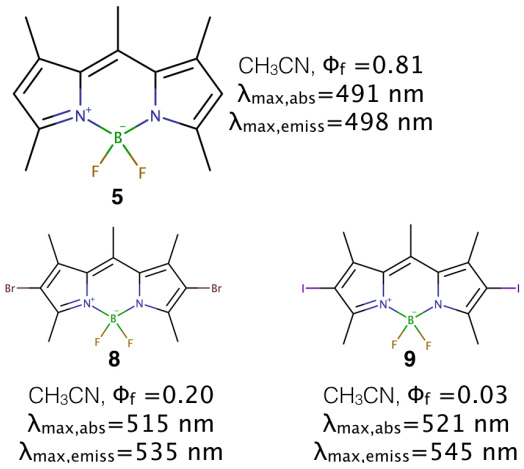

Figure 3.8. Halogenation of the 1,3,5,7,8-pentamethyl-substitued BODIPY.

The fluorescence of the BODIPY dyes can also be quenched by photoinduced electron transfer processes, as in the case of the meso-modified BODIPY (Figure 3.9) dyes[49]. It is worth to note that the substituent can act as electron donors or acceptors (Figure 3.9*)* depending on their oxidation potentials, relative to the excited-state of the BODIPY core.

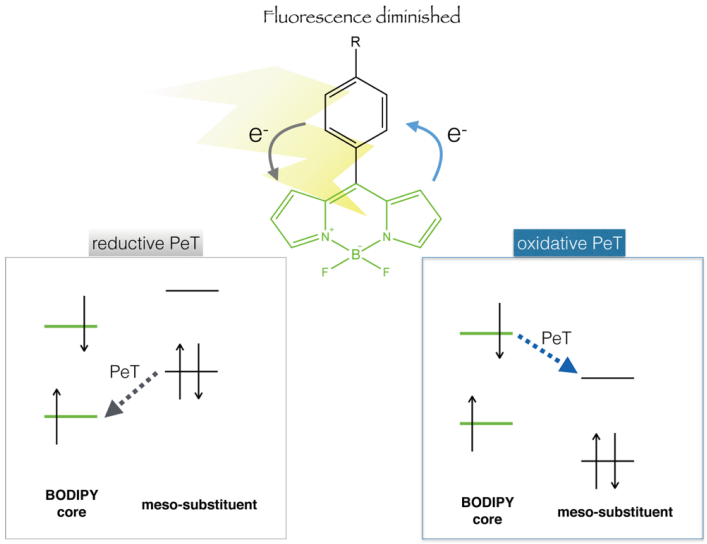

Figure 3.9. The meso-substituent provides electrons to the excited-state *'reductive PeT'*, or a low lying LUMO to accept electrons from the excited-state '*oxidative PeT*', both cases involve a decrease of the fluorescence.

The feasibility of electron transfer can be judged from the change in free energy (ΔG_{PeT}), as described by Rehm-Weller equation (section 2.4.1):

$$\Delta G_{PeT} = E^0 (D^+/D) - E^0 (A/A^-) - wp - \Delta G_{00},$$

where $E^0 (D^+/D)$ is the ground-state oxidation potential of the donor, $E^0 (A/A^-)$ is the ground-state reduction potential of the acceptor, ΔG_{00} is the free energy corresponding to the equilibrium energy E_{00}, and w_p is an electrostatic interaction term.

Another interesting class of BODIPY is the so-called aza-BODIPY[50], in which a nitrogen atom substitutes the meso-carbon atom (Figure 3.10).

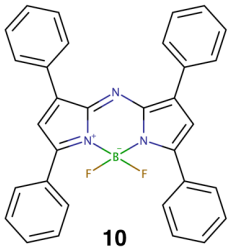

10

$CHCl_3$, Φ_f =0.34

$\lambda_{max,abs}$=650 nm

$\lambda_{max,emiss}$=672 nm

Figure 3.10. Structure of tetraphenyl azapyrromethene BF2 chelates, the first synthesized aza-BODIPY dye.

The importance of these compounds has been highlighted in 2002, when O'Shea and co-workers[51,52] proposed the aza-BODIPY (BF2 chelated of 3,5-diaryl-1H-pyrrol-2-yl-3,5-diarylpyrrol-2-ylidene amines 'tetraarylazadipyrromethenes') derivatives as promising photosensitizers for PDT. They reported the synthesis, the photophysical properties, a test for singlet oxygen production, the cellular localization, and in vitro light-induced cytotoxicity assays for this new class of potential PDT agents. The triplet quantum yield of the aza-BODIPY derivatives increases upon the attachment of a heavy atom in the core of the photosensitizer. This substitution ensures the enhancing of the spin-orbit coupling (SOC) which results in a fast ISC.

3.3.1 Halogen Atom Effect on the Photophysical Properties in Substituted Aza-BODIPY Derivatives (PAPER IV)

Recently, a series of aza-BODIPYs differently substituted with bromine or iodine atoms (Figure 3.11), with high stability under irradiation condition, have been found as a promising class of red-light absorbing photosensitizers[53].

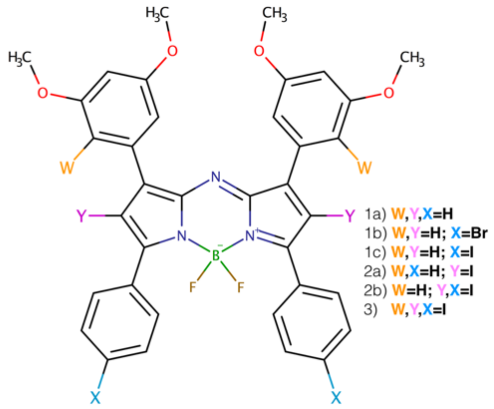

Figure 3.11. Schematic representation of the investigated compounds.

In particular, in paper IV, the following systems have been studied:

-**1a**: tetraaryl-BF_2-aza-dipyrromethene

-**1b**,**1c** and **2b**: the halogen atoms (Br and, I) are substituted in the peripheral position.

- **2a**: two iodine are inserted in the two pyrrole rings of aza-BODIPY core.

- **3**: six iodine atoms are contained at both peripheral and aza-BODIPY core.

DFT and TD-DFT have been employed to investigate the substituent effects of halogen atom (Br, I) in different amounts and positions in aza-BODIPY skeleton on the photophysical properties of these aza-BODIPY derivatives (Figure 3.11).

The heavy atom effect on excitation energies, singlet and triplet energy gaps and spin-orbit matrix elements have been studied together with the most probable ISC pathways for the activation of the lowest triplet states. On the basis of the results, the available experimental data were rationalized and the potential therapeutic usage of these compounds as photosensitizers in PDT were discussed.

3.3.2 Theoretical Insights on the Switch on/off Photosensitization in Chemicontrolled Photodynamic Therapy (MANUSCRIPT)

Recently, a design of a dormant singlet oxygen photosensitizer, that is activated upon its reaction with reactive oxygen species (ROS), including singlet oxygen itself, in what constitutes an autocatalytic process, was reported in the literature[54]. The main advantage of these PSs is the high selectivity for the cancer cells, which are characterized by high concentration of ROS than normal healthy cells. This kind of PSs are composed combining the photosensitization of BODIPY dye with the antioxidant ability of chromanol ring of α-tocopherol. The chemically controlled photosensitization is due to the intramolecular photo-electron transfer that causes the inactivation of PS until it reaches the cell in which the singlet oxygen photosensitization is triggered thanks to the chromanol oxidation.

DFT and its time-dependent extension (TDDFT) have been used to explore the photophysical properties of a series of recently synthetized BODIPY-based photosensitizers in order to gain more insight into the ability of a Br-substituted BODIPY derivative as ROS-activatable photosensitizer. The reaction mechanism of the oxidation process by $^1O_2$ and cumyloxyl radical has been also elucidated.

From our results, all the investigated BODIPY-based dyes can be considered potential tipe II 'photodynamic PSs' and the two segments photosensitizer-trap molecule Br-substituted could be also used in chemicontrolled photodynamic therapy as it is activated by ROS through oxidation of hydroxyl group on chromanol ring.

➢ BIBLIOGRAPHY

ANALOGUES OF NITROGENOUS BASES

1. Dahm, R. Discovering DNA: Friedrich Miescher and the Early Years of Nucleic Acid Research. *Hum. Genet.* **2008**, *122*, 565–81.
2. Altmann, R. Ueber Nucleinsäuren. *Arch. f. Anatomie u. Physiol.* **1889**, 524–536.
3. Kossel, A. Beziehungen der Chemie zur Physiologie. (In: Meyer Ev (ed) Die Kultur der Gegenwart, ihre Entwicklung und ihre Ziele: Chemie. Teubner, Leipzig, **1913**, pp 376–412).
4. Avery, O.; Macleod, C.; Mccarty, M. Studies on the chemical nature of the substance inducing transformation of pneumococcal types induction of transformation by a desoxyribonucleic acid fraction isolated from pneumococcus type III. *J Exp Medicine.* **1944**, *79*, 137–158.
5. Hershey, A. D.; Chase, M. Independent Functions of Viral Protein and Nucleic Acid in Growth of Bacteriophage. *J. Gen. Physiol.* **1952**, *36*, 39–56.
6. Watson, J.D.; Crick, F.H.C. Molecular structure of nucleic acids; a structure for deoxyribose nucleic acid. *Nature* **1953**, 171, 737-738.
7. Watson, J.D.; Crick, F.H.C. Genetical implications of the structure of deoxyribonucleic acid. *Nature* **1953**, 171, 964-967.
8. Downes, A.; Blunt, T. Researches on the Effect of Light upon Bacteria and Other Organisms. *P R Soc London* **1877**, *26*, 488–500.
9. Ward, M. The Action of Light on Bacteria. III. *P R Soc London* **1893**, *54*, 472–475.
10. Findlay, G.M. Ultraviolet light and skin cancer. Lancet **1928**, 2, 1070-1073.
11. Gates, F. A study of the bactericidal action of ultra violet light III. The absorption of ultra violet light by bacteria. *J Gen Physiology* **1930**, *14*, 31–42.
12. Henshaw, P. S., The action of the x-rays on nucleated and non-nucleated egg fragments. *Am. J. Cancer* **1938**, 33, 258.
13. Swanson. Differential sensitivity of prophase pollen tube chromosomes to x-rays and ultraviolet radiation. *J Gen Physiology* **1943**, *26*, 485–494.
14. Setlow, R.; Setlow, J. Evidence that ultraviolet-induced thymine dimers in dna cause biological damage. *Proc National Acad Sci* **1962**, *48*, 1250–1257.
15. Wacker, A. Molecular mechanisms of radiation effects. *Prog. Nucl. Acids Res. Molec. Biol.* **1963**, 1, 369-399.
16. Morrison, H. Photochemistry and the Nucleic Acid; (Wiley-Interscience: New York, **1990)**.
17. Davis, R. J. H. Ultraviolet Radiation Damage in DNA. *Biochem. Soc. Trans.* **1995**, 23, 407–418.
18. Pfeifer, G. P. Formation and Processing of UV Photoproducts: Effects of DNA Sequence and Chromatin Environment. *Photochem. Photobiol.* **1997**, 65, 270–283.
19. Cadet, J.; Sage, E.; Douki, T. Ultraviolet Radiation-Mediated Damage to Cellular DNA. *Mutat. Res.* **2005**, 571, 3–17.
20. Mouret, S.; Baudouin, C.; Charveron, M.; Favier, A.; Cadet, J.; Douki, T. Cyclobutane Pyrimidine Dimers Are Predominant DNA Lesions in Whole Human Skin Exposed to UVA Radiation. *Proc National Acad Sci* **2006**,*103*, 13765–13770.
21. Clark, L.B., Peschel, G.G., Tinoco, I. Vapor spectra and heats of vaporization of some purine and pyrmidine bases. *J. Phys. Chem.* **1965**, 69, 3615.
22. Middleton, C.T., de La Harpe, K., Su, C., Law, Y.K., Crespo-Hernández, C.E., Kohler, B. DNA Excited-State Dynamics: From Single Bases to the Double Helix. *Annu. Rev. Phys. Chem.* **2009**, 60, 217.
23. Daniels, M.; Hauswirth, W. Fluorescence of the purine and pyrimidine bases of the nucleic acids in neutral aqueous solution at 300°K. *Science.* **1971**, 171, 675.

24. Shugar, D.; Fox, J.J. Spectrophotometric studies on nucleic acid derivatives and related compounds as a function of pH. I. Pyrimidines. Biochem. *Biochim. Biophys. Acta.* **1952**, 9, 199.
25. Dixon, J.M.; Taniguchi, M.; Lindsey, J.S. PhotochemCAD 2: a refined program with accompanying spectral databases for photochemical calculations. *Photochem. Photobiol.* **2005**, 81, 212.
26. Callis, P.R. Electronic states and luminescence of nucleic acid systems. *Annu. Rev. Phys. Chem.* **1983**, 34, 329.
27. Ellison, R.R. et al. Clinical evaluation of a new antimetabolite, 6-mercaptopurine, in the treatment of acute leukemia and allied diseases. *Blood.* **1953**, 8, 965–999.
28. Hitchings, G.H.; Elion, G.B. The chemistry and biochemistry of purine analogs. *Ann N Y Acad Sci.* **1954**, 60, 195–199.
29. O'Donovan, P.; Perrett, C.M.; Zhang, X., Montaner, B.; Xu, Y.Z.; Harwood, C.A.; McGregor, J.M.; Walker, S.L.; Hanaoka, F.; Karran; P. Azathioprine and UVA light generate mutagenic oxidative DNA damage. Science. **2005**, 309, 1871.
30. Karran, P.; Attard, N. Thiopurines in current medical practice: molecular mechanisms and contributions to therapy-related cancer. *Nat. Rev. Cancer.* **2008**, 8, 24.
31. Reelfs, O.; Karran, P.; Young, A.R. 4-Thiothymidine sensitization of DNA to UVA offers potential for a novel photochemotherapy. *Photochem Photobiol Sci.* **2012**, 11, 148.
32. Pridgeon; Heer; Taylor; Newell; O'Toole; Robinson; Xu, Y.-Z.; Karran; Boddy Thiothymidine Combined with UVA as a Potential Novel Therapy for Bladder Cancer. *Brit J Cancer* **2011**, *104*, 1869–1876.
33. Massey, A.; Xu, Y. Z.; Karran, P. Photoactivation of DNA Thiobases as a Potential Novel Therapeutic Option. *Curr. Biol.* **2001**, *11*, 1142–6.
34. Marvin Pollum; Steffen Jockusch; Carlos E Crespo-Hernández; 2,4-Dithiothymine as a Potent UVA Chemotherapeutic Agent. *J. Am. Chem. Soc.* **2014**, 136, 17930−17933.

Ru(II)POLYPYRIDIL COMPLEXES

35. Rillema, D.; Jones, D. S. Structure of tris(2,2'-bipyridyl)ruthenium(II) hexafluorophosphate, $[Ru(bipy)_3][PF_6]_2$; X-ray crystallographic determination *Chem. Commun.* **1979**, *412*, 849-851.
36. Balzani, V.; Juris, A.; Venturi, M.; Campagna, S.; Serroni, S.; Balzani, V.; Juris, A.; Venturi, M.; Campagna, S.; Serroni, S. Luminescent and Redox-Active Polynuclear Transition Metal Complexes. *Chemical Reviews.* **1995**.
37. Damrauer; Cerullo; Yeh; Boussie; Shank. Femtosecond Dynamics of Excited-State Evolution. (JK McCusker, Science. New York. **1997**, PMID: 8974388).
38. Yeh, A.T.; Shank, C.V. Ultrafast Electron Localization Dynamics Following Photo-Induced Charge Transfer. (JK McCusker Science. New York. **2000**).
39. Balzani, V.; Campagna, S.; Denti, G.; Juris, A.; Serroni, S.; Venturi, M. Designing Dendrimers Based on Transition-Metal Complexes. Light-Harvesting Properties and Predetermined Redox Patterns. *Accounts Chem. Res.* **1998**, *31*, 26–34.
40. Balzani, V.; Juris, A.; Venturi, M.; Campagna, S.; Serroni, S.; Balzani, V.; Juris, A.; Venturi, M.; Campagna, S.; Serroni, S. Luminescent and Redox-Active Polynuclear Transition Metal Complexes. *Chemical Reviews* **1995**.
41. Durham, B.; Caspar, J.; Nagle, J.; Meyer, T. Photochemistry of tris(2,2'-bipyridine)ruthenium(2+) Ion. *J Am Chem Soc* **1982**, *104*, 4803–4810.
42. Kilah, N. L.; Meggers, E. Sixty years young: the diverse biological activities of metal polypyridyl complexes pioneered by Francis P. Dwyer. *Aust. J. Chem* **2012,** *65*, 1325-1332.
43. Maksimoska, J.; Feng, L.; Harms, K.; Yi, C.; Kissil, J.; Marmorstein, R.; Meggers, E. Targeting Large Kinase Active Site with Rigid, Bulky Octahedral Ruthenium Complexes. *J Am Chem Soc* **2008**, *130*, 15764–5.
44. Dörr, M.; Meggers, E. Metal Complexes as Structural Templates for Targeting Proteins.*Curr Opin Chem Biol* **2014**, *19*, 76–81.

45. Kratz, F.; Hartmann, M.; Keppler B.; Messori, L. The binding properties of two antitumor ruthenium(III) complexes to apotransferrin. *J. Biol. Chem*., **1994**, 269, 2581–2588.
46. McFarland, S. A. Metal-based Thiophene Photodynamic Compounds and Their Use. (US provisional **patent 61624391** led April 15, 2012, PCT/US13/36595 led April 15, 2013).
47. Shi, G.; Monro, S.; Hennigar, R.; Colpitts, J.; Fong, J.; Kasimova, K.; Yin, H.; DeCoste, R.; Spencer, C.; Chamberlain, L.; Mandel, A.; Lilge, L.; McFarland, S. A. Ru(II) Dyads Derived from A-Oligothiophenes: A New Class of Potent and Versatile Photosensitizers for PDT, *Coord. Chem. Rev.* **2014**, *282*, 127–138.
48. Arenas, Y.; Monro, S.; Shi, G.; Mandel, A.; McFarland, S.; Lilge, L. Photodynamic Inactivation of Staphylococcus Aureus and Methicillin-Resistant Staphylococcus Aureus with Ru(II)-Based Type I/Type II Photosensitizers. *Photodiagn. Photodyn. Ther.*, **2013**, *10*, 615–625.

BODIPY DERIVATIVES

49. Gabe, Y.; Urano, Y.; Kikuchi, K.; Kojima, H.; Nagano, T. Highly Sensitive Fluorescence Probes for Nitric Oxide Based on Boron Dipyrromethene Chromophore Rational Design of Potentially Useful Bioimaging Fluorescence Probe. *J. Am. Chem. Soc.* **2004**, *126*, 3357–3367.
50. Zhao, W.; Carreira, E. Conformationally Restricted Aza-Bodipy: A Highly Fluorescent, Stable, Near-Infrared-Absorbing Dye. *Angew Chem-ger Edit* **2005**,*117*, 1705–1707.
51. Killoran, J.; Allen, L.; Gallagher, J.; Gallagher, W.; O'Shea, D. Synthesis of BF 2 Chelates of Tetraarylazadipyrromethenes and Evidence for Their Photodynamic Therapeutic Behaviour. *Chem. Commun.* **2002**, *0*, 1862–1863.
52. Gorman, A.; Killoran, J.; O'Shea, C.; Kenna, T.; Gallagher, W.; O'Shea, D. In Vitro Demonstration of the Heavy-Atom Effect for Photodynamic Therapy. *J. Am. Chem. Soc.* **2004**, *126*, 10619–10631.
53. Adarsh, N.; Shanmugasundaram, M.; Avirah, R.; Ramaiah, D. Aza-BODIPY Derivatives: Enhanced Quantum Yields of Triplet Excited States and the Generation of Singlet Oxygen and Their Role as Facile Sustainable Photooxygenation Catalysts. *Chem - European J.* **2012**, *18*, 12655–12662.
54. Durantini, A.; Greene, L.; Lincoln, R.; Martínez, S.; Cosa, G. Reactive Oxygen Species Mediated Activation of a Dormant Singlet Oxygen Photosensitizer: From Autocatalytic Singlet Oxygen Amplification to Chemicontrolled Photodynamic Therapy.*J Am Chem Soc* **2016**, *138*, 1215–1225.

➢ Paper I

Photophysical Properties Prediction of Selenium- and Tellurium-Substituted Thymidine as Potential UVA Chemotherapeutic Agents.

Jenny Pirillo, Bruna de Simone, Nino Russo.

*Theoretical Chemistry Accounts. (**2016**)*

Theor Chem Acc (2016) 135:8
DOI 10.1007/s00214-015-1744-1

REGULAR ARTICLE

Photophysical properties prediction of selenium- and tellurium-substituted thymidine as potential UVA chemotherapeutic agents

Jenny Pirillo[1] · Bruna Clara De Simone[1] · Nino Russo[1]

Received: 31 August 2015 / Accepted: 30 September 2015 / Published online: 21 December 2015

Abstract Density functional theory and time-dependent density functional theory calculation for a series of photophysical properties (absorption spectra, singlet and triplet excitation energies and spin–orbit matrix elements) have been performed on the sulfur-, selenium- and tellurium-substituted thymine. The heavy atoms have been substituted in 2 or 4 and in both 2,4 position of the thymine ring. Different pathways for the population of the lowest triplet state have been considered. We find that all the considered systems are potential UVA chemotherapeutic agents since the lowest triplet states lie above the energy required for the production of the highly cytotoxic $^1\Delta_g$ excited oxygen molecule and due to the possible and efficient intersystem crossings ensured by high spin–orbit coupling values.

Keywords TDDFT · Photodynamic therapy · Excited states · Substituted thymidines

1 Introduction

Photodynamic therapy (PDT) is a promising and less invasive method for treating a variety of diseases by using visible light irradiation in conjunction with a photosensitizer (PS) that must be non-toxic in the dark [1]. One of the advantages of PDT is its capability to selectively act on the damaged tissue preserving the surrounding normal tissues. Starting from the preparation of Photofrin® (a mixture of dimers and oligomers of hematoporphyrin in which porphyrin units are linked by ether, ester and C–C bonds) in 1983 [2], a series of first- and second-generation PSs have been synthesized or extracted from plants [3–6], tested in vitro and in vivo.

PDT PSs must meet several criteria, and the more important properties are: (1) chemical stability; (2) water solubility; (3) high quantum yield of $^1O_2$ ($^1\Delta_g$) generation; (4) no cytotoxicity in the dark; (5) selectivity and rapid accumulation in target tissues; (6) rapid clearance from patients; (7) a high molar absorption coefficient (ε) in the long wavelength (600–800 nm) that can penetrate deeper tissues.

Although a large number of potential candidates are proposed, very few have shown ideal properties and have been approved for their clinical use (see Ref. [6] and reference therein). For these reasons, recent studies have focused on the development and efficacy of new PSs.

The two most important physical aspects of PDT can be summarized as the processes of light absorption and the energy transfer. The absorption of light in the form of photons induces a transition from the PS ground state S_0 to the excited one S_n with a short lived and loses its energy by emitting fluorescent light or by internal conversion (IC) into heat. Alternatively, it may also undergo a process known as intersystem crossing (ISC) whereby the spin of the excited electron inverts to form a relatively long-lived excited triplet state T_1 [7, 8]. This PS excited triplet state can transfer its energy directly to molecular oxygen that is, consequently excited from the triplet ground state ($^3\Sigma_g$) to the singlet excited state ($^1\Delta_g$), highly reactive and cytotoxic. Alternatively, the excited triplet state can react with a substrate in the environment producing reactive anion and cation radical species that, in turn, may further react with oxygen to produce reactive oxygen species (ROS) that react with the

Published as part of the special collection of articles “Health and Energy from the Sun”.

✉ Nino Russo
nrusso@unical.it

[1] Dipartimento di Chimica e Tecnologie Chimiche, Università della Calabria, Via P. Bucci, Cubo 14 c, 87036 Rende, Italy

tissue. The production of excited singlet oxygen is preferred in PDT and is possible only if the T_1 state of the PS has an energy higher of 0.98 eV necessary to excite the oxygen molecule [9].

Due to their photophysical and photochemical properties and to their possible use in PDT, the thio-substituted nucleobases have been the subject of many experimental and theoretical investigations [10–16]. Special emphasis has been reserved to thymidine since the substitution of oxygen in position 4 or in both 2 and 4 strongly enhances the production of the cytotoxic singlet excited oxygen [10–13]. Although these systems show absorption band that falls down to the so-called therapeutic window (about 600–800 nm) and, consequently, possess a limited light penetration power, they remain good candidates for PDT antimicrobial and antivirus disinfection and UVA chemotherapeutic agents. The available experimental characterization for 2-thiothymine [10], 4-thiothymidine [11, 12] and 2,4-dithiothymidine [13] and the recent accurate theoretical studies on 4-thiothymidine [14] and 2-thiothymine [15] have stimulated our attention to consider the selenium (2-SeT, 4-SeT, 2,4-DiSeT) and tellurium (2-TeT, 4-TeT, 2,4-DiTeT) thymidines also in view of the fact that Se- and Te-containing systems have been previously indicated as potential PSs in PDT since the presence of these heavy atoms redshifts the absorption band and enhances the intersystem crossing [17–19]. In order to assets our computational protocol, we have performed the computations for the thiothymidine derivatives (2-ThioT, 4-ThioT, 2,4-DiThioT) for which a comparison with experimental data and previous theoretical results is possible.

2 Computational details

Our investigation has been performed by using DFT and TDDFT levels of theory previously and extensively tested as reliable tools for the determination of excited-state properties [20–23]. All computations have been performed employing the Gaussian 09 code [24]. Molecular geometries were optimized using the meta-GGA functional M06 [25] coupled with 6-31G* basis set, whereas for the excited-state properties M06/6-31+G* time TDDFT approach has been adopted. This protocol was previously used in a series of systems and properties including the simulation of the photophysical properties of different dye molecules [26–28]. The impact of solvation effects (water) on the considered properties has been estimated by means of the integral equation formalism polarizable continuum model (IEFPCM), which corresponds to a linear response in non-equilibrium solvation [29]. Spin–orbit matrix elements have been computed by using the atomic-mean field approximation [30] as implemented in DALTON code [31], since previous studies have demonstrated as Breit–Pauli method [32] and atomic-mean field approximation provide very similar values [26], the latter of which requires a lower computational cost. Because of the presence of only few hybrid functionals available in DALTON to perform these calculations, B3LYP [33, 34] has been selected and used on the previously M06-optimized geometries, in conjunction with the cc-pVDZ basis set for all the atoms.

3 Results and discussion

The computed electronic transitions are reported in Fig. 1. As a general feature, we observe that the substitution of oxygen atom with sulfur, selenium and tellurium atoms shifts the absorption spectrum to the red. This shift is more pronounced when the substitution concerns the position 4 and increases with the atomic size of the substituent (0.73, 1.02, 1.16 and 1.42 Å for oxygen, sulfur, selenium and tellurium, respectively). This behavior is due to the weakness of the C=X strength in going from C=O to C=S, C=Se and C=Te bonds. Furthermore, the increases of the metallic character and the electron delocalizability along the chalcogens family contribute to the increase in the observed redshift spectral lines. In the case of the 2,4 double substitution, the observed redshift does not correspond to a simple linear combination of the shifts observed in the corresponding 2 and 4 substitution, but is more similar to that occurring when the chalcogens are present in position 4. In all the 2 and 4 substitutions, the transitions are mainly HOMO-1 → LUMO in nature with contribution of HOMO → LUMO ones, while for 2,4 species the contamination coming from other excitations (e.g., HOMO-2 → L, HOMO-3 → L, HOMO → LUMO + 1) appears. From the molecular orbital picture reported in Fig. 2, it is clear that in all the considered systems the S_1 transition and S_2 transition have $n\pi^*$ and $\pi\pi^*$ nature, respectively. The computed absorption maxima well agree with the experimental results available for thymidine (264 nm) [16], 2-thiothymidine (278 nm) [10, 13], 4-thiothymidine (335 nm) [13, 35], 2,4-dithiothymidine (278 and 360 nm) [13] and 4-selenothymidine 369 nm) [36].

As previously mentioned, in a series of recent papers the thioderivatives of thymine and thymidine have been the subject of accurate experimental and theoretical analysis in order to establish their possible use as PS in PDT [10–16]. At this purpose, the excited singlet and triplet states, the spin–orbit matrix elements and the singlet oxygen production upon excitation have been computed or measured. Computational studies have been performed by employing DFT as well as CASCF and CASPT2 levels of theory [14, 15]. In the work of Cui and Fang [15] on the 2-thiothymine, it is shown as DFT, especially when M06-like

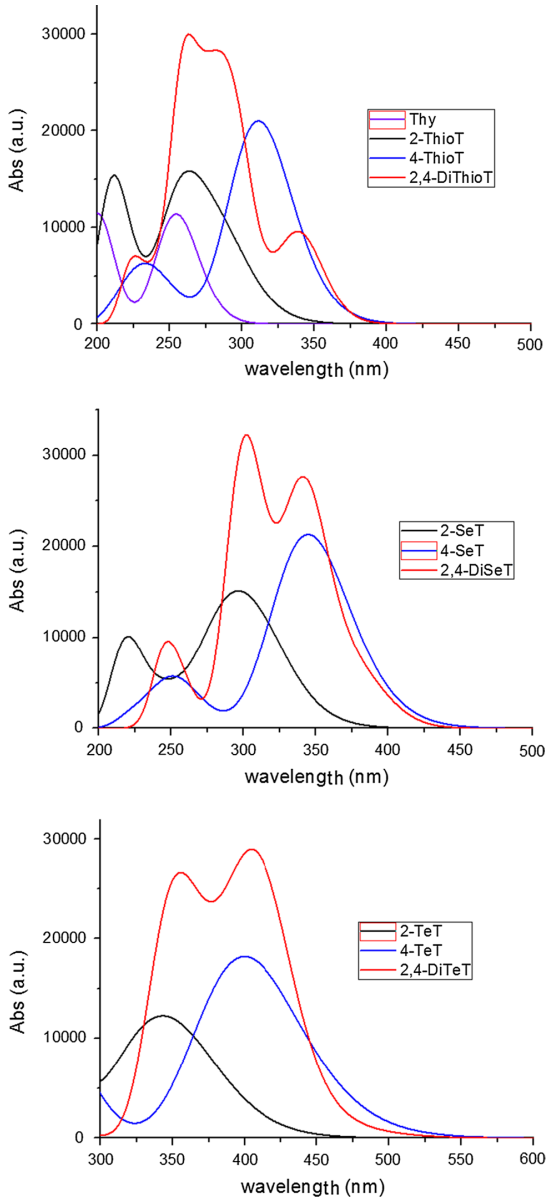

Fig. 1 M06-simulated electronic spectra in water solvent for the studied compounds

exchange–correlation functional is employed, gives singlet and excited states energetic close to the corresponding CASPT2 values. On the other hand, in a series of previous paper our group demonstrated the reliability of DFT in the computations of the spin–orbit matrix elements in a series of PSs active in PDT [23, 37, 38]. The computed main vertical singlet and triplet electronic states and the spin–orbit

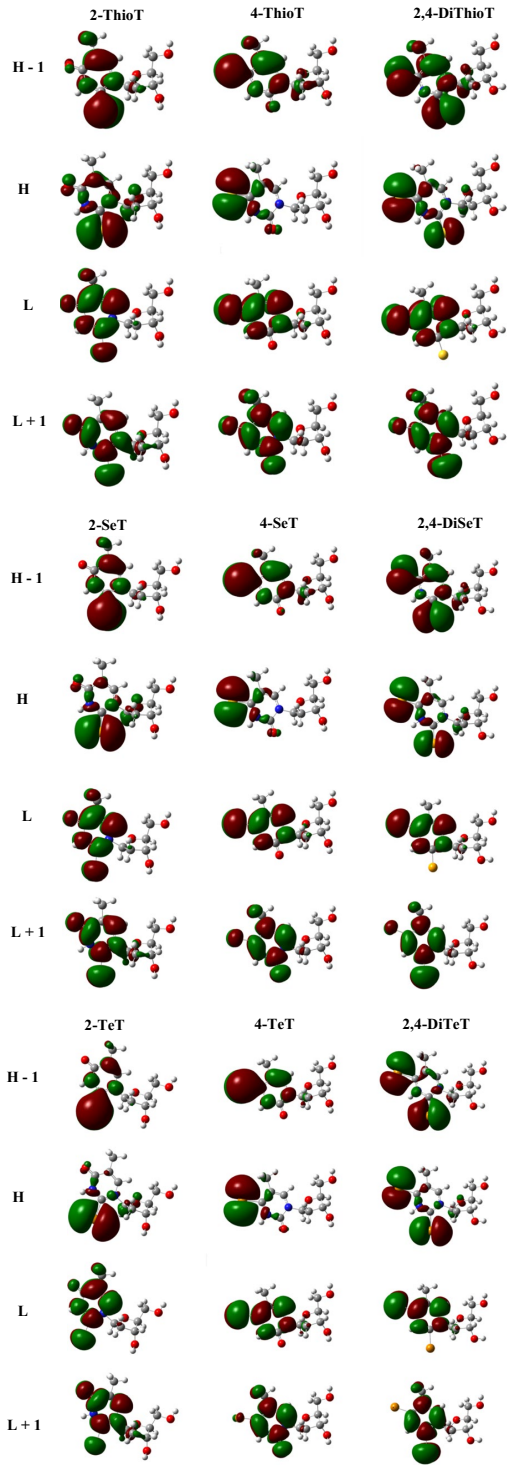

Fig. 2 Orbital composition for the ground state of the studied compounds

matrix elements for all the considered systems are reported in Table 1. For thymidine, the spectroscopically bright state is the S_1 ($n\pi^*$), while for all the considered derivatives is the S_2 with a $\pi\pi^*$ character as previously demonstrated in the experimental and theoretical works on the thiothymine and thiothymidines [10–16]. From Table 1, it emerges that all the investigated molecules have a first excited triplet state (T_1) that is higher than the energy required activating the $^1\Delta_g$ excited state of oxygen molecules that is the key cytotoxic agent in PDT. We underline as our computed vertical T_1 value for 2-ThioT is in good agreement with the available experimental counterpart (4.30 vs. 4.14 eV) [15]. Good agreement is also found for the vertical values for S_1, S_2, T_1 and T_2 states computed at CASPT2 level of theory [15]. The activation of singlet excited O_2 is possible if the energy is transferred by the singlet excited state to the triplet one via an intersystem spin crossing that will depend from the values of the spin–orbit matrix elements ($|\hat{H}_{SO}|$) involved in a given transition. As previously suggested in the theoretical study on 4-thiothymidine [11, 14] and on 2-thiothymine [10, 15] and in the experimental investigation on 2-thymine [10], the following most probable pathways for the activation of the lowest triplet state (T_1) are possible: (1) pathI: $S_2 \rightarrow S_1 \rightarrow T_1$; (2) pathII: $S_2 \rightarrow T_2 \rightarrow T_1$. In the first one, the S_2 undergoes a fast IC to S_1 via minimum energy conical insertion S_2S_1. This transition is allowed since the small energy difference between the two singlet excited states. Then the system decays to the T_1 state throughout a ISC process. In the second pathway, the first ISC between the S_2 and T_2 states is followed by an IC from T_2 to T_1. In order to predict the more efficient ISC processes, it is mandatory to compute the spin–orbit matrix elements. As a general rule, the presence of a heavy atom increases the ISC probability via the so-called heavy atom effect. From Table 1, it is evident as the increase in the atom size contributes to significantly increase the $|\hat{H}_{SO}|$. According to the El-Sayed rules [39, 40], the rate of the ISC sensibly increases if the radiationless transition involves a change of orbital type. Therefore, the magnitude of the $|\hat{H}_{SO}|$ between the initial $\Psi(S_n)$ and final $\Psi(T_n)$ wave functions not only depends on the effective nuclear mass of heavy atoms eventually present in the molecular system, but also depends on the nature of the orbitals involved in the coupling. Due to the $\pi\pi^*$ and $n\pi^*$ nature of S_2 and T_1 and S_1 and T_2 states, respectively, we expect high $|\hat{H}_{SO}|$ values for the S_1T_1 and S_2T_2 couplings. Table 1 shows as all the spin–orbit coupling matrix elements increase in going from thymidine (Thy) to the substituted species with high effective nuclear mass. Furthermore, it is evident that the substitution on the position 4 is preferred over the position 2. As expected from the El-Sayed rule and from the lower energetics the $S_1T_1|\hat{H}_{SO}|$ values result to be very high than the corresponding S_2T_2 ones. In any case, from the computed properties, both the investigated paths show efficient intersystem crossing.

We have explored also the possibility that, after the efficient S_2S_1 IC, S_1 can transfer the energy to the T_2 state that in turn can generate singlet oxygen throughout a fast T_2T_1 IC. The $|\hat{H}_{SO}|$ values for this ISC (see Table 1) suggest that, contrary to the previously discussed ISC, the substitution of the heavy atoms in position 2 is more efficient than that in 4. This alternative route is less probable since the smallest spin–orbit coupling obtained. A deep examination of the considered pathway for the formation of the lowest triple state (T_1) shows that only the path I follows the Kasha's rule [41] that indicate as, in a given spin manifold, the transition $S_n \rightarrow S_1(n > 1)$ should be very fast and triplet-state population (as well as other photophysical properties) should start from the lowest singlet exited state (S_1).

4 Conclusions

The possibility that the sulfur, selenium and tellurium derivatives of thymidine can be proposed as PSs in PDT have been explored theoretically employing density functional theory. The computed singlets and triplets excitations

Table 1 Vertical singlet and triplet energies computed in water at M06/6-31+G* level of theory and spin–orbit matrix elements (cm^{-1}) calculated at the B3LYP/6-31G(d)//M06

	T_1 (eV)	T_2 (eV)	S_1 (eV)	S_2 (eV)	$\lvert\langle\Psi_{S_1}\lvert\hat{H}_{so}\rvert\Psi_{T_1}\rangle\rvert$	$\lvert\langle\Psi_{S_1}\lvert\hat{H}_{so}\rvert\Psi_{T_2}\rangle\rvert$	$\lvert\langle\Psi_{S_2}\lvert\hat{H}_{so}\rvert\Psi_{T_2}\rangle\rvert$
Thy	3.32	4.78	4.87	5.04	31.40	1.13	11.08
2-ThioT	3.18	3.70	3.81	4.30	133.91	25.86	3.53
4-ThioT	2.68	2.94	3.08	3.98	176.02	2.91	64.73
2,4-DiThioT	2.66	2.89	3.03	3.65	172.11	11.62	19.09
2-SeT	2.91	3.28	3.43	3.97	744.56	127.00	22.49
4-SeT	2.20	2.54	2.75	3.60	891.49	17.31	303.67
2,4-DiSeT	2.13	2.47	2.68	3.26	877.92	67.95	74.41
2-TeT	2.67	2.82	2.92	3.45	4716.5	283.13	438.37
4-TeT	1.99	2.13	2.25	3.10	5668.7	35.87	521.43
2,4-DiTeT	1.88	2.01	2.15	2.62	1256.3	159.11	336.73

and the spin–orbit coupling matrix elements and the consideration of different pathways for the production of cytotoxic singlet molecular oxygen allow us to outline the following conclusions:

- absorption energies are short enough to penetrate into the tissue. Consequently, these systems cannot be proposed in the therapy of a series of tumors, but should be used in killing microbes and virus as well in other diseases in which a deeper penetration into the tissue is not requested;
- the lowest triplet excited state (T_1) lies up to the energy requested for the $^1\Delta_g$ singlet oxygen production in all the considered thymidine substituted;
- the spin–orbit coupling matrix elements increase with the atomic size of the substituent and are large enough to ensure efficient intersystem crossing;
- the substitution in position 4 is more efficient that that in position 2 of the thymine ring;

Although more detailed information can be obtained employing excited-state simulations, the obtained results clearly emerge that these systems can be considered potential UVA chemotherapeutic agents.

Acknowledgments This work has been financially supported by Universita della Calabria and FP7-PEOPLE-2011-IRSES, Project No. 295172.

References

1. Ackroyd R, Kelty C, Brown N, Reed M (2001) Photochem Photobiol 74:656
2. Dougherty TJ (1983) Photochem Photobiol 38:377
3. Dennis EJ, Dolmans GJ, Fukumura D, Jain RK (2003) Nat Rev Cancer 3:381
4. Robertson CA, Evans DH, Abrahamse H (2009) J Photochem Photobiol B Biol 96:1
5. Juzeniene A, Peng Q, Moan J (2007) Photochem Photobiol Sci 6:1234
6. Yanoa S, Hirohara S, Obata M, Hagiya Y, Ogura S, Ikeda A, Kataoka H, Tanaka M, Joh T (2011) J Photochem Photobiol C 12:46
7. Castano AP, Demidova TN, Hamblin MR (2004) Photodiagn Photodyn Ther 1:279
8. Szaciłowski K, Macyk W, Drzewiecka-Matuszek A, Brindell M, Stochel G (2005) Chem Rev 105:2647
9. Herzberg G (1950) In: Van Nostrand D Company (ed) Spectra of diatomic molecules, 2nd edn. New York
10. Kuramochi H, Kobayashi T, Suzuki T, Ichimura T (2010) J Phys Chem B 114:8782
11. Harada Y, Okabe C, Kobayashi T, Suzuki T, Ichimura T, Nishi N, Xu YZ (2010) J Phys Chem Lett 1:480
12. Reichardt C, Crespo-Hernandez CE (2010) J Phys Chem Lett 1:2239
13. Pollum M, Jockusch S, Crespo-Hernández CE (2014) J Am Chem Soc 136:17930
14. Cui G, Thiel W (2014) J Phys Chem Lett 5:2682
15. Cui G, Fang W (2013) J Chem Phys 138:044315
16. Pollum M, Crespo-Hernández CE (2014) J Chem Phys 140:071101
17. Sheng J, Huang Z (2010) Chem Biodivers 7:753
18. Jiang J, Sheng J, Carrasco N, Huang Z (2007) Nucleic Acids Res 35:477
19. Sheng J (2009) Synthesis, structure and function studies of selenium and tellurium derivatized nucleic acids. Dissertation, Georgia State University. http://scholarworks.gsu.edu/chemistry_diss/30
20. Jacquemin D, Perpete EA, Ciofini I, Adamo C (2009) Acc Chem Res 42:326
21. Eriksson ESE, Eriksson LA (2011) Phys Chem Chem Phys 13:7207
22. Adamo C, Jacquemin D (2013) Chem Soc Rev 42:845
23. Alberto ME, Mazzone G, Quartarolo AD, Fortes Ramos Sousa F, Sicilia E, Russo N (2014) J Comput Chem 35:2107
24. Frisch MJ, Trucks GW, Schlegel HB, Scuseria GE, Robb MA, Cheeseman JR, Scalmani G, Barone V, Mennucci B, Petersson GA, Nakatsuji H, Caricato M, Li X, Hratchian HP, Izmaylov AF, Bloino J, Zheng G, Sonnenberg JL, Hada M, Ehara M, Toyota K, Fukuda R, Hasegawa J, Ishida M, Nakajima T, Honda Y, Kitao NakaiH, Vreven T, Montgomery JA Jr, Peralta JE, Ogliaro F, Bearpark M, Heyd JJ, Brothers E, Kudin KN, Staroverov VN, Kobayashi R, Normand J, Raghavachari K, Rendell A, Burant JC, Iyengar SS, Tomasi J, Cossi M, Rega N, Millam JM, Klene M, Knox JE, Cross JB, Bakken V, Adamo C, Jaramillo J, Gomperts R, Stratmann RE, Yazyev O, Austin AJ, Cammi R, Pomelli C, Ochterski JW, Martin RL, Morokuma K, Zakrzewski VG, Voth GA, Salvador P, Dannenberg JJ, Dapprich S, Daniels AD, Farkas Ö, Foresman JB, Ortiz JV, Cioslowski J, Fox DJ (2009) Gaussian 09. Gaussian, Wallingford
25. Zhao Y, Truhlar DG (2008) Theor Chem Acc 120:215
26. Alberto ME, Marino T, Quartarolo AD, Russo N (2013) Phys Chem Chem Phys 15:16167
27. Alberto ME, Iuga C, Quartarolo AD, Russo N (2013) J Chem Inf Model 53:2334
28. Mazzone G, Russo N, Sicilia E (2013) Can J Chem 91:902
29. Cossi M, Barone V (2000) J Chem Phys 112:2427
30. Ruud K, Schimmelpfennig B, Ågren H (1999) Chem Phys Lett 310:215
31. (2011) DALTON, a molecular electronic structure program. http://daltonprogram.org/
32. Vahtras O, Ågren H, Jørgensen P, Jensen HJA, Helgaker T, Olsen J (1992) J Chem Phys 96:2118
33. Becke AD (1993) J Chem Phys 98:5648
34. Lee C, Yang W, Parr RG (1988) Phys Rev B 37:785
35. Zhang X, Xu YZ (2011) Molecules 16:5655
36. Caton-Williams J, Huang Z (2008) Angew Chem Int Ed 47:1723
37. Alberto ME, De Simone BC, Mazzone G, Quartarolo AD, Russo N (2014) J Chem Theory Comput 10:4006
38. Alberto ME, De Simone BC, Mazzone G, Marino T, Russo N (2015) Dyes Pigment 120:335
39. El-Sayed MA (1962) J Chem Phys 36:573
40. El-Sayed MA (1963) J Chem Phys 38:2834
41. Kasha M (1950) Discuss Faraday Soc 9:14

➢ Paper II

Photophysical Properties of S, Se and Te-Substituted Deoxyguanosines: Insight into Their Ability to Act as Chemotherapeutic Agents

Jenny Pirillo, Gloria Mazzone, Nino Russo and Luca Bertini.

Journal of Chemical Information and Modeling. (***2016)***

JOURNAL OF CHEMICAL INFORMATION AND MODELING

Article

pubs.acs.org/jcim

Photophysical Properties of S, Se and Te-Substituted Deoxyguanosines: Insight into Their Ability To Act as Chemotherapeutic Agents

Jenny Pirillo,[†] Gloria Mazzone,*[,†] Nino Russo,[†] and Luca Bertini[‡]

[†]Dipartimento di Chimica e Tecnologie Chimiche, University of Calabria, Via P. Bucci, 87036 Rende, Italy

[‡]Department of Biotechnologies and Biosciences, University of Milano-Bicocca, Piazza della Scienza 2, I-20126 Milano, Italy

Supporting Information

ABSTRACT: Guanine and guanosine derivatives have long been in use as anticancer drugs and recently have been proposed also as photosensitizers in photodynamic therapy. By means of density functional theory and its time-dependent formulation, the potential power as UVA chemotherapeutic agents has been investigated computing the photophysical properties (absorption spectra, excitation energies, and spin−orbit matrix elements) of sulfur, selenium, and tellurium-substituted deoxyguanosines. Different pathways for the population of the lowest triplet state have been considered. Results show that all the examined systems have the lowest triplet state lying above the energy required for the production of the highly cytotoxic excited molecular oxygen $^1\Delta_g$ and that the heavy atom effect ensures an efficient intersystem spin crossing.

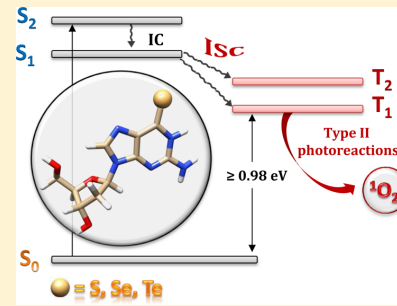

1. INTRODUCTION

Photodynamic therapy (PDT) is a medical treatment that combines the action of a photosensitizing drug, light, and an adequate concentration of molecular oxygen to cause selective damage of the targeted tissues. PDT has several potential advantages over surgery and radiotherapy: (i) it is comparatively noninvasive and can be targeted accurately; (ii) repeated doses can be given without the total-dose limitations associated with radiotherapy, and the healing process results in little or no scarring; and (iii) it can usually be done in an outpatient or day-case setting and has no side-effects. PDT is currently used to treat a variety of diseases.[1,2] Other applications include antiviral, antimicrobial, and antibacterial, and sterilization of blood plasma and water.[3−14]

In the last decades, a series of first- and second-generation photosensitizers have been proposed and tested in vitro and in vivo.[3−5,15] Drugs that are presently approved in a series of states include: Photofrin, a mixture of dimers and oligomers of hematoporphyrin in which porphyrin units are linked by ether, ester, and C−C bonds;[16] Foscan, the 5,10,15,20-tetrakis(m-hydroxyphenyl)chlorin;[17] Verteporfin, a benzoporphyrin derivative;[18] and Lutex, a lutetium complex of Texaphyrin.[19]

The desired therapeutic effect is related to a series of specific physical, chemical, and biological properties of the photosensitizer (PS). An effective PS is typically characterized by chemical stability, water-solubility, high quantum yield of $^1O_2$ ($^1\Delta_g$) production, no cytotoxicity in the dark, selectivity and rapid accumulation in target tissues, rapid clearance from patients, and a high molar absorption coefficient (ε) in the long wavelength (600−800 nm) range. The latter requirement is pivotal in the treatment of several types of cancers, since it allows the penetration of the radiation in deeper tissues, but is less important in antiviral, antimicrobial, and sterilization applications.[1]

The photochemical process involved in PDT begins with the excitation of the PS from its ground state to the lowest-energy spectroscopic state, usually the S_1 state, as an effect of the absorption of light radiation. The S_1 state can then transfer its energy to a low-lying triplet state, T_1, via nonradiative intersystem crossing (ISC).[20] If the lifetime of the triplet state is in the micro- to millisecond range and its energy is sufficiently high, T_1 can be considered the main mediator of the photodynamic reactions. It can give rise to two types of photoreactions generally essential in PDT, called type I and type II.[21] In the type I reaction, the PS T_1 directly transfers an electron or hydrogen to a biomolecule, producing reactive intermediates (i.e., O_2^-, H_2O_2, OH^-, and NO·) able to cause the diseased cells death. In the type II reaction, the PS transfers energy to molecular oxygen, yielding the production of singlet oxygen ($^1O_2$), which requires 0.98 eV of energy to occur. Being an extremely powerful oxidant, the $^1O_2$ is the principal cytotoxic species in PDT. Although the T_1 deactivating pathways are in competition among them, type II reactions generally predominate over the other.

Since 1950, the sulfur analogues of guanine DNA base have reached medical significance, being prescribed as immunosuppressants and for the treatment of some cancer types.[22−24]

Received: August 18, 2016
Published: December 23, 2016

DOI: 10.1021/acs.jcim.6b00486
J. Chem. Inf. Model. XXXX, XXX, XXX−XXX

More recently, a series of studies have shown that thiopurines are able to generate $^1O_2$ as well as other reactive oxygen species.[25,26] In addition, it has been found that 6-thioguanine and 6-tioguanosine are UVA chromophores absorbing at about 340 nm. These indications have stimulated several experimental and theoretical studies on the photophysical and photochemical properties of sulfur analogues of natural guanine bases.[27−32] Although these systems show an absorption band that falls down the so-called therapeutic window and, consequently, they possess a limited light penetration power, they remain good candidates for PDT for antimicrobial and antivirus disinfection and as UVA chemotherapeutic agents.

Selenium analogues of guanine and guanosines have also been synthesized and structurally characterized as potential antitumor agents,[33,34] while, for tellurium derivatives, the information is limited to some oligonucleotide derivatives.[35]

By means of the time-dependent extension of DFT,[36] the photophysical properties of S, Se, and Te-deoxyguanosine derivatives (labeled as S6-dGuo, Se6-dGuo, and Te6-dGuo, respectively) Scheme 1 have been investigated with the aim to

Scheme 1. X6-Deoxyguanosine, with X = S, Se, or Te

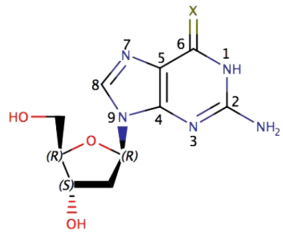

gain more insights into the ability of these compounds to act as UVA chemotherapeutic agents and to rationalize the influence of chalcogen atoms on the photophysical properties of deoxyguanosine.

2. COMPUTATIONAL DETAILS

All the calculations have been done by using the Gaussian 09 software package[37] at the DFT and TDDFT levels of theory. The structures have been optimized without any constraints in aqueous solution by using the hybrid three-parameter B3LYP[38,39] and M06[40] exchange and correlation funcionals. The standard 6-31+G* basis sets of Pople and co-workers have been used for all the atoms, with the exception of tellurium, for which an effective core pseudopotential[41] has been employed.

Absorption spectra have been obtained as vertical electronic excitations from the minima of the ground-state structures by using time-dependent density functional response theory (TD-DFT).[36] The solvent environment, water, has been simulated, with a dielectric constant of 78, by means of the integral equation formalism polarizable continuum model (IEFPCM),[42,43] which corresponds to a linear response in equilibrium and nonequilibrium solvation, in geometries optimization of the excited and ground states, respectively.

Spin−orbit matrix elements have been computed using the quadratic-response TD-DFT approach,[44,45] as implemented in the Dalton code,[46] at their involved excited state optimized geometries. The TD-B3LYP/cc-pVDZ//TD-B3LYP/6-31+G* level of theory has been used in the framework of both the atomic-mean field approximation[47] and the Breit−Pauli method[48] for thio- and seleno-derivatives, while for a tellurium-containing system, the same level of theory has been used in conjunction with the SDD pseudopotential for Te atom by using the spin−orbit coupling operators for effective core potentials with the effective nuclear charge given in ref 49. The spin−orbit couplings (SOCs) have been defined according to the following formula:

$$SOC_{ij} = \sqrt{\sum_n |\langle \psi_{S_i} | \hat{H}_{SO} | \psi_{T_{j,n}} \rangle|^2}; \quad n = x, y, z \tag{1}$$

where $\hat{H}_{SO}$ is the spin−orbit Hamiltonian.

The excitation energies of S6-dGuo have also been computed employing the coupled cluster with the approximate singlets and doublets method and the resolution of identity approximation (RICC2),[50] as implemented in Turbomole code,[51] using the def2-TZVP basis set for all the atoms.[52]

In addition, to explicitly consider solvation effects, S6-deoxyguanosine (S6-dGuo) has been solvated in a spherical water box with a radius of 18 Å (equal to 1264 water molecules) by using the TYP3PBOX solvent model as implemented in Chimera software.[53] All QM:MM computations have been performed considering the ONIOM procedure.[54−58] In the geometry optimizations, all water molecules have been allowed to move, and no constraints have been imposed on the peripheral solvent molecules. The B3LYP/6-31+G* level has been chosen for the QM region, while the Amber force field[59] has been chosen for the MM region. To compute the electronic spectrum of S6-dGuo by using such a model, two procedures have been followed. In the first one, labeled as QM:MM, the TDDFT calculation has been conducted on the optimized structure just described. While, in the second procedure, labeled as QM1:MM, the QM region has been reoptimized including the first solvation sphere (equal to 42 water molecules) and then the TDDFT has been used to achieve the electronic spectrum.

The Rehm−Weller equation,[60] which defines the free change for photoinduced electron transfer, has been used to calculate the driving force for electron transfer from the T_1 state of the investigated X6-dGuo to molecular oxygen, already applied by Pollum et al.,[61] according to eq 2:

$$\Delta G_{ET} = E_{ox}^{X6\text{-}dGuo} - E_{red}^{O_2} - E_{triplet} - C \tag{2}$$

where $E_{ox}^{X6\text{-}dGuo}$ is the oxidation potential of X6-dGuo, estimated by using the methodology described in ref 62, $E_{red}^{O_2}$ is the reduction potential of triplet molecular oxygen (−0.78 V vs SCE in acetonitrile),[63] $E_{triplet}$ is the energy of the T_1 state of the investigated compounds, and C is the Coulombic interaction term, estimated in acetonitrile as $e^2/\varepsilon a \approx 0.06$ eV.[64]

3. RESULTS

3.1. Benchmark and UV−vis Spectra. Though the reliability of the methodology used to investigate the properties of all deoxyguanosine derivatives has been previously and extensively tested on studying the photophysical properties of a wide range of photosensitizers,[65−75] the electronic spectrum of S6-dGuo has been computed by employing two different exchange and correlation functionals, the RICC2 method and QM:MM models.

As an initial step, the absorption properties of S6-dGuo have been explored in the solvents used in the experiments,[30] which are water and acetonitrile, which show maximum absorption peaks at 342 and 346 nm, respectively. As reported in Table S1

DOI: 10.1021/acs.jcim.6b00486
J. Chem. Inf. Model. XXXX, XXX, XXX−XXX

Table 1. Vertical Absorption (ΔE) in eV, Wavelengths in nm, MO Contribution (%), and Oscillator Strengths (f) from the Low-Lying Singlet State of S6-, Se6-, and Te6-Deoxyguanosine Calculated at the TD-B3LYP and -M06/6-31+G* Levels of Theory in Water

		B3LYP		M06	
S6-dGuo	MO contribution	ΔE, λ	f	ΔE, λ	f
S_1 ($n\pi^*$)	H-1→L (100%)	3.5, 359	0.000	3.5, 357	0.000
S_2 ($\pi\pi^*$)	H→L (95%)	3.9, 319	0.434	4.0, 314	0.455
T_1 ($\pi\pi^*$)	H→L (99%)	2.7, 457	0.000	2.9, 432	0.000
T_2 ($n\pi^*$)	H-1→L (99%)	3.2, 382	0.000	3.4, 369	0.000
Se6-dGuo					
S_1 ($n\pi^*$)	H-1→L (100%)	3.1, 400	0.000	3.1, 395	0.000
S_2 ($\pi\pi^*$)	H→L (96%)	3.6, 341	0.460	3.6, 344	0.473
T_1 ($\pi\pi^*$)	H→L (99%)	2.5, 487	0.000	2.5, 493	0.000
T_2 ($n\pi^*$)	H-1→L (99%)	2.9, 425	0.000	3.0, 416	0.000
Te6-dGuo					
S_1($n\pi^*$)	H-1→L (100%)	2.7, 457	0.000	2.7, 468	0.000
S_2 ($\pi\pi^*$)	H→L (98%)	3.2, 385	0.414	3.2, 391	0.427
T_1 ($\pi\pi^*$)	H→L (99%)	2.3, 531	0.000	2.3, 533	0.000
T_2 ($n\pi^*$)	H-1→L (100%)	2.56, 479	0.000	2.6, 486	0.000

of the Supporting Information (SI), according to the experimental observations, no significant differences have been found in the reproduction of the absorption spectrum of S6-dGuo in the two environments (λ_{max} = 319 nm in both cases at the B3LYP/6-31+G* level); hence, the water solvent has been used to describe the photophysical properties by using different approaches (Table S2 of the SI) as well as those of Se and Te derivatives (Table 1), and accordingly, only data obtained in water will be discussed.

For S6-dGuo, the vertical excitation energies for the first two excited singlet states have been computed to be 3.5 eV and 3.9 or 4.0 eV, respectively, at the B3LYP and M06 levels of theory. The S_1 state, originated mainly from the H-1 → L transition, is spectroscopically dark, whereas the S_2 one, resulted predominantly from the H → L transition, is bright and is the major contributor to the first band of the absorption spectrum.[27,30,31] The associated absorption band at 319 nm is in satisfactory accordance with the experimental data,[30] as a difference of 23 and 28 nm has been found at the B3LYP and M06 levels of theory, respectively.

As can be seen in Figures 1 and 2, the S_1 and T_2 states arise from the $n\pi^*$ electronic excitation, being the H-1 localized on the chalcogen atom lone-pair and the L delocalized over the whole guanine moiety, while the S_2 and T_1 states are mainly of $\pi\pi^*$ character. These assignments agree with previous results reported for 6-thioguanosine[30] and 6-thioguanine (6-TG)[27] and confirm how the presence of the deoxyribose does not significantly influence the spectroscopic properties of the 6-thioguanine absorption core. Therefore, we are confident to keep the higher level of theory used in studying the absorption properties of 6-TG, MS-CASPT2//SA-CASSCF,[27] as a reference to confirm the reliability of the computed excitation energies. In their study, Corral and co-workers compared the absorption spectrum of 6-TG computed according to the MS-CASPT2//SA-CASSCF and TD-B3LYP approaches. The authors found that the excitation energies for the key singlet states differ less than 0.2 eV while those of the triplet states are mainly underestimated by the TD-DFT method by 0.4−0.8 eV, though the maximum absorption wavelength has been found blue-shifted by 34 nm at the highest level of theory under consideration. Looking at the TD-DFT data reported in Table 1, a good agreement in the location of the vertical values of the

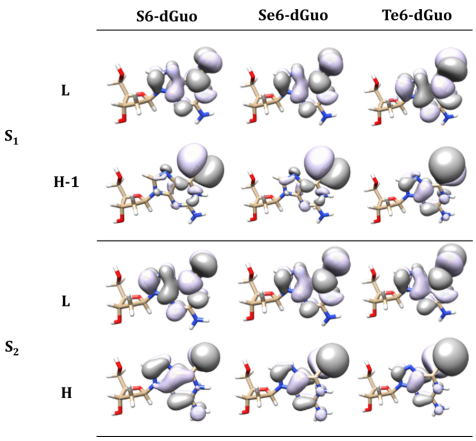

Figure 1. Graphical representation of the highest occupied and lowest unoccupied MOs involved in the vertical transitions for S6-, Se6-, and Te6-dGuo obtained from the equilibrium geometries of the excited states S_1 and S_2 by using the B3LYP functional. The plots of the orbitals were accomplished with an isodensity value of 2×10^{-2} a.u.

S_1, S_2, T_1 and T_2 states computed at the CASPT2 level of theory for 6-TG results.[27] A mean error in reproducing the singlet and triplet states excitation energies of 0.1 and 0.3 eV at the B3LYP level emerges, while 0.1 and 0.2 eV are the mean errors found at the M06 level, resulting in a satisfactory estimation of the excitation energies at the TD-DFT level of theory.

As further confirmation of the proper choice of the computational protocol, additional calculations by using the coupled cluster with the approximate singles and doubles method within resolution of the identity approximation (RICC2) have been carried out. Data reported in Table S2 show how the inclusion of the double excitation to the excited state wave functions, that result to be of less than 10% (see Table S3), slightly contributes to the proper estimation of the excitation energies. A better match of the excitation energies with the data reported by Corral and co-workers[27] with respect to the TD-DFT calculations has been found. Despite this,

DOI: 10.1021/acs.jcim.6b00486
J. Chem. Inf. Model. XXXX, XXX, XXX−XXX

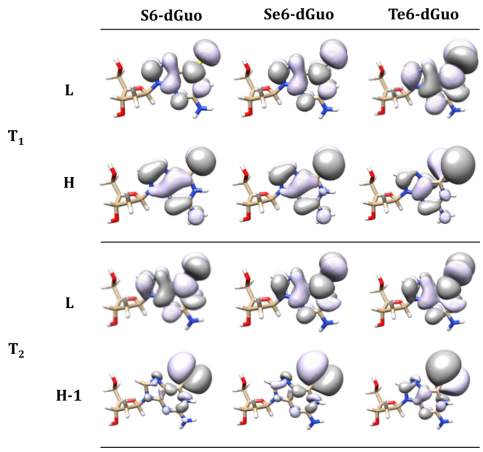

Figure 2. Graphical representation of the highest occupied and lowest unoccupied MOs involved in the vertical transitions for S6-, Se6-, and Te6-dGuo obtained from the equilibrium geometries of the excited states T_1 and T_2 by using the B3LYP functional. The plots of the orbitals were accomplished with an isodensity value of 2×10^{-2} a.u.

employing such a method, the computed energies result very similar to those obtained at the M06/6-31+G* level of theory and the absorption band results to be blue-shifted about 30 nm with respect to the experimental spectrum.

A similar performance in reproducing the electronic spectrum of S6-dGuo has been shown by QM:MM methods. The maximum absorption wavelength is found to be 327 (QM1:MM) or 312 nm (QM:MM), by including or not the first solvation sphere in the QM region (see Figure S1). Also the estimation of the other excited state energies is not so different from the excitation energies computed in the implicit solvent model discussed above, since the QM region is described by the same level of theory. Therefore, a slight gain has been found only considering explicitly a key number of water molecules in the QM region (QM1:MM model).

Putting together these considerations, we found accurate the TD-DFT level of theory in studying the spectroscopic properties of deoxyguanosine chalcogen-derivatives.

From data reported in Table 1 it appears clear that the substitution of sulfur with selenium and tellurium atoms entails a red shift of the maximum absorption band, and consequently a decreasing of all the excitation energies. This behavior can be related to (i) the increasing of the atomic size of the chalcogen atom (atomic radius 1.02, 1.16, and 1.42 Å for sulfur, selenium, and tellurium, respectively); (ii) the weakness of the C═X strength in going from C═S to C═Se and C═Te bonds; (iii) the increasing of the metallic character and the propensity to electron delocalization along the chalcogens' family.

Similarly to the thioderivative, also for Se and Te ones, the S_1 and S_2 excited states arise from H-1 → L and H → L transitions, respectively. Looking at the plot of the orbitals reported in Figure 1, it can be noted that, similarly to that found for S6-dGuo, the S_1 excited states are originated by transitions involving orbitals with different composition ($n\pi^*$), while, for the bright S_2 state, the n contribution in the HOMO results to be more pronounced in Se6- and Te6-dGuo than in the thioderivative, due to the increasing of chalcogen atom size.

Table 2. Selected Bond Lengths (Å) and Valence and Dihedral Angles (degrees) of Ground (S_0) and Excited States (S_1, S_2, T_1, T_2) Fully Optimized at the DFT (B3LYP and M06 in parentheses) and TD-DFT Levels, respectively, in Water for S6-, Se6-, and Te6-Deoxyguanosine[a]

	Bond lengths		Valence angles		Dihedral Angles		
	C_6X	C_8N_7	φ_1	φ_2	Φ_1	Φ_2	Φ_3
S6-dGuo							
S_0	1.691	1.311	128.6	117.5	−179.8	−0.3	−0.1
	(1.682)	(1.304)	(128.3)	(117.3)	(179.8)	(−0.2)	(−0.1)
S_1	1.773	1.325	123.4	116.2	156.0	−2.5	4.3
	(1.763)	(1.319)	(121.6)	(116.1)	(152.1)	(−2.2)	(5.0)
S_2	1.741	1.340	126.3	118.5	158.0	−0.7	−1.5
	(1.740)	(1.331)	(124.6)	(118.4)	(151.7)	(−1.0)	(−2.3)
T_1	1.708	1.367	128.6	120.0	173.7	−0.6	0.2
	(1.701)	(1.375)	(128.3)	(120.0)	(176.2)	(−0.4)	(0.0)
T_2	1.708	1.323	122.3	116.1	146.0	−3.4	0.4
	(1.774)	(1.317)	(121.8)	(116.0)	(144.9)	(−3.2)	(0.8)
Se6-dGuo							
S_0	1.839	1.310	128.6	117.6	180.0	−0.2	−0.2
S_1	1.917	1.324	123.3	116.3	156.7	−3.3	3.0
S_2	1.999	1.320	118.8	118.2	139.1	−4.1	0.3
T_1	1.851	1.357	128.8	119.5	177.6	−0.4	−0.4
T_2	1.940	1.322	121.3	116.3	145.9	−4.5	0.2
Te6-dGuo							
S_0	2.074	1.310	128.0	117.8	180.0	−0.2	−0.1
S_1	2.144	1.323	121.2	116.5	151.1	−3.0	1.8
S_2	2.281	1.315	117.4	117.9	134.3	−3.7	−0.4
T_1	2.130	1.326	120.4	118.2	140.7	−2.5	−0.5
T_2	2.248	1.317	118.6	116.8	137.7	−3.4	−3.1

[a] $\varphi_1 = C_5C_6X$; $\varphi_2 = N_1C_2N$; $\Phi_1 = XC_6C_5C_4$; $\Phi_2 = C_6C_5C_4N_3$; $\Phi_3 = C_6N_1C_2N_3$.

DOI: 10.1021/acs.jcim.6b00486
J. Chem. Inf. Model. XXXX, XXX, XXX−XXX

Anyhow, the spectroscopic properties of Se6-dGuo and Te6-dGuo remain similar to that of S6-dGuo.

The computation of the absorption band of Se6-dGuo at 341 and 344 nm, with B3LYP and M06 functionals, respectively, well fits with the experimental band found at 357 nm.[34]

3.2. Ground and Excited State Properties. Although the presence of the solvation sphere in the QM region for S6-dGuo allows prediction of the main absorption band with a smaller error, the full excited states structure optimization would be really expensive. To balance computational accuracy and efficiency, the geometry optimization of the excited states has been computed at the TD-B3LYP/6-31+G* level of theory.

Selected structural parameters for the optimized structures of the ground (S_0), low lying singlet (S_1, S_2), and triplet (T_1, T_2) states for the S6-dGuo, Se6-dGuo, and Te6-dGuo are collected in Table 2, while the Cartesian coordinates are reported in the SI.

As can be seen from data reported in Table 2, in all the considered molecules, the π system moiety, including the lone pair of the chalcogen atoms, results to be approximately planar in the ground state, but significantly distorted in the excited ones. This behavior agrees with what has already been reported for 6-thioguanine,[27,29,32] for which conical intersection, linear interpolated Cartesian coordinates, and minimum energy paths for the description of the deactivation pathway were computed. The major deviation from the planarity can be observed looking at the values of the Φ_1 dihedral angle. In S6-dGuo it switches from 179.8 degrees in the ground state to 156 and 158 degrees in the singlet excited ones. Since such a parameter accounts for the deviation of the chalcogen atom from the condensed-rings' plane, an elongation of the C_6–S bond has been observed. From 1.691 Å in the ground state, it becomes 1.773 and 1.741 Å in the S_1 and S_2 optimized structures, respectively, which is really similar to what has been found for 6-thioguanine (1.781 and 1.749 Å, respectively).[27] While, a different scenario has been observed for the orientation of the NH_2 group with respect to the ring plane, as contrariwise to what has been reported for the excited state S_2 of 6-thioguanine,[27] no significant out-of-plane deviation of the NH_2 group, see φ_2, has been found.

Regarding the Se and Te derivatives, a very similar behavior can be observed, with a significant difference in the S_2 optimized structure, which results to be further distorted (Φ_1 of 139.1 and 134.3 degrees for Se and Te-derivatives, respectively) with respect to that of the thio-derivative. While, as regards the triplet excited states, the values of such an angle show a major distortion for T_2 compared to T_1 for all the deoxyguanosine derivatives, also the Φ_2 and Φ_3 dihedral angles suffer a small distortion, albeit obviously much less pronounced being defined by atoms belonging to the planar ring. Therefore, it can be concluded that the distortion of the π structure increases with the increasing of the dimensions of the chalcogen atom.

Furthermore, comparing the optimized structures of the excited states, it can be observed that the states that are characterized by a structure significantly different from that of the ground state are the S_2 and T_2 states (see also Table S4), which can play a pivotal role in the ability of these compounds to promote the singlet oxygen production.

In order to elucidate how the geometry optimization of the excited states has an impact on the energetics, the adiabatic energies are collected in Table 3.

Table 3. Adiabatic Energies (eV) of the Excited States S_1, S_2, T_1, and T_2 Computed for S6-dGuo, Se6-dGuo, and Te6-dGuo at the TD-B3LYP/6-31+G* Level of Theory

	S6-dGuo	Se6-dGuo	Te6-dGuo
S_1	3.3	2.9	2.5
S_2	3.5	3.4	2.8
T_1	2.5	2.4	2.2
T_2	3.0	2.7	2.3

Comparing the adiabatic energies with the vertical excitation ones, it emerges that, as often occurs, the structural relaxation leads to a reduction of the energy gaps for all the considered excited states. The stabilization upon optimization of the excited state energies is directly related to the structural rearrangement. Indeed, looking at singlet states, it can be noted that for all the investigated deoxyguanosine derivatives the greater decrease of the energy gap has been found for S_2, being the stabilization energies for S6-, Se6-, and Te6-dGuo 0.4, 0.2, and 0.4 eV, respectively, with reference to the correspondent vertical energies. As pointed out above, the S_2 is the singlet excited state that entails the greatest structural rearrangement with respect to the S_0. Similarly, for the triplet excited states, the adiabatic energies of T_2 result to be 0.2, 0.2, and 0.3 eV above the correspondent vertical ones for S6-, Se6-, and Te6-dGuo, respectively.

3.3. Excited States Deactivation Pathways. Though the absorption of the title molecules in the range 300–400 nm, falling below the therapeutic window, limits their use in anticancer therapy that requires a deeper penetration into the tissue, their potential use as UVA chemotherapeutic agents could be first investigated by evaluating their ability to populate the low-lying excited triplet state and then to excite the molecular oxygen.

First of all, as can be seen in Table 1, the first triplet excited state of all the examined deoxyguanosine derivatives has enough energy to activate the triplet molecular oxygen (0.9 eV).[74] Also considering the adiabatic singlet–triplet energy gap, included in Table 3, resulting from the energies at their equilibrium geometry, these compounds should be able to activate molecular oxygen.

Whereas the absorption of the light entails the population of the S_2 excited state, the population of the lowest triplet state could be achieved by the following three plausible nonradiative decay pathways:

(a)

$$S_0 \xrightarrow{A} S_2 \xrightarrow{IC} S_1 \xrightarrow{ISC} T_1$$

(b)

$$S_0 \xrightarrow{A} S_2 \xrightarrow{IC} S_1 \xrightarrow{ISC} T_2 \xrightarrow{IC} T_1$$

(c)

$$S_0 \xrightarrow{A} S_2 \xrightarrow{ISC} T_2 \xrightarrow{IC} T_1$$

As established by an approximate expression of the Fermi Golden Rule, the intersystem crossing kinetics is directly related to the spin–orbit matrix elements $\langle S_n|\hat{H}_{SO}|T_m\rangle$ and the Franck–Condon weighted density of states FCWD:

$$k_{isc}^{nm} = \frac{2\pi}{\hbar}\langle S_n|\hat{H}_{SO}|T_m\rangle^2 \times \mathrm{FCWD}$$

DOI: 10.1021/acs.jcim.6b00486
J. Chem. Inf. Model. XXXX, XXX, XXX–XXX

While the computation of SOC values has been performed for a series of photosensitizers,[69−74] the estimation of FCWD results to be really expensive. It is common to assume that for similar compounds its contribution to the k_{isc} is of the same magnitude. Anyhow, in the framework of Marcus−Levich−Jortner theory[76] the FCWD is proportional to the exponential factor:

$$\text{FCWD} \propto \exp\left[-\frac{(\Delta E_{S-T})^2}{4\lambda k_B T}\right]$$

where λ is the Marcus reorganization energy and ΔE is the difference between the energies of the singlet and triplet states at their equilibrium geometry. From accurate ab initio electronic structure data, it has been established that SOCs and small S_n-T_m energy gaps define the efficiency of ISC processes.[77]

In Table 4 are, thus, reported the computed SOCs, while in Table 5 are collected the adiabatic energy differences between the excited states that could take part in the nonradiative decay pathways. Following path a, due to the dark nature of S_1, it can be hypothesized that a fast internal conversion (IC) process from S_2 to S_1 occurs before the T_1 state results to be populated through an efficient intersystem spin crossing (ISC). The associated SOCs are quite high and increase with the dimension of the substituent. In particular, passing from the S6- to the Te6-deoxyguanosine derivatives, an increase of SOC values of 1 order of magnitude (from 190 to 1903 cm^{-1}) can be noted, while the singlet−triplet energy difference decreases with the atomic size of the substituent. According to path b after the IC from S_2 to S_1, the T_1 state can be populated by an ISC from S_1 to T_2 states and a subsequent IC process. Also in this case the SOCs increase in going from sulfur- to tellurium-substituted deoxyguanosine derivatives, but they result to be considerably smaller than those computed for the ISC process from S_1 to T_1. This behavior can be explained considering the El-Sayed rule[78,79] which established that the rate of the ISC sensibly increases if the radiationless transition involves a change of orbital type. Indeed, in the former case the ISC is characterized by a $(n\pi^*) \rightsquigarrow (\pi\pi^*)$ transition, while in the latter the SOCs are computed between states characterized by orbitals of the same nature $(n\pi^*) \rightsquigarrow (n\pi^*)$ (see Figures 1 and 2). Therefore, although the $\Delta E(S_1\text{-}T_2)$ are smaller than the $\Delta E(S_1\text{-}T_1)$, the greater magnitude of the SOCs values computed for the ISC involved in path a suggests the latter as the most probable one.

Channel c is the only pathway in which the ISC has been supposed to occur before any other nonradiative process. The energy difference between S_2 and T_2 is found to be 0.5 (S6-dGuo), 0.7 (Se6-dGuo), and 0.5 eV (Te6-dGuo) at the TD-B3LYP/6-31+G* level of theory. In agreement with the different orbital natures of S_2 $(\pi\pi^*)$ and T_2 $(n\pi^*)$, SOCs rather high have been obtained, though smaller than those found between S_1 and T_1. Therefore, on the basis of SOC values, energy gaps, and the nature of the involved molecular orbitals, the favored deactivation channels should be those involving an ISC between $S_1 \rightsquigarrow T_1$ or $S_2 \rightsquigarrow T_2$ states. According to Kasha's rule,[80] in a given spin manifold, the transition $S_n \rightsquigarrow S_1$(with $n > 1$) should be very fast, and the triplet state population, as well as other photophysical properties, should start from the lowest singlet exited state (S_1). Hence, pathway a should be the fastest deactivation channel.

It is worthy of note that, the necessary requirements of high SOC values and low-lying triplet state with enough energy to excite the molecular oxygen do not guarantee that these compounds will be an efficient $^1O_2$ generator, as other competitive deactivation processes from the T_1 state could occur. Very recently,[61] it has been shown that S6-dGuo generates $^1O_2$ in only ca. 20% yield, contrariwise to what was previously reported for 6-TG.[81] The authors, measuring also the fraction of quenching events, hypothesized that most of the triplet quenching by molecular oxygen occurs through nonradiative decay pathways. In particular, due to the estimated exergonic driving force for electron transfer, they proposed the formation of a charge-transfer complex that obviously reduces the probability of $^1O_2$ generation. Therefore, as the occurrence of the electron-transfer event can be first predicted evaluating the Gibbs free energy for electron transfer (ΔG_{ET}) from T_1 of the photosensitizer to the ground states of molecular oxygen, such a parameter has been computed according to eq 2 (see Table 6) for all the deoxyguanosine chalcogen derivatives investigated here.

As can be seen in Table 6, the lowest value of the oxidation potential has been found for Te6-dGuo, essentially due to the vertical ionization energy computed for such a compound. This means that, among the deoxyguanosine derivatives considered here, the Te6-dGuo results to be the most susceptible to ionization. Nevertheless, it is noteworthy that there is no evidence supporting the formation of a radical cation for any of the X6-dGuo derivatives, especially for Te6-dGuo, which has not been under investigation so far. Looking instead at the

Table 4. SOC (cm^{-1}) between Low-Lying Singlet and Triplet Excited States at the B3LYP/cc-pVDZ//B3LYP/6-31+G* Level of Theory, for S6-dGuo and Se6-dGuo, Obtained in the Framework of Both Atomic Mean Field and Breit−Pauli (in parentheses) Methods, on the Optimized Geometry of the First and Second Singlet Excited States, for Coupling of S_1 and S_2, respectively[a]

	S6-dGuo	Se6-dGuo	Te6-dGuo
$\lvert\langle\psi_{S_1}\lvert\hat{H}_{so}\rvert\psi_{T_1}\rangle\rvert$	190.3 (237.1)	932.6 (913.6)	1902.8
$\lvert\langle\psi_{S_1}\lvert\hat{H}_{so}\rvert\psi_{T_2}\rangle\rvert$	17.3 (21.4)	67.4 (74.6)	186.4
$\lvert\langle\psi_{S_2}\lvert\hat{H}_{so}\rvert\psi_{T_2}\rangle\rvert$	86.4 (107.4)	828.1 (919.8)	1334.0

[a]For Te6-dGuo the correspondent data obtained by using the effective core one electron Hamiltonian in conjunction with the ECP for Te atom are reported.

Table 5. Adiabatic Energy Differences (eV) between the Excited States, among which the Intersystem Crossing Could Occur, at Their Equilibrium Geometries Computed at the TDB3LYP/6-31+G* Level of Theory

S6-dGuo	transition	ΔE
$\Delta E(S_1\text{-}T_1)$	$(n\pi^*) \rightsquigarrow (\pi\pi^*)$	0.8
$\Delta E(S_1\text{-}T_2)$	$(n\pi^*) \rightsquigarrow (n\pi^*)$	0.2
$\Delta E(S_2\text{-}T_2)$	$(\pi\pi^*) \rightsquigarrow (n\pi^*)$	0.5
Se6-dGuo		
$\Delta E(S_1\text{-}T_1)$	$(n\pi^*) \rightsquigarrow (\pi\pi^*)$	0.6
$\Delta E(S_1\text{-}T_2)$	$(n\pi^*) \rightsquigarrow (n\pi^*)$	0.2
$\Delta E(S_2\text{-}T_2)$	$(\pi\pi^*) \rightsquigarrow (n\pi^*)$	0.7
Te6-dGuo		
$\Delta E(S_1\text{-}T_1)$	$(n\pi^*) \rightsquigarrow (\pi\pi^*)$	0.4
$\Delta E(S_1\text{-}T_2)$	$(n\pi^*) \rightsquigarrow (n\pi^*)$	0.2
$\Delta E(S_2\text{-}T_2)$	$(\pi\pi^*) \rightsquigarrow (n\pi^*)$	0.5

DOI: 10.1021/acs.jcim.6b00486
J. Chem. Inf. Model. XXXX, XXX, XXX−XXX

Table 6. Vertical Ionization Energy (VIE), Oxidation Potential (E_{ox}), and Adiabatic Energy of the Low-Lying Triplet Excited State (E_T) and Gibbs Free Energy of Electron Transfer (ΔG_{ET}) of X6-dGuo (X = S, Se, Te) in kJ mol^{-1}

	S6-dGuo	Se6-dGuo	Te6-dGuo
VIE	689.8	693.9	641.6
E_{ox}	136.4	138.7	109.4
E_T	232.3	221.0	202.7
ΔG_{ET}	−50.5	−36.4	−47.4

ΔG_{ET} values, Te6-dGuo exhibits the same propensity of S6-dGuo in forming a charge-transfer complex, with the net exothermicity being 47.4 vs 50.5 kJ mol^{-1}, because of the smallest gap S-T found for the Tellurium derivative with respect to the thio one (202.7 kJ mol^{-1} vs 232.3 kJ mol^{-1}). Schweitzer et al. estimated that charge-transfer interactions play a significant role in quenching of the T_1 state by $^3O_2$ when $\Delta G_{ET} < -30$ kJ mol^{-1}.[63] Therefore, for all the X6-dGuo derivatives the charge-transfer complex formation could be a viable route for deactivation of the photosensitizer's triplet state, even though the ΔG_{ET} computed for Se6-dGuo is only −36.4 kJ mol^{-1}. Therefore, it could be possible that the behavior of the Se-derivative is not dominated by the formation of a charge-transfer complex and, then, it should be able to excite the molecular oxygen.

To the best of our knowledge, only for S6-dGuo have the $^1O_2$ quantum yields been estimated, while for Se and Te derivatives this parameter has not been measured so far. Therefore, our data can stimulate further investigations aiming at establishing whether these compounds can be efficient singlet oxygen generators.

4. CONCLUSIONS

In this paper DFT and its time-dependent extension (TDDFT) have been used to compute the photophysical properties of deoxyguanosine chalcogen-derivatives (S6-dGuo, Se6-dGuo, Te6-dGuo) with the aim to rationalize the influence of the chalcogen substituent on the ability of deoxyguanosine to act as photosensitizer in cancer therapy. Analyzing the electronic spectra, the spin−orbit couplings, and the energy gaps between the excited states, the following conclusions can be outlined:

- all the investigated systems have the lowest triplet excited state (T_1) with sufficiently higher energy to excite the molecular oxygen;
- the magnitude of the spin−orbit coupling matrix elements increases with the atomic size of the substituent and, according to the El-Sayed rules, is larger when orbitals with different nature are involved in the intersystem crossing process;
- among the hypothesized deactivation channels, considering both SOCs and ΔE(S-T), path a, $S_0 \xrightarrow{A} S_2 \xrightarrow{IC} S_1 \xrightarrow{ISC} T_1$, seems to be the favored one, although, due to the high spin−orbit values found for the S_2-T_2 coupling, also channel b, $S_0 \xrightarrow{A} S_2 \xrightarrow{IC} S_1 \xrightarrow{ISC} T_2 \xrightarrow{IC} T_1$, should have a fast kinetics;
- the exoergonic driving force computed for the electron transfer from the photosensitizer T_1 to the ground states of molecular oxygen opens the possibility that charge-transfer interactions play a role in quenching the triplet state of X6-dGuo derivatives.

■ ASSOCIATED CONTENT

Supporting Information

The Supporting Information is available free of charge on the ACS Publications website at DOI: 10.1021/acs.jcim.6b00486.

Electronic spectrum of S6-deoxyguanosine in water and acetonitrile calculated at the TD-B3LYP/6-31+G* level of theory; electronic spectrum of S6-deoxyguanosine in water performed by TDDFT, RICC2, and QM:MM methods; contribution of the excitation levels to the excited states wave functions computed at the RICC2/def2-TZVP level of theory for S6-dGuo; QM:MM and QM1:MM models; optimized structures and Cartesian coordinates of the ground and excited states of S6-dGuo, Se6-dGuo, and Te6-dGuo (PDF)

■ AUTHOR INFORMATION

Corresponding Author

*(G.M.) E-mail: gloria.mazzone@unical.it.

ORCID

Gloria Mazzone: 0000-0002-4686-6876

Notes

The authors declare no competing financial interest.

■ ACKNOWLEDGMENTS

University of Calabria is gratefully acknowledged.

■ REFERENCES

(1) Yano, S.; Hirohara, S.; Obata, M.; Hagiya, Y.; Ogura, S. I.; Ikeda, A.; Kataoka, H.; Tanaka, M.; Joh, T. Current States and Future Views in Photodynamic Therapy. *J. Photochem. Photobiol., C* **2011**, *12*, 46−67.

(2) Brown, S. B.; Brown, E. A.; Walker, I. The Present and Future Role of Photodynamic Therapy in Cancer Treatment. *Lancet Oncol.* **2004**, *5* (8), 497−508.

(3) Moan, J.; Berg, K. The Photodegradation of Porphyrins in Cells Can Be Used to Estimate the Lifetime of Singlet Oxygen. *Photochem. Photobiol.* **1991**, *53*, 549−553.

(4) Juarranz, A.; Jaen, P.; Sanz-Rodriguez, F.; Cuevas, J.; Gonzalez, S. Photodynamic Therapy of Cancer. Basic Principles and Applications. *Clin. Transl. Oncol.* **2008**, *10*, 148−154.

(5) Castano, A. P.; Demidova, T. N.; Hamblin, M. R. Mechanisms in Photodynamic Therapy: Part One-Photosensitizers, Photochemistry and Cellular Localization. *Photodiagn. Photodyn. Ther.* **2004**, *1*, 279−293.

(6) Garland, M. J.; Cassidy, C. M.; Woolfson, D.; Donnelly, R. F. Designing Photosensitizers for Photodynamic Therapy: Strategies, Challenges and Promising Developments. *Future Med. Chem.* **2009**, *1*, 667−691.

(7) Spikes, J. D. Quantum Yields and Kinetics of the Photobleaching of Hematoporphyrin, Photofrin II, Tetra(4-Sulfonatophenyl)-Porphine and Uroporphyrin. *Photochem. Photobiol.* **1992**, *55*, 797−808.

(8) Macalpine, J. K.; Boch, R.; Dolphin, D. Evaluation of Tetraphenyl-2,3-Dihydroxychlorins as Potential Photosensitizers. *J. Porphyrins Phthalocyanines* **2002**, *6*, 146−155.

(9) Isakau, H. A.; Parkhats, M. V.; Knyukshto, V. N.; Dzhagarov, B. M.; Petrov, E. P.; Petrov, P. T. Toward Understanding the High PDT Efficacy of Chlorine e6−Polyvinylpyrrolidone Formulations: Photophysical and Molecular Aspects of Photosensitizer−Polymer Interaction *in Vitro*. *J. Photochem. Photobiol., B* **2008**, *92*, 165−174.

(10) Senge, M. O.; Brandt, J. C. Temoporfin (Foscan®, 5,10,15,20-Tetra(*m*-Hydroxyphenyl) Chlorin) A Second-Generation Photosensitizer. *Photochem. Photobiol.* **2011**, *87*, 1240−1296.

(11) Kiesslich, T.; Berlanda, J.; Plaetzer, K.; Krammer, B.; Berr, F. Comparative Characterization of the Efficiency and Cellular Pharmacokinetics of Foscan- and Foslip-Based Photodynamic Treat-

DOI: 10.1021/acs.jcim.6b00486
J. Chem. Inf. Model. XXXX, XXX, XXX−XXX

ment in Human Biliary Tract Cancer Cell Lines. *Photochem. Photobiol. Sci.* **2007**, *6*, 619−627.
(12) Houle, J. M.; Strong, A. Clinical Pharmacokinetics of Verteporfin. *J. Clin. Pharmacol.* **2002**, *42*, 547−557.
(13) Dolmans, D. E.; Fukumura, D.; Jain, R. K. Photodynamic Therapy for Cancer. *Nat. Rev. Cancer* **2003**, *3*, 380−387.
(14) Robertson, C. A.; Evans, D. H.; Abrahamse, H. Photodynamic Therapy (PDT): a Short Review on Cellular Mechanisms and Cancer Research Applications for PDT. *J. Photochem. Photobiol., B* **2009**, *96*, 1−8.
(15) Juzeniene, A.; Peng, Q.; Moan, J. Milestones in the Development of Photodynamic Therapy and Fluorescence Diagnosis. *Photochem. Photobiol. Sci.* **2007**, *6*, 1234−1245.
(16) Bonnett, R.; White, R. D.; Winfield, U. J.; Berenbaum, C. Hydroporphyrins of the Meso-Tetra(Hydroxyphenyl)Porphyrin Series as Tumour Photosensitizers. *Biochem. J.* **1989**, *261*, 277−280.
(17) Grahn, M. F.; McGuinness, A.; Benzie, R.; Boyle, R.; de Jode, M. L.; Dilkes, M. G.; Abbas, B.; Williams, N. S. Intracellular Uptake, Absorption Spectrum and Stability of the Bacteriochlorin Photo-Sensitizer 5,10,15,20-Tetrakis (m-Hydroxyphenyl) Bacteriochlorin (m-THPBC). Comparison with 5,10,15,20-Tetrakis(m-Hydroxyphenyl) Chlorin (m-THPC). *J. Photochem. Photobiol., B* **1997**, *37*, 261−266.
(18) Aveline, B.; Hasan, T.; Redmond, R. W. Photophysical and Photosensitizing Properties of Benzoporphyrin Derivative Monoacid Ring A (BPD-MA). *Photochem. Photobiol.* **1994**, *59*, 328−335.
(19) Sessler, J. L.; Hemmi, G.; Mody, T. D.; Murai, T.; Burrell, A.; Young, S. W. Texaphyrins: Synthesis and Applications. *Acc. Chem. Res.* **1994**, *27*, 43−50.
(20) Szaciłowski, K.; Macyk, W.; Drzewiecka-Matuszek, A.; Brindell, M.; Stochel, G. Bioinorganic Photochemistry: Frontiers and Mechanisms. *Chem. Rev.* **2005**, *105*, 2647−2694.
(21) Foote, C. S. Definition of Type I and Type II Photosensitized Oxidation. *Photochem. Photobiol.* **1991**, *54*, 659.
(22) Elion, G. B. The Purine Path to Chemotherapy. *Science* **1989**, *244*, 41−47.
(23) Euvrard, S.; Kanitakis, J.; Claudy, A. Skin Cancers After Organ Transplantation. *N. Engl. J. Med.* **2003**, *348*, 1681−1691.
(24) Attard, N. R.; Karran, P. UVA Photosensitization of Thiopurines and Skin Cancer in Organ Transplant Recipients. *Photochem. Photobiol. Sci.* **2012**, *11*, 62−68.
(25) Karran, P.; Attard, N. Thiopurines in Current Medical Practice: Molecular Mechanisms and Contributions to Therapy-Related Cancer. *Nat. Rev. Cancer* **2008**, *8*, 24−36.
(26) Brem, R.; Li, F.; Karran, P. Reactive Oxygen Species Generated by Thiopurine/UVA Cause Irreparable Transcription-Blocking DNA Lesions. *Nucleic Acids Res.* **2009**, *37*, 1951−1961.
(27) Martínez-Fernández, L.; González, L. Corral, I. An Ab Initio Mechanism for Efficient Population of Triplet States in Cytotoxic Sulfur Substituted DNA Bases: The Case of 6-Thioguanine. *Chem. Commun.* **2012**, *48*, 2134−2136.
(28) Massey, A.; Xu, Y.-Z.; Karran, P. Photoactivation of DNA Thiobases as a Potential Novel Therapeutic Option. *Curr. Biol.* **2001**, *11*, 1142−1146.
(29) Martínez-Fernández, L. Corral, I.; Granucci, G.; Persico, M. Competing Ultrafast Intersystem Crossing and Internal Conversion: a Time Resolved Picture for the Deactivation of 6-Thioguanine. *Chem. Sci.* **2014**, *5*, 1336−1347.
(30) Reichardt, C.; Guo, C.; Crespo-Hernández, C. E. Excited-State Dynamics in 6-Thioguanosine from the Femtosecond to Microsecond Time Scale. *J. Phys. Chem. B* **2011**, *115*, 3263−3270.
(31) Gomzi, V. TDDFT Study of Nucleobase Thioanalogues and Oxo-Derivatives Excited States. *J. Theor. Comput. Chem.* **2009**, *8*, 71−83.
(32) Pollum, M.; Martínez-Fernández, L.; Crespo-Hernández, C. E. Photochemistry of Nucleic Acid Bases and Their Thio- and Aza-Analogues in Solution. *Top. Curr. Chem.* **2014**, *355*, 245−327.
(33) Milne, G. H.; Townsend, L. B. Synthesis and Antitumor Activity of Alpha-and Beta-20-Deoxy-6-Selenoguanosine and Certain Related Derivatives. *J. Med. Chem.* **1974**, *17*, 263−268.
(34) Kaur, M.; Huang, Z. Synthesis and Optical Behaviors of 6-Seleno-Deoxyguanosine. *Sci. China: Chem.* **2014**, *57*, 314−321.
(35) Sheng, J.; Hassan, A.; Huang, Z. Synthesis of the First Tellurium-Derivatized Oligonucleotides for Structural and Functional Studies. *Chem. - Eur. J.* **2009**, *15*, 10210−10216.
(36) Casida, M. E. In *Recent Advances in Density Functional Methods, Part I*; Chong, D. P., Ed.; World Scientific: Singapore: 1995; pp 155−192.
(37) *Gaussian 09*, Revision D.01; Frisch, M. J.; Trucks, G. W.; Schlegel, H. B.; Scuseria, G. E.; Robb, M. A.; Cheeseman, J. R.; Scalmani, G.; Barone, V.; Mennucci, B.; Petersson, G. A.; Nakatsuji, H.; Caricato, M.; Li, X.; Hratchian, H. P.; Izmaylov, A. F.; Bloino, J.; Zheng, G.; Sonnenberg, J. L.; Hada, M.; Ehara, M.; Toyota, K.; Fukuda, R.; Hasegawa, J.; Ishida, M.; Nakajima, T.; Honda, Y.; Kitao, O.; Nakai, H.; Vreven, T.; Montgomery, J. A., Jr.; Peralta, J. E.; Ogliaro, F.; Bearpark, M.; Heyd, J. J.; Brothers, E.; Kudin, K. N.; Staroverov, V. N.; Kobayashi, R.; Normand, J.; Raghavachari, K.; Rendell, A.; Burant, J. C.; Iyengar, S. S.; Tomasi, J.; Cossi, M.; Rega, N.; Millam, J. M.; Klene, M.; Knox, J. E.; Cross, J. B.; Bakken, V.; Adamo, C.; Jaramillo, J.; Gomperts, R.; Stratmann, R. E.; Yazyev, O.; Austin, A. J.; Cammi, R.; Pomelli, C.; Ochterski, J. W.; Martin, R. L.; Morokuma, K.; Zakrzewski, V. G.; Voth, G. A.; Salvador, P.; Dannenberg, J. J.; Dapprich, S.; Daniels, A. D.; Farkas, Ö.; Foresman, J. B.; Ortiz, J. V.; Cioslowski, J.; Fox, D. J. Gaussian, Inc.: Wallingford, CT, 2009.
(38) Becke, A. D. Density-Functional Thermochemistry. III. The Role of Exact Exchange. *J. Chem. Phys.* **1993**, *98*, 5648−5652.
(39) Lee, C.; Yang, W.; Parr, R. G. Development of the Colle-Salvetti Correlation-Energy Formula Into a Functional of the Electron Density. *Phys. Rev. B: Condens. Matter Mater. Phys.* **1988**, *37*, 785−789.
(40) Zhao, Y.; Truhlar, D. G. The M06 Suite of Density Functionals for Main Group Thermochemistry, Thermochemical Kinetics, Noncovalent Interactions, Excited States, and Transition Elements: Two New Functionals and Systematic Testing of Four M06-Class Functionals and 12 Other Functionals. *Theor. Chem. Acc.* **2008**, *120*, 215−241.
(41) Bergner, A.; Dolg, M.; Küchle, W.; Stoll, H.; Preuß, H. Molecular Physics: An International Journal at the Interface Between Chemistry and Physics. *Mol. Phys.* **1993**, *80*, 1431−1441.
(42) Cossi, M.; Barone, V. Solvent Effect on Vertical Electronic Transitions by the Polarizable Continuum Model. *J. Chem. Phys.* **2000**, *112*, 2427−2435.
(43) Tomasi, J.; Menucci, B.; Cammi, R. Quantum Mechanical Continuum Solvation Models. *Chem. Rev.* **2005**, *105*, 2999−3094.
(44) Rinkevicius, Z.; Tunell, I.; Sałek, P.; Vahtras, O.; Ågren, H. Restricted Density Functional Theory of Linear Time-Dependent Properties in Open-Shell Molecules. *J. Chem. Phys.* **2003**, *119*, 34−46.
(45) Ågren, H.; Vahtras, O.; Minaev, B. Response Theory and Calculations of Spin-Orbit Coupling Phenomena in Molecules. *Adv. Quantum Chem.* **1996**, *27*, 71−162.
(46) DALTON. A Molecular Electronic Structure Program. Release Dalton 2011. Available online: http://daltonprogram.org/.
(47) Ruud, K.; Schimmelpfennig, B.; Ågren, H. Internal and External Heavy-Atom Effects on Phosphorescence Radiative Lifetimes Calculated Using a Mean-Field Spin-Orbit Hamiltonian. *Chem. Phys. Lett.* **1999**, *310*, 215−221.
(48) Heß, B. A.; Marian, C. M.; Wahlgren, U.; Gropen, O. A Mean-Field Spin-Orbit Method Applicable to Correlated Wavefunctions. *Chem. Phys. Lett.* **1996**, *251*, 365.
(49) Koseki, S.; Schmidt, M. W.; Gordon, M. S. Effective Nuclear Charges for the First- Through Third-Row Transition Metal Elements in Spin-Orbit Calculations. *J. Phys. Chem. A* **1998**, *102*, 10430.
(50) Hättig, C.; Weigend, F. CC2 Excitation Energy Calculations on Large Molecules Using the Resolution of the Identity Approximation. *J. Chem. Phys.* **2000**, *113*, 5154−5161.
(51) Ahlrichs, R.; Bär, M.; Häser, M.; Horn, H.; Kölmel, C. Electronic Structure Calculations on Workstation Computers: the Program System TURBOMOLE. *Chem. Phys. Lett.* **1989**, *162*, 165−169.

DOI: 10.1021/acs.jcim.6b00486
J. Chem. Inf. Model. XXXX, XXX, XXX−XXX

(52) Weigend, F.; Ahlrichs, R. Balanced Basis Sets of Split Valence, Triple Zeta Valence and Quadruple Zeta Valence Quality for H to Rn: Design and Assessment of Accuracy. *Phys. Chem. Chem. Phys.* **2005**, *7*, 3297−3305.
(53) Pettersen, E. F.; Goddard, T. D.; Huang, C. C.; Couch, G. S.; Greenblatt, D. M.; Meng, E. C.; Ferrin, T. E. UCSF Chimera–a Visualization System for Exploratory Research and Analysis. *J. Comput. Chem.* **2004**, *25*, 1605−1612.
(54) Dapprich, S.; Komáromi, I.; Byun, K. S.; Morokuma, K.; Frisch, M. J. A New ONIOM Implementation in Gaussian 98. 1. The Calculation of Energies, Gradients and Vibrational Frequencies and Electric Field Derivatives. *J. Mol. Struct.: THEOCHEM* **1999**, *462*, 1−21.
(55) Vreven, T.; Byun, K. S.; Komáromi, I.; Dapprich, S.; Montgomery, J. A., Jr; Morokuma, K.; Frisch, M. J. Combining Quantum Mechanics Methods with Molecular Mechanics Methods in ONIOM. *J. Chem. Theory Comput.* **2006**, *2*, 815−26.
(56) Vreven, T.; Morokuma, K. In *Annual Reports in Computational Chemistry*; Spellmeyer, D. C., Ed.; Elsevier: 2006; Vol. 2, pp 35−51.
(57) Clemente, F.; Vreven, T.; Frisch, M. J. In *Quantum Biochemistry*; Matta, C, Ed.; Wiley VCH: Weinheim, 2010; pp 61−84.
(58) Vreven, T.; Morokuma, K. In *Continuum Solvation Models in Chemical Physics: From Theory to Applications*; Mennucci, B, Cammi, R, Eds.; Wiley: 2008.
(59) Cornell, W. D.; Cieplak, P.; Bayly, C. I.; Gould, I. R.; Merz, K. M., Jr.; Ferguson, D. M.; Spellmeyer, D. C.; Fox, T.; Caldwell, J. W.; Kollman, P. A. A Second Generation Force-Field for the Simulation of Proteins, Nucleic-Acids, and Organic-Molecules. *J. Am. Chem. Soc.* **1995**, *117*, 5179−5197.
(60) Rehm, D.; Weller, A. H. Kinetics of Fluorescence Quenching by Electron and H-Atom Transfer. *Isr. J. Chem.* **1970**, *8*, 259−271.
(61) Pollum, M.; Ortiz-Rodríguez, L. A.; Jockusch, S.; Crespo-Hernández, C. E. The Triplet State of 6-thio-2′-deoxyguanosine: Intrinsic Properties and Reactivity Toward Molecular Oxygen. *Photochem. Photobiol.* **2016**, *92*, 286−292.
(62) Crespo-Hernández, C. E.; Close, D. M.; Gorb, L.; Leszczynski, J. Determination of Redox Potentials for the Watson-Crick Base Pairs, DNA Nucleosides, and Relevant Nucleoside Analogues. *J. Phys. Chem. B* **2007**, *111*, 5386−5395.
(63) Schweitzer, C.; Schmidt, R. Physical Mechanisms of Generation and Deactivation of Singlet Oxygen. *Chem. Rev.* **2003**, *103*, 1685−1757.
(64) Lakowicz, J. R. *Principles of Fluorescence Spectroscopy*; Springer: Boston, MA, 2006.
(65) Jacquemin, D.; Perpète, E. A.; Ciofini, I.; Adamo, C. Accurate Simulation of Optical Properties in Dyes. *Acc. Chem. Res.* **2009**, *42*, 326−334.
(66) Eriksson, E. S. E.; Eriksson, L. A. Predictive Power of Long-Range Corrected Functionals on the Spectroscopic Properties of Tetrapyrrole Derivatives for Photodynamic Therapy. *Phys. Chem. Chem. Phys.* **2011**, *13*, 7207−7217.
(67) Adamo, C.; Jacquemin, D. The Calculations of Excited-State Properties with Time-Dependent Density Functional Theory. *Chem. Soc. Rev.* **2013**, *42*, 845−856.
(68) Yang, W.; Zhao, J.; Sonn, C.; Escudero, D.; Karatay, A.; Yaglioglu, G. H.; Küçüköz, B.; Hayvali, M.; Li, C.; Jacquemin, D. Efficient Intersystem Crossing in Heavy-Atom-Free Perylenebisimide Derivatives. *J. Phys. Chem. C* **2016**, *120*, 10162−10175.
(69) Alberto, M. E.; Mazzone, G.; Quartarolo, A. D.; Sousa, F. F. R.; Sicilia, E.; Russo, N. Electronic Spectra and Intersystem Spin-Orbit Coupling in 1,2- and 1,3-Squaraines. *J. Comput. Chem.* **2014**, *35*, 2107−2113.
(70) Alberto, M. E.; De Simone, B. C.; Mazzone, G.; Quartarolo, A. D.; Russo, N. Theoretical Determination of Electronic Spectra and Intersystem Spin−Orbit Coupling: The Case of Isoindole-BODIPY Dyes. *J. Chem. Theory Comput.* **2014**, *10*, 4006−4013.
(71) Alberto, M. E.; De Simone, B. C.; Mazzone, G.; Marino, T.; Russo, N. Photophysical Properties of Free and Metallated Meso-Substituted Tetrabenzotriazaporphyrin from Density Functional Theory Investigation. *Dyes Pigm.* **2015**, *120*, 335−339.
(72) Alberto, M. E.; De Simone, B. C.; Mazzone, G.; Sicilia, E.; Russo, N. The Heavy Atom Effect on Zn(II) Phthalocyanine Derivatives: a Theoretical Exploration of the Photophysical Properties. *Phys. Chem. Chem. Phys.* **2015**, *17*, 23595−601.
(73) Mazzone, G.; Quartarolo, A. D.; Russo, N. PDT-Correlated Photophysical Properties of Thienopyrrole BODIPY Derivatives. Theoretical Insights. *Dyes Pigm.* **2016**, *130*, 9−15.
(74) Mazzone, G.; Alberto, M. E.; De Simone, B. C.; Marino, T.; Russo, N. Can Expanded Bacteriochlorins Act as Photosensitizers in Photodynamic Therapy? Good News from Density Functional Theory Computations. *Molecules* **2016**, *21*, 288.
(75) Pirillo, J.; De Simone, B. C.; Russo, N. Photophysical Properties Prediction of Selenium- and Tellurium-Substituted Thymidine as Potential UVA Chemotherapeutic Agents. *Theor. Chem. Acc.* **2016**, *135*, 8.
(76) Brédas, J. L.; Beljonne, D.; Coropceanu, V.; Cornil, J. Charge-Transfer and Energy-Transfer Processes in π-Conjugated Oligomers and Polymers: A Molecular Picture. *Chem. Rev.* **2004**, *104*, 4971−5004.
(77) Marian, C. M. Spin−Orbit Coupling and Intersystem Crossing in Molecules. *WIREs Comput. Mol. Sci.* **2012**, *2*, 187−203.
(78) El-Sayed, M. A. The Radiationless Processes Involving Change of Multiplicity in the Diazenes. *J. Chem. Phys.* **1962**, *36*, 573−574.
(79) El-Sayed, M. A. Spin-Orbit Coupling and the Radiationless Processes in Nitrogen Heterocycles. *J. Chem. Phys.* **1963**, *38*, 2834−2838.
(80) Kasha, M. Characterization of Electronic Transitions in Complex Molecules. *Discuss. Faraday Soc.* **1950**, *9*, 14−19.
(81) Zhang, Y.; Zhu, X.; Smith, J.; Haygood, M. T.; Gao, R. Direct observation and quantitative characterization of singlet oxygen in aqueous solution upon UVA excitation of 6-thioguanines. *J. Phys. Chem. B* **2011**, *115*, 1889−1894.

DOI: 10.1021/acs.jcim.6b00486
J. Chem. Inf. Model. XXXX, XXX, XXX−XXX

Supporting Information

Photophysical Properties of S, Se and Te-Substituted Deoxyguanosines: Insight into Their Ability To Act as Chemotherapeutic Agents

Jenny Pirillo,[†] Gloria Mazzone,[†]* Nino Russo[†] and Luca Bertini[‡]

[†] *Dipartimento di Chimica e Tecnologie Chimiche, University of Calabria, Via P. Bucci, cubo 14 c, 87036 Rende, Italy*

[‡] *Department of Biotechnologies and Biosciences, University of Milano-Bicocca, Piazza della Scienza 2, I-20126 Milano, Italy*.

***** E-mail: gloria.mazzone@unical.it.

Table of Contents

-Table S1-

Vertical absorption (ΔE) reported in eV and nm, MO contribution (%) and oscillator strengths (*f*) from the low-lying singlet state of S6-deoxyguanosine calculated at TD-B3LYP/6-31+G* level of theory in water and acetonitrile.

		water		acetonitrile	
State	MO contribution	ΔE	*f*	ΔE	*f*
S_1 (nπ*)	H-1→L (100%)	3.46,359	0.000	3.45,360	0.000
S_2 (ππ*)	H→L (95%)	3.89,319	0.434	3.89,319	0.437
T_1 (ππ*)	H→L (99%)	2.71,457	0.000	2.71,457	0.000
T_2 (nπ*)	H-1→L (99%)	3.24,382	0.000	3.23,383	0.000

-Table S2-

Vertical absorption (ΔE) reported in eV and nm, MO contribution (%) and oscillator strengths (*f*) from the low-lying singlet state of S6-deoxyguanosine calculated in water at TD-B3LYP and –M06/6-31+G* levels of theory, with RICC2/def2-TZVP method, QM:MM and QM1:MM approaches.

	MS-CASPT2// SA-CASSCF[a]	B3LYP		M06		RICC2		*QM/MM*		*QM1/MM*	
		ΔE	*f*	ΔE	*f*	ΔE	*f*				
S_1	3.36,369	3.46,359	0.000	3.47,357	0.000	3.25,381	0.000	3.16,392	0.000	3.62,343	0.001
S_2	4.05,306	3.89,319	0.434	3.95,314	0.455	3.97,312	0.355	3.97,312	0.225	3.79,327	0.235
T_1	3.10,400	2.71,457	0.000	2.87,432	0.000	2.93,423	0.000	2.61,475	0.000	2.74,453	0.000
T_2	3.31,375	3.24,382	0.000	3.36,369	0.000	3.11,399	0.000	2.87,431	0.000	3.42,362	0.000

[a] from ref 27 of the main manuscript.

-Table S3-

Contribution of the excitation levels to the excited states wavefunctions computed at RICC2/def2-TZVP level of theory for S6-dGuo.

	E/eV	% singles	% doubles
S_1 (nπ*)	3.25	90.38	9.62
S_2 (ππ*)	3.97	89.34	10.66
T_1 (ππ*)	2.93	92.77	7.23
T_2 (nπ*)	3.11	91.24	8.76

-Figure S1-

QM:MM and QM1:MM models, the QM region without or with the first solvation sphere (equal to 42 water molecules), respectively has been highlighted.

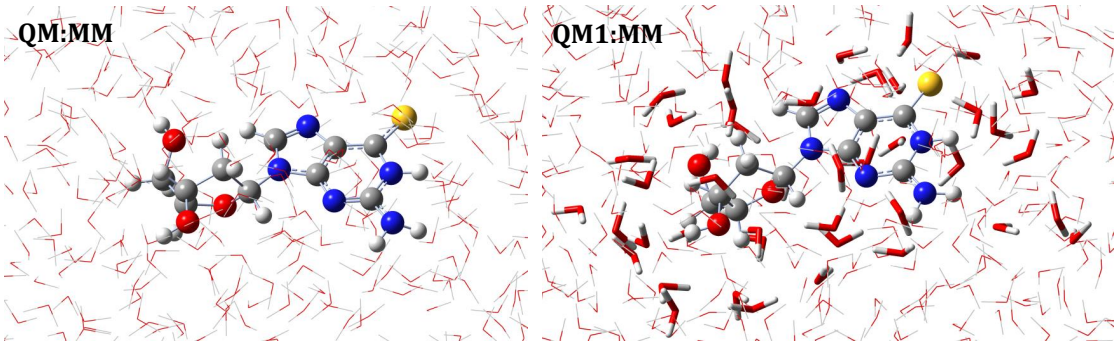

-Table S4-

Cartesian Coordinates of the optimized structures of ground and excited states S_1, S_2, T_1 and T_2 of S6-dGuo, Se6-dGuo and Te6-dGuo.

S6-dGuo	S0			S1			S2			T1			T2		
	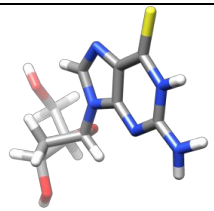			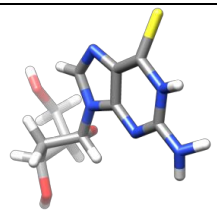			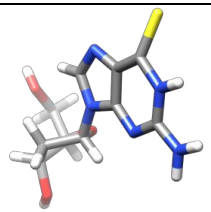			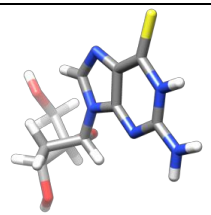			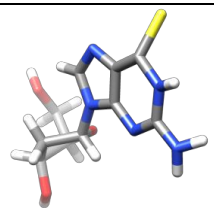		
Atom	X	Y	Z	X	Y	Z	X	Y	Z	X	Y	Z	X	Y	Z
H	-9.542250	0.623168	-2.083705	-9.553036	0.514887	-2.046461	-9.540364	0.651731	-2.084785	-9.541538	0.641663	-2.065589	-9.550583	0.471702	-2.046747
O	-8.581260	0.756233	-2.080506	-8.599869	0.695150	-2.039968	-8.578386	0.777298	-2.077545	-8.579771	0.769050	-2.066240	-8.599745	0.663838	-2.039971
C	-7.976836	-0.275628	-1.293048	-7.942892	-0.336047	-1.295649	-7.983561	-0.271540	-1.305216	-7.978076	-0.269106	-1.285001	-7.930367	-0.358100	-1.293872
H	-8.191280	-1.263309	-1.721904	-8.130862	-1.318560	-1.748395	-8.205157	-1.250686	-1.749647	-8.200629	-1.254034	-1.716004	-8.107397	-1.343730	-1.744238
H	-8.361170	-0.252732	-0.263614	-8.305861	-0.356752	-0.258115	-8.369593	-0.261318	-0.276239	-8.357270	-0.247129	-0.253675	-8.292241	-0.380625	-0.255972
C	-6.467650	-0.074633	-1.248974	-6.441196	-0.081691	-1.276349	-6.472906	-0.083422	-1.255417	-6.467586	-0.077789	-1.247332	-6.431698	-0.086196	-1.276538
H	-6.055539	-0.837098	-0.577267	-5.988967	-0.844506	-0.630616	-6.068061	-0.859662	-0.595308	-6.056994	-0.845055	-0.580324	-5.969954	-0.842133	-0.629381
O	-5.882746	-0.290508	-2.554412	-5.877900	-0.241787	-2.597175	-5.886624	-0.284120	-2.563023	-5.890033	-0.294136	-2.556527	-5.867937	-0.242406	-2.597443
C	-5.290799	0.905831	-3.057711	-5.315798	0.985609	-3.070852	-5.292149	0.916349	-3.050342	-5.293763	0.898222	-3.059101	-5.319945	0.990556	-3.074254
H	-4.202656	0.803302	-3.063469	-4.225427	0.908846	-3.070423	-4.204799	0.807581	-3.065538	-4.206852	0.787283	-3.077705	-4.228761	0.926202	-3.073721
N	-5.675479	1.071232	-4.456258	-5.693946	1.181295	-4.462752	-5.683551	1.109173	-4.446282	-5.691787	1.074258	-4.455994	-5.700198	1.178817	-4.466093
C	-6.963657	1.153891	-4.968226	-6.969964	1.324045	-4.972628	-6.957872	1.211503	-4.943255	-6.970038	1.169345	-4.943735	-6.976584	1.305106	-4.977553
H	-7.820470	1.112525	-4.308123	-7.836192	1.312419	-4.326228	-7.819806	1.164503	-4.290898	-7.833785	1.117670	-4.296649	-7.843986	1.282153	-4.332833
N	-6.997158	1.255554	-6.274854	-6.983563	1.430824	-6.292839	-6.991482	1.317217	-6.278706	-6.993245	1.279574	-6.306000	-6.988103	1.416933	-6.295611
C	-5.666573	1.238451	-6.664396	-5.654247	1.357525	-6.669107	-5.686865	1.274025	-6.675934	-5.703566	1.254402	-6.690957	-5.657623	1.362338	-6.669834
C	-5.071011	1.316533	-7.941344	-5.038904	1.439748	-7.935453	-5.085614	1.400725	-7.959772	-5.090061	1.351802	-7.978737	-5.047659	1.455652	-7.951553
N	-3.677620	1.252713	-7.866367	-3.633829	1.230994	-7.889021	-3.657969	1.297659	-7.895282	-3.648867	1.247683	-7.893134	-3.633090	1.308628	-7.881251
H	-3.192103	1.318742	-8.756917	-3.099858	1.439459	-8.725348	-3.165197	1.376284	-8.778420	-3.154350	1.301556	-8.777131	-3.095286	1.551018	-8.706033
C	-2.937652	1.128016	-6.712794	-2.930711	1.077709	-6.716645	-2.943286	1.127830	-6.743796	-2.948280	1.110710	-6.756303	-2.932504	1.115135	-6.712398
N	-1.584610	1.133016	-6.832029	-1.564750	1.034275	-6.830774	-1.606092	1.009032	-6.829469	-1.608230	1.035999	-6.799085	-1.564820	1.079653	-6.827861
H	-1.148133	0.908860	-7.716789	-1.167617	0.651999	-7.681396	-1.103091	1.071104	-7.704081	-1.083599	1.048946	-7.663159	-1.169956	0.695189	-7.678659
H	-1.065039	0.859257	-6.007491	-1.087557	0.734413	-5.988786	-1.076700	0.862254	-5.980336	-1.104376	0.910670	-5.931555	-1.087460	0.775910	-5.987275
N	-3.489489	1.054644	-5.511676	-3.482838	1.026092	-5.520639	-3.499774	1.066816	-5.525741	-3.514308	1.046407	-5.516688	-3.486760	1.036125	-5.520706
C	-4.832900	1.116054	-5.538229	-4.840760	1.180423	-5.545142	-4.840392	1.120457	-5.537621	-4.849371	1.111996	-5.539505	-4.846409	1.192615	-5.550468
C	-6.000846	1.331219	-0.807856	-6.019053	1.328734	-0.804290	-5.994861	1.311355	-0.792609	-5.988483	1.323371	-0.804765	-6.026198	1.330231	-0.807678
H	-6.753966	1.835872	-0.193438	-6.783280	1.791273	-0.170658	-6.743672	1.812393	-0.169985	-6.735729	1.832435	-0.186832	-6.795811	1.784978	-0.174915
C	-5.758840	2.042242	-2.135527	-5.814254	2.080155	-2.115401	-5.748912	2.041622	-2.109144	-5.746345	2.036275	-2.131445	-5.830507	2.081087	-2.120449
H	-6.695225	2.468870	-2.501785	-6.768106	2.483267	-2.462399	-6.682340	2.481044	-2.467439	-6.680680	2.471490	-2.492720	-6.789024	2.472680	-2.467847
H	-5.014034	2.837062	-2.048949	-5.096973	2.898498	-2.014744	-4.997621	2.828982	-2.011344	-4.994197	2.824229	-2.046113	-5.122588	2.907783	-2.021695
O	-4.748750	1.278520	-0.110750	-4.759646	1.302657	-0.117398	-4.742738	1.238065	-0.097673	-4.734468	1.259866	-0.112228	-4.766543	1.320661	-0.120718
H	-4.884651	0.852218	0.751698	-4.873400	0.846657	0.732974	-4.880959	0.797902	0.757410	-4.870733	0.834209	0.750482	-4.875045	0.865841	0.730970
S	-5.823476	1.469606	-9.447958	-5.872611	1.052110	-9.451988	-5.843473	1.067564	-9.491229	-5.836856	1.377861	-9.514916	-5.819088	0.812080	-9.422065

Se6-dGuo	S0			S1			S2			T1			T2		
	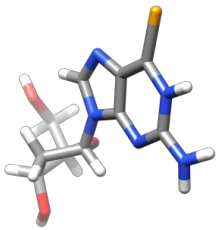			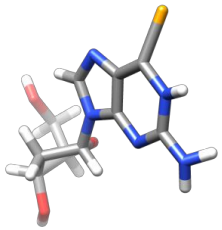			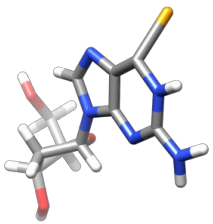			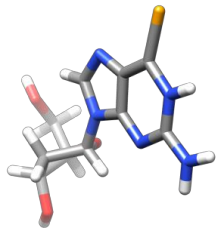			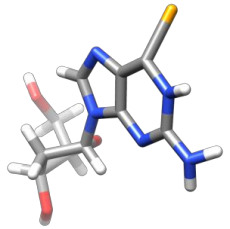		
Atom	X	Y	Z	X	Y	Z	X	Y	Z	X	Y	Z	X	Y	Z
H	-9.541370	0.640760	-2.085919	-9.550764	0.515332	-2.039387	-9.542702	0.653270	-2.084871	-9.546037	0.630806	-2.051086	-9.555205	0.518240	-2.042889
O	-8.579508	0.767388	-2.082859	-8.596855	0.691723	-2.036785	-8.580589	0.777688	-2.079441	-8.584748	0.761540	-2.056141	-8.601178	0.693950	-2.039201
C	-7.981924	-0.267509	-1.293990	-7.941155	-0.341477	-1.294063	-7.984478	-0.280229	-1.320586	-7.976292	-0.272717	-1.275088	-7.946966	-0.340518	-1.296956
H	-8.201302	-1.254096	-1.722779	-8.131840	-1.323193	-1.747418	-8.208276	-1.254214	-1.775182	-8.198121	-1.259470	-1.702350	-8.139870	-1.321841	-1.750208
H	-8.367516	-0.241865	-0.265139	-8.302946	-0.362236	-0.256138	-8.367524	-0.281141	-0.290420	-8.350452	-0.249162	-0.241915	-8.307982	-0.360666	-0.258733
C	-6.471740	-0.074743	-1.248041	-6.438852	-0.090431	-1.276336	-6.473540	-0.093558	-1.273464	-6.466140	-0.076951	-1.245570	-6.444213	-0.092279	-1.280567
H	-6.064327	-0.839515	-0.576188	-5.987589	-0.855133	-0.632169	-6.066903	-0.877186	-0.623094	-6.050017	-0.841290	-0.578466	-5.993505	-0.858692	-0.638013
O	-5.886543	-0.294007	-2.553155	-5.877503	-0.250015	-2.598020	-5.892731	-0.279009	-2.585282	-5.895365	-0.294190	-2.557130	-5.885432	-0.250808	-2.603411
C	-5.289274	0.899255	-3.056167	-5.314207	0.977013	-3.071273	-5.290647	0.925475	-3.056958	-5.300464	0.898600	-3.063343	-5.317431	0.975208	-3.074131
H	-4.201560	0.792233	-3.062400	-4.223936	0.898575	-3.073000	-4.203528	0.812620	-3.067083	-4.213279	0.789276	-3.079373	-4.227408	0.893131	-3.074874
N	-5.673925	1.065296	-4.455192	-5.694684	1.174752	-4.462033	-5.675160	1.135317	-4.449425	-5.696142	1.070089	-4.459867	-5.695708	1.177437	-4.464411
C	-6.962861	1.143373	-4.967942	-6.971827	1.311361	-4.970307	-6.959423	1.259636	-4.951817	-6.973111	1.166297	-4.952479	-6.970699	1.327484	-4.974440
H	-7.819078	1.099890	-4.307016	-7.837159	1.291595	-4.322805	-7.816534	1.216823	-4.292317	-7.837127	1.120244	-4.305020	-7.837725	1.309202	-4.328874
N	-6.997897	1.244748	-6.273997	-6.987663	1.420911	-6.290113	-6.996239	1.386087	-6.264994	-6.996320	1.274554	-6.304609	-6.982097	1.452512	-6.290340
C	-5.667314	1.232849	-6.664908	-5.658331	1.357187	-6.669393	-5.676716	1.342002	-6.667953	-5.699694	1.247788	-6.691878	-5.652552	1.381996	-6.667795
C	-5.070295	1.310264	-7.933328	-5.045884	1.458561	-7.932528	-5.075764	1.534644	-7.929077	-5.083911	1.333266	-7.970420	-5.043562	1.508447	-7.944051
N	-3.682347	1.254553	-7.865947	-3.640121	1.271118	-7.887900	-3.671299	1.386550	-7.870477	-3.647086	1.248760	-7.890465	-3.635735	1.337124	-7.876043
H	-3.198280	1.319092	-8.757434	-3.107504	1.487485	-8.722727	-3.171328	1.523727	-8.743330	-3.150677	1.303117	-8.772807	-3.094605	1.570778	-8.701185
C	-2.938938	1.133317	-6.714154	-2.934084	1.099833	-6.720380	-2.941855	1.174490	-6.732985	-2.945739	1.109953	-6.750115	-2.933726	1.108297	-6.715515
N	-1.588120	1.141913	-6.834087	-1.567999	1.056594	-6.837213	-1.589679	1.110779	-6.840140	-1.602119	1.049449	-6.801307	-1.567485	1.050354	-6.833376
H	-1.147194	0.936948	-7.721054	-1.173283	0.683033	-7.692820	-1.154731	0.926266	-7.735055	-1.086865	1.030533	-7.670581	-1.179115	0.683532	-7.694764
H	-1.062756	0.879768	-6.009606	-1.090321	0.744385	-5.999998	-1.091174	0.765537	-6.029656	-1.095633	0.892810	-5.940649	-1.094364	0.716780	-6.001799
N	-3.490591	1.057791	-5.511648	-3.484643	1.033792	-5.524004	-3.496171	1.076737	-5.525590	-3.511036	1.038981	-5.518130	-3.487394	1.017540	-5.523041
C	-4.832179	1.113407	-5.535994	-4.842877	1.183398	-5.545555	-4.836387	1.162448	-5.536677	-4.851501	1.108061	-5.543137	-4.843229	1.189521	-5.549259
C	-5.997563	1.328559	-0.807138	-6.012954	1.318404	-0.803013	-5.994275	1.295734	-0.795042	-5.989686	1.326789	-0.807997	-6.015125	1.315024	-0.805256
H	-6.747707	1.837150	-0.192339	-6.775052	1.781617	-0.167300	-6.742765	1.790237	-0.166819	-6.735998	1.834790	-0.188036	-6.776203	1.778998	-0.168863
C	-5.752714	2.038222	-2.135020	-5.808923	2.071187	-2.113455	-5.747301	2.040262	-2.103256	-5.755033	2.037005	-2.137275	-5.809428	2.069137	-2.114542
H	-6.687606	2.467882	-2.501555	-6.762557	2.476456	-2.458612	-6.680576	2.484216	-2.456417	-6.692492	2.466966	-2.496796	-6.762297	2.476973	-2.458839
H	-5.004837	2.830172	-2.048945	-5.089897	2.888015	-2.012908	-4.995773	2.826270	-1.996515	-5.006151	2.828612	-2.056584	-5.088659	2.884317	-2.013014
O	-4.745211	1.269504	-0.111050	-4.752336	1.288615	-0.118460	-4.742351	1.213699	-0.100505	-4.732703	1.268734	-0.119990	-4.754605	1.281578	-0.120663
H	-4.882419	0.843461	0.751323	-4.865409	0.831107	0.731200	-4.881265	0.762996	0.748933	-4.864411	0.844427	0.744101	-4.868823	0.823535	0.728543
Se	-5.882249	1.468194	-9.575935	-5.947994	1.054687	-9.574689	-5.869462	0.626080	-9.524111	-5.882794	1.456585	-9.635099	-5.904819	0.827961	-9.543095

Te6-dGuo	S0			S1			S2			T1			T2		
	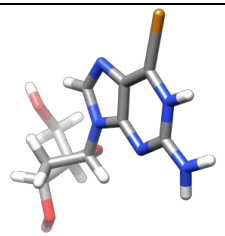			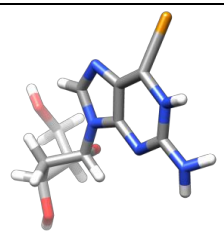			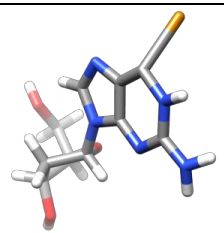			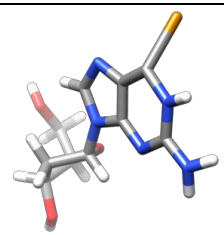			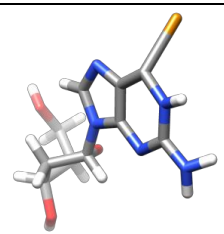		
Atom	X	Y	Z	X	Y	Z	X	Y	Z	X	Y	Z	X	Y	Z
H	-9.538027	0.648566	-2.098473	-9.549610	0.514256	-2.055954	-9.542601	0.643169	-2.091882	-9.546847	0.591271	-2.062985	-9.548708	0.562917	-2.064722
O	-8.575850	0.772672	-2.091523	-8.596139	0.692805	-2.046910	-8.581499	0.774604	-2.079931	-8.588402	0.741074	-2.057088	-8.592053	0.723602	-2.056245
C	-7.984059	-0.263188	-1.299403	-7.941955	-0.344868	-1.309086	-7.980607	-0.294040	-1.340266	-7.963328	-0.313600	-1.317790	-7.956474	-0.328206	-1.321964
H	-8.202946	-1.249423	-1.729199	-8.130165	-1.323632	-1.769766	-8.200519	-1.260858	-1.811782	-8.173876	-1.286628	-1.780865	-8.158030	-1.301230	-1.789064
H	-8.374971	-0.236615	-0.272627	-8.307292	-0.373044	-0.272570	-8.363255	-0.314746	-0.310103	-8.333988	-0.333891	-0.283114	-8.326155	-0.356588	-0.287077
C	-6.473847	-0.072941	-1.245656	-6.439985	-0.092517	-1.284567	-6.470426	-0.101815	-1.290321	-6.455641	-0.098753	-1.286297	-6.450890	-0.099074	-1.290531
H	-6.071157	-0.837997	-0.571374	-5.990116	-0.861117	-0.644092	-6.060757	-0.893379	-0.651436	-6.027516	-0.880396	-0.646999	-6.015057	-0.878969	-0.654173
O	-5.881801	-0.294440	-2.547583	-5.874077	-0.242573	-2.605428	-5.888583	-0.264444	-2.604237	-5.887288	-0.259501	-2.605461	-5.882301	-0.248945	-2.610516
C	-5.283126	0.897698	-3.050075	-5.310349	0.988144	-3.068460	-5.289226	0.949880	-3.056742	-5.302791	0.960380	-3.067872	-5.304077	0.977261	-3.065920
H	-4.195467	0.789930	-3.055624	-4.220014	0.910404	-3.067496	-4.201779	0.840008	-3.064796	-4.214375	0.861705	-3.077220	-4.214762	0.886365	-3.068242
N	-5.666871	1.062693	-4.450297	-5.686706	1.195851	-4.458913	-5.669913	1.179484	-4.445971	-5.687485	1.179825	-4.455717	-5.681335	1.197772	-4.454625
C	-6.956954	1.136328	-4.963280	-6.962757	1.339825	-4.969995	-6.954307	1.326743	-4.949075	-6.963120	1.335026	-4.955814	-6.959451	1.347921	-4.964361
H	-7.811874	1.091684	-4.300498	-7.829418	1.320522	-4.324123	-7.811270	1.295318	-4.288919	-7.825593	1.318792	-4.303532	-7.823376	1.325686	-4.314060
N	-6.995104	1.235799	-6.268439	-6.974930	1.459550	-6.287276	-6.988618	1.462880	-6.256725	-6.988309	1.461149	-6.275304	-6.976437	1.483406	-6.274753
C	-5.664379	1.226684	-6.663885	-5.645016	1.395864	-6.666985	-5.663933	1.404072	-6.661814	-5.673733	1.384314	-6.675596	-5.645714	1.420989	-6.660373
C	-5.070619	1.303382	-7.928748	-5.043288	1.489474	-7.938245	-5.071328	1.563221	-7.929436	-5.076072	1.513065	-7.966701	-5.056645	1.531562	-7.944838
N	-3.685896	1.249867	-7.866542	-3.638730	1.299012	-7.879802	-3.674976	1.405786	-7.863647	-3.650298	1.364168	-7.872036	-3.656639	1.400668	-7.864313
H	-3.196106	1.312067	-8.755497	-3.100285	1.495148	-8.715983	-3.164338	1.546857	-8.730058	-3.128194	1.500920	-8.730245	-3.121594	1.593707	-8.704798
C	-2.938044	1.133447	-6.716082	-2.930813	1.106360	-6.718475	-2.942495	1.173236	-6.728670	-2.944440	1.148491	-6.733989	-2.937510	1.143233	-6.719518
N	-1.588846	1.142573	-6.836913	-1.564981	1.046168	-6.835841	-1.587683	1.101976	-6.847177	-1.584037	1.088194	-6.821235	-1.575110	1.075613	-6.846955
H	-1.144323	0.953863	-7.725517	-1.175036	0.674996	-7.694605	-1.173104	0.861457	-7.738978	-1.150463	0.839395	-7.701667	-1.187816	0.739208	-7.720738
H	-1.058793	0.891367	-6.012168	-1.091433	0.720445	-6.001453	-1.094642	0.749416	-6.036123	-1.111625	0.736546	-5.997785	-1.092927	0.731512	-6.025134
N	-3.488135	1.059577	-5.511319	-3.479839	1.040814	-5.519556	-3.492635	1.075344	-5.523154	-3.500647	1.053180	-5.522230	-3.485620	1.042935	-5.522563
C	-4.826912	1.111096	-5.531001	-4.833796	1.206985	-5.541630	-4.831774	1.203810	-5.533309	-4.845669	1.187332	-5.547442	-4.833533	1.218514	-5.540974
C	-5.999128	1.329774	-0.803714	-6.017036	1.313380	-0.800095	-5.997977	1.281998	-0.789885	-5.998916	1.294637	-0.797220	-6.007682	1.296715	-0.795665
H	-6.751176	1.840232	-0.192812	-6.781845	1.771605	-0.164019	-6.749678	1.763711	-0.155578	-6.752279	1.769072	-0.159363	-6.766042	1.761647	-0.156730
C	-5.747003	2.038307	-2.130981	-5.808958	2.075365	-2.104575	-5.751763	2.047572	-2.086077	-5.773543	2.056113	-2.099265	-5.787599	2.064950	-2.094612
H	-6.679130	2.470855	-2.501141	-6.761770	2.482497	-2.449814	-6.686287	2.493677	-2.433150	-6.716730	2.487415	-2.441568	-6.734367	2.488021	-2.437367
H	-4.997140	2.828037	-2.042161	-5.090868	2.891978	-1.995978	-5.003537	2.834799	-1.965762	-5.035644	2.854545	-1.988731	-5.057858	2.870289	-1.979845
O	-4.750087	1.268965	-0.102081	-4.758899	1.280059	-0.111227	-4.747100	1.194668	-0.093886	-4.741584	1.228786	-0.109831	-4.750525	1.239781	-0.106836
H	-4.891927	0.844140	0.760139	-4.874600	0.816375	0.734708	-4.886054	0.729396	0.747645	-4.867608	0.765272	0.734709	-4.873134	0.770675	0.735119
Te	-6.006542	1.477418	-9.771302	-6.085537	0.872286	-9.707564	-5.973578	0.388617	-9.664529	-5.986201	0.614518	-9.669520	-6.036820	0.480477	-9.673384

➢ Paper III

Theoretical Exploration of Type I/Type II Dual Photoreactivity of Promising Ru(II) Dyads for PDT Approach

Marta Erminia Alberto, Jenny Pirillo, Nino Russo, Carlo Adamo.

*Inorganic Chemistry. (**2016**)*

Inorganic Chemistry

Article

pubs.acs.org/IC

Theoretical Exploration of Type I/Type II Dual Photoreactivity of Promising Ru(II) Dyads for PDT Approach

Marta Erminia Alberto,*[,†] Jenny Pirillo,[‡] Nino Russo,[‡] and Carlo Adamo[†,§]

[†]Chimie ParisTech, PSL Research University, CNRS, Institut de Recherche de Chimie Paris (IRCP), F-75005 Paris, France

[‡]Dipartimento di Chimica e Tecnologie Chimiche, Università della Calabria, Via P. Bucci, 87036 Rende, Italy

[§]Institut Universitaire de France, 103 Boulevard Saint Michel, F-75005 Paris, France

Supporting Information

ABSTRACT: Ru(II) dyads are a class of bioactive molecules of interest as anticancer agents obtained incorporating an organic chromophore in the light-absorbing metallic scaffold. A careful DFT and TDDFT investigation of the photophysical properties of a series of Ru(II)−polypiridyl dyads containing polythiophene chains of different lengths bound to a coordinating imidazo[4,5-*f*][1,10]phenanthroline ligand is herein reported. The modulation of the crucial chemical and physical properties of the photosensitizer with increasing number of thiophene units has been accurately described by investigating the UV−vis spectra and type I and type II photoreactions, also including spin−orbit coupling values (SOC). Results show that the low-lying ^{3}IL states afforded as the number of thiophene ligands increases (n = 3, 4) are energetically high enough to ensure singlet oxygen production and can be also involved in electron transfer reaction, showing a dual type I/type II photoreactivity.

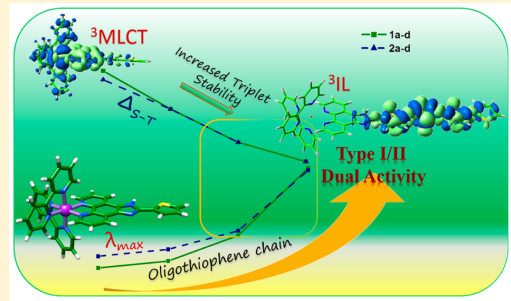

1. INTRODUCTION

Due to their appealing physicochemical properties, Ru(II) compounds have found wide applications in biological and medical fields and are now attracting increasing interest as potential candidates for photodynamic therapy (PDT).[1] The latter is a noninvasive medical approach used for the treatment of several skin diseases and, more recently, for the treatment of some types of cancer.[2] The so-called photodynamic effect rests on the oxidative damage of biological material by reactive forms of oxygen generated by sensitized reactions. As currently practiced, a photosensitizing agent (PS) is injected intravenously and is excited from its ground state S_0 to the first excited state S_1 by using light of a specific wavelength. The S_1 state can relax back to the ground state via a radiative process, the singlet−singlet emission called fluorescence, or via nonradiative intersystem crossing (ISC) from the singlet to triplet state. The triplet state generated by the radiationless intersystem crossing can be quenched through two kinds of processes.

In oxygenated environment and under particular conditions, the chromophore in its excited triplet state can transfer its energy to ground-state molecular oxygen ($^3O_2$), undergoing type II photoreactions.[2] The interaction between electronically excited triplet sensitizer and ground-state molecular oxygen ($^3O_2$) usually involves energy transfer to yield chemically highly active singlet oxygen $^1O_2$, which reacts with many biological molecules, including lipids, proteins, and nucleic acids, leading to cancer cell death. Singlet lowest-energy oxygen $^1O_2(^1\Delta_g)$ can be generated provided that the energy difference Δ_{S-T} of the sensitizer exceeds the energy required to promote the O_2 $^3\Sigma_g^- \rightarrow {}^1\Delta_g$ transition (0.98 eV).[2,3]

On the other hand, the excited PS can react directly with organic substrates by electron exchange producing radical intermediates that are subsequently scavenged by oxygen, with the formation of the superoxide oxygen radical species $O_2^{\bullet(-)}$ and other highly reactive radicals. Collectively these reactions are classified as type I photoreactions.[2,3]

Type II processes are believed to predominate in the induction of cell damage, and their efficiency depends on many factors, among them the triplet state lifetime and the triplet quantum yield (Φ_T) of the photosensitizer. Moreover, sensitizers suitable for PDT should possess (i) a red-shifted electronic absorption band falling in the so-called therapeutic window (600−800 nm) to penetrate human tissues allowing the treatment of deeper tumors, (ii) a high intersystem spin crossing probability, and (iii) a Δ_{S-T} higher than the energy required to generate the singlet oxygen. Other requested properties include solubility in aqueous media, redox stability, absence of intermolecular aggregation phenomena which decreases the photodynamic action, and no toxicity in the dark.

There are a number of photosensitizers whose excited triplet lifetimes are too short to permit a type II process to occur. For this reason, many efforts are devoted to the synthesis of

Received: July 28, 2016
Published: October 18, 2016

DOI: 10.1021/acs.inorgchem.6b01782
Inorg. Chem. 2016, 55, 11185−11192

compounds with excited triplet state having long lifetimes. The strategy to incorporate organic chromophores into Ru(II) scaffolds attempts to accomplish this requirement. The resulting dyad systems are characterized by the installation of an additional low-lying ^{3}IL state of organic triplet character and are able to extend the excited state lifetimes compared to traditional Ru(II) complexes that do not invoke ^{3}IL states. Pyrene chromophore has been employed so far to establish excited state equilibration between the organic ^{3}IL state and the Ru(II)-based ^{3}MLCT.[4] The energy of the organic triplet was further lowered by using spacers to link pyrene to the Ru's phenanthroline ligand,[5] achieving the longest lifetime for Ru(II) dyads to date.[6]

In view of their interesting properties, α-oligothiophenes have been recently used to obtain Ru(II) dyads with promising physicochemical characteristics.[7,8] The in vitro PDT effect of these compounds was found to increase with the polythiophene chain length.[8] Among them, Ru(II)−polypyridyl complexes with three thiophene units (Scheme 1) have been suggested to

Scheme 1. Investigated Molecules

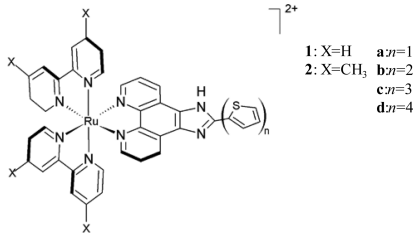

act via a dual type I/II photosensitization process, depending on the tissue oxygen tension, broadening the spectra of applicability of PDT, and it is currently under optimization for clinical phase I trials.[7,8] Moreover, it has been suggested to photocleave DNA when exposed to visible light. Both type I and II pathways hence could play a pivotal role in inducing light-mediated damage to DNA.

In order to shed light on the photochemistry of these molecules, we report a careful DFT and TDDFT investigation of the photophysical properties of Ru(II) dyads containing either 2,2′-bipyridine (bpy) (**1**) or 4,4′-dimethyl-2,2′-bipyridine (dmb) (**2**) as coligands, and in which polythiophene chains of different lengths (**a**, **b**) are incorporated at C2 of the coordinating imidazo[4,5-*f*][1,10]phenanthroline ligand (IP) (Scheme 1).

The influence of the increasing number of thiophene units on the crucial chemical and physical properties of the photosensitizer has been accurately described by investigating the UV−vis spectra and type I and type II photoreactions, also including spin−orbit coupling values (SOC).

Results reveal that all the investigated compounds (**1a−d** and **2a−d**) possess a Δ_{S-T} gap high enough to ensure the O_2 $^3\Sigma_g^- \rightarrow {}^1\Delta_g$ transition, combined with non-negligible SOC values. Nevertheless, 3 or 4 thiophene units are required to allow the installation of a low energy absorption band with an organic character, which could be useful for application in PDT. Inspection of the excited states of all the compounds reveals that a very low lying ^{3}IL state is afforded with the increasing of the thiophene ligands, which could be populated by ISC mechanism and can promote also type I photoreactions, generating a reducing form of the sensitizer subsequently scavenged from oxygen leading to the superoxide anion. A fast bimolecular decay to yield oxidizing species as H_2O_2 and $OH^\bullet$ can, thus, easily take place. Moreover, our results show that $O_2^{\bullet(-)}$ can act itself as reducing agent for other Ru(II) dyads in the triplet state, which may be one rationale for the high phototoxicity induced by these compounds even at low oxygen concentration.

2. COMPUTATIONAL DETAILS

All the calculations herein presented have been performed at DFT and its time-dependent TD-DFT formulation[9] by using the Gaussian 09 program code.[10] A preliminary benchmark study was conducted testing several exchange-correlation functionals (M06,[11] M06L,[12] M062X,[11] B3LYP,[13,14] Cam-B3LYP,[15] PBE0,[16] and ωB97XD[17]) against the experimental data available for molecule **1a**,[18] in methanol. The XC functionals and their performances have been evaluated comparing both calculated geometrical parameters and absorption electronic spectra with available experimental data. The 6-31+G** basis set was used for all atoms except for Ru, which was described by the quasi-relativistic Stuttgart−Dresden pseudopotential.[19] Water environment was simulated by means of the integral equation formalism polarizable continuum model (IEFPCM),[20] which corresponds to a linear response in nonequilibrium solvation. Along the text, λ_{max} will be used to indicate the transition computed at the longest wavelength in each molecule's visible absorption spectra (i.e. the lowest energy transition). Spin−orbit matrix elements were computed by using the quadratic-response TDDFT approach,[21,22] as implemented in the Dalton code,[23] at their ground-state optimized geometries, using the approximate 1-electron spin−orbit operator with scaled nuclear charges.[24] For this purpose, B3LYP was used coupled

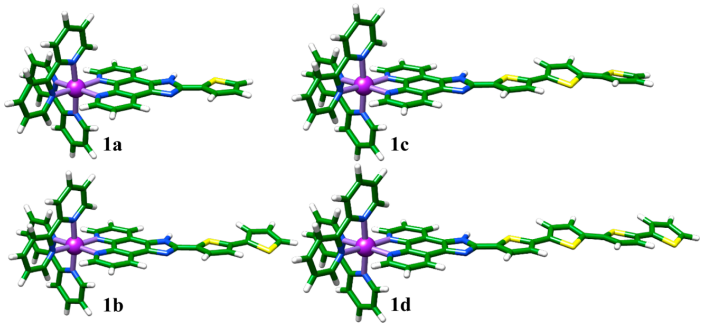

Figure 1. Optimized **1a−1d** molecules, in the most stable conformations.

DOI: 10.1021/acs.inorgchem.6b01782
Inorg. Chem. 2016, 55, 11185−11192

i)

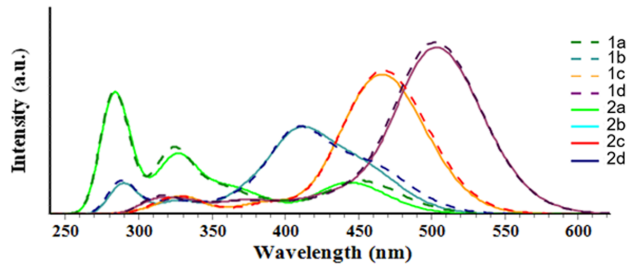

ii)

Ru(II)-Dyad	λ_{max} nm	Main Configuration (%)	f	Ass.
1a *(2a)*	460 *(465)*	H-1→L (72%)	0.067	MLCT
1b *(2b)*	463 (468)	H-2→L (56%); H→L (30%)	0.199	MLCT
1c *(2c)*	474 *(476)*	H→L (33%);H→L+1 (24%)	1.208	LL
1d *(2d)*	503 *(502)*	H→L+1 (48%), H→L+3 (25%), H→L (16%)	2.063	LL

Figure 2. (i) Computed absorption spectra of **1a−d** and **2a−d**, in water, at the M06/6-31+G(d,p)/SDD level of theory. (ii) λ_{max} (above 450 nm) reported in nm, oscillator strengths, *f*, main configuration, and theoretical peak assignment, for **1a−1d** (**2a−2d** in parentheses), in water solvent; see also Figure S2 for more details.

with the cc-pVDZ basis set for all atoms and SDD pseudopotential on the metal ion. Spin−orbit couplings (SOCs) have been defined according to the following formula:

$$SOC_{ij} = \sqrt{\sum_{n} |\langle \psi_{S_i} | \hat{H}_{SO} | \psi_{T_{j,n}} \rangle|^2}\ ;\ n = x, y, z$$

where $\hat{H}_{SO}$ is the spin−orbit Hamiltonian.

3. RESULTS AND DISCUSSION

3.1. Benchmark of XC Functionals and Ground-State Properties. In order to select the most appropriate XC functional to accurately describe geometrical parameters and electronic transition energies for the systems under evaluation, a series of preliminary computations have been carried out testing several XC density functionals against the experimental data available for molecule **1a**,[18] in methanol (see Table S1 and Figure S1). Results, collected in Table S1, show that PBE0[16] reproduces with great accuracy the geometrical parameters, and it has been chosen as the most suitable XC functional for the ground-state molecular optimizations. Nevertheless, the computed absorption spectra reveal that M06[11] outperforms significantly the other XC functionals in the reproduction of the absorption spectra, and in particular at high wavelengths, although PBE0 gives also good results (see Figure S1). The computed absorption peaks for **1a** in methanol are in good agreement with the experimental bands, as is reported in Figure S2. Each band has been assigned on the basis of the involved molecular orbitals. The very good performances of M06 have emerged also in previous studies on metallic compounds.[25,26]

The optimized **1a−1d** structures are reported in Figure 1. The very similar structures obtained for **2a−2d** and selected geometrical parameters are reported in Figure S3.

The introduction of the electron-donating thiophene group onto the Ru-coordinated electron-withdrawing IP unit extends the molecular planarity of the rigid imidazole-containing phenanthroline ligand. The dihedral angles between the adjacent imidazole and thiophene ring are found to be equal to 3.5° in the presence of one thiophene ligand (**1a**, **2a**) and slightly vary as the chain grows, reaching the minimum value with a 4-unit chain (**1d**, **2d**).

The Ru(II) center maintains its nearly ideal octahedral geometry along the **a−d** series, and the sequential addition of thiophene units does not have any effect on the Ru−N distances, which keeps the same average values in all the complexes. The increasing of the chain provides more conformational flexibility, and the additional thio units (**b−d**) adopt positions which deviate from the thiophene−IP plane.

Different conformations have been tested for complexes with more than 2 thiophene units. The addition of the groups with sulfur atoms in trans between them resulted in more stable structures, although the cis conformations lie in a range of very few kcal/mol compared with trans analogues. Anyway, cis and trans isomers display very similar photophysical properties, and the conclusion herein derived for trans compounds can be easily transferred also on cis isomers. (see Figures S4, S5)

3.2. UV−Vis Absorption Spectra. In order to evaluate the effect of the variable number of thiophene units on the photophysical properties of Ru^{II}-dyads, the electronic absorption spectra of molecules **1a−d** and **2a−d** have been computed in water and their superposition is reported in Figure 2, together with main photophysical parameters. The visible region of the spectrum is the most interesting one for the purpose of this investigation, and will be discussed in detail along the text. Nevertheless, absorption bands falling in the UV region are also reported in Figure 2.

Looking at Figure 2, significant differences can be underlined in going from **1a** and **2a** to dyads containing more than one thiophene unit. Actually, with the increasing of the delocalized π-system, the Ru(II)-dyads become more efficient light absorbers in the visible region.

Compounds **1a** and **2a** show the most intense bands in the UV region, computed at 282 and 330 nm in both cases and characterized as IL bands. The computed values are in great agreement with the experimental ones available for molecule **1a**[18] (289 and 330 nm). On the contrary, at higher wavelengths

DOI: 10.1021/acs.inorgchem.6b01782
Inorg. Chem. 2016, 55, 11185−11192

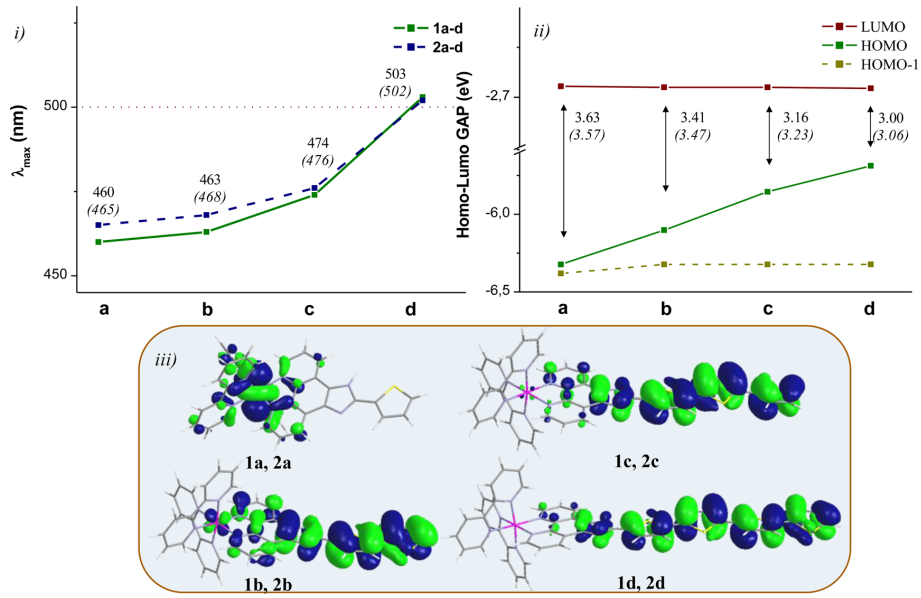

Figure 3. Plot of (i) maximum absorption wavelength λ_{max} and (ii) HOMO−LUMO gap, for **1a−d** and **2a−d** (in parentheses), and (iii) Ru(II)-based HOMO for **1a** and **2a** and IP-based HOMOs for molecules **1b−d** and **2b−d**, at the M06/6-31+G(d,p)/SDD level of theory, in water.

only two weaker bands were experimentally observed, at 425 and 461 nm.[18] Both of them have been characterized by the computed absorption spectrum. According to our results, the band experimentally found at 425 nm, arises from two transitions of comparable intensity, computed at 439 and 443 nm, MLCT in nature, while the lowest energy transition has been computed at 460 nm. (See Figure S2 for more detailed information).

On the contrary, Ru(II)-dyads with polythiophene chains mostly absorb visible light. The intensity and wavelenght of λ_{max} increase systematically with n reaching, in the case of n = 3 and n = 4, the highest values.

Such effect is a direct consequence of the reduced HOMO−LUMO gap observed as the number of thiophenes increases, as reported in Figure 3. Actually, the highest-occupied molecular orbital changes in nature along the **a−d** series, being clearly metal-based in the case of **1a** and **2a** whereas it is localized on the imidazo-phenanthroline (IP) ligand when n = 2, 3, and 4. The incorporation of a polythiophene chain into the Ru(II) scaffold, thus, produce the installation of an additional HOMO orbital of organic character lying at higher energies in the case of n >1, leaving the HOMO-1 orbitals at the same energy and with the same Ru(II)-based character of the **1a** and **2a** HOMO (see Figure 3 and Figure S6). On the contrary, the LUMO orbital does not suffer any change with the chain extension, being localized on the polypiridyl ligand in all cases (see Figures S6, S7).

The lowest energy transition is then MLCT in nature in the case of **1a** and **1b** (and **2a** and **2b**), while neither in **1c** (**2c**) nor in **1d** (**2d**) does it include the metal contribution, the donor and acceptor orbitals, in both cases, being localized on the ligands. This effect produces a shift of the λ_{max} at high wavelengths and enables compounds with n = 3 and n = 4 to absorb in region above 475 nm not accessible to classical Ru(II)-polypiridyl compunds. The increasing of n results to be useful to move the visible absorption band to lower energy, changing its nature from a MLCT to a ligand-ligand one, opening interesting perspective on the use of Ru-polypiridyl polythiophene complexes (n = 3, 4) as candidate photosensitizers for PDT.

3.3. Type I/II Photoreactions. The ability of a sensitizer to promote type II photoreactions depends on the efficiency of the energy transfer process between the excited triplet photosensitizer and molecular oxygen required to generate the singlet cytotoxic species $^1O_2$. To ensure the O_2 $^3\Sigma_g^- \rightarrow {}^1\Delta_g$ transition and to achieve a good singlet oxygen quantum yield, a PS must possess a singlet−triplet energy gap larger than that of O_2 to allow the energy transfer process to take place. Obviously, an efficient triplet state population by ISC mechanism from a singlet state is an indispensable requirement. The lowest singlet state for oxygen has been computed to be 0.90 eV,[27] in good agreement with the experimental value of 0.98 eV.

The plot of singlet−triplet energy gap (Δ_{S-T}) reported in Figure 4 shows that all compounds could promote the formation of singlet oxygen, the first triplet state of all the investigated dyads lying above the O_2 $^3\Sigma_g^-$ one.

Interestingly, the plot reveals that the first triplet state experiences a great stabilization as a function of n. Indeed, the triplet state of **1a** and **2a** dyads has been localized at 2.30 and 2.23 eV, respectively, and reduces in energy systematically as the polythiophene chain increases, reaching the minimum value of 1.59 and 1.60 eV for **1d** and **2d**, respectively. The observed drop in the triplet state energy derives from the π-expansive polythiophene chromophore which confers an organic IL character to the excited state. Actually, while the T_1 state for **1a** and **2a** is a ^{3}MLCT state, in Ru(II) dyads with polythiophene chains from 2 to 4 we observe the installation of low-lying ^{3}IL states. The analysis of the electronic difference density plots between S_0 and T_1 excited state (Figure 4ii) shows the

DOI: 10.1021/acs.inorgchem.6b01782
Inorg. Chem. 2016, 55, 11185−11192

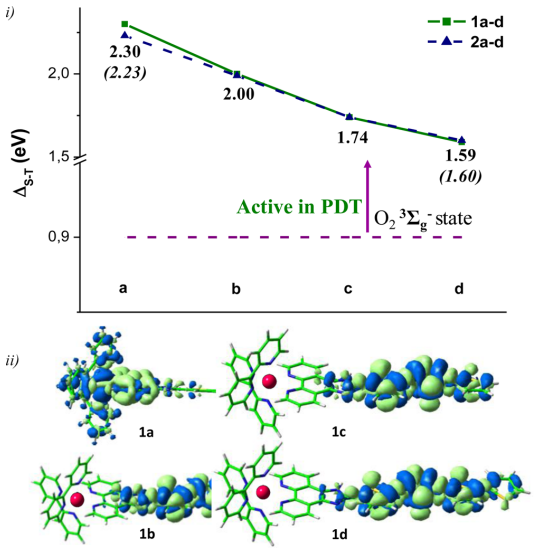

Figure 4. (i) Singlet−triplet energy gap(Δ_{S-T}) for **1a−d** and **2a−d**, in water, at the M06/6-31+G(d,p)/SDD level of theory. If different, values relative to **2a−d** compounds are reported in italics, in parentheses. (ii) Electron density difference plots between S_0 and T_1, for **1a−1d** molecules.

involvement of Ru metal in the case of **1a** while it confirms the triplet IL nature for $n \geq 2$. It is not surprising that the triplet state energy computed for dyads with more than one thiophene unit is similar to that found for the corresponding free α-oligothiophene (see Figure S8), confirming the increasing organic nature of the triplet state with n (i.e., 2.00 eV vs 2.31 eV for **1b** and dithiophene (**2T**), 1.74 eV against 1.96 eV for **1c** and trithiophene (**3T**), and 1.59 vs 1.62 eV for **1d** and **4T**). In the case of **1a** (and **2a**) compounds, the same it is not true, the triplet state energy of the dyad being greatly stabilized with respect to that computed for the free thiophene ligand, sustaining the metal involvement in the triplet state (2.30 eV vs 3.44 eV for **1a** and thiophene, respectively). It should be recalled that the drop in ^{3}IL state energy has been connected with longer lifetimes[8] for Ru(II) dyads.

The energy diagram for the lowest S_n and T_m excited states is reported in Figure S9. A large number of triplet states lie below the first bright excited singlet one, and each one could contribute to populate the T_1 state by internal conversion, provided that an efficient intersystem spin crossing process takes place from excited singlet states. To establish the feasibility of the intersystem crossing process, spin−orbit coupling values (SOC) between several excited singlet and triplet states have been computed for molecules **1a−1d** and **2a−2d**. Values are reported in Table S2. The rationalization of the obtained data is not trivial, but the comparison between them allows us to devise some considerations. The highest SOC values are obtained for compounds **1a** and **2a**, in which just one thiophene group is linked to the IP ligand. The most favorable channel for them involves high excited singlet and triplet states. It is noteworthy that, in the case of **1a** and **2a** molecules, the S_5 is the first bright state. Actually, the highest values are found for the channels involving S_5 and the lower S_4 state, with triplet states very close in energy to them (T_7, T_8, T_9, and T_{10}). Table 1 lists the SOC values of the major ISC channels (S_n to T_m) of **1a** and **2a**, together with the S_n-T_m

Table 1. SOC Values (cm^{-1}) and Singlet−Triplet Energy Gap ΔS_n-T_m (eV) for the Major ISC Channels Involving S_n (n = 4, 5) and T_m (m = 7, 8, 9, 10) States, for 1a and 2a Molecules

	1a (2a)				
n, m	SOC (S_n-T_m)	ΔS_n-T_m	n, m	SOC (S_n-T_m)	ΔS_n-T_m
4, 7	229 (193)	0.14 (0.14)	5,7	354 (291)	0.20 (0.17)
4, 8	306 (43)	0.14 (0.06)	5,8	283 (41)	0.17 (0.09)
4, 9	47 (311)	0.04 (0.00)	5,9	46 (204)	0.07 (007)
4, 10	345 (56)	0.02 (−0.02)	5,10	168 (158)	0.05 (0.05)

energy gaps. In view of the high spin−orbit values computed for them, a direct ISC channel from S_5 and S_4 states to very close triplet states could be then hypothesized. SOC of comparable order of magnitude (>150 cm^{-1}) have been also recently reported for another Ru(II) compound.[26]

On the contrary, compounds containing an increasing number of thiophenes (n > 2) display SOC values relatively small and equal to few tens of cm^{-1} (see Table S2). This result can be ascribed to the increasing organic character imparted to the occupied molecular orbitals by the polythiophene chain. Accordingly, the smallest values are those displayed by **1d** and **2d** dyads. Nevertheless, it should be recalled that values between 0.2 and 5.0 cm^{-1} are considered large enough to induce ISC on a nanosecond time scale[28] and that organic molecules approved for PDT display very small SOC values even though they are able to efficiently produce the cytotoxic singlet oxygen.[29] As a consequence, a population of triplet states can be hypothesized for all the investigated compounds.

The populated excited triplet state could also follow a different deactivation pathway photogenerating the superoxide anion $O_2^{\bullet(-)}$ and ROS, instead of transferring its energy to produce the singlet oxygen species. For **1c** and **2c** dyads, the possibility to switch to a type I mechanism mediating photoinduced electron transfer reactions was previously suggested.[8] The feasibility of such kinds of photoreactions can be established computing the vertical electron affinity (VEA) and ionization potentials (VIP) for each molecule and molecular oxygen.[30] Results are listed in Table 2.

Type I reactions involve electron or hydrogen atom transfer between the excited sensitizer (usually T_1) and substrate molecules, such as the cell membrane or the sensitizer itself, to yield radical ions and free radicals. These radicals can then

Table 2. VEA and VIP Values (eV) in Water, for $^3O_2$ Molecule and for 1a−1d and 2a−2d Ru(II) Dyads in Their Singlet and Triplet States, Computed at PBE0/6-31+G/SDD[a]**

	1a (*2a*)	1b (*2b*)	1c (*2c*)	1d (*2d*)
VEA	−2.87 (*−2.81*)	−2.88 (*−2.82*)	−2.88 (*−2.82*)	−2.88 (*−2.82*)
VIP	5.94 (*5.61*)	5.72 (*5.71*)	5.48 (*5.48*)	5.33 (*5.33*)
VEA (T_1)	−4.90 (*−5.04*)	−4.88 (*−4.82*)	−4.62 (*−4.56*)	−4.47 (*−4.42*)
VIP (T_1)	3.64 (*3.38*)	3.72 (*3.71*)	3.74 (*3.74*)	3.74 (*3.73*)

[a]The O_2 electron affinity (−3.42 eV) has been computed at the same level of theory.

DOI: 10.1021/acs.inorgchem.6b01782
Inorg. Chem. 2016, 55, 11185−11192

interact with oxygen to produce oxygenated products. Different pathways can be followed to generate $O_2^{\bullet(-)}$ species which then undergo fast bimolecular decay to yield oxidizing species as H_2O_2 and $OH^{\bullet}$, able to promote reactions with biomolecules.[2]

The superoxide anion $O_2^{\bullet(-)}$ can be produced by direct electron transfer from the photosensitizer to molecular oxygen according to reaction 1:

$$Ps(S_0) + {}^3O_2 \rightarrow Ps^{\cdot(+)} + O_2^{\cdot(-)} \quad (1)$$

Such a reaction is still of type II oxygen reactions and results to be less feasible as the thiophene chain grows. With the increasing of n indeed, the triplet state becomes weaker as electron donors and is not able to promote the direct electron transfer in water. According to our data, only in the case of **2a** is the process, to some extent, likely to occur, the sum of VIP(T_1) and the electron affinity of $^3O_2$ (−3.43 eV at the same level of theory) being slightly negative.

An alternative pathway to generate $O_2^{\bullet(-)}$ may proceed through electron transfer from the reduced form of dyads to molecular oxygen, provided that the summation of the electron affinity of $^3O_2$ and VEA PS (S_0/T_1) is negative:

$$Ps^{\cdot(-)} + {}^3O_2 \rightarrow {}^1Ps + O_2^{\cdot(-)} \quad (2)$$

The $Ps^{\bullet(-)}$ species could be formed in solution in the presence of electron donors in the near vicinity, e.g., a DNA base, or through the so-called autoionization reactions (eq 3 and eq 4), which imply the reduction of the T_1 state of Ps by neighboring S_0 or the T_1 state of Ps itself (type I photoreactions):

$$Ps(T_1) + Ps(S_0) \rightarrow Ps^{\cdot(+)} + Ps^{\cdot(-)} \quad (3)$$

$$Ps(T_1) + Ps(T_1) \rightarrow Ps^{\cdot(+)} + Ps^{\cdot(-)} \quad (4)$$

According to our results, the T_1 states of all the compounds can be reduced through autoionization reactions by neighboring T_1 ones, the sum of VEA (T_1) and VIP (T_1) being negative. More interestingly, all the reduced dyads can transfer an electron to the molecular oxygen in its ground state through reaction 2 producing the superoxide anion, as confirmed by the higher electron affinity of oxygen if compared with that of the sensitizer. Moreover, the superoxide anion can act itself as reducing agent for dyads in the triplet state, which may be one rationale for the fact that the phototoxicity induced by these compounds is high even at low oxygen concentration.

Based on our results, all the investigated dyads can undergo type I photoreactions. Nevertheless, only compounds containing 3 and 4 thiophene ligands display a low energy absorption band to be useful in PDT through type II mechanism. They are, accordingly, able to afford low-lying ^{3}IL states which can contribute to the dual type I/II photoreactivity, and exert their phototoxicity at different oxygen tension.

4. CONCLUSIONS

A careful DFT and TDDFT investigation has been carried out on very promising Ru(II) dyads incorporating polythiophene chains of different lengths. The influence of the increasing number of thiophene units ($1 \leq n \leq 4$) on the crucial chemical and physical properties of the photosensitizer has been accurately described by investigating the UV−vis spectra and type I and type II photoreactions, also including spin−orbit coupling values (SOC).

Results reveal that the incorporation of a polythiophene chain into Ru(II) scaffold produces the installation of an additional HOMO orbital of organic character lying at higher energies in the case of $n > 1$, shifting the λ_{max} toward higher wavelengths and enabling compounds with $n = 3$ and $n = 4$ to absorb in region above 475 nm not accessible to classical Ru(II)-polypiridyl compunds. The organic chromophore produces a change of the absorption band which acquires an increased ^{1}LL nature as the chain grows. More importantly, results reveal that the increasing of the π-expansive polythiophene chromophore confers an organic IL character to the first triplet excited state producing a systematic drop in its energy. The first triplet state changes from being a ^{3}MLCT to a pure ^{3}IL state when $n = 3$ and 4. In all cases, the Δ_{S-T} gap is high enough to ensure the O_2 $^3\Sigma_g^- \rightarrow {}^1\Delta_g$ transition combined with non-negligible SOC values which indicate an efficient triplet population by ISC mechanism. The magnitudes of SOC values are inversely proportional to the chain length and decrease with the increasing of the organic character of the involved states. The high activity experimentally found for compound **1c** can be then ascribed to the efficient energy transfer from the stable ^{3}IL state to oxygen, accessible by ISC mechanism after irradiation with a low energy source. The same conclusion can be extended to **2c**, **1d**, and **2d** compounds.

Results show that the populated triplet states can undergo also type I photoreactions, generating a reducing form of the sensitizer subsequently scavenged from oxygen leading to the superoxide anion. A fast bimolecular decay to yield oxidizing species as H_2O_2 and $OH^{\bullet}$ can, thus, easily take place in all cases. Moreover, our results show that $O_2^{\bullet(-)}$ can act itself as reducing agent for other Ru(II) dyads in the triplet state, which may be one rationale for the high phototoxicity induced by these compounds even at low oxygen concentration.

■ ASSOCIATED CONTENT

Supporting Information

The Supporting Information is available free of charge on the ACS Publications website at DOI: 10.1021/acs.inorgchem.6b01782.

Selected geometrical parameters of optimized molecules, detailed computed UV−vis spectra, MO plots, diagram of S_n and T_n vertical excitation states, energy and SOC values for **1a−d** and **2a−d**, and additional data on less stable conformers (PDF)

■ AUTHOR INFORMATION

Corresponding Author

*E-mail: marta.alberto@chimie-paristech.fr.

Funding

This project has received funding from the European Union's Horizon 2020 research and innovation program under the Marie Sklodowska-Curie Grant Agreement No. 652999.

Notes

The authors declare no competing financial interest.

■ ACKNOWLEDGMENTS

M.E.A. gratefully acknowledges the Research Executive Agency (REA) for the MSCA Individual Fellowship grant.

■ REFERENCES

(1) (a) Padilla, R.; Rodriguez-Corrales, J. A.; Donohoe, L. E.; Winkel, B. S. J.; Brewer, K. J. A new class of Ru(II) polyazine agents with potential for photodynamic therapy. *Chem. Commun.* **2016**, *52*, 2705−2708. (b) Wachter, E.; Heidary, K.; Howerton, B. S.; Parkin, S.; Glazer,

DOI: 10.1021/acs.inorgchem.6b01782
Inorg. Chem. 2016, 55, 11185−11192

E. C. Light-activated ruthenium complexes photobind DNA and are cytotoxic in the photodynamic therapy window. *Chem. Commun.* **2012**, *48*, 9649−9651. (c) Mari, C.; Pierroz, V.; Ferrari, S.; Gasser, G. Combination of Ru(II) complexes and light: new frontiers in cancer therapy. *Chem. Sci.* **2015**, *6*, 2660−2686. (d) Farrer, N. J.; Salassa, L.; Sadler, P. J. Photoactivated chemotherapy (PACT): the potential of excited-state d-block metals in medicine. *Dalton Trans.* **2009**, 10690−10701. (e) Liu, Y.; Hammitt, R.; Lutterman, D. A.; Joyce, L. E.; Thummel, R. P.; Turro, C. Ru(II) complexes of new tridentate ligands: unexpected high yield of sensitized $^1O_2$. *Inorg. Chem.* **2009**, *48*, 375−385.

(2) (a) Quirk, B. J.; Brandal, G.; Donlon, S.; Vera, J. C.; Mang, T. S.; Foy, A. B.; Lew, S. M.; Girotti, A. W.; Jogal, S.; LaViolette, P. S.; Connelly, J. M.; Whelan, H. T. Photodynamic therapy (PDT) for malignant brain tumors−where do we stand? *Photodiagn. Photodyn. Ther.* **2015**, *12*, 530−544. (b) Dolmans, D.E.J.G.J.; Fukumura, D.; Jain, R. K. Photodynamic therapy for cancer. *Nat. Rev. Cancer* **2003**, *3*, 380−387. (c) Yano, S.; Hirohara, S.; Obata, M.; Hagiya, Y.; Ogura, S.-I.; Ikeda, A.; Kataoka, H.; Tanaka, M.; Joh, T. Current states and future views in photodynamic therapy. *J. Photochem. Photobiol., C* **2011**, *12*, 46−67. (d) Castano, A. P.; Mroz, P.; Hamblin, M. R. Photodynamic therapy and anti-tumour immunity. *Nat. Rev. Cancer* **2006**, *6*, 535−545. (e) Castano, A. P.; Demidova, T. N.; Hamblin, M. R. Mechanisms in photodynamic therapy: part one-photosensitizers, photochemistry and cellular localization. *Photodiagn. Photodyn. Ther.* **2004**, *1*, 279−293.

(3) (a) Lang, K.; Mosinger, J.; Wagnerová, D. M. Photosensitized singlet oxygen and its applications. *Coord. Chem. Rev.* **2004**, *248*, 321−350. (b) DeRosa, M. C.; Crutchley, R. J. *Coord. Chem. Rev.* **2002**, *233*−*234*, 351−371.

(4) (a) McClenaghan, N. D.; Leydet, Y.; Maubert, B.; Indelli, M. T.; Campagna, S. Excited-state equilibration: a process leading to long-lived metal-to-ligand charge transfer luminescence in supramolecular systems. *Coord. Chem. Rev.* **2005**, *249*, 1336−1350. (b) Reichardt, C.; Pinto, M.; Wächtler, M.; Stephenson, M.; Kupfer, S.; Sainuddin, T.; Guthmuller, J.; McFarland, S. A.; Dietzek, B. Photophysics of Ru(II) Dyads Derived from Pyrenyl-Substitued Imidazo[4,5-f][1,10]-phenanthroline Ligands. *J. Phys. Chem. A* **2015**, *119*, 3986−3994.

(5) Monro, S.; Scott, J.; Chouai, A.; Lincoln, R.; Zong, R.; Thummel, R. P.; McFarland, S. A. Photobiological Activity of Ru(II) Dyads Based on (Pyren-1-yl)ethynyl Derivatives of 1,10-Phenanthroline. *Inorg. Chem.* **2010**, *49*, 2889−2900.

(6) Lincoln, R.; Kohler, L.; Monro, S.; Yin, H.; Stephenson, M.; Zong, R.; Chouai, A.; Dorsey, C.; Hennigar, R.; Thummel, R. P.; McFarland, S. A. Exploitation of Long-Lived ^{3}IL Excited States for Metal−Organic Photodynamic Therapy: Verification in a Metastatic Melanoma Model. *J. Am. Chem. Soc.* **2013**, *135*, 17161−17175.

(7) (a) McFarland, S. A. Metal-based Thiophene Photodynamic Compounds and Their Use. US provisional patent 61624391 filed April 15, 2012, PCT/US13/36595 filed April 15, 2013. (b) http://theralase.com/pressrelease/theralase-files-us-patent-applicationincreased-targeting-photo-dynamic-therapy/.

(8) (a) Shi, G.; Monro, S.; Hennigar, R.; Colpitts, J.; Fong, J.; Kasimova, K.; Yin, H.; DeCoste, R.; Spencer, C.; Chamberlain, L.; Mandel, A.; Lilge, L.; McFarland, S. A. Ru(II) dyads derived from α-oligothiophenes: A new class of potent and versatile photosensitizers for PDT. *Coord. Chem. Rev.* **2015**, *282*−*283*, 127−138. (b) Arenas, Y.; Monro, S.; Shi, G.; Mandel, A.; McFarland, S.; Lilge, L. Photodynamic inactivation of *Staphylococcus aureus* and methicillin-resistant *Staphylococcus aureus* with Ru(II)-based type I/type II photosensitizers. *Photodiagn. Photodyn. Ther.* **2013**, *10*, 615−625. (c) Kaspler, P.; Lazic, S.; Forward, S.; Arenas, Y.; Mandel, A.; Lilge, L. A ruthenium(II) based photosensitizer and transferrin complexes enhance photo-physical properties, cell uptake, and photodynamic therapy safety and efficacy. *Photochem. Photobiol. Sci.* **2016**, *15*, 481−495.

(9) Casida, M. E. In *Recent Developments and Applications of Modern Density Functional Theory*; Seminario, J. M., Ed.; Elsevier: Amsterdam, The Netherlands, 1996; pp 155−192.

(10) Frisch, M. J.; Trucks, G. W.; Schlegel, H. B.; Scuseria, G. E.; Robb, M. A.; Cheeseman, J. R.; Scalmani, G.; Barone, V.; Mennucci, B.; Petersson, G. A.; Nakatsuji, H.; Caricato, M.; Li, X.; Hratchian, H. P.; Izmaylov, A. F.; Bloino, J.; Zheng, G.; Sonnenberg, J. L.; Hada, M.; Ehara, M.; Toyota, K.; Fukuda, R.; Hasegawa, J.; Ishida, M.; Nakajima, T.; Honda, Y.; Kitao, O.; Nakai, H.; Vreven, T.; Montgomery, J. A., Jr.; Peralta, J. E.; Ogliaro, F.; Bearpark, M.; Heyd, J. J.; Brothers, E.; Kudin, K. N.; Staroverov, V. N.; Kobayashi, R.; Normand, J.; Raghavachari, K.; Rendell, A.; Burant, J. C.; Iyengar, S. S.; Tomasi, J.; Cossi, M.; Rega, N.; Millam, J. M.; Klene, M.; Knox, J. E.; Cross, J. B.; Bakken, V.; Adamo, C.; Jaramillo, J.; Gomperts, R.; Stratmann, R. E.; Yazyev, O.; Austin, A. J.; Cammi, R.; Pomelli, C.; Ochterski, J. W.; Martin, R. L.; Morokuma, K.; Zakrzewski, V. G.; Voth, G. A.; Salvador, P.; Dannenberg, J. J.; Dapprich, S.; Daniels, A. D.; Farkas, Ö.; Foresman, J. B.; Ortiz, J. V.; Cioslowski, J.; Fox, D. J. *Gaussian 09, Revision E.01*; Gaussian, Inc.: Wallingford, CT, 2009.

(11) Zhao, Y.; Truhlar, D. G. The M06 suite of density functionals for main group thermochemistry, thermochemical kinetics, noncovalent interactions, excited states, and transition elements: two new functionals and systematic testing of four M06-class functionals and 12 other functionals. *Theor. Chem. Acc.* **2008**, *120*, 215−241.

(12) Zhao, Y.; Truhlar, D. G. A new local density functional for main-group thermochemistry, transition metal bonding, thermochemical kinetics, and noncovalent interactions. *J. Chem. Phys.* **2006**, *125*, 194101.

(13) Becke, D. Density-functional thermochemistry. III. The role of exact exchange. *J. Chem. Phys.* **1993**, *98*, 5648−5652.

(14) Lee, C.; Yang, W.; Parr, R. G. Development of the Colle-Salvetti correlation-energy formula into a functional of the electron density. *Phys. Rev. B: Condens. Matter Mater. Phys.* **1988**, *37*, 785−789.

(15) Yanai, T.; Tew, D.; Handy, N. A new hybrid exchange? Correlation functional using the Coulomb-attenuating method (CAM-B3LYP). *Chem. Phys. Lett.* **2004**, *393*, 51−57.

(16) Adamo, C.; Barone, V. Toward reliable density functional methods without adjustable parameters: The PBE0 model. *J. Chem. Phys.* **1999**, *110*, 6158−6169.

(17) Chai, J.-D.; Head-Gordon, M. Long-range corrected hybrid density functionals with damped atom−atom dispersion corrections. *Phys. Chem. Chem. Phys.* **2008**, *10*, 6615−6620.

(18) Xu, F.; Peng, Y.-X.; Hu, B.; Tao, T.; Huang, W. Comparative structural and spectral analyses for mononuclear and dinuclear metal complexes of 2-thiophen and 2-(5-bromothiophen) imidazo[4,5-f][1,10]phenanthroline. *CrystEngComm* **2012**, *14*, 8023−8032.

(19) Andrae, D.; Haussermann, U.; Dolg, M.; Stoll, H.; Preuss, H. Energy-adjusted *ab initio* pseudopotentials for the second and third row transition elements. *Theor. Chim. Acta* **1990**, *77*, 123−141.

(20) (a) Cossi, M.; Barone, V. Solvent effect on vertical electronic transitions by the polarizable continuum model. *J. Chem. Phys.* **2000**, *112*, 2427−35. (b) Tomasi, J.; Mennucci, B.; Cammi, R. Quantum mechanical continuum solvation models. *Chem. Rev.* **2005**, *105*, 2999−3094.

(21) Rinkevicius, Z.; Tunell, I.; Sałek, P.; Vahtras, O.; Ågren, H. Restricted density functional theory of linear time-dependent properties in open-shell molecules. *J. Chem. Phys.* **2003**, *119*, 34−46.

(22) Ågren, H.; Vahtras, O.; Minaev, B. Response Theory and Calculations of Spin-Orbit Coupling Phenomena in Molecules. *Adv. Quantum Chem.* **1996**, *27*, 71−162.

(23) *DALTON. A molecular electronic structure program*. Release Dalton 2016. http://daltonprogram.org/.

(24) Koseki, S.; Schmidt, M. W.; Gordon, M. S. Effective Nuclear Charges for the First- through Third-Row Transition Metal Elements in Spin−Orbit Calculations. *J. Phys. Chem. A* **1998**, *102*, 10430−10435.

(25) Latouche, C.; Skouteris, D.; Palazzetti, F.; Barone, V. TD-DFT Benchmark on Inorganic Pt(II) and Ir(III) Complexes. *J. Chem. Theory Comput.* **2015**, *11*, 3281−3289.

(26) Alberto, M. E.; Russo, N.; Adamo, C. Synergistic Effects of Metals in a Promising Ru^{II}−Pt^{II} Assembly for a Combined Anticancer Approach: Theoretical Exploration of the Photophysical Properties. *Chem. - Eur. J.* **2016**, *22*, 9162−9168.

(27) Alberto, M. E.; De Simone, B. C.; Mazzone, G.; Sicilia, E.; Russo, N. The heavy atom effect on Zn(II) phthalocyanine derivatives:

DOI: 10.1021/acs.inorgchem.6b01782
Inorg. Chem. 2016, 55, 11185−11192

a theoretical exploration of the photophysical properties. *Phys. Chem. Chem. Phys.* **2015**, *17*, 23595−23601.
(28) Klessinger, M. In *Theoretical and Computational Chemistry*, Cyril, P., Ed.; Elsevier: 1998; Vol. *5*, pp 581−610.
(29) Alberto, M. E.; Marino, T.; Quartarolo, A. D.; Russo, N. Photophysical origin of the reduced photodynamic therapy activity of temocene compared to Foscan®: insights from theory. *Phys. Chem. Chem. Phys.* **2013**, *15*, 16167−16171.
(30) Llano, J.; Raber, J.; Eriksson, L. A. Theoretical study of phototoxic reactions of psoralens. *J. Photochem. Photobiol., A* **2003**, *154*, 235−243.

DOI: 10.1021/acs.inorgchem.6b01782
Inorg. Chem. 2016, 55, 11185−11192

-Supporting Information-

A theoretical exploration of TypeI/TypeII dual photoreactivity of promising Ru(II)-dyads for PDT approach

Marta Erminia Alberto,[a] Jenny Pirillo,[b] Nino Russo,[b] Carlo Adamo [a,c]*

[a] *Chimie ParisTech, PSL Research University, CNRS, Institut de Recherche de Chimie Paris (IRCP), F-75005 Paris, France. E-mail: marta.alberto@chimie-paristech.fr*

[b]*Dipartimento di Chimica e Tecnologie Chimiche, Università della Calabria, Via P. Bucci, 87036 Rende, Italy*

[c] *Institut Universitaire de France, 103 Boulevard Saint Michel, F-75005 Paris, France*

-Table S1-

Table S1. Selected bond lengths (Å) and torsion angles (°) for complex **1a**, obtained by using different XC functional, in methanol solvent

Table S1.

	X-ray	M06	M06L	M062X	B3LYP	Cam-B3LYP	PBE0	wB97XD
Ru-N1	2.082(3)	2.089(3)	2.097(9)	2.119(3)	2.105(5)	2.100(4)	2.077(4)	2.095(4)
Ru-N2	2.056(1)	2.087(7)	2.096(8)	2.118(6)	2.104(9)	2.099(5)	2.076(9)	2.097(6)
Ru-N3	2.065(7)	2.081(2)	2.089(1)	2.110(5)	2.097(9)	2.093(7)	2.070(8)	2.089(0)
Ru-N4	2.029(4)	2.082(1)	2.089(5)	2.109(8)	2.098(5)	2.093(5)	2.070(7)	2.086(1)
Ru-N5	2.049(5)	2.080(1)	2.088(0)	2.108(7)	2.096(8)	2.092(2)	2.069(2)	2.086(9)
Ru-N6	2.051(2)	2.083(5)	2.090(1)	2.111(9)	2.098(8)	2.094(2)	2.071(3)	2.088(9)
N7-C1-C2-S	9.0(5)	4.3(9)	3.3(9)	9.4(5)	2.5(6)	4.4(4)	3.5(4)	14.7(8)

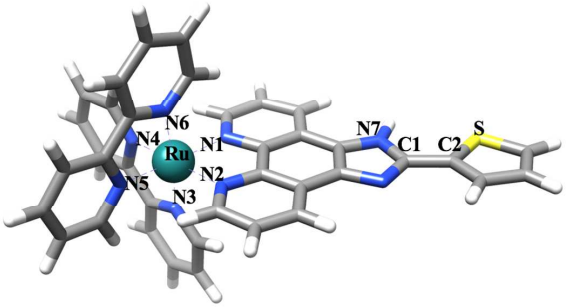

- Figure S1-

Figure S1. a) Computed Absorption Spectra of molecule **1a**, obtained by using several XC functional, in methanol solvent, on PBE0/6-31+G**/SDD optimized geometries; b) B3LYP, PBE0 and M06 spectra extracted from a) for clarity

a)

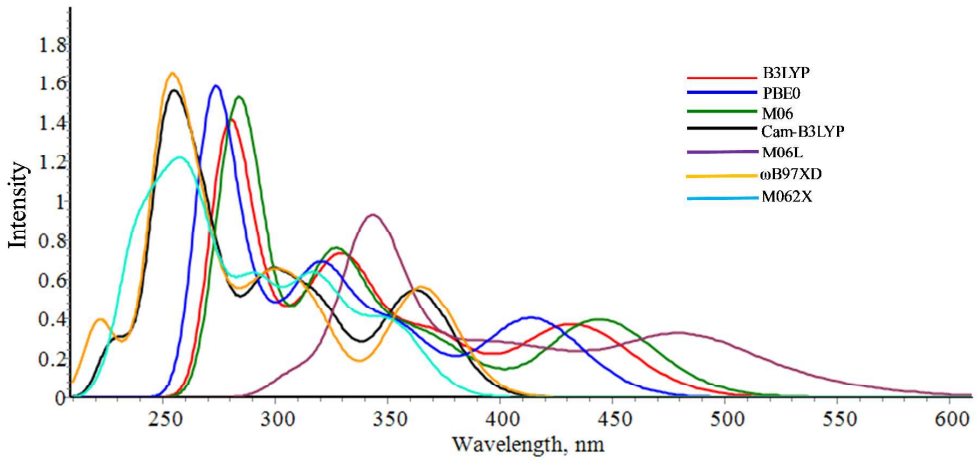

b)

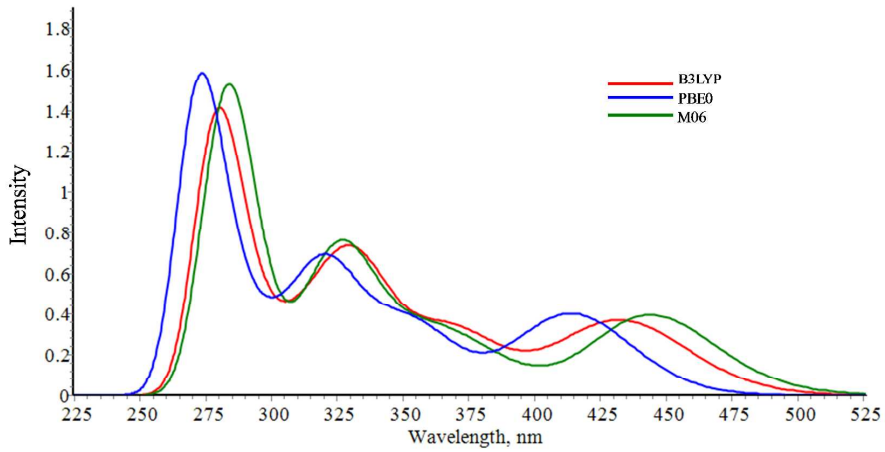

-Figure S2-

Figure S2. Detailed Computed Absorption Spectrum of molecule **1a,** at M06/6-31+G**/SDD level of theory and experimental values in the box, in methanol solvent.

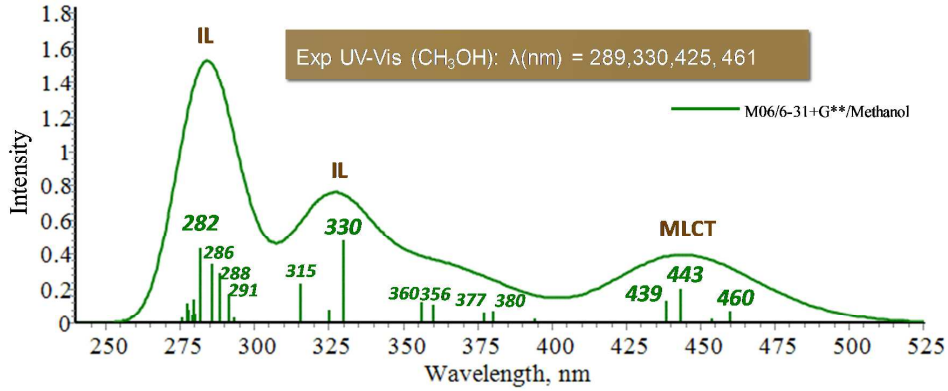

1a

Exp (nm)	*ΔE (eV, nm)[2a]*	*Main Configuration (%)*	*f*	*Theoretical Assignment*
461	2.69, 460*[465]*	H-1→L (70%)	0.0651	MLCT
425	2.80, 443*[451]*	H-2→L+1 (36%), H-1→L+2 (46%)	0.1936	MLCT
	2.83, 439*[444]*	H-2→L+2 (49%), H-1→L+1 (25%)	0.1282	
330	3.76, 330*[330]*	H-3→L+4 (26%), H-1→L+4 (15%), H-1→L+5 (47%)	0.474	IL
289	4.40, 282*[283]*	H-7→L(25%), H-3→L+6 (26%), H-1→L+9 (19%)	0.4295	IL

-Figure S3-

Figure S3. a) Optimized **2a-2d** molecules, in the most stable conformations, at PBE0/6-31+G**/SDD level of theory, in water solvent; b) Selected bond lengths (Å) and torsion angles (°) for complexes **1a-d** and **2a-d** in water solvent

a)

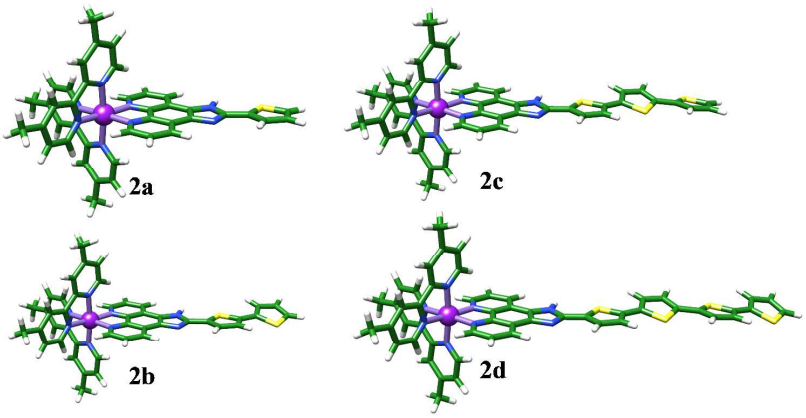

b)

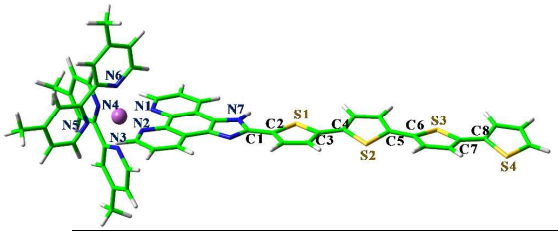

	1a	2a	1b	2b	1c	2c	1d	2d
Ru-N1	2.077	2.075	2.077	2.075	2.077	2.075	2.077	2.075
Ru-N2	2.077	2.075	2.077	2.075	2.077	2.075	2.077	2.075
Ru-N3	2.071	2.071	2.071	2.071	2.071	2.071	2.071	2.072
Ru-N4	2.071	2.071	2.070	2.071	2.070	2.071	2.070	2.071
Ru-N5	2.069	2.070	2.069	2.070	2.069	2.070	2.069	2.070
Ru-N6	2.071	2.072	2.071	2.072	2.071	2.072	2.071	2.072
N7-C1-C2-S1	-3.5	-3.5	-3.3	-3.5	-2.4	-2.4	-0.9	-1.4
S1-C3-C4-S2			-163.4	-163.5	-166.5	-166.4	-167.3	-166.9
S2-C5-C6-S3					161.7	162.0	164.6	164.3

S3-C7-C8-S4	-161.7	-161.3

-Figure S4-

Figure S4. Optimized **1a-1d** molecules in less stable conformations and relative energies in kcal/mol, compared with most stable conformations.

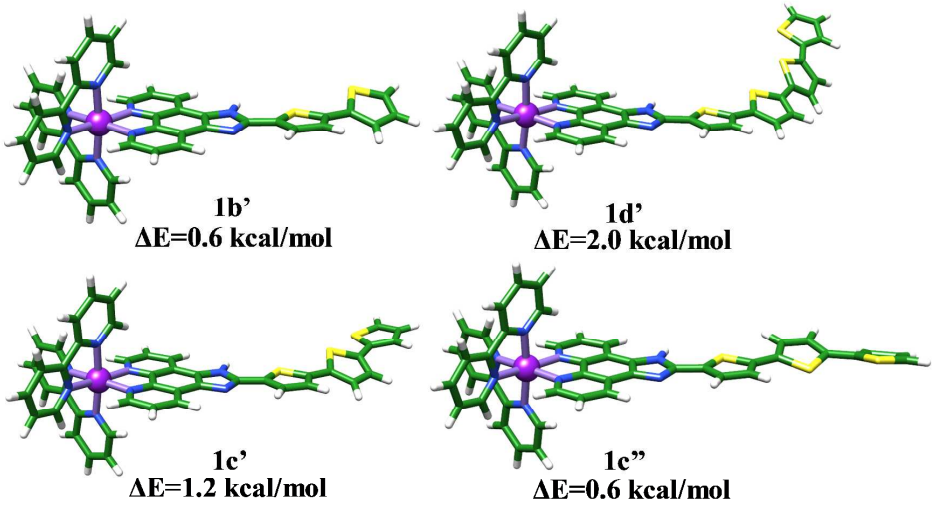

-Figure S5-

Figure S5. Main photophysical properties of “cis” isomers 1b’,1c’ and 1d’: a) Superposition between cis and trans UV-Vis spectra obtained for 1a-1d molecules; b) Singlet-triplet energy gaps; c) Comparison between SOC values obtained for 1c and 1c’ molecules

a)

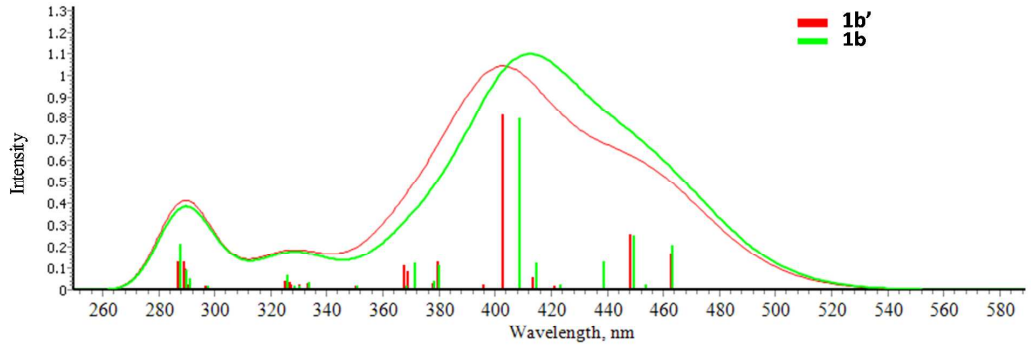
1b'
1b
Intensity
Wavelength, nm

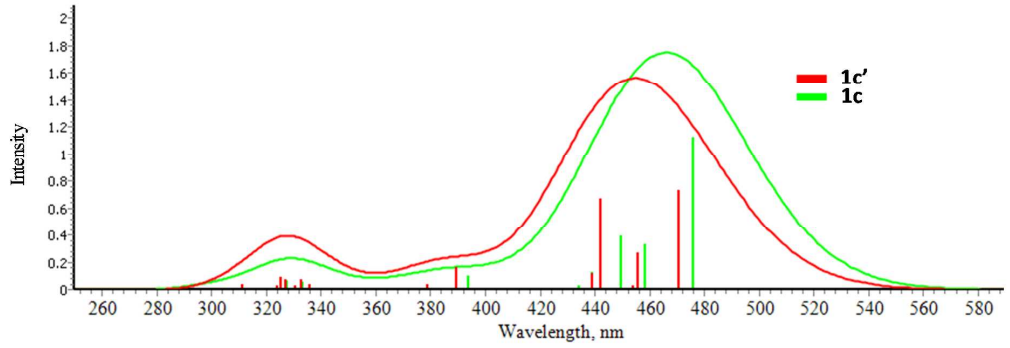
1c'
1c
Intensity
Wavelength, nm

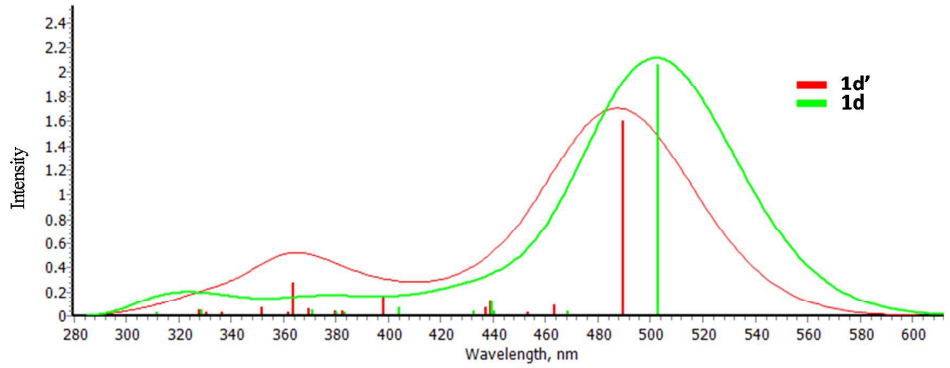
1d'
1d
Intensity
Wavelength, nm

b)

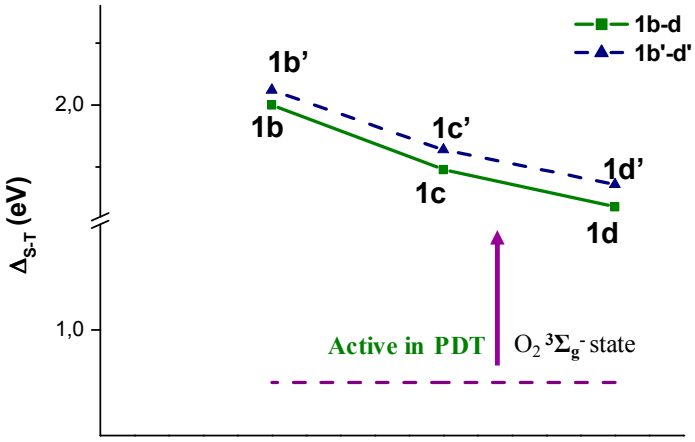

c)

SOC VALUES 1C (1C')

	T1	T2	T3	T4	T5	T6	T7
S1	0.14(0.13)	10.26(10.17)	2.23(2.18)	5.44(5.51)	1.60(1.37)	1.85(1.40)	8.90(8.88)
S2		0.21(0.21)	23.66(23.82)	17.02 (17.16)	8.90 (8.80)	9.70 (8.49)	13.57(14.33)
S3			0.39 (0.11)	11.49 (11.57)	2.73(2.65)	6.03 (5.13)	18.83 (19.29)
S4				0.97(1.45)	4.71(0.35)	4.71(6.30)	10.83 (12.22)

-Figure S6-

Figure S6. ***1)*** Molecular Orbitals (MOs) energetic diagram (eV), for **1a-1d** complexes and ***2)*** Plots of the MOs involved in the UV-Vis spectrum transitions, with the contribution of bpy (cyan), IP (yellow) and Ru (red) fragments to each MO

1)

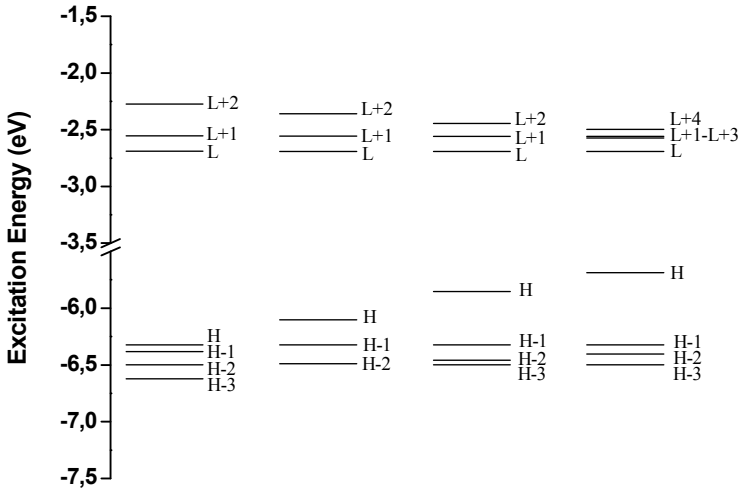
Excitation Energy (eV)
-1,5
-2,0
-2,5
-3,0
-3,5
-6,0
-6,5
-7,0
-7,5
L+2
L+1
L
H
H-1
H-2
H-3
L+2
L+1
L
H
H-1
H-2
L+2
L+1
L
H
H-1
H-2
H-3
L+4
L+1-L+3
L
H
H-1
H-2
H-3

2)

1a)

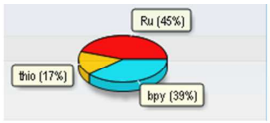

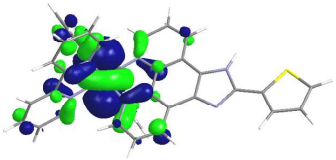

Homo

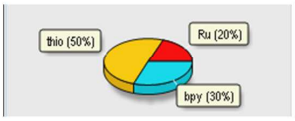

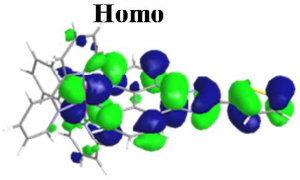

Homo-1

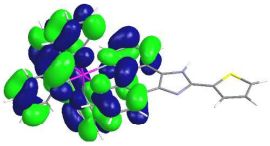

bpy-based Lumo, Lumo+1, Lumo+2

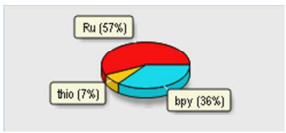

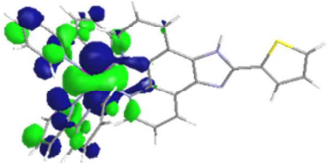

Homo-2

1b)

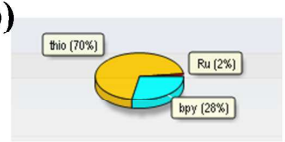

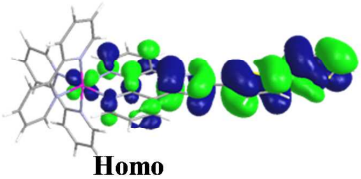

Homo

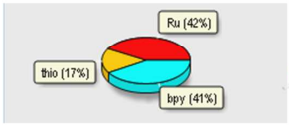

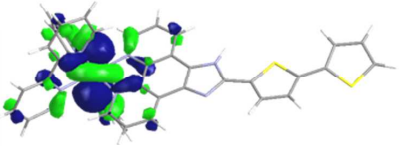

Homo-1

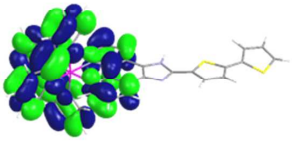

bpy-based Lumo, Lumo+1, Lumo+2

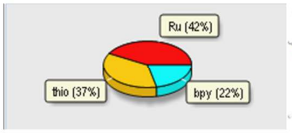

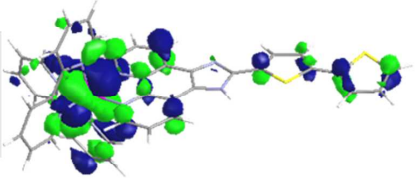

Homo-2

1c)

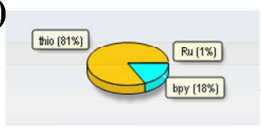

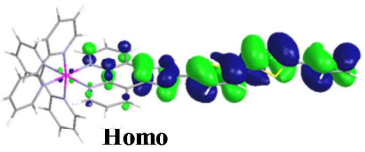

Homo

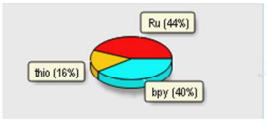

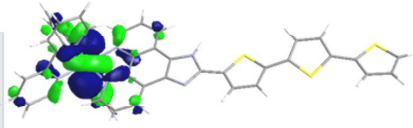

Homo-1

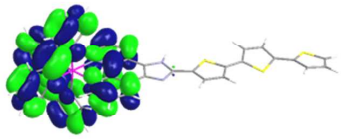

bpy-based Lumo, Lumo+1, Lumo+2

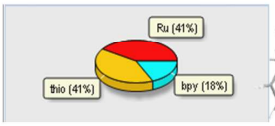

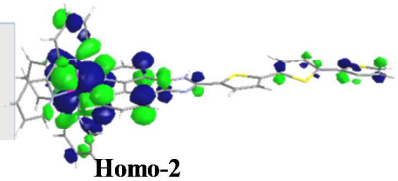

Homo-2

1d)

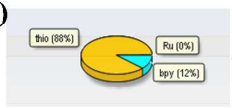

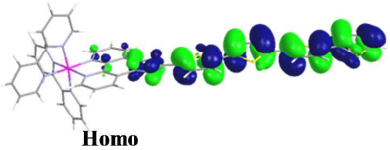

Homo

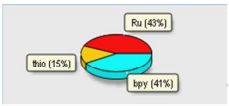

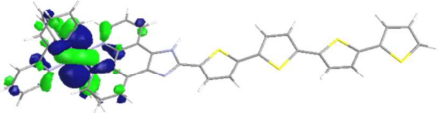

Homo-1

bpy-based Lumo, Lumo+1, L+2,L+3,L+4

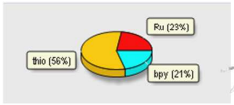

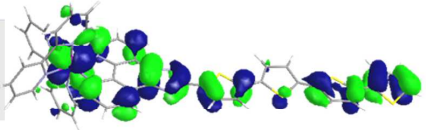

Homo-2

-Figure S7-

Figure S7. Plots of the MOs involved in the UV-Vis spectrum transitions for 2a-2d molecules

2a)

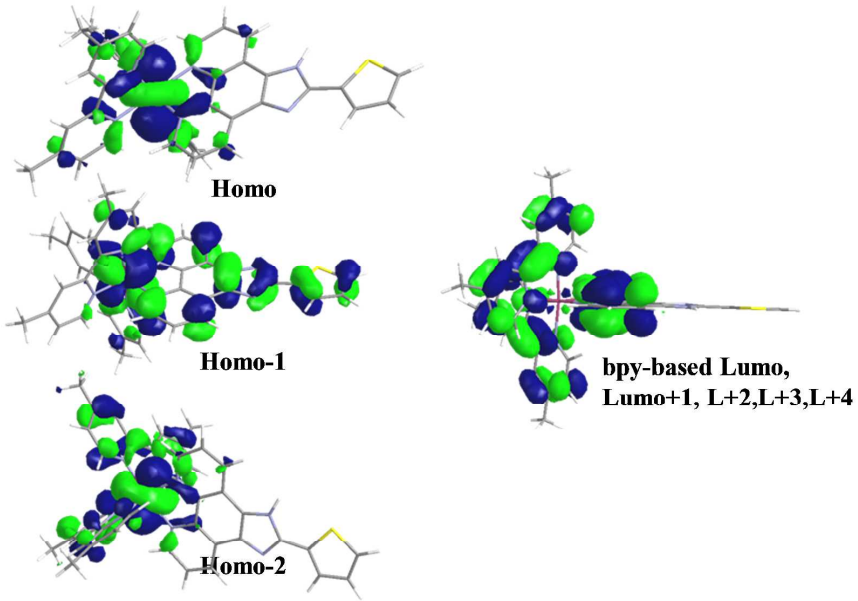

2b)

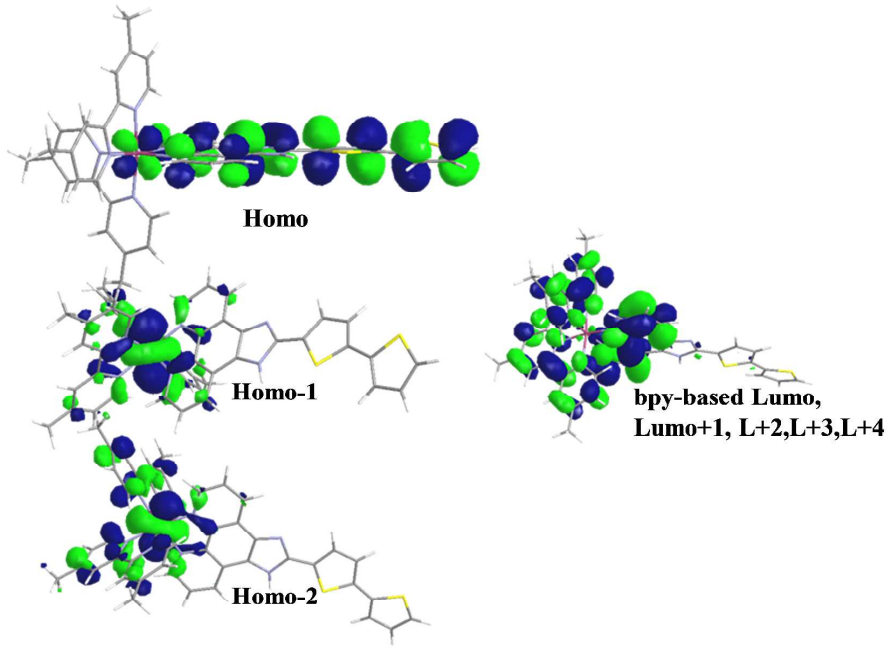
Homo
Homo-1
Homo-2
bpy-based Lumo,
Lumo+1, L+2,L+3,L+4

2c)

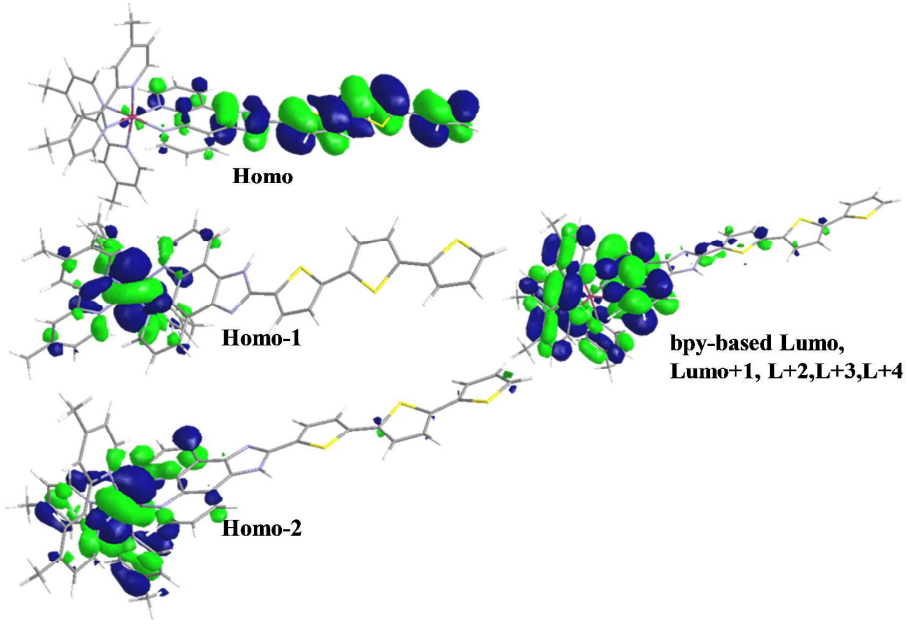
Homo
Homo-1
Homo-2
bpy-based Lumo,
Lumo+1, L+2,L+3,L+4

2d)

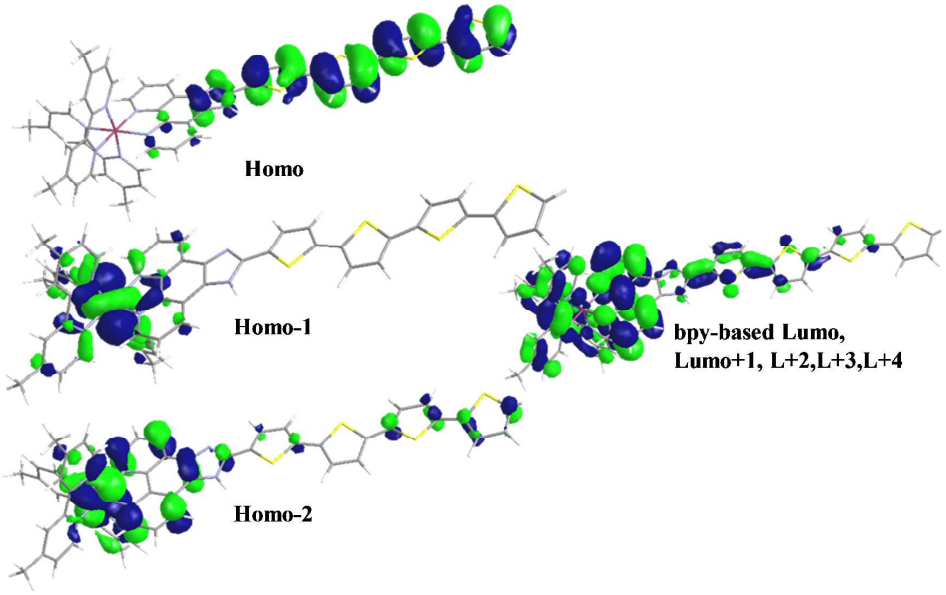

-Figure S8-

Figure S8. ***a)*** Comparison between singlet-triplet energy gap(Δ_{S-T}) of **1a-d** and (oligo)thiophene ligands **1-4T**, in water, at the M06/6-31+G(d,p) level of theory. Optimized structures of **1-4T** are displayed in the figure;

b) Comparison between λ_{max} of **1a-d** and (oligo)thiophene ligands **1-4T**, in water, at the M06/6-31+G(d,p) level of theory.

a)

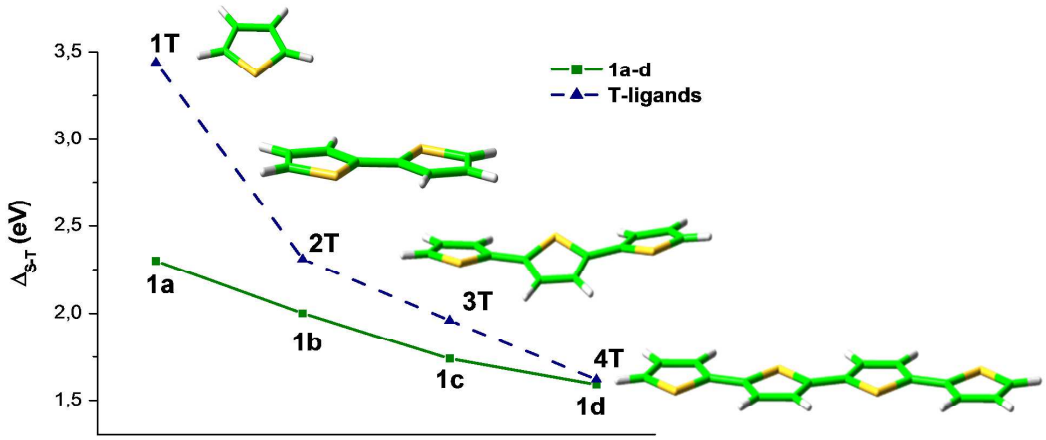

b)

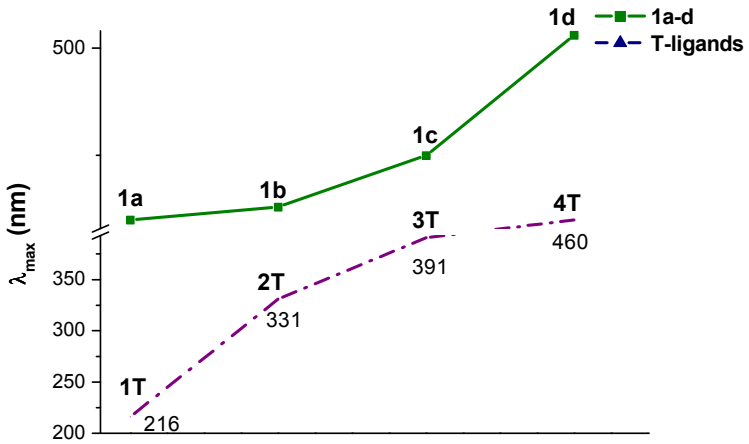

-Figure S9-

Figure S9. ***a)*** Diagram of S_n and T_n vertical excitation states and ***b)*** energy values (eV), for **1a-d** and **2a-d** molecules

a)

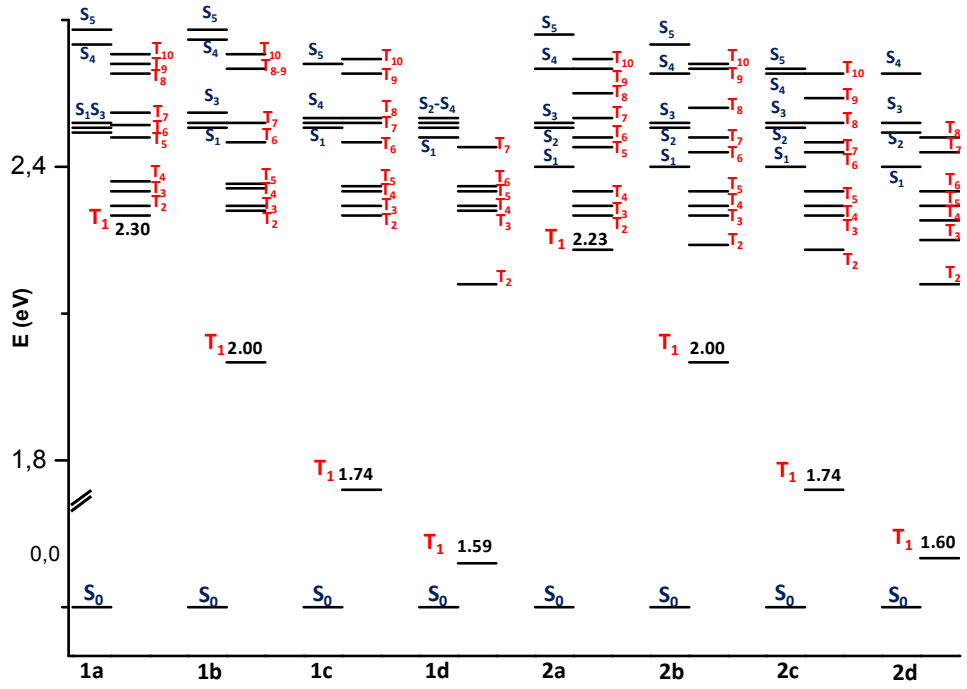

b) Excited States Energy (eV) for **1a-d** and **2a-d** molecules. The first bright singlet excited state energy is reported in bolt

	1a	**1b**	**1c**	**1d**	**2a**	**2b**	**2c**	**2d**
T1	2.30 MLCT	2.00 IL	1.74 IL	1.59 IL	2.23 MLCT	2.00 IL	1.74 IL	1.60 IL
T2	2.32	2.31	2.30	2.16	2.30	2.24	2.23	2.16
T3	2.35	2.32	2.32	2.31	2.32	2.30	2.30	2.25
T4	2.37	2.36	2.35	2.32	2.35	2.32	2.32	2.29
T5	2.46	2.36	2.36	2.35	2.44	2.35	2.35	2.32
T6	2.48	2.45	2.45	2.36	2.46	2.43	2.43	2.35
T7	2.51	2.49	2.49	2.44	2.50	2.46	2.45	2.43
T8	2.59	2.60	2.50	2.49	2.55	2.52	2.49	2.46
T9	2.61	2.60	2.59	2.58	2.60	2.60	2.54	2.52
T10	2.63	2.63	2.62	2.59	2.62	2.61	2.59	2.58
S1	2.47	2.48	2.48	**2.46**	2.40	2.40	2.40	**2.40**
S2	2.48	2.49	2.49	2.48	2.48	2.48	2.48	2.47
S3	2.49	2.51	2.50	2.49	2.49	2.49	2.49	2.48
S4	2.65	2.66	**2.61**	2.50	2.60	2.59	2.59	2.49
S5	**2.68**	**2.68**	2.66	2.65	**2.67**	**2.65**	**2.60**	2.59
S6	2.71	2.73	2.71	2.66	2.67	2.67	2.67	2.65
S7	2.78	2.76	2.73	2.72	2.75	2.73	2.70	2.67

-Table S2-

Table S2. SOC values between relevant singlet states and triplet states lying below them (cm^{-1}) for ***a)*** **1a-1d** and ***b)*** **2a-2d** molecules

a)

	T1	**T2**	**T3**	**T4**	**T5**	**T6**	**T7**	**T8**	**T9**	**T10**
					1a					
S1	1.09	0.80	2.37	3.10	13.16	40.47	6.44	25.03	16.78	5.02
S2	16.33	14.48	14.34	7.09	54.13	11.26	44.83	9.78	4.93	13.10
S3	6.34	15.54	17.68	23.47	18.55	20.54	5.93	17.00	22.19	10.81
S4	11.34	68.78	30.54	21.49	74.58	29.36	228.85	306.12	47.22	345.38
S5	6.31	14.68	43.96	81.30	67.06	70.14	354.45	282.80	46.45	167.64
					1b					
S1	0.38	7.91	2.93	4.13	2.48	1.46	6.78	3.28	7.00	2.39
S2	3.18	3.39	24.97	15.47	9.52	11.09	12.11	6.46	3.63	5.31
S3	2.11	24.11	2.58	10.99	6.91	5.20	18.75	8.30	1.69	2.48
S4	2.78	19.24	14.30	1.21	1.14	6.08	12.00	6.21	4.91	1.71
S5	0.58	8.50	2.05	4.47	6.56	1.80	6.79	2.29	0.69	0.69
					1c					
S1	0.14	10.26	2.23	5.44	1.60	1.85	8.90	12.17	2.35	2.26
S2	8.90	0.21	23.66	17.02	8.90	9.70	13.57	17.85	15.74	0.84
S3	2.30	23.24	0.39	11.49	2.73	6.03	18.83	26.63	8.26	1.49
S4	5.81	19.43	13.23	0.97	4.71	4.71	10.83	10.13	3.57	0.69
S5	0.47	8.99	1.07	5.00	1.23	2.13	7.35	11.25	2.37	0.20
					1d					
S1	0.52	11.49	2.02	6.07	1.94	9.80	2.96	/	/	/

b)

	T1	T2	T3	T4	T5	T6	T7	T8	T9	T10
					2a					
S1	4.80	17.57	7.04	24.42	31.53	6.26	3.61	36.81	26.83	15.22
S2	7.47	25.12	30.68	45.63	43.19	29.41	34.06	12.26	40.37	14.88
S3	17.02	11.52	68.71	44.48	27.65	37.96	70.53	8.86	20.47	25.41
S4	12.43	13.48	119.59	71.61	81.64	31.53	192.90	43.29	310.61	56.22
S5	11.80	26.09	50.45	112.81	107.46	217.67	291.34	40.91	203.56	158.26
					2b					
S1	0.56	1.46	1.79	0.99	1.19	3.57	7.64	1.35	0.80	5.77
S2	8.83	16.17	16.01	12.93	11.86	9.74	2.58	6.59	7.06	5.10
S3	5.89	15.47	19.11	12.27	10.13	6.20	2.90	4.85	3.80	5.00
S4	5.06	13.69	18.19	2.33	1.77	8.70	6.40	4.94	3.88	11.72
S5	0.64	0.57	7.75	1.77	3.60	4.10	0.87	0.55	1.53	1.91
					2c					
S1	0.23	4.17	2.75	3.07	1.84	0.92	4.18	1.77	6.06	1.32
S2	1.70	3.69	24.03	15.65	9.47	10.07	7.89	2.18	17.68	9.50
S3	2.12	23.95	3.56	12.11	7.41	4.21	18.43	1.51	27.94	6.13
S4	2.32	18.21	14.58	1.45	0.35	6.30	12.22	1.87	9.13	1.99
S5	0.60	7.58	2.54	4.64	2.72	1.34	5.81	0.57	10.31	1.50
					2d					
S1	0.18	6.64	2.17	4.38	1.18	1.28				

➢ Paper IV

Halogen Atom Effect on the Photophysical Properties in Substituted Aza-BODIPY Derivatives

Bruna Clara De Simone, Gloria Mazzone, Jenny Pirillo, Nino Russo, Emilia Sicilia.

Physical Chemistry Chemical Physics. ***(2016)***

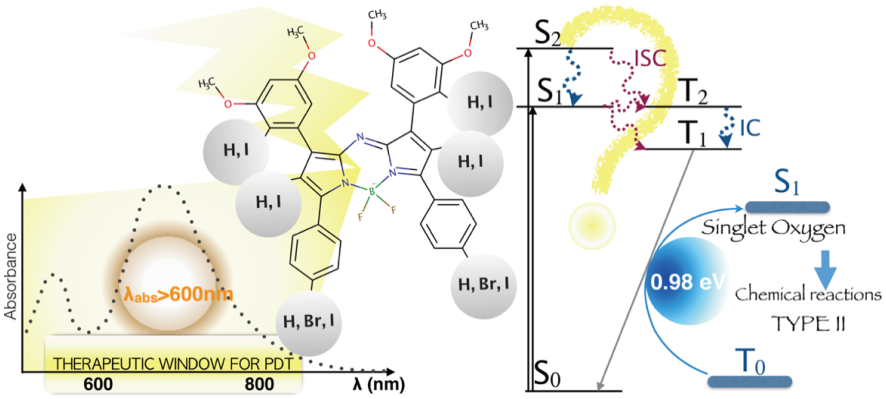

PCCP

PAPER

View Article Online
View Journal | View Issue

Cite this: *Phys. Chem. Chem. Phys.*, 2017, **19**, 2530

Halogen atom effect on the photophysical properties of substituted aza-BODIPY derivatives†

B. C. De Simone, G. Mazzone,* J. Pirillo, N. Russo and E. Sicilia

Received 17th November 2016,
Accepted 14th December 2016

DOI: 10.1039/c6cp07874e

www.rsc.org/pccp

The influence of halogen atom substitution (Br and I), in different amounts and positions in an aza-BODIPY skeleton, on the photophysical properties of some aza-BODIPY derivatives has been investigated by using density functional theory and its time-dependent extension. The heavy atom effect on excitation energies, singlet–triplet energy gaps and spin–orbit matrix elements has been considered. The maximum absorption within the therapeutic window has been confirmed for all the aza-BODIPY derivatives. The feasible intersystem spin crossing pathways for the population of the lowest triplet state, that will depend on the values of the spin–orbit matrix elements, the energy gap as well as the orbital composition of the involved states have been found to most likely involve the S_1 and T_1 or T_2 states. The outcomes of computations support the potential therapeutic use of these compounds as photosensitizers in photodynamic therapy.

1. Introduction

4,4-Difluoro-4-bora-3*a*,4*a*-diaza-*s*-indacene (BODIPY) and its aza (aza-BODIPY) derivatives have been proposed for several technological applications such as biological labelling, electroluminescent devices, tunable laser dyes, solid-state solar concentrators, fluorescent switches, fluorophores in sensors, thanks to the relatively simple synthesis, high redox and thermodynamic stability, and peculiar photophysical properties (large absorption extinction coefficients, sharp emission and quantum fluorescence yields).[1–6] Starting from the seminal works of O'Shea and co-workers,[7] BODIPY derivatives have also been proposed as promising photosensitizers in photodynamic therapy (PDT).[8–10] The photosensitizer's photodynamic action starts with the absorption of a photon followed by competing radiative and nonradiative reactions which ultimately lead to the oxidative degradation of essential biomolecules. Molecular oxygen plays a crucial role in propagating the initial biomolecule damage, leading to the formation of organic radicals and activated oxygen species which act to cause diseased cell death. The basic mechanism of PDT includes the excitation of the photosensitizer with appropriate wavelength light ($S_0 \rightarrow S_n$) and a successive energy transfer to a triplet state ($S_n \rightarrow T_n$) *via* a nonradiative intersystem spin crossing (ISC).[2,3,11] The photophysical processes that follow the photosensitizer's triplet state population can essentially give rise to two types of photoreactions, called type I and type II. In the former electron or hydrogen-atom transfer between the T_1 sensitizer and the substrate molecules occurs yielding radical ions and free radicals. While, the latter involves an energy transfer between the excited triplet sensitizer and ground-state molecular oxygen ($^3O_2$) to yield singlet oxygen ($^1\Delta_g$) species. Thus, the photodynamic effect mainly results from the energy and/or electron transfer of the excited triplet photosensitizer to an organic substrate or molecular oxygen. Most of the photosensitizers currently under evaluation degrade the biological target mainly *via* Type II photoreactions. Accordingly, $^1O_2$ is considered the principal cytotoxic agent in PDT.

Several porphyrin-like photosensitizers have been proposed so far and some of them are in various phases of clinical trials or are currently used in the PDT for the treatment of various cancers and other diseases,[3,12–16] such as ®Foscan[17] and temocene.[18,19] Several non-porphyrin systems such as squaraine dyes,[20,21] substituted perylenediimides,[22] bisanthracene bis(dicarboxylic imide)s[23] and ipericine[24] have also been investigated. Nevertheless, most of these systems possess intrinsic drawbacks, such as dark toxicity and low absorption in the NIR region and, consequently, low penetration power in the tissue. BODIPY dyes, although generally have the wavelength for maximum absorption falling outside the therapeutic window and are highly fluorescent, hardly undergo efficient ISC, have the advantage of being surely non-toxic in the dark and, once structurally modified, can be able to absorb within the right range and to efficiently generate excited singlet oxygen.[1,8–10] Furthermore, their chemical functionalization is relatively inexpensive and they are stable against redox reactions that can occur in the body.

Dipartimento di Chimica e Tecnologie Chimiche, Università della Calabria, I-87036 Arcavacata di Rende, Italy. E-mail: gloria.mazzone@unical.it

† Electronic supplementary information (ESI) available: B3LYP and TD-B3LYP/6-31G* optimized structures of ground and excited states, respectively, of **1a–c**, **2a,b** and **3**; graphical representation of the highest occupied and lowest unoccupied MOs involved in the vertical transitions obtained from the equilibrium geometries of ground, S_0, and excited states, S_1, S_2, T_1 and T_2 at the M06/6-31G* level of theory for **1a–c** and **2b**. See DOI: 10.1039/c6cp07874e

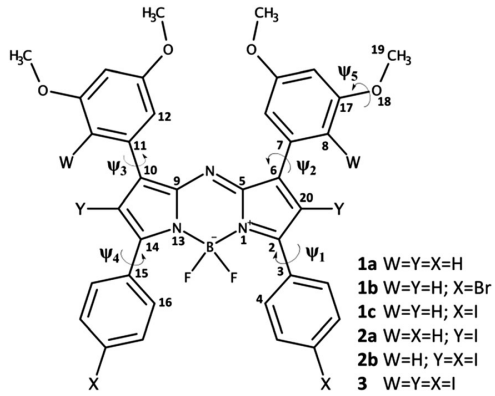

Scheme 1 Schematic representation of the investigated compounds.

Recently, a series of aza-BODIPYs differently substituted with bromine or iodine atoms, with an intense absorption band in the near infrared region, have been found to be able to generate singlet oxygen in high yield.[1] Thanks to their non-dark toxicity, high stability and the enhanced quantum yields of triplet excited states, some of them can be proposed as promising PDT photosensitizers.

The application of first principles methods in the elucidation of photophysical properties, such as excitation energies, singlet–triplet energy gaps and spin–orbit matrix elements, of relatively large molecules is well established.[19,21,23–30] We report here a computational study, at DFT and TDDFT levels of theory, on the photophysical properties of systems reported in Scheme 1 with the aim of elucidating the origin of the improved $^1O_2$ production.

2. Computational section

All the computations have been carried out by using the Gaussian 09[31] code at DFT and its time dependent formulation TDDFT[32] levels of theory.

On the basis of our previous experiences on the photophysical properties of similar and other systems,[27–30] ground and excited state optimization has been performed by using the M06[33] exchange correlation functional coupled with the 6-31G* basis sets for all the atoms with the exception of bromine and iodine, for which the SSD pseudopotential has been employed[34] in the framework of DFT and TDDFT levels of theory, respectively. The excitation energies have been calculated by substituting the 6-31G* basis set with the 6-31+G* ones. The inclusion of the solvent effects has been made by means of the integral equation formalism polarizable continuum model (IEFPCM)[35,36] which corresponds to a linear response in equilibrium and non-equilibrium solvation, and in geometry optimization of excited and ground states, respectively. A dielectric constant of 46.826 has been used in order to take into account the dielectric media of the solvent used in the experiments,[1] dimethyl sulfoxide.

As in all cases the ground and first excited singlet states exhibit approximately the same structural parameters, spin–orbit matrix elements have been computed by using the DALTON code[37] at the ground state equilibrium geometries. The quadratic-response TDDFT approach has been applied by employing the exchange and correlation functional B3LYP.[38,39] As suggested by the authors, the cc-pVDZ basis set has been selected for H, C, N, F and O, while the SDD pseudopotential has been used for Br and I atoms. Therefore, while the atomic-mean field approximation[40] has been employed for **1a**, the spin–orbit coupling operators for effective core potentials with the effective nuclear charge[41] have been used for the other derivatives.

3. Results and discussion

The investigated systems differ in the position and the number of halogens substituted in the aza-BODIPY skeleton of compound **1a** (see Scheme 1). In **1b** and **1c**, halogen atoms (Br and I) occupy the peripheral position, while in **2a** two iodine atoms are inserted in the two pyrrole rings of the aza-BODIPY core. Compound **2b** is characterized by the presence of two extra iodine atoms in the peripheral position. Finally, system **3** contains the highest amount of halogen atoms investigated here, six iodine atoms in both the peripheral and aza-BODIPY core.

3.1 Ground and excited state geometries

The optimization of ground (S_0) and low lying singlet (S_1, S_2) and triplet (T_1, T_2) excited states reveals that in all cases the structural parameters that undergo a significant variation in going from ground to excited states are the dihedral angles (see Table 1), and no significant changes have been found in both bond lengths and valence angles, including those involving the halogen atoms. For example, it can be seen that in **3** the bond distance between C20 and I atoms on the BODIPY core assumes approximately the same value in going from S_0, S_1, S_2, T_1 and T_2 states.

The aza-BODIPY core retains the planarity in the ground and excited states for all the investigated systems. While, the torsional angles, which account for the orientation of the aryl substituent with respect to the BODIPY core, show some interesting variations, such as Ψ_2 that in compounds **1a–c** for the S_1 and T_1 states assumes values about 20 degrees higher than in S_0 and T_2 ones. In compound **3**, the presence of iodine atoms in both the core and peripheral position causes a significant variation in Ψ_2 and Ψ_3 as the aromatic ring rotates in order to alleviate the conformational strength with a consequent reduction of the electron delocalization. In **3** also the electron-donor methoxy group undergoes conformational changes (see Ψ_5 values in Table 1) because of the steric effect generated by the adjacent iodine atom.

3.2 Electronic excitations

The computed vertical excitation energies are reported in Table 2, while molecular orbital plots are depicted in Fig. 1 and Fig. S2 (ESI†).

Table 1 Bond length (Å) C20-I for **3** and dihedral angles (degrees) of ground (S_0) and excited states (S_1, S_2, T_1, and T_2) computed at the M06/6-31G* level

	Bond	Dihedral angles				
	$d_{C20\text{-}I}$	Ψ_1	Ψ_2	Ψ_3	Ψ_4	Ψ_5
1a						
S_0		31.3	142.8	22.9	33.9	−0.4
S_1		29.6	168.1	−26.5	27.6	1.1
T_1		28.7	165.9	−28.4	26.6	1.1
T_2		30.3	147.6	−0.5	33.4	0.3
1b						
S_0		31.1	143.0	22.7	33.3	−0.5
S_1		29.6	168.9	−28.0	27.0	1.1
T_1		28.2	165.8	−28.6	26.3	1.0
T_2		30.1	147.7	−0.4	32.4	0.5
1c						
S_0		30.7	142.9	22.7	32.9	−0.5
S_1		27.6	154.3	−13.1	29.1	0.3
T_1		28.1	165.8	−28.9	25.8	1.0
T_2		29.7	147.7	−0.3	32.0	0.5
2a						
S_0	2.111	48.8	130.6	40.9	60.7	1.6
S_1	2.117	48.2	132.0	38.4	61.2	3.4
T_1	2.110	44.5	131.4	38.8	56.6	1.6
T_2	2.114	51.6	132.2	29.2	67.8	2.5
2b						
S_0	2.111	48.1	131.0	40.8	60.6	1.6
S_1	2.116	47.4	131.8	39.8	58.4	3.3
T_1	2.110	43.4	131.4	38.6	55.9	1.6
T_2	2.114	50.1	132.3	29.7	66.8	2.6
3						
S_0	2.102	48.6	74.5	96.3	47.8	92.9
S_1	2.112	49.9	67.3	102.2	46.9	97.6
S_2	2.115	43.4	93.3	117.5	49.7	8.8
T_1	2.102	40.9	73.4	100.7	42.7	−87.2
T_2	2.112	50.0	66.4	100.2	47.0	98.6

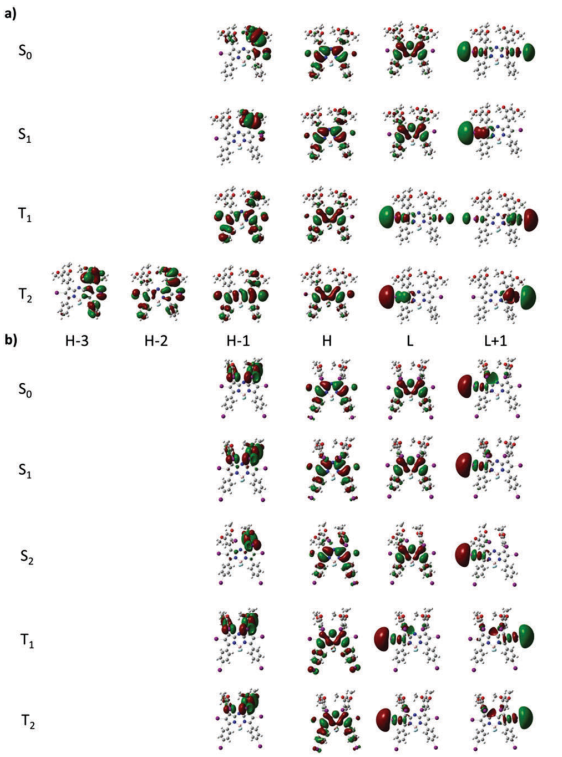

Fig. 1 Graphical representation of the highest occupied and lowest unoccupied MOs involved in the vertical transitions obtained from the equilibrium geometries of ground, GS, and excited states, S_1, S_2, T_1 and T_2 at the M06/6-31G* level of theory for (a) **2a** and (b) **3**. The plots of the orbitals were accomplished with an isodensity value of 2×10^{-2} a.u.

Table 2 Singlet excitation energies (eV), absorption wavelengths (nm), MO contribution (%) and oscillator strength (*f*) computed in DMSO at the M06/6-31+G* level of theory. Experimental values are taken from ref. 1

Compound	States	ΔE	λ	f	Transitions	λ_{exp}
1a	S_1	1.990	623	0.810	H → L, 99%	680
	S_2	2.329	532	0.055	H−1 → L, 99%	
1b	S_1	1.948	636	0.846	H → L, 99%	664
	S_2	2.255	550	0.058	H−1 → L, 99%	
1c	S_1	1.930	642	0.870	H → L, 100%	675
	S_2	2.257	549	0.060	H−1 → L, 98%	
2a	S_1	2.065	600	0.814	H → L, 97%	660
	S_2	2.144	578	0.042	H−1 → L, 97%	
2b	S_1	2.019	614	0.833	H → L, 97%	670
	S_2	2.089	594	0.046	H−1 → L, 97%	
3	S_1	1.914	648	0.092	H−1 → L, 79%	
	S_2	1.997	621	0.704	H → L, 79%	676

From data in Table 2 it emerges that most of the aza-BODIPY investigated showed absorption in the red region (620–750 nm). The effect of including the iodine atoms to the BODIPY core in **2a, b** derivatives results in a slight hypsochromic shift of about 20 nm with respect to the derivative that does not contain any heavy atoms (**1a**), while a blue-shift of more than 30 nm has been found with respect to compounds which contain halogen atoms in peripheral positions (**1b, c**).

The aza-BODIPY derivative which had both periphery and core substitution exhibits a maximum absorption at approximately the same wavelength of **1a**, that does not contain halogen atoms (621 *vs.* 623 nm), according to what has been reported by Ramaiah and co-workers.[1] Anyhow, the comparison between computed and experimental wavelengths shows a reasonable agreement with an error of few tens of nm, typically found for these systems.[29,31] However, it is noteworthy that the deviations between theory and experiment can be in part ascribable to the inherent limits of TDDFT, which does not take into account double excitations, and in part to the use of vertical approximation and the linear response solvent effects, as recently shown.[42]

For **1a–c** and **2a, b** compounds the oscillator strength (*f*) of the first singlet excited state, S_1, assumes values higher than 0.8, while S_2 is found to be dark in nature. In contrast, in **3** the S_2 state has an *f* value of 0.704 and S_1 is found to be very weak in intensity ($f = 0.092$). In **1a–c** and **2a, b** systems, S_1 is originated by a HOMO → LUMO transition, while in **3** the transition

HOMO−1 → LUMO dominates about 80% of the dark first excited state. The plot of molecular orbitals reported in Fig. 1 and Fig. S1 (ESI†) clearly reveals that the electronic transition occurs from π to π* orbitals. Similar to the first excited state in the other molecules, S_2 in **3** is due to a HOMO → LUMO excitation and results to be ππ* in nature (Fig. 1). The low lying triplet state T_1 involves ππ* transition (HOMO → LUMO) in compounds in which the halogen substitution is accomplished exclusively in the *para* position of the peripheral aryl groups (**1b, c**, see Fig. S2, ESI†), while in compound **2a**, where the iodine atoms occupy a position on the BODIPY core, the transition involves orbitals with different nature, πn*, as the LUMO is dominated by the lone pairs of the heavy atom directly bound to the core. Interestingly, in **2b** and **3** in which the iodine atoms are present, in different amounts, in both peripheral and core positions (see Scheme 1), the effect of the heavy atom on the BODIPY core plays the major role in the characterization of the state, with the LUMO being again localized on the lone pairs of one iodine atom.

Concerning the T_2 state it can be noted that a transition between orbitals with different nature significantly contributes to this excited state for **1c**, **2a, b** and **3**, as the transition involves the LUMO (HOMO−3 → LUMO for **1c** and **2a, b**, and HOMO−1 → LUMO for **3**). In contrast in **1a, b**, although T_2 is originated by the same transition as **1c**, the LUMO is characterized by the delocalization on the BODIPY core, then the transition is of type ππ* (see Fig. S2, ESI†).

In order to verify if the investigated aza-BODIPY derivatives can be proposed as efficient photosensitizers for PDT, the computed vertical energy gaps between singlet ground and low lying triplet electronic states (ΔE_{S-T}), included in Table 3, will be discussed. As can be seen, a common feature in the computed excited states is the T_1 energy below the S_1 one, together with the T_2 excited state. In addition, it is evident that $\Delta E(S_0–T_1)$ gaps are closer to 0.9 eV,[32] the energy computed to be necessary to activate O_2 from its ground triplet ($^3\Sigma_g$) to the excited singlet state ($^1\Delta_g$). The highest T_1 state has been found for **2a, b** (approximately 1 eV). Similar values have been previously found at the DFT level of theory in a series of BODIPY and aza-BODIPY systems.[29,31]

3.3 Spin–orbit coupling constants

High quantum yields of cytotoxic singlet O_2 species, fundamental in PDT, can be correlated with the rate constants of the intersystem crossing (radiationless transition $S_n \rightarrow T_m$). The ISC efficiency, in the golden rule approximation[43] and in the framework of Marcus–Levich–Jortner theory,[44] can be expressed as:

$$K_{isc} = \frac{4\pi^2}{h}\left|\left\langle \Psi_{S_n}\left|\hat{H}_{so}\right|\Psi_{T_m}\right\rangle\right|^2 \cdot \mathrm{FCWD}$$

where $\left\langle \Psi_{S_n}\left|\hat{H}_{so}\right|\Psi_{T_m}\right\rangle$ is the spin–orbit coupling (SOC) integral between the singlet (S_n) and triplet (T_m) pure spin states and FCWD represents the Franck–Condon weighted density of the states. In this case, compounds very similar in structural behaviour will be compared, so it can be reasonable to consider the relative FCWDs approximately of the same magnitude. Anyhow, this term is proportional to an exponential term in which the ΔE_{S-T} plays the major role.[44] As, from accurate *ab initio* electronic structure data, it has been established that SOCs and small S_n–T_m energy gaps define the efficiency of ISC processes,[43] the computed singlet–triplet energy gap reported in Table 3, combined with SOC values, can be considered as a reliable parameter in evaluating the ISC kinetics.

The spin–orbit matrix elements between the initial $\Psi(S_1)$ and final $\Psi(T_1)$ wave functions, following the El Sayed rules,[45] depend on the nature of the orbitals involved in the transition (internal effect). The presence in the molecular system of a heavy atom can also affect the SOCs in two ways: (i) contributing to changing the orbital nature of the excited states; (ii) varying the SOC with values proportional to the atomic number and inversely proportional to the mean cubic radial distribution (r^{-3}) of the electron (heavy atom effect).

As in all cases two excited triplet states, T_1 and T_2 originated by H → L and H−3 → L transitions, respectively, have been found to be lying below the energy of the first singlet excited one, S_1, SOCs have been computed for S_1 with the two triplet states. From Table 4 it emerges that the presence of halogen atoms increases in all cases the SOC amplitude. Comparison between the values obtained for **1c** (two iodine atoms in peripheral positions) and **2a** (two iodine atoms in the BODIPY core) well evidences as the substitutional position strongly affects both the $\left\langle \Psi_{S_1}\left|\hat{H}_{so}\right|\Psi_{T_1}\right\rangle$ and $\left\langle \Psi_{S_1}\left|\hat{H}_{so}\right|\Psi_{T_2}\right\rangle$ values. Looking at Fig. 1 and Fig. S2 (ESI†), it appears clear that the inclusion of iodine atoms directly in the BODIPY core entails a change in the orbital composition of the LUMO in the triplet excited states, with respect to **1c** bearing halogen atoms in peripheral positions, enhancing the SOC amplitude. The addition of further iodine atoms (compound **2b**) does not cause strong variations in the computed SOC values, because of occupying

Table 3 Vertical singlet–triplet energy gap ($\Delta E(S_0–T_1)$) and energy differences between the excited states among which the intersystem crossing could occur are computed at the TD-B3LYP/cc-pVDZ level of theory. Values are reported in eV

	1a	1b	1c	2a	2b	3
$\Delta E(S_0–T_1)$	0.94	0.93	0.93	1.02	1.01	0.95
$\Delta E(S_1–T_1)$	1.18	1.12	1.12	0.89	0.84	0.77
$\Delta E(S_1–T_2)$	0.25	0.24	0.23	0.16	0.14	0.01
$\Delta E(S_2–T_2)$						0.32

Table 4 Spin–orbit matrix elements (cm^{-1}) calculated at the B3LYP/cc-pVDZ//M06/6-31G* level of theory in the ground state optimized geometry

Compound	$\left\langle \Psi_{S_1}\left\|\hat{H}_{so}\right\|\Psi_{T_1}\right\rangle$	$\left\langle \Psi_{S_1}\left\|\hat{H}_{so}\right\|\Psi_{T_2}\right\rangle$	$\left\langle \Psi_{S_2}\left\|\hat{H}_{so}\right\|\Psi_{T_2}\right\rangle$
1a	0.3	0.5	
1b	1.3	3.5	
1c	3.6	9.9	
2a	256.4	394.4	
2b	238.8	324.3	
3	202.5	470.8	89.8

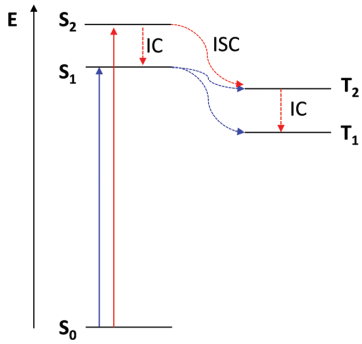

Scheme 2 Representative energy diagram of the excited singlet and triplet states and plausible deactivation pathways, denoted with blue, for **1** and **2**, and red arrows for compound **3**.

peripheral positions. Finally, the increasing number of iodine atoms in **3** (addition of other two I atoms in the *ortho* position of the peripheral aryl rings) causes an increase of about 150 cm^{-1} and a modest decrease of $\langle \Psi_{S_1} | \hat{H}_{so} | \Psi_{T_2} \rangle$ and $\langle \Psi_{S_1} | \hat{H}_{so} | \Psi_{T_1} \rangle$, respectively. This is probably due to the similar energy of S_1 and T_2 states, that in turn enhances the probability of the intersystem crossing.

Nevertheless, for all the derivatives, different intersystem spin crossing pathways for the population of the lowest triplet states have been explored, considering a series of plausible non-radiative decay pathways depending on the excited state electron energies, as depicted in Scheme 2. For **1a–c** and **2a, b**, for which the absorption generates the S_1 state, the population of the lowest triplet excited state can reasonably follow two ways (blue lines in Scheme 2):

$$S_0 \xrightarrow{A} S_1 \xrightarrow{ISC} T_1 \quad (a)$$

$$S_0 \xrightarrow{A} S_1 \xrightarrow{ISC} T_2 \xrightarrow{IC} T_1 \quad (b)$$

In the first pathway a direct ISC from S_1 to T_1 is hypothesized and looking at the $\langle \Psi_{S_1} | \hat{H}_{so} | \Psi_{T_1} \rangle$ values, it is found that this transition has increasing probability to occur in going from **1a** to **2b**. The computed energy gaps (Table 3) are between 0.8 and 1.2 eV, the lowest of which has been found for the compounds which contain the iodine atoms directly bound to the BODIPY core, **2a** and **2b**, and for which substantial SOCs have been calculated, 256.4 and 238.8 cm^{-1}, respectively. Indeed, as previously underlined, the SOC values depend on the nature of orbitals in the two involved states: in **1a–c** the nonradiative transition occurs between states with ππ* character, while in **2a, b** the T_1 states have πn* character, due to the iodine lone-pair contributions. In path (b) an ISC, that occurs between S_1 and T_2 states, should be followed by a fast $T_2 \rightarrow T_1$ internal conversion. Also in this case the computed SOCs almost increase in the series and the energy gaps are very small (the maximum value is 0.25 eV). The T_2 molecular orbital composition results to be ππ* in nature for **1a, b** and becomes πn* in the case of **2a, b** systems. Due to the SOC, ΔE_{S-T} values and the change in orbital composition both channels should be possible, especially for **2a, b** molecules, for which significant SOCs have been computed.

For compound **3**, as the absorption involves the S_2 state, three deactivation pathways can be hypothesized (red lines in Scheme 2):

$$S_0 \xrightarrow{A} S_2 \xrightarrow{ISC} T_2 \xrightarrow{IC} T_1 \quad (c)$$

$$S_0 \xrightarrow{A} S_2 \xrightarrow{IC} S_1 \xrightarrow{ISC} T_1 \quad (d)$$

$$S_0 \xrightarrow{A} S_2 \xrightarrow{IC} S_1 \xrightarrow{ISC} T_2 \xrightarrow{IC} T_1 \quad (e)$$

In path (c) the intersystem crossing can occur between the populated S_2 state and the T_2 one that in turn undergoes a fast internal conversion to T_1. Assuming that the energy difference between the involved states is rather small (0.32 eV), the relative SOC is found to be considerably smaller than those computed for the coupling with the S_1 state. In addition, taking into account Kasha' rule[46] that indicates as, in a given spin manifold, the transition $S_n \rightarrow S_1$ (with $n > 1$) should be very fast and triplet state population should start from the lowest singlet excited state (S_1), this pathway seems to be unlikely to occur.

The other two decay channels (d) and (e) share the first step (a fast IC from S_2 to S_1) but in the former the T_1 population occurs by a direct $S_1 \rightarrow T_1$ ISC, while in the latter by the $S_1 \rightarrow T_2$ one. $S_1 \rightarrow T_1$ intersystem crossing is dominated by a high SOC value (202.5 cm^{-1}) and the $\Delta E(S_1\text{–}T_1)$ energy gap assumes a value of 0.77 eV. Channel (e) is characterized by the highest SOC (470.8 cm^{-1}) and a negligible ΔE_{S-T}, and therefore it seems to be the most probable one.

For all the considered systems it can be possible to compare the computed SOC values involved in the intersystem crossing between S_1 and low lying excited triplet states with the experimental data, that are singlet oxygen (ϕ_Δ) and sensitizer's triplet (ϕ_T) quantum yields (Fig. 2).[1]

The experimental and theoretical behaviours are quite similar. In particular, it can be noted that both singlet oxygen (ϕ_Δ) and triplet (ϕ_T) quantum yields slightly increase in going from **1a** to

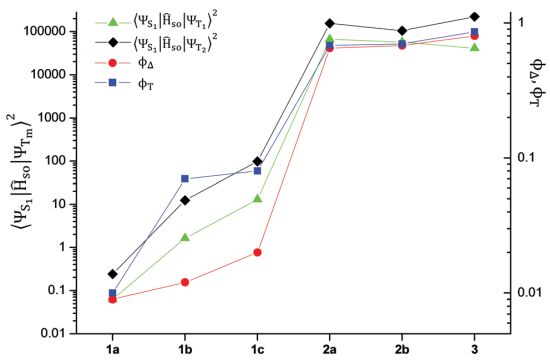

Fig. 2 Computed SOC for $S_1 \rightarrow T_m$ (with m = 1, 2) radiationless transition and measured[1] quantum yields of singlet oxygen ϕ_Δ and triplet excited states ϕ_T for the investigated systems.

1c while a drastic enhancement in **2a,** where iodine atoms occupy a position of the BODIPY core, has been found. The addition of extra heavy atoms produces only a modest increase of the singlet oxygen and triplet quantum yields. The reported SOC values approximately show the same trend. In particular for derivatives containing iodine atoms in the core region of the molecule (**2a, b** and **3**), the experimental trend is finely reproduced by the SOCs computed for $S_1 \rightarrow T_2$ radiationless transition.

4. Conclusions

The halogen atom effect on the photophysical properties of a series of recently synthesized aza-BODIPY derivatives has been elucidated by using DFT and TDDFT approaches. In particular, the maximum absorption wavelengths, singlet–triplet energy gaps, spin–orbit matrix elements for the radiationless $S_n \rightarrow T_m$, and the preferred channels for the photosensitizer's triplet state population have been determined. The following conclusions can be drawn:

– All the studied systems show a Q band that falls within the so-called therapeutic window;

– The $\Delta E(S_0–T_1)$ gaps are higher than 0.90 eV and, accordingly, all the aza-BODIPY investigated should be able to generate the cytotoxic singlet molecular oxygen;

– The introduction of halogen atoms induces an increase of the spin–orbit matrix elements, which are even more substantial when heavy atoms occupy a position in the core region of the molecular system;

– Following the El-Sayed and Kasha rules, the most probable channel for the triplet state population starts from the S_1 state ($\pi\pi^*$) and involves intersystem spin crossing between the states characterized by different orbital compositions, that in both low lying triplet excited states possibly involved is πn^*.

Putting together these considerations, all the halogenated aza-BODIPY derivatives studied here could be proposed as candidates to be tested as photosensitizers in type II photodynamic therapy.

Acknowledgements

Università della Calabria is gratefully acknowledged for financial support.

References

1 N. Adarsh, M. Shanmugasundaram, R. Avirah and D. Ramaiah, *Chem. – Eur. J.*, 2012, **18**, 12655–12662.
2 A. Kamkaew, S. Lim, H. Lee, L. Kiew, L. Chung and K. Burgess, *Chem. Soc. Rev.*, 2012, **42**, 77–88.
3 S. Awuah and Y. You, *RSC Adv.*, 2012, **2**, 11169–11183.
4 J. Zhao, K. Xu, W. Yang, Z. Wang and F. Zhong, *Chem. Soc. Rev.*, 2015, **44**, 8904–8939.
5 S. Ji, J. Ge, D. Escudero, Z. Wang, J. Zhao and D. Jacquemin, *J. Org. Chem.*, 2015, **80**, 5958–5963.
6 A. Charaf-Eddin, B. Guennic and D. Jacquemin, *RSC Adv.*, 2014, **4**, 49449–49456.
7 J. Killoran, L. Allen, J. Gallagher, W. Gallagher and D. O'Shea, *J. Cheminf.*, 2002, **33**, 177.
8 A. T. Byrne, A. E. O'Connor, M. Hall, J. Murtagh, K. O'Neill, K. M. Curran, K. Mongrain, J. A. Rousseau, R. Lecomte, S. McGee, J. J. Callanan, D. F. O'Shea and W. M. Gallagher, *Br. J. Cancer*, 2009, **101**, 1565–1573.
9 A. Gorman, J. Killoran, C. O'Shea, T. Kenna, W. Gallagher and D. O'Shea, *J. Am. Chem. Soc.*, 2004, **126**, 10619–10631.
10 P. Batat, M. Cantuel, G. Jonusauskas, L. Scarpantonio, A. Palma, D. O'Shea and N. McClenaghan, *J. Phys. Chem.*, 2011, **115**, 14034–14039.
11 C. Schweitzer and R. Schmidt, *J. Cheminf.*, 2003, **34**, 1685–1757.
12 T. J. Dougherty, G. B. Grindey, R. Fiel, K. R. Weishaupt and D. G. Boyle, *J. Natl. Cancer Inst.*, 1975, **55**, 115–121.
13 A. Juzeniene, Q. Peng and J. Moan, *Photochem. Photobiol. Sci.*, 2007, **6**, 1234–1245.
14 P. Babilas, S. Schreml, M. Landthaler and R. Szeimies, *Photodermatol., Photoimmunol. Photomed.*, 2010, **26**, 118–132.
15 S. Kossodo and G. LaMuraglia, *Am. J. Cardiovasc. Drugs*, 2001, **1**, 15–21.
16 J. Garrier, L. Bezdetnaya, C. Barlier, S. Grafe, F. Guillemin and M. A. D'Hallewin, *Photodiagn. Photodyn. Ther.*, 2011, **8**, 321–327.
17 M. Chen, X. Liu and A. Fahr, *Int. J. Pharm.*, 2011, **408**, 223–234.
18 M. García-Díaz, D. Sánchez-García, J. Soriano, L. Sagristà, M. Mora, Á. Villanueva, J. Stockert, M. Cañete and S. Nonell, *MedChemComm*, 2011, **2**, 616–619.
19 M. Alberto, T. Marino, A. Quartarolo and N. Russo, *Phys. Chem. Chem. Phys.*, 2013, **15**, 16167–16171.
20 D. Ramaiah, A. Joy, N. Chandrasekhar, N. Eldho, S. Das and M. George, *Photochem. Photobiol.*, 1997, **65**, 783–790.
21 M. Alberto, G. Mazzone, A. Quartarolo, F. Sousa, E. Sicilia and N. Russo, *J. Comput. Chem.*, 2014, **35**, 2107–2113.
22 I. Macdonald and T. Dougherty, *J. Porphyrins Phthalocyanines*, 2001, **5**, 105–129.
23 M. Alberto, C. Iuga, A. Quartarolo and N. Russo, *J. Chem. Inf. Model.*, 2013, **53**, 2334–2340.
24 E. Eriksson and L. Eriksson, *Phys. Chem. Chem. Phys.*, 2011, **13**, 7207–7217.
25 D. Jacquemin, E. Perpète, I. Ciofini and C. Adamo, *Acc. Chem. Res.*, 2009, **42**, 326–334.
26 C. Adamo and D. Jacquemin, *Chem. Soc. Rev.*, 2012, **42**, 845–856.
27 M. Alberto, B. Simone, G. Mazzone, A. Quartarolo and N. Russo, *J. Chem. Theory Comput.*, 2014, **10**, 4006–4013.
28 M. Alberto, B. Simone, G. Mazzone, T. Marino and N. Russo, *Dyes Pigm.*, 2015, **120**, 335–339.
29 G. Mazzone, A. Quartarolo and N. Russo, *Dyes Pigm.*, 2016, **130**, 9–15.
30 G. Mazzone, M. Alberto, B. Simone, T. Marino and N. Russo, *Molecules*, 2016, **21**, 288.
31 M. J. Frisch, G. W. Trucks, H. B. Schlegel, G. E. Scuseria, M. A. Robb, J. R. Cheeseman, G. Scalmani, V. Barone,

B. Mennucci, G. A. Petersson, H. Nakatsuji, M. Caricato, X. Li, H. P. Hratchian, A. F. Izmaylov, J. Bloino, G. Zheng, J. L. Sonnenberg, M. Hada, M. Ehara, K. Toyota, R. Fukuda, J. Hasegawa, M. Ishida, T. Nakajima, Y. Honda, O. Kitao, H. Nakai, T. Vreven, J. A. Montgomery, Jr., J. E. Peralta, F. Ogliaro, M. Bearpark, J. J. Heyd, E. Brothers, K. N. Kudin, V. N. Staroverov, R. Kobayashi, J. Normand, K. Raghavachari, A. Rendell, J. C. Burant, S. S. Iyengar, J. Tomasi, M. Cossi, N. Rega, J. M. Millam, M. Klene, J. E. Knox, J. B. Cross, V. Bakken, C. Adamo, J. Jaramillo, R. Gomperts, R. E. Stratmann, O. Yazyev, A. J. Austin, R. Cammi, C. Pomelli, J. W. Ochterski, R. L. Martin, K. Morokuma, V. G. Zakrzewski, G. A. Voth, P. Salvador, J. J. Dannenberg, S. Dapprich, A. D. Daniels, Ö. Farkas, J. B. Foresman, J. V. Ortiz, J. Cioslowski and D. J. Fox, *Gaussian 09, Revision A.2*, Gaussian, Inc., Wallingford CT, 2009.

32 M. E. Casida, in *Recent Advances in Density Functional Methods, Part I*, ed. D. P. Chong, World Scientific, Singapore, 1995, p. 155.

33 Y. Zhao and D. Truhlar, *Theor. Chem. Acc.*, 2008, **119**, 525.

34 D. Andrae, U. Haussermann, M. Dolg, H. Stoll and H. Preuss, *Theor. Chim. Acta*, 1990, **77**, 123–141.

35 M. Cossi and V. Barone, *J. Chem. Phys.*, 2000, **112**, 2427.

36 J. Tomasi, B. Menucci and R. Cammi, *Chem. Rev.*, 2005, **105**, 2999–3094.

37 *DALTON. A Molecular Electronic Structure Program. Release Dalton 2011*, http://daltonprogram.org/.

38 A. Becke, *J. Chem. Phys.*, 1993, **98**, 5648–5652.

39 C. Lee, W. Yang and R. Parr, *Phys. Rev. B: Condens. Matter Mater. Phys.*, 1988, **37**, 785–789.

40 K. Ruud, B. Schimmelpfennig and H. Ågren, *Chem. Phys. Lett.*, 1999, **310**, 215–221.

41 S. Koseki, M. Schmidt and M. Gordon, *J. Phys. Chem.*, 1998, **102**, 10430–10435.

42 B. Le Guennic and D. Jacquemin, *Acc. Chem. Res.*, 2015, **48**, 530–537.

43 C. Marian, *Wiley Interdiscip. Rev.: Comput. Mol. Sci.*, 2012, **2**, 187–203.

44 J.-L. Brédas, D. Beljonne, V. Coropceanu and J. Cornil, *Chem. Rev.*, 2004, **104**, 4971–5004.

45 M. A. El-Sayed, *J. Chem. Phys.*, 1963, **38**, 2834–2838.

46 M. Kasha, *Discuss. Faraday Soc.*, 1950, **9**, 14–19.

Electronic Supplementary Material (ESI) for Physical Chemistry Chemical Physics.

Electronic Supplementary Information

Halogen atom effect on the photophysical properties of substituted aza-BODIPY derivatives

Bruna Clara De Simone, Gloria Mazzone, Jenny Pirillo, Nino Russo, Emilia Sicilia,*

Dipartimento di Chimica e Tecnologie Chimiche, Università della Calabria, I-87036 Arcavacata di Rende, Italy

* To whom correspondence should be addressed. E-mail: gloria.mazzone@unical.it

Table of contents

Table S1

1a

	S_0			S_1		
Atomic Number	X	Y	Z	X	Y	Z
6	0.683437	1.645267	-1.987281	0.545036	1.827086	-1.985439
6	-0.274319	0.723168	-1.437262	-0.356978	0.843968	-1.441777
6	0.6276	2.0183	0.199715	0.380581	2.2362	0.192278
6	-0.268828	0.964787	-0.076143	-0.414179	1.113503	-0.080431
1	-0.861815	0.457161	0.675387	-1.045395	0.61604	0.64786
7	1.178712	2.451648	-0.959309	0.951404	2.679562	-0.990635
6	-1.125963	-0.243321	-2.124786	-1.027999	-0.203103	-2.182014
6	-2.281481	-0.679354	-1.45745	-1.42828	-1.373413	-1.510191
6	-0.812896	-0.743399	-3.39385	-1.304567	-0.050904	-3.553096
6	-3.113595	-1.620851	-2.05617	-2.07408	-2.381606	-2.214716
1	-2.534649	-0.250149	-0.492913	-1.185601	-1.485947	-0.457298
6	-1.658783	-1.691899	-3.974677	-1.971328	-1.063044	-4.238406
1	0.074551	-0.38273	-3.90549	-0.999501	0.861769	-4.053463
6	-2.800669	-2.130897	-3.311233	-2.346706	-2.231637	-3.578851
1	-3.448737	-2.869058	-3.776907	-2.863936	-3.022356	-4.116591
6	0.896489	2.517992	1.545772	0.551261	2.827691	1.505014
6	1.1883	3.859117	1.827678	0.83487	4.188409	1.7153
6	0.805528	1.610433	2.613943	0.379745	2.001681	2.633411
6	1.381386	4.271507	3.138518	0.936754	4.692062	3.003459
1	1.250755	4.577968	1.017497	0.962733	4.849164	0.863583
6	1.008566	2.027136	3.920414	0.485734	2.511381	3.915525
1	0.606679	0.55969	2.408491	0.196503	0.9379	2.491668
6	1.29432	3.362816	4.187998	0.763736	3.863426	4.108309
1	1.6002	5.318394	3.340934	1.150994	5.750041	3.145276
1	0.947664	1.304959	4.732532	0.362076	1.849787	4.771175
1	1.450584	3.693589	5.213346	0.849968	4.267502	5.115563
7	1.085448	1.720809	-3.238276	0.996195	1.838242	-3.236079
6	2.006737	2.60041	-3.58851	1.965841	2.687266	-3.562343
6	2.427559	2.897446	-4.921554	2.505658	2.873887	-4.887215
6	3.225396	4.020692	-4.823104	3.389563	3.940741	-4.771152
6	3.337107	4.371077	-3.459212	3.418744	4.364354	-3.436118
1	3.767641	4.495585	-5.633471	4.034204	4.337945	-5.54723
6	2.128425	2.169189	-6.150483	2.203194	2.085588	-6.061622
6	2.162408	0.780332	-6.184001	1.532281	0.856693	-5.95707
6	1.910708	2.903913	-7.329137	2.610576	2.536184	-7.333744
6	2.01964	0.11864	-7.409496	1.27309	0.090585	-7.099861
1	2.362993	0.198689	-5.286342	1.208938	0.477738	-4.991131
6	1.7298	2.229931	-8.528918	2.340535	1.766061	-8.454228
1	1.867678	3.988272	-7.271898	3.108633	3.496619	-7.426508
6	1.791994	0.831888	-8.578056	1.665519	0.534823	-8.352682
1	1.664456	0.353481	-9.544722	1.483932	-0.021632	-9.267783
6	4.137048	5.489217	-2.970482	4.220017	5.468625	-2.942799
6	4.306943	6.598346	-3.81489	4.550307	6.500828	-3.843098
6	4.785772	5.486061	-1.728119	4.72235	5.545968	-1.632316
6	5.093235	7.672737	-3.429213	5.346517	7.56345	-3.453191
1	3.787795	6.626137	-4.771786	4.139844	6.477448	-4.851269
6	5.577251	6.561517	-1.350816	5.522847	6.612267	-1.250422
1	4.674689	4.633751	-1.065511	4.495185	4.758153	-0.921606
6	5.735492	7.65639	-2.194237	5.840188	7.624415	-2.15113
1	5.201499	8.528525	-4.093015	5.575473	8.35549	-4.164179
1	6.079839	6.54005	-0.385567	5.907409	6.649578	-0.232604
1	6.35608	8.497558	-1.890159	6.46537	8.460025	-1.841085
7	2.611794	3.499873	-2.713363	2.563935	3.565376	-2.69325
8	-4.25081	-2.102974	-1.496205	-2.486055	-3.552901	-1.675949
8	-1.451573	-2.255637	-5.185983	-2.315212	-0.994652	-5.545789
8	2.129602	-1.233234	-7.362565	0.617056	-1.07083	-6.868883
8	1.494381	2.832458	-9.718947	2.679881	2.109401	-9.717367
6	-4.61745	-1.61999	-0.229023	-2.261726	-3.760121	-0.302823
1	-3.845647	-1.832775	0.526334	-1.188062	-3.753838	-0.06314
1	-4.809498	-0.536422	-0.246567	-2.769595	-2.998629	0.307656
1	-5.538043	-2.141825	0.044614	-2.676435	-4.743773	-0.069101
6	-0.286508	-1.895583	-5.889465	-2.189077	0.255768	-6.184791
1	-0.29977	-2.480651	-6.81291	-2.576459	0.12012	-7.198797
1	-0.271373	-0.823056	-6.135647	-2.782061	1.025283	-5.668462
1	0.623901	-2.139737	-5.322993	-1.142149	0.587674	-6.2392
6	2.032744	-1.940589	-8.574881	0.187063	-1.816701	-7.980782
1	1.049071	-1.797445	-9.048703	-0.458267	-1.214322	-8.639708
1	2.817629	-1.635719	-9.282414	1.037265	-2.197727	-8.566164
1	2.161563	-2.997329	-8.326193	-0.38771	-2.656454	-7.583177
6	1.419513	4.236999	-9.738587	3.374485	3.318137	-9.911672
1	0.604672	4.606816	-9.098818	2.776783	4.182428	-9.586989
1	2.365588	4.696296	-9.41518	4.333482	3.321155	-9.373394
1	1.218919	4.519683	-10.774979	3.563309	3.394069	-10.985252
5	2.274928	3.551789	-1.181771	2.101069	3.729099	-1.200491
9	1.791748	4.814612	-0.906141	1.655459	5.025071	-1.037884
9	3.363452	3.229924	-0.400091	3.113269	3.418264	-0.314339

	T_1			T_2		
Atomic Number	X	Y	Z	X	Y	Z
6	0.554203	1.836454	-1.982831	0.693574	1.618744	-2.017261
6	-0.366171	0.848712	-1.444309	-0.263906	0.722952	-1.48438
6	0.353129	2.251687	0.190354	0.608109	2.054991	0.19595
6	-0.442082	1.125532	-0.092829	-0.28906	1.002666	-0.079821
1	-1.082152	0.628674	0.627815	-0.920479	0.540431	0.66991
7	0.944399	2.69108	-0.996654	1.16476	2.442249	-0.974059
6	-1.025181	-0.212513	-2.186274	-1.112713	-0.208088	-2.15624
6	-1.398331	-1.383214	-1.50668	-2.037065	-0.984763	-1.385644
6	-1.314097	-0.067121	-3.550373	-1.093885	-0.343137	-3.562515
6	-2.041068	-2.404427	-2.200778	-2.928276	-1.836708	-2.012637
1	-1.141141	-1.490099	-0.456436	-2.037193	-0.8986	-0.304538
6	-1.973995	-1.09437	-4.225052	-2.006351	-1.184684	-4.171301
1	-1.021487	0.843891	-4.061222	-0.374489	0.242037	-4.127554
6	-2.330375	-2.262314	-3.557104	-2.931226	-1.940891	-3.408082
1	-2.842592	-3.060695	-4.088155	-3.634399	-2.600714	-3.908834
6	0.50407	2.847952	1.500492	0.839394	2.583616	1.538589
6	0.803883	4.205432	1.709493	1.126369	3.929591	1.804296
6	0.294566	2.029379	2.628373	0.71621	1.69727	2.622139
6	0.886288	4.713153	2.997173	1.281482	4.365072	3.112344
1	0.95714	4.861251	0.858511	1.216813	4.631524	0.98193
6	0.384415	2.543003	3.91017	0.87651	2.138343	3.926502
1	0.094315	0.968622	2.488293	0.527401	0.640812	2.433459
6	0.67927	3.891397	4.101601	1.157487	3.478194	4.17743
1	1.112099	5.768445	3.139293	1.498571	5.414899	3.300768
1	0.231917	1.888006	4.76597	0.789559	1.431257	4.749503
1	0.751198	4.298848	5.108491	1.281852	3.829305	5.200278
7	1.000738	1.840491	-3.235435	1.137465	1.685503	-3.259551
6	1.97267	2.690318	-3.54735	2.061455	2.588305	-3.587924
6	2.527465	2.863507	-4.882828	2.536368	2.845103	-4.902154
6	3.414044	3.918287	-4.767698	3.33482	3.980607	-4.801533
6	3.44186	4.353849	-3.43092	3.383599	4.378372	-3.459655
1	4.064546	4.305501	-5.54367	3.911044	4.43276	-5.601877
6	2.215053	2.073649	-6.061164	2.268565	2.070516	-6.107526
6	1.562817	0.844834	-5.9589	2.153288	0.684329	-6.061312
6	2.603837	2.549553	-7.332086	2.19455	2.735927	-7.345723
6	1.289871	0.097332	-7.109486	1.992534	-0.039933	-7.246226
1	1.249352	0.452464	-4.995637	2.225513	0.146664	-5.118231
6	2.328587	1.793995	-8.46022	2.004563	2.003785	-8.508671
1	3.088563	3.517759	-7.416733	2.262743	3.820487	-7.36378
6	1.664999	0.560952	-8.362061	1.899601	0.606792	-8.471069
1	1.472373	0.013615	-9.280546	1.766268	0.083129	-9.413271
6	4.250725	5.451252	-2.941029	4.137251	5.525566	-2.967431
6	4.608482	6.46506	-3.851823	4.351258	6.601983	-3.846018
6	4.734565	5.538655	-1.624572	4.702845	5.596717	-1.686033
6	5.411592	7.523473	-3.464087	5.102151	7.702171	-3.463628
1	4.215471	6.432119	-4.86653	3.894129	6.579836	-4.83416
6	5.544686	6.598737	-1.246266	5.452014	6.702208	-1.30761
1	4.488295	4.763217	-0.907026	4.566279	4.774803	-0.991051
6	5.887087	7.594581	-2.156226	5.65921	7.758312	-2.188854
1	5.661846	8.302373	-4.182058	5.246022	8.524821	-4.162331
1	5.916885	6.644335	-0.224433	5.88601	6.733628	-0.30945
1	6.519225	8.425605	-1.848389	6.248417	8.621864	-1.884784
7	2.569444	3.56035	-2.683802	2.619236	3.508852	-2.714691
8	-2.42945	-3.579051	-1.645136	-3.840982	-2.606569	-1.378445
8	-2.322627	-1.037418	-5.532751	-2.123995	-1.366546	-5.49407
8	0.63574	-1.068841	-6.890861	1.928811	-1.391659	-7.09542
8	2.652525	2.159153	-9.725536	1.903347	2.546416	-9.74834
6	-2.180585	-3.771394	-0.275812	-3.88631	-2.548698	0.026897
1	-1.1037	-3.744516	-0.050681	-2.937305	-2.881099	0.473468
1	-2.692532	-3.015659	0.339201	-4.115636	-1.532607	0.381027
1	-2.573204	-4.760682	-0.027241	-4.685843	-3.225504	0.336725
6	-2.202898	0.206171	-6.185458	-1.189986	-0.713629	-6.337157
1	-2.59811	0.059224	-7.19502	-1.480176	-0.963181	-7.360924
1	-2.794172	0.981289	-5.675269	-1.222324	0.376464	-6.204714
1	-1.157012	0.536662	-6.252448	-0.172065	-1.075046	-6.14095
6	0.191123	-1.795444	-8.009024	1.777791	-2.174391	-8.252665
1	-0.454776	-1.179555	-8.65486	0.832707	-1.95327	-8.774261
1	1.032794	-2.175767	-8.607244	2.610799	-2.023335	-8.955025
1	-0.387825	-2.635641	-7.618214	1.769453	-3.216419	-7.923022
6	3.332676	3.375984	-9.903836	2.004731	3.943855	-9.85976
1	2.730405	4.230898	-9.56123	1.200986	4.454124	-9.307829
1	4.296434	3.381744	-9.37281	2.97525	4.310129	-9.492689
1	3.513971	3.473321	-10.977287	1.912597	4.175742	-10.924029
5	2.099051	3.736047	-1.196074	2.241209	3.589811	-1.216467
9	1.657388	5.033805	-1.040547	1.680677	4.824098	-0.958382
9	3.10299	3.425445	-0.300917	3.295521	3.310239	-0.372352

1b

	S_0			S_1		
Atomic Number	X	Y	Z	X	Y	Z
6	0.684012	1.644699	-1.98983	0.545215	1.832157	-1.990953
6	-0.273479	0.722435	-1.437888	-0.353729	0.84536	-1.450305
6	0.629579	2.01929	0.196591	0.376541	2.239147	0.185597
6	-0.266906	0.965897	-0.07594	-0.413935	1.111735	-0.088957
1	-0.860342	0.458951	0.675822	-1.044848	0.60997	0.637001
7	1.18002	2.452125	-0.963258	0.947236	2.686607	-0.993606
6	-1.124259	-0.245067	-2.12358	-1.016102	-0.205229	-2.196833
6	-2.277792	-0.683847	-1.453644	-1.382229	-1.392426	-1.53602
6	-0.811985	-0.743146	-3.394127	-1.314583	-0.038752	-3.560888
6	-3.110061	-1.626147	-2.051863	-2.016755	-2.405508	-2.245827
1	-2.530414	-0.255945	-0.48826	-1.122025	-1.513418	-0.488101
6	-1.656968	-1.693229	-3.974449	-1.969241	-1.055495	-4.251987
1	0.073855	-0.380321	-3.907161	-1.036852	0.887684	-4.052186
6	-2.797262	-2.134141	-3.308463	-2.310655	-2.24136	-3.603685
1	-3.444875	-2.873156	-3.773653	-2.818851	-3.035127	-4.14576
6	0.902032	2.522559	1.539985	0.541513	2.832605	1.497024
6	1.207759	3.862082	1.816375	0.827828	4.193595	1.705088
6	0.802929	1.622112	2.613149	0.365227	2.01169	2.628449
6	1.404022	4.288883	3.122164	0.92791	4.710423	2.987808
1	1.279862	4.578854	1.004595	0.959741	4.855225	0.854357
6	1.006417	2.035108	3.920964	0.466074	2.51698	3.913059
1	0.595741	0.571328	2.417121	0.180332	0.947338	2.494398
6	1.301093	3.371219	4.157999	0.745231	3.869152	4.077284
1	1.632174	5.33133	3.330891	1.141765	5.765889	3.138339
1	0.942236	1.327385	4.743925	0.342023	1.868704	4.777364
7	1.084812	1.721068	-3.241328	0.999332	1.84458	-3.237871
6	2.004686	2.602424	-3.592235	1.966068	2.700548	-3.563906
6	2.424347	2.901651	-4.925587	2.509201	2.887144	-4.883957
6	3.221646	4.026644	-4.826107	3.393652	3.954883	-4.766577
6	3.334038	4.373213	-3.462005	3.416877	4.378437	-3.431665
1	3.76321	4.502192	-5.636739	4.040098	4.351876	-5.541614
6	2.12547	2.173079	-6.153977	2.207298	2.094483	-6.057491
6	2.160196	0.783737	-6.184772	1.517473	0.874868	-5.944288
6	1.907945	2.906803	-7.333645	2.624701	2.523855	-7.330579
6	2.017913	0.11953	-7.409556	1.246289	0.099377	-7.080357
1	2.361379	0.203417	-5.286272	1.182373	0.511914	-4.976309
6	1.726618	2.230656	-8.532796	2.347146	1.742638	-8.445581
1	1.8641	3.991369	-7.278259	3.13851	3.475066	-7.433982
6	1.789841	0.832023	-8.578883	1.651557	0.521991	-8.335501
1	1.662384	0.352391	-9.545087	1.46831	-0.042388	-9.245581
6	4.133179	5.488585	-2.967246	4.216467	5.480059	-2.931191
6	4.306238	6.602898	-3.803815	4.553608	6.515282	-3.825058
6	4.778395	5.479364	-1.722809	4.712531	5.553399	-1.617811
6	5.089242	7.679954	-3.417169	5.351797	7.577642	-3.437085
1	3.792358	6.639667	-4.763128	4.148995	6.50057	-4.835658
6	5.570546	6.548009	-1.328244	5.516258	6.611278	-1.219858
1	4.669018	4.624858	-1.062477	4.482469	4.765545	-0.907635
6	5.716113	7.634793	-2.178584	5.828613	7.610426	-2.13147
1	5.206421	8.544326	-4.066288	5.591551	8.377145	-4.134119
1	6.075493	6.530783	-0.365546	5.902887	6.653597	-0.204373
7	2.610157	3.500299	-2.716048	2.557916	3.579922	-2.693201
8	-4.244709	-2.110345	-1.491222	-2.395053	-3.592091	-1.717629
8	-1.450736	-2.255661	-5.185548	-2.334191	-0.975863	-5.553262
8	2.128232	-1.231358	-7.360886	0.566252	-1.041677	-6.832784
8	1.490502	2.830312	-9.722974	2.69801	2.066523	-9.707264
6	-4.611803	-1.630007	-0.223365	-2.144622	-3.814546	-0.351776
1	-3.838975	-1.842344	0.531256	-1.067562	-3.786065	-0.128705
1	-4.806297	-0.546734	-0.239596	-2.660696	-3.074556	0.2782
1	-5.531122	-2.154176	0.050233	-2.532088	-4.811249	-0.126531
6	-0.287112	-1.895493	-5.890626	-2.231936	0.282287	-6.179526
1	-0.301413	-2.480887	-6.813923	-2.636653	0.15509	-7.187977
1	-0.272815	-0.822859	-6.137205	-2.822506	1.040463	-5.643876
1	0.624212	-2.139139	-5.325081	-1.188609	0.62469	-6.248096
6	2.033857	-1.941138	-8.571902	0.09112	-1.783277	-7.929896
1	1.050529	-1.799795	-9.047208	-0.494641	-1.149657	-8.614526
1	2.819427	-1.636411	-9.278848	0.915181	-2.249358	-8.490454
1	2.163681	-2.99735	-8.321189	-0.558055	-2.557695	-7.514193
6	1.414048	4.234421	-9.747186	3.412843	3.261901	-9.917463
1	0.600034	4.605387	-9.106816	2.82678	4.139154	-9.60734
1	2.360563	4.695772	-9.427606	4.369899	3.256378	-9.376241
1	1.210866	4.513621	-10.784081	3.605541	3.318183	-10.991419
5	2.272823	3.552621	-1.186405	2.09498	3.736845	-1.200927
9	1.78836	4.816646	-0.909954	1.650388	5.03395	-1.031392
9	3.362069	3.236297	-0.400828	3.109571	3.426419	-0.314858
35	1.576205	3.965486	5.97886	0.888541	4.593628	5.865885
35	6.818205	9.126178	-1.624441	6.950458	9.085472	-1.573575

	T_1			T_2		
Atomic Number	X	Y	Z	X	Y	Z
6	0.551255	1.835897	-1.983688	0.695642	1.622321	-2.015673
6	-0.363845	0.844537	-1.441681	-0.259552	0.723675	-1.479817
6	0.351015	2.253455	0.18894	0.610421	2.055494	0.193551
6	-0.438415	1.122821	-0.089137	-0.284979	0.999908	-0.082146
1	-1.076383	0.624263	0.632423	-0.91527	0.535984	0.667817
7	0.939405	2.69358	-0.999426	1.167351	2.445853	-0.976717
6	-1.018344	-0.219151	-2.182615	-1.105624	-0.211667	-2.156758
6	-1.382163	-1.393646	-1.503585	-2.030264	-0.990741	-1.384711
6	-1.31179	-0.07204	-3.546223	-1.084137	-0.348309	-3.558186
6	-2.019319	-2.418348	-2.198383	-2.921739	-1.848832	-2.007201
1	-1.121413	-1.500902	-0.45414	-2.030288	-0.90104	-0.303784
6	-1.96774	-1.101665	-4.221659	-1.994893	-1.196089	-4.164899
1	-1.026482	0.842202	-4.055601	-0.367206	0.237982	-4.125296
6	-2.313484	-2.273781	-3.554205	-2.922101	-1.955795	-3.400661
1	-2.821816	-3.0746	-4.085547	-3.621604	-2.617844	-3.903665
6	0.499776	2.859623	1.494084	0.841249	2.587378	1.532946
6	0.795749	4.219949	1.69198	1.144244	3.931777	1.794131
6	0.293496	2.051764	2.630086	0.705486	1.709802	2.622498
6	0.877602	4.748716	2.970988	1.299963	4.382398	3.096849
1	0.947469	4.872499	0.837876	1.246742	4.631287	0.970534
6	0.378742	2.569331	3.910995	0.86334	2.148256	3.928099
1	0.097047	0.988596	2.504322	0.50758	0.653556	2.443851
6	0.668423	3.920287	4.06587	1.156128	3.487677	4.148617
1	1.098061	5.803607	3.114784	1.527073	5.427793	3.29149
1	0.231633	1.931822	4.779519	0.769975	1.45675	4.762075
7	0.996095	1.840855	-3.236748	1.134247	1.687948	-3.261194
6	1.967837	2.690573	-3.549222	2.057051	2.591765	-3.591088
6	2.520457	2.86797	-4.885446	2.528569	2.852456	-4.906869
6	3.410539	3.920926	-4.768085	3.327933	3.987613	-4.805206
6	3.441877	4.349455	-3.429573	3.381068	4.379218	-3.461452
1	4.061419	4.306966	-5.544468	3.902526	4.441028	-5.606241
6	2.204506	2.082176	-6.064914	2.258699	2.079143	-6.112603
6	1.554055	0.851721	-5.962358	2.145845	0.692378	-6.065766
6	2.588797	2.561937	-7.33606	2.181911	2.745029	-7.350511
6	1.278633	0.105222	-7.113614	1.98477	-0.032503	-7.250811
1	1.244685	0.45651	-4.998894	2.222182	0.154761	-5.122833
6	2.310499	1.808304	-8.465269	1.991724	2.012536	-8.513949
1	3.071866	3.531129	-7.420375	2.248349	3.829828	-7.368837
6	1.649125	0.573288	-8.366271	1.889269	0.614853	-8.475421
1	1.45467	0.027679	-9.285548	1.756237	0.091162	-9.417789
6	4.256961	5.437877	-2.93221	4.137835	5.520509	-2.963939
6	4.629635	6.45224	-3.836199	4.355364	6.602342	-3.834968
6	4.734392	5.517247	-1.612445	4.704079	5.582778	-1.681793
6	5.442564	7.503727	-3.449356	5.108806	7.702081	-3.454429
1	4.243192	6.43125	-4.853593	3.89927	6.59183	-4.823599
6	5.555208	6.562782	-1.217375	5.459306	6.678858	-1.287958
1	4.477852	4.743963	-0.89559	4.568236	4.758721	-0.988943
6	5.90103	7.543447	-2.137482	5.655241	7.724263	-2.178188
1	5.710093	8.288222	-4.153082	5.260756	8.53465	-4.13742
1	5.92877	6.610552	-0.197408	5.899946	6.712789	-0.294334
7	2.568333	3.556095	-2.683735	2.618468	3.507932	-2.716757
8	-2.396623	-3.596566	-1.645684	-3.830875	-2.61707	-1.368893
8	-2.321558	-1.043622	-5.526962	-2.111463	-1.382675	-5.483239
8	0.628195	-1.062088	-6.895482	1.92266	-1.38396	-7.100329
8	2.628582	2.176013	-9.730013	1.888339	2.554451	-9.752554
6	-2.140854	-3.793329	-0.278397	-3.879626	-2.550541	0.0362
1	-1.063144	-3.758121	-0.057827	-2.931298	-2.879329	0.487012
1	-2.657016	-3.044766	0.342001	-4.111692	-1.532513	0.383072
1	-2.523913	-4.787127	-0.032836	-4.678948	-3.226594	0.348152
6	-2.208144	0.200487	-6.179162	-1.184609	-0.72788	-6.335115
1	-2.606346	0.053199	-7.187585	-1.481364	-0.981735	-7.355756
1	-2.800506	0.973267	-5.666418	-1.221498	0.361804	-6.203074
1	-1.163373	0.534426	-6.249278	-0.165197	-1.086598	-6.142938
6	0.183706	-1.789547	-8.013042	1.778557	-2.167465	-8.257832
1	-0.465227	-1.175065	-8.657341	0.833959	-1.950168	-8.782261
1	1.025662	-2.166858	-8.612874	2.613051	-2.012417	-8.957591
1	-0.392135	-2.631696	-7.621593	1.773935	-3.209679	-7.928402
6	3.305188	3.394397	-9.910238	1.990907	3.951435	-9.866317
1	2.70201	4.247515	-9.564439	1.187469	4.463175	-9.315057
1	4.271113	3.401627	-9.382973	2.962	4.317159	-9.499911
1	3.481983	3.49314	-10.984338	1.898869	4.181864	-10.930948
5	2.097362	3.732991	-1.198077	2.243643	3.586202	-1.217623
9	1.663725	5.034765	-1.041524	1.693287	4.826947	-0.956032
9	3.099261	3.419381	-0.299363	3.302313	3.307001	-0.375457
35	0.787132	4.66192	5.847873	1.371202	4.118758	5.96501
35	7.045113	9.000761	-1.582764	6.712919	9.25432	-1.627848

1c

	S_0			S_1		
Atomic Number	X	Y	Z	X	Y	Z
6	0.683495	1.647325	-1.991522	1.478251	-1.21818	-0.169302
6	-0.276018	0.726775	-1.440203	2.01824	-2.553505	-0.145116
6	0.629918	2.02068	0.195213	-0.250559	-2.609793	-0.135397
6	-0.2694	0.969785	-0.078302	0.913482	-3.393352	-0.093527
1	-0.863959	0.463386	0.672884	0.926706	-4.47752	-0.126745
7	1.181021	2.453013	-0.964556	0.107576	-1.273747	-0.203378
6	-1.12763	-0.239888	-2.126001	3.424323	-2.902795	-0.158586
6	-2.281467	-0.677831	-1.456075	3.834978	-4.128746	0.397162
6	-0.815371	-0.738689	-3.396274	4.370733	-2.039156	-0.738869
6	-3.113987	-1.620124	-2.05388	5.183584	-4.466556	0.390282
1	-2.533971	-0.249474	-0.490856	3.093389	-4.772657	0.862173
6	-1.660641	-1.688753	-3.97616	5.714844	-2.403873	-0.757312
1	0.070756	-0.376469	-3.909309	4.032824	-1.098372	-1.161785
6	-2.801239	-2.128884	-3.310186	6.12551	-3.607227	-0.18527
1	-3.448949	-2.868039	-3.775012	7.176471	-3.885901	-0.194384
6	0.906111	2.519247	1.539617	-1.599927	-3.13577	-0.132094
6	1.226197	3.854024	1.8208	-2.688214	-2.480949	-0.734457
6	0.798675	1.61767	2.610608	-1.829277	-4.390934	0.464184
6	1.4292	4.273472	3.12835	-3.948757	-3.058745	-0.74539
1	1.304395	4.57364	1.01199	-2.539375	-1.517096	-1.212093
6	1.008326	2.02539	3.91924	-3.08532	-4.97234	0.462564
1	0.580539	0.569351	2.412739	-1.010858	-4.901631	0.969269
6	1.31928	3.357843	4.168046	-4.141288	-4.300308	-0.148546
1	1.669807	5.314705	3.33041	-4.77573	-2.540897	-1.22652
1	0.934161	1.308563	4.733778	-3.242604	-5.93608	0.942146
7	1.084851	1.72355	-3.242851	2.196734	-0.106464	-0.065215
6	2.005434	2.604357	-3.593465	1.567837	1.057732	0.072815
6	2.426789	2.901488	-4.926725	2.201112	2.351213	0.113941
6	3.224481	4.026162	-4.827933	1.155303	3.268048	0.125559
6	3.335121	4.37513	-3.464155	-0.05955	2.569227	0.133547
1	3.766661	4.500467	-5.638864	1.238354	4.345929	0.212049
6	2.128329	2.171156	-6.154232	3.625015	2.608551	0.168725
6	2.163637	0.781773	-6.183206	4.530533	1.575218	0.459788
6	1.910009	2.903179	-7.334806	4.120701	3.909284	-0.04431
6	2.021416	0.115852	-7.407059	5.905684	1.831611	0.533403
1	2.365078	0.202668	-5.283984	4.183101	0.561612	0.637411
6	1.728515	2.225297	-8.532954	5.486502	4.146262	0.036115
1	1.865584	3.987797	-7.280803	3.431595	4.710914	-0.293566
6	1.792684	0.826658	-8.577273	6.397094	3.109537	0.321057
1	1.665255	0.345802	-9.542864	7.453527	3.358785	0.367469
6	4.131679	5.492605	-2.969913	-1.368748	3.19119	0.139883
6	4.311354	6.603147	-3.809632	-1.500395	4.474692	-0.42514
6	4.766269	5.491635	-1.720448	-2.508928	2.602919	0.714484
6	5.087885	7.684224	-3.419738	-2.710746	5.14659	-0.422453
1	3.807173	6.634923	-4.774397	-0.641661	4.935837	-0.910506
6	5.550093	6.565748	-1.323612	-3.723761	3.271274	0.7268
1	4.656139	4.639659	-1.057042	-2.437074	1.620091	1.169911
6	5.704556	7.654709	-2.173291	-3.820094	4.537322	0.15893
1	5.204498	8.541007	-4.079629	-2.793307	6.129519	-0.881038
1	6.040249	6.545812	-0.352825	-4.592179	2.802085	1.184462
7	2.609976	3.503235	-2.717827	0.205072	1.20861	0.133129
8	-4.248787	-2.103756	-1.492949	5.692595	-5.605028	0.914775
8	-1.454308	-2.252058	-5.186871	6.695478	-1.662513	-1.322807
8	2.132367	-1.234957	-7.356559	6.667066	0.747154	0.803593
8	1.491239	2.823146	-9.723863	6.062489	5.352831	-0.152794
6	-4.614977	-1.623608	-0.224778	4.797405	-6.515483	1.504002
1	-3.841751	-1.83631	0.529341	4.277933	-6.069982	2.365617
1	-4.809205	-0.540279	-0.240584	4.049896	-6.87258	0.779639
1	-5.534268	-2.147599	0.049292	5.399073	-7.361647	1.8452
6	-0.289558	-1.894134	-5.891185	6.307779	-0.547148	-2.091695
1	-0.303922	-2.480879	-6.81365	7.228371	-0.133656	-2.514015
1	-0.273652	-0.821826	-6.13917	5.634589	-0.844785	-2.909431
1	0.620875	-2.138132	-5.324349	5.811662	0.221708	-1.480327
6	2.038261	-1.946374	-8.566587	8.064983	0.892202	0.753516
1	1.055139	-1.805497	-9.042458	8.390852	1.294753	-0.218546
1	2.824127	-1.642775	-9.273707	8.431269	1.553049	1.553461
1	2.167693	-3.002281	-8.31438	8.481269	-0.109871	0.883599
6	1.412371	4.227069	-9.749793	5.229634	6.449692	-0.446147
1	0.598417	4.597475	-9.109013	4.702575	6.307765	-1.40107
1	2.358413	4.69055	-9.43192	4.491216	6.617393	0.35133
1	1.207539	4.504554	-10.786834	5.884632	7.320947	-0.521154
5	2.272878	3.554341	-1.187874	-0.788806	0.003962	-0.033457
9	1.786448	4.817164	-0.909785	-1.562587	0.245136	-1.152084
9	3.362845	3.238133	-0.403351	-1.566651	-0.178787	1.094252
53	1.636231	4.000374	6.17665	-6.077928	-5.188411	-0.156635
53	6.898887	9.307587	-1.548016	-5.695541	5.548048	0.156682

	T_1			T_2		
Atomic Number	X	Y	Z	X	Y	Z
6	0.559129	1.833685	-1.982578	0.692853	1.627046	-2.018271
6	-0.354997	0.842001	-1.440118	-0.264554	0.730288	-1.482937
6	0.356632	2.254231	0.189197	0.609932	2.058102	0.191799
6	-0.431195	1.121867	-0.088388	-0.28881	1.005742	-0.084733
1	-1.07021	0.623778	0.632509	-0.920447	0.542785	0.664604
7	0.946165	2.692918	-0.999141	1.166731	2.448285	-0.978758
6	-1.008307	-0.223205	-2.180223	-1.111429	-0.204256	-2.159387
6	-1.366496	-1.399188	-1.501028	-2.03787	-0.980975	-1.387466
6	-1.306501	-0.075581	-3.542636	-1.08791	-0.343254	-3.560963
6	-2.003042	-2.425125	-2.194664	-2.928542	-1.839479	-2.010042
1	-1.101863	-1.506371	-0.452545	-2.039976	-0.889158	-0.306737
6	-1.962453	-1.106161	-4.216644	-1.998023	-1.191436	-4.167723
1	-1.02474	0.839787	-4.052063	-0.369278	0.241308	-4.127724
6	-2.302609	-2.279939	-3.549157	-2.926614	-1.949005	-3.403567
1	-2.810629	-3.081588	-4.079541	-3.62573	-2.611727	-3.906247
6	0.496081	2.864601	1.49309	0.847034	2.583132	1.532746
6	0.79315	4.224495	1.690487	1.167258	3.921693	1.801414
6	0.273236	2.062739	2.629954	0.703619	1.702372	2.618401
6	0.854216	4.758517	2.968939	1.334555	4.361818	3.106749
1	0.958134	4.874111	0.83655	1.274627	4.625734	0.982213
6	0.337407	2.587485	3.909132	0.872609	2.132302	3.925378
1	0.077162	0.999079	2.506974	0.491973	0.649397	2.43564
6	0.623864	3.94058	4.070338	1.185392	3.466962	4.160528
1	1.07361	5.815718	3.10138	1.577423	5.404852	3.296605
1	0.170854	1.9475	4.772611	0.770689	1.429954	4.749537
7	1.002676	1.83841	-3.236022	1.131897	1.692507	-3.263582
6	1.973448	2.688695	-3.549704	2.055462	2.595684	-3.593255
6	2.521393	2.869182	-4.887369	2.528822	2.854166	-4.908784
6	3.411781	3.921905	-4.770668	3.327855	3.989606	-4.807976
6	3.448221	4.346678	-3.430994	3.379237	4.383534	-3.46472
1	4.06022	4.309633	-5.54827	3.902924	4.442012	-5.609232
6	2.201159	2.085785	-6.067372	2.260535	2.07788	-6.113014
6	1.552181	0.854561	-5.964823	2.148896	0.69112	-6.062754
6	2.579666	2.568678	-7.339054	2.183723	2.740475	-7.352679
6	1.272815	0.110235	-7.116503	1.988958	-0.037015	-7.245955
1	1.247127	0.45701	-5.000953	2.225083	0.15595	-5.118422
6	2.297399	1.817184	-8.468726	1.99459	2.004754	-8.514271
1	3.061395	3.538563	-7.423211	2.249246	3.82529	-7.374109
6	1.637739	0.581284	-8.36969	1.893357	0.607087	-8.472289
1	1.44005	0.037413	-9.289311	1.761164	0.080834	-9.413361
6	4.268635	5.430493	-2.93285	4.13328	5.526633	-2.967375
6	4.641522	6.447525	-3.833128	4.356377	6.606161	-3.83939
6	4.753168	5.502076	-1.615737	4.689587	5.595189	-1.681687
6	5.46139	7.493314	-3.444496	5.102229	7.710061	-3.454599
1	4.250348	6.433298	-4.849012	3.90988	6.591587	-4.832518
6	5.581883	6.541843	-1.221145	5.435922	6.696384	-1.285107
1	4.497098	4.726832	-0.900707	4.553725	4.772493	-0.987243
6	5.931768	7.530575	-2.134484	5.638809	7.746108	-2.172229
1	5.724451	8.275371	-4.153257	5.253316	8.53594	-4.146431
1	5.957696	6.573467	-0.200901	5.862869	6.726268	-0.284998
7	2.576899	3.551979	-2.68408	2.615587	3.513195	-2.719635
8	-2.374497	-3.605125	-1.641613	-3.839273	-2.606201	-1.372106
8	-2.321638	-1.047532	-5.520493	-2.112356	-1.380384	-5.486206
8	0.624389	-1.05823	-6.898169	1.927825	-1.388102	-7.091908
8	2.609817	2.188029	-9.734024	1.891138	2.543503	-9.754312
6	-2.112037	-3.802439	-0.2757	-3.889752	-2.537786	0.032808
1	-1.03353	-3.763054	-0.059772	-2.941979	-2.866005	0.485225
1	-2.628455	-3.05667	0.347855	-4.122071	-1.519249	0.378023
1	-2.48994	-4.798072	-0.029563	-4.689531	-3.213314	0.344745
6	-2.211642	0.197059	-6.172316	-1.183125	-0.727851	-6.336949
1	-2.61285	0.049896	-7.179579	-1.478067	-0.982615	-7.357906
1	-2.80333	0.96887	-5.65731	-1.218815	0.362116	-6.206544
1	-1.167469	0.532285	-6.245413	-0.164398	-1.087377	-6.142351
6	0.176938	-1.784291	-8.015419	1.785378	-2.174768	-8.247449
1	-0.474424	-1.169396	-8.656855	0.841119	-1.959547	-8.773334
1	1.017299	-2.160082	-8.618442	2.620405	-2.020921	-8.946847
1	-0.397053	-2.627462	-7.623415	1.781204	-3.216115	-7.915272
6	3.283407	3.408055	-9.914285	1.991688	3.940338	-9.871225
1	2.679918	4.259279	-9.564378	1.187492	4.452157	-9.321142
1	4.25129	3.416087	-9.390632	2.962232	4.30826	-9.505557
1	3.455916	3.509384	-10.98885	1.899372	4.168232	-10.936383
5	2.107073	3.729553	-1.197698	2.242952	3.588663	-1.219603
9	1.677489	5.032539	-1.04136	1.692057	4.828012	-0.953446
9	3.107587	3.412544	-0.29893	3.303283	3.306992	-0.38041
53	0.69553	4.771348	6.031095	1.449167	4.139926	6.166189
53	7.207753	9.124189	-1.521279	6.781481	9.440342	-1.550067

2a

	S_0			S_1		
Atomic Number	X	Y	Z	X	Y	Z
6	0.696469	1.607157	-1.960111	0.704566	1.581017	-1.940814
6	-0.25329	0.676092	-1.414647	-0.226104	0.683286	-1.392383
6	0.718435	1.935391	0.230257	0.722087	1.930356	0.268077
6	-0.19711	0.88496	-0.040962	-0.186809	0.905519	-0.00573
7	1.226743	2.382219	-0.931964	1.231672	2.349998	-0.930706
6	-1.113651	-0.21648	-2.189743	-1.112184	-0.195132	-2.167112
6	-2.446415	-0.377583	-1.789898	-2.438735	-0.374795	-1.791804
6	-0.624565	-0.884291	-3.318733	-0.685382	-0.825647	-3.329784
6	-3.28184	-1.233827	-2.504503	-3.301459	-1.287213	-2.488773
1	-2.824297	0.18926	-0.945738	-2.839149	0.206019	-0.967455
6	-1.476624	-1.740881	-4.020114	-1.579643	-1.673374	-4.075909
1	0.40399	-0.725874	-3.628172	0.31947	-0.62748	-3.689594
6	-2.79529	-1.92146	-3.610701	-2.872817	-1.931862	-3.633062
1	-3.446734	-2.590757	-4.167221	-3.526589	-2.600145	-4.183824
6	1.092055	2.487367	1.537032	1.10967	2.490561	1.569968
6	0.857529	3.833098	1.834601	0.895672	3.839793	1.869849
6	1.662931	1.65557	2.506291	1.664653	1.659013	2.548455
6	1.182284	4.333585	3.089088	1.226875	4.34066	3.122715
1	0.423036	4.481207	1.07868	0.478859	4.494055	1.109177
6	2.002673	2.166512	3.751618	1.996519	2.163084	3.800197
1	1.862866	0.611082	2.270567	1.855767	0.612349	2.313078
6	1.755569	3.504264	4.0476	1.774735	3.505416	4.091655
1	0.988677	5.380326	3.316095	1.054498	5.393084	3.342806
1	2.461483	1.516184	4.494069	2.436595	1.5048	4.547779
1	2.014403	3.901817	5.027599	2.034481	3.902161	5.072088
7	1.058503	1.716731	-3.221116	1.058535	1.66117	-3.242352
6	1.970638	2.604987	-3.570199	1.961545	2.570236	-3.582029
6	2.379858	2.903873	-4.905154	2.388782	2.867035	-4.911942
6	3.181255	4.028784	-4.79575	3.181214	4.00793	-4.795679
6	3.30692	4.37041	-3.419341	3.290026	4.361862	-3.43419
6	2.062914	2.121257	-6.099552	2.08565	2.087334	-6.110627
6	2.358914	0.763869	-6.124378	2.333276	0.717363	-6.136321
6	1.550838	2.76224	-7.237355	1.619374	2.733798	-7.265842
6	2.183508	0.041613	-7.31146	2.152137	0.001072	-7.323747
1	2.773852	0.257412	-5.254834	2.727456	0.203359	-5.261221
6	1.355649	2.025691	-8.398739	1.432899	2.006881	-8.434493
1	1.309445	3.819983	-7.188651	1.416518	3.799931	-7.224288
6	1.676707	0.662438	-8.444556	1.696566	0.631287	-8.47359
1	1.522306	0.140785	-9.384709	1.549069	0.114043	-9.417343
6	4.085873	5.466837	-2.845031	4.045123	5.472537	-2.855646
6	3.966274	6.753023	-3.38777	3.932031	6.75062	-3.420547
6	4.964898	5.254118	-1.776319	4.900593	5.292481	-1.760836
6	4.706378	7.805706	-2.868572	4.656345	7.818252	-2.908874
1	3.265384	6.93065	-4.201622	3.245929	6.908935	-4.250834
6	5.715364	6.308331	-1.27327	5.629541	6.362088	-1.258692
1	5.051315	4.261804	-1.342662	4.980862	4.310501	-1.303738
6	5.589474	7.583611	-1.815732	5.513906	7.625979	-1.829644
1	4.592148	8.80358	-3.288156	4.545304	8.80664	-3.352339
1	6.402508	6.130783	-0.448205	6.294212	6.204575	-0.410925
1	6.176954	8.407793	-1.414466	6.08594	8.462087	-1.430033
7	2.583799	3.493861	-2.691671	2.553618	3.468597	-2.707087
8	-4.582871	-1.454843	-2.197654	-4.543557	-1.525394	-2.084687
8	-1.112298	-2.454677	-5.109546	-1.211293	-2.268276	-5.194021
8	2.53836	-1.266574	-7.256967	2.438717	-1.331941	-7.254465
8	0.868697	2.537584	-9.552921	0.997698	2.538913	-9.602269
6	-5.105265	-0.8152	-1.060048	-5.035987	-0.938202	-0.88497
1	-4.550827	-1.091106	-0.149664	-4.394449	-1.187596	-0.030608
1	-5.091705	0.280108	-1.166871	-5.119567	0.15049	-0.987286
1	-6.140978	-1.151814	-0.966273	-6.028699	-1.365994	-0.73764
6	0.126563	-2.159185	-5.708631	0.057226	-1.982999	-5.793896
1	0.181676	-2.783355	-6.604987	0.063623	-2.539085	-6.731709
1	0.187435	-1.097706	-5.990601	0.155603	-0.909683	-5.989256
1	0.977123	-2.402817	-5.054099	0.880169	-2.326806	-5.15751
6	2.42247	-2.025345	-8.435991	2.371828	-2.074828	-8.445458
1	1.380403	-2.063798	-8.790174	1.351068	-2.086072	-8.861903
1	3.058321	-1.622558	-9.23805	3.058366	-1.678906	-9.207871
1	2.754259	-3.036557	-8.185735	2.667559	-3.09692	-8.191698
6	0.572564	3.912851	-9.582831	0.787536	3.929672	-9.646018
1	-0.22519	4.168807	-8.869675	-0.017877	4.23909	-8.96309
1	1.461794	4.521229	-9.357076	1.702886	4.484815	-9.390383
1	0.232025	4.132668	-10.597758	0.497263	4.164745	-10.673431
5	2.372755	3.449754	-1.126765	2.351136	3.427799	-1.149554
9	1.983172	4.685642	-0.69048	1.949448	4.664173	-0.706311
9	3.502106	2.986287	-0.495727	3.496111	2.992114	-0.51193
53	4.313272	4.877528	-6.362112	4.338006	4.843703	-6.359223
53	-1.227912	-0.155169	1.482451	-1.249564	-0.168065	1.482682

	T_1			T_2		
Atomic Number	X	Y	Z	X	Y	Z
6	0.72481	1.589508	-1.95095	0.700942	1.523911	-1.99745
6	-0.247778	0.650813	-1.395615	-0.283962	0.66311	-1.459645
6	0.692532	1.93057	0.25085	0.672996	1.977621	0.218789
6	-0.201921	0.876419	-0.021117	-0.255622	0.946382	-0.031673
7	1.207505	2.383466	-0.953827	1.202648	2.332372	-0.9638
6	-1.113112	-0.219746	-2.179492	-1.15339	-0.227447	-2.180677
6	-2.437457	-0.423297	-1.759968	-2.450068	-0.517966	-1.677898
6	-0.638444	-0.844044	-3.342924	-0.737523	-0.79002	-3.405606
6	-3.267309	-1.276924	-2.480572	-3.281807	-1.390812	-2.361584
1	-2.814437	0.114792	-0.897433	-2.807822	-0.005161	-0.792653
6	-1.48378	-1.702311	-4.047843	-1.582139	-1.663683	-4.07449
1	0.375159	-0.644068	-3.673912	0.237615	-0.521049	-3.79645
6	-2.789408	-1.925415	-3.615904	-2.850611	-1.980148	-3.553217
1	-3.439234	-2.59143	-4.178243	-3.501385	-2.663484	-4.092752
6	1.07743	2.497691	1.541561	1.040858	2.583282	1.50855
6	0.923386	3.865887	1.7996	0.712616	3.912289	1.787869
6	1.581238	1.663797	2.548814	1.717464	1.824558	2.468155
6	1.253384	4.381112	3.045814	1.043821	4.466477	3.017873
1	0.547147	4.517632	1.016634	0.215697	4.509047	1.027344
6	1.927554	2.188835	3.785728	2.052137	2.384648	3.694235
1	1.728784	0.60441	2.345338	2.002897	0.798131	2.239196
6	1.756452	3.547035	4.039821	1.710407	3.704798	3.972774
1	1.119427	5.443806	3.239318	0.784894	5.502435	3.228515
1	2.335295	1.534054	4.553701	2.589433	1.790623	4.431348
1	2.021012	3.956808	5.013271	1.972175	4.143802	4.934097
7	1.090441	1.6574	-3.233163	1.107784	1.617573	-3.256866
6	1.990707	2.585877	-3.557291	2.018479	2.535804	-3.583161
6	2.401338	2.894445	-4.912873	2.460741	2.831495	-4.900109
6	3.194246	4.020709	-4.80276	3.267989	3.966083	-4.769766
6	3.330074	4.365214	-3.428925	3.356278	4.318727	-3.412093
6	2.079199	2.113376	-6.105475	2.144027	2.075894	-6.11131
6	2.358901	0.751939	-6.135406	2.338238	0.699372	-6.152978
6	1.575442	2.761274	-7.244337	1.709251	2.760188	-7.257748
6	2.174765	0.034978	-7.323706	2.132639	0.007453	-7.351904
1	2.761363	0.235603	-5.265828	2.696447	0.15405	-5.281823
6	1.376104	2.03147	-8.408944	1.495685	2.057825	-8.435833
1	1.341159	3.820436	-7.192416	1.548708	3.832703	-7.200108
6	1.679802	0.664583	-8.457686	1.707637	0.67427	-8.492811
1	1.518935	0.146063	-9.398481	1.540786	0.174996	-9.44296
6	4.091089	5.45847	-2.848931	4.112708	5.418379	-2.810452
6	4.024585	6.734592	-3.433274	3.976903	6.712748	-3.329258
6	4.910119	5.26869	-1.724253	4.996362	5.205399	-1.745642
6	4.756371	7.788843	-2.908985	4.70275	7.768239	-2.794576
1	3.361503	6.904304	-4.279144	3.276962	6.890042	-4.144383
6	5.654043	6.324004	-1.218184	5.725882	6.263475	-1.218858
1	4.957162	4.290024	-1.255817	5.104093	4.206671	-1.332109
6	5.58145	7.584532	-1.805768	5.583747	7.545718	-1.740234
1	4.677722	8.776334	-3.359999	4.576985	8.770044	-3.20223
1	6.294369	6.160306	-0.353617	6.413619	6.082205	-0.394594
1	6.162403	8.410679	-1.399168	6.156189	8.372613	-1.322646
7	2.601377	3.449556	-2.690607	2.598002	3.433391	-2.697352
8	-4.557532	-1.534462	-2.157683	-4.530995	-1.728017	-1.970433
8	-1.126478	-2.373892	-5.165796	-1.28968	-2.281491	-5.2307
8	2.504331	-1.28029	-7.270065	2.371246	-1.331928	-7.304638
8	0.897952	2.552716	-9.56306	1.0841	2.622606	-9.597187
6	-5.073453	-0.93592	-0.995118	-5.014241	-1.177541	-0.769486
1	-4.495668	-1.220745	-0.102173	-4.378453	-1.454748	0.085491
1	-5.087965	0.16166	-1.074739	-5.083096	-0.080768	-0.825615
1	-6.098901	-1.29986	-0.890874	-6.014593	-1.59197	-0.622555
6	0.113742	-2.05527	-5.750699	-0.069669	-1.950655	-5.864463
1	0.17653	-2.637376	-6.674315	-0.044594	-2.522556	-6.79501
1	0.177029	-0.982789	-5.985735	-0.019723	-0.875367	-6.086176
1	0.960353	-2.327298	-5.102225	0.796966	-2.2274	-5.247798
6	2.356442	-2.041289	-8.443535	2.240766	-2.059062	-8.499692
1	1.311783	-2.04597	-8.79284	1.214195	-2.006642	-8.897024
1	3.001257	-1.666024	-9.251882	2.936837	-1.696615	-9.270721
1	2.654417	-3.06199	-8.188873	2.47981	-3.098636	-8.258147
6	0.616083	3.930798	-9.588913	0.913433	4.018549	-9.617569
1	-0.182182	4.192546	-8.878385	0.120334	4.339866	-8.925693
1	1.510364	4.529541	-9.356956	1.845535	4.543884	-9.358257
1	0.28246	4.158178	-10.604524	0.625136	4.278503	-10.639559
5	2.350328	3.441759	-1.138961	2.324721	3.451398	-1.17045
9	1.951766	4.693954	-0.744884	1.833875	4.668512	-0.777691
9	3.464225	3.003735	-0.456672	3.415567	3.049457	-0.43666
53	4.326136	4.855411	-6.376092	4.442733	4.819436	-6.306378
53	-1.238973	-0.163363	1.500925	-1.124423	-0.141025	1.510898

2b

	S_0			S_1		
Atomic Number	X	Y	Z	X	Y	Z
6	0.693119	1.605546	-1.96411	0.70438	1.583462	-1.940036
6	-0.25443	0.672975	-1.416973	-0.220042	0.679784	-1.391099
6	0.716962	1.932729	0.225638	0.734819	1.918383	0.270275
6	-0.196186	0.881024	-0.042458	-0.172699	0.890609	-0.004464
7	1.223429	2.381518	-0.936761	1.235203	2.348869	-0.928926
6	-1.115476	-0.220199	-2.189571	-1.107392	-0.196807	-2.168712
6	-2.446624	-0.383206	-1.784706	-2.438442	-0.360905	-1.80403
6	-0.629103	-0.885859	-3.321083	-0.674191	-0.838804	-3.321725
6	-3.283905	-1.238912	-2.49789	-3.304085	-1.267706	-2.505813
1	-2.822582	0.182659	-0.939038	-2.8391	0.225877	-0.983881
6	-1.482544	-1.743053	-4.02008	-1.570287	-1.679384	-4.074513
1	0.398326	-0.726495	-3.633778	0.337909	-0.658403	-3.669948
6	-2.799758	-1.92489	-3.606299	-2.870099	-1.921697	-3.642876
1	-3.452334	-2.594362	-4.161261	-3.526135	-2.58397	-4.198242
6	1.091746	2.488524	1.530563	1.125989	2.472689	1.572301
6	0.857804	3.834048	1.825832	0.960804	3.83044	1.864078
6	1.665618	1.663162	2.502289	1.638655	1.629783	2.563399
6	1.179305	4.346691	3.076448	1.288074	4.333806	3.117383
1	0.421874	4.483535	1.071957	0.585252	4.499782	1.095274
6	2.008345	2.171055	3.748323	1.97078	2.119869	3.820881
1	1.86936	0.617768	2.274411	1.80349	0.576241	2.340922
6	1.751855	3.50922	4.026024	1.784453	3.470423	4.086191
1	0.984438	5.392718	3.301594	1.152919	5.391898	3.330733
1	2.47037	1.526531	4.492453	2.377749	1.453625	4.578132
7	1.054337	1.716265	-3.225237	1.053043	1.666958	-3.241973
6	1.966037	2.605125	-3.574259	1.955219	2.575838	-3.583123
6	2.375274	2.905488	-4.909028	2.380439	2.873117	-4.913447
6	3.176532	4.031236	-4.798981	3.17208	4.014386	-4.799012
6	3.30182	4.370037	-3.422644	3.281795	4.367737	-3.437453
6	2.060199	2.122975	-6.103753	2.078978	2.089648	-6.110585
6	2.355078	0.765183	-6.12658	2.337771	0.721844	-6.133075
6	1.552536	2.764193	-7.243477	1.604027	2.73004	-7.265347
6	2.1837	0.04246	-7.314154	2.158678	0.000642	-7.318042
1	2.767675	0.258728	-5.255943	2.738211	0.212927	-5.257825
6	1.360581	2.02701	-8.405136	1.419255	1.998155	-8.431529
1	1.310922	3.821935	-7.19644	1.391228	3.794347	-7.226221
6	1.681369	0.663548	-8.449067	1.694284	0.624625	-8.467641
1	1.530333	0.141824	-9.389725	1.547337	0.103856	-9.409552
6	4.081069	5.463965	-2.844234	4.033712	5.479903	-2.859216
6	3.972841	6.750591	-3.38632	3.928192	6.755357	-3.430006
6	4.948905	5.251096	-1.767239	4.878481	5.307768	-1.75549
6	4.709315	7.805838	-2.86658	4.647109	7.830268	-2.925131
1	3.280911	6.936433	-4.205787	3.249846	6.915807	-4.265999
6	5.702284	6.297222	-1.251814	5.608167	6.373872	-1.246575
1	5.030903	4.26065	-1.328264	4.95745	4.330447	-1.28827
6	5.576521	7.565462	-1.806622	5.489159	7.625032	-1.838943
1	4.603746	8.804127	-3.285158	4.542854	8.81647	-3.372185
1	6.380784	6.119386	-0.420901	6.26486	6.223451	-0.392832
7	2.579409	3.492772	-2.694689	2.54894	3.4729	-2.708208
8	-4.583319	-1.461036	-2.187864	-4.552192	-1.491142	-2.113912
8	-1.121487	-2.455842	-5.110656	-1.196937	-2.280845	-5.18707
8	2.537732	-1.265391	-7.257808	2.455637	-1.329306	-7.245618
8	0.877489	2.537963	-9.560722	0.975432	2.522821	-9.598659
6	-5.104563	-0.821366	-1.049405	-5.054797	-0.89058	-0.924743
1	-4.548932	-1.097385	-0.139825	-4.430233	-1.144851	-0.059396
1	-5.091482	0.273848	-1.156678	-5.122315	0.19845	-1.03425
1	-6.139956	-1.158331	-0.954402	-6.055162	-1.304359	-0.790379
6	0.116706	-2.162161	-5.712256	0.07732	-2.003395	-5.779104
1	0.169767	-2.788303	-6.607207	0.086138	-2.55857	-6.717396
1	0.177198	-1.101279	-5.996589	0.182919	-0.930538	-5.972846
1	0.968082	-2.404991	-5.05859	0.893328	-2.353714	-5.137311
6	2.428381	-2.024862	-8.437505	2.393801	-2.076375	-8.434794
1	1.388579	-2.062472	-8.798115	1.372406	-2.098812	-8.849068
1	3.069999	-1.623129	-9.235381	3.07516	-1.67584	-9.199286
1	2.757614	-3.03616	-8.184448	2.700187	-3.094606	-8.178521
6	0.582431	3.913603	-9.593879	0.752269	3.911657	-9.646368
1	-0.217806	4.171091	-8.884125	-0.054295	4.215509	-8.962367
1	1.471408	4.521504	-9.366022	1.663263	4.475669	-9.394873
1	0.245899	4.132007	-10.610373	0.457375	4.140696	-10.673718
5	2.369213	3.446382	-1.131332	2.344331	3.434482	-1.15263
9	1.98281	4.682648	-0.690695	1.931708	4.671544	-0.715755
9	3.499393	2.981898	-0.50071	3.492129	3.014255	-0.508977
53	4.30898	4.881975	-6.36362	4.324103	4.849783	-6.365414
53	-1.216605	-0.165039	1.483246	-1.245624	-0.188063	1.472316
53	6.730898	9.173122	-1.014059	6.616086	9.264927	-1.060737
53	2.24753	4.291021	5.948085	2.277485	4.233529	6.021805

	T_1			T_2		
Atomic Number	X	Y	Z	X	Y	Z
6	0.71925	1.590463	-1.953892	0.69821	1.525979	-1.997715
6	-0.251046	0.649618	-1.397822	-0.280661	0.658997	-1.458831
6	0.685665	1.930675	0.247831	0.674406	1.97018	0.21683
6	-0.205318	0.874984	-0.02216	-0.250416	0.934309	-0.035763
7	1.199572	2.385907	-0.957252	1.200722	2.333025	-0.964973
6	-1.114689	-0.221959	-2.180813	-1.146255	-0.235184	-2.183234
6	-2.437446	-0.431434	-1.758035	-2.446883	-0.521714	-1.6835
6	-0.640097	-0.842292	-3.346945	-0.727839	-0.798634	-3.403962
6	-3.265785	-1.286585	-2.478268	-3.279884	-1.395545	-2.365472
1	-2.81507	0.104291	-0.894338	-2.805492	-0.004031	-0.801318
6	-1.483349	-1.703289	-4.050768	-1.573356	-1.671285	-4.073185
1	0.372075	-0.63853	-3.679771	0.248179	-0.531699	-3.793936
6	-2.787319	-1.931542	-3.615831	-2.845947	-1.986748	-3.554208
1	-3.435877	-2.599323	-4.177538	-3.495186	-2.669498	-4.09625
6	1.071057	2.500378	1.537021	1.039438	2.577759	1.505716
6	0.929145	3.870063	1.790559	0.717257	3.908896	1.77997
6	1.566879	1.669908	2.549975	1.710669	1.823912	2.471945
6	1.257427	4.39664	3.032609	1.041305	4.474533	3.006704
1	0.56101	4.5256	1.006961	0.225082	4.508492	1.018648
6	1.915241	2.19011	3.788499	2.04667	2.381313	3.699234
1	1.710303	0.608217	2.356536	1.99757	0.795913	2.253005
6	1.747555	3.55091	4.021131	1.699944	3.702653	3.956569
1	1.131923	5.460354	3.221614	0.785185	5.510924	3.213856
1	2.316529	1.53844	4.561083	2.581412	1.791975	4.440622
7	1.085161	1.659918	-3.235785	1.100962	1.621981	-3.25872
6	1.985958	2.587599	-3.559079	2.010349	2.541574	-3.584572
6	2.39714	2.897288	-4.914221	2.449312	2.840573	-4.902126
6	3.190915	4.023084	-4.803789	3.256421	3.975017	-4.771921
6	3.326781	4.365444	-3.429723	3.348165	4.323352	-3.413078
6	2.075269	2.116572	-6.106958	2.132417	2.084136	-6.112818
6	2.356674	0.755438	-6.136158	2.329498	0.707858	-6.152392
6	1.571281	2.76422	-7.24583	1.69636	2.766316	-7.259832
6	2.174323	0.038051	-7.324602	2.126534	0.014017	-7.350769
1	2.759973	0.239725	-5.266596	2.689754	0.164583	-5.280748
6	1.372861	2.033776	-8.410339	1.484711	2.061874	-8.437286
1	1.335412	3.823056	-7.19436	1.533238	3.838554	-7.204037
6	1.678687	0.667202	-8.458521	1.700231	0.678727	-8.492363
1	1.518796	0.148424	-9.399343	1.535235	0.178185	-9.442163
6	4.09058	5.454695	-2.847746	4.108822	5.417818	-2.809467
6	4.044913	6.728365	-3.438108	3.997456	6.710701	-3.336261
6	4.893839	5.267226	-1.711769	4.973968	5.204268	-1.730098
6	4.779776	7.783073	-2.919214	4.7277	7.765889	-2.806254
1	3.393671	6.905611	-4.291442	3.309925	6.898078	-4.1593
6	5.646215	6.31257	-1.198089	5.714802	6.250801	-1.19592
1	4.9268	4.293701	-1.231067	5.064174	4.20967	-1.302424
6	5.585768	7.562319	-1.806704	5.586851	7.522282	-1.741359
1	4.717047	8.768591	-3.375021	4.621214	8.766471	-3.219486
1	6.27432	6.149987	-0.325386	6.38888	6.069171	-0.362031
7	2.597559	3.449588	-2.691314	2.592394	3.435745	-2.697624
8	-4.553703	-1.549572	-2.154007	-4.529563	-1.729305	-1.97609
8	-1.126706	-2.372352	-5.169702	-1.282236	-2.290291	-5.22654
8	2.505462	-1.276334	-7.270502	2.36882	-1.324455	-7.301822
8	0.894025	2.553544	-9.564181	1.072151	2.623771	-9.599014
6	-5.070892	-0.9555	-0.989261	-5.015957	-1.173402	-0.778224
1	-4.490559	-1.239887	-0.097909	-4.383163	-1.448605	0.079499
1	-5.090476	0.142051	-1.067092	-5.08345	-0.076907	-0.839281
1	-6.094408	-1.324388	-0.884496	-6.017088	-1.586221	-0.633066
6	0.113077	-2.052742	-5.755489	-0.060621	-1.964766	-5.862567
1	0.17591	-2.635396	-6.678668	-0.039456	-2.537866	-6.792233
1	0.174719	-0.980344	-5.991265	-0.007963	-0.889873	-6.084516
1	0.959953	-2.32364	-5.106973	0.804321	-2.244526	-5.245339
6	2.362565	-2.037609	-8.44488	2.244711	-2.053142	-8.497109
1	1.31876	-2.045166	-8.796466	1.218788	-2.005764	-8.896628
1	3.008343	-1.660021	-9.251251	2.940958	-1.687757	-9.266421
1	2.662997	-3.057381	-8.189673	2.488305	-3.091307	-8.254243
6	0.60975	3.931363	-9.591461	0.898809	4.019604	-9.62267
1	-0.188913	4.192225	-8.881126	0.104458	4.340718	-8.932215
1	1.503203	4.531615	-9.360411	1.829849	4.547045	-9.363997
1	0.275662	4.156979	-10.607226	0.61092	4.276581	-10.64544
5	2.34202	3.44251	-1.14205	2.327159	3.442525	-1.169423
9	1.944469	4.696399	-0.748787	1.854523	4.663037	-0.762767
9	3.45404	3.005685	-0.454097	3.421602	3.026887	-0.445362
53	4.323583	4.854628	-6.378155	4.42808	4.826807	-6.311444
53	-1.236753	-0.170731	1.499628	-1.119902	-0.15838	1.504449
53	6.738658	9.168957	-1.015521	6.731478	9.131764	-0.928953
53	2.256509	4.353569	5.930356	2.1996	4.567252	5.842269

3

	S_0			S_1			S_2		
Atomic Number	X	Y	X	X	X	Z	X	X	Z
6	0.865451	1.872195	-2.060645	0.878127	1.819662	-2.06977	1.057348	1.862936	-2.158471
6	-0.113975	0.930485	-1.6464	-0.093832	0.892282	-1.629502	0.108945	0.885205	-1.768388
6	0.795413	2.002258	0.145595	0.809331	1.984211	0.154854	0.947946	1.964112	0.062387
6	-0.132932	0.999615	-0.270214	-0.108918	0.991565	-0.243024	0.075561	0.948896	-0.374843
7	1.379968	2.532357	-0.950695	1.395848	2.49037	-0.978144	1.53654	2.523607	-1.041911
6	-0.882314	0.100549	-2.584539	-0.88764	0.055501	-2.535589	-0.540545	-0.065058	-2.677205
6	-1.998194	0.599924	-3.254379	-1.963349	0.566475	-3.26961	-1.367772	0.294344	-3.74511
6	-0.434643	-1.199072	-2.842295	-0.540794	-1.287707	-2.701397	-0.292339	-1.427983	-2.448996
6	-2.646396	-0.190746	-4.21132	-2.655726	-0.239233	-4.183062	-1.923836	-0.688229	-4.582861
6	-1.09245	-1.990218	-3.782546	-1.237053	-2.09913	-3.597444	-0.857729	-2.399878	-3.261942
1	0.440746	-1.560383	-2.307386	0.296083	-1.668586	-2.121269	0.360083	-1.69014	-1.621116
6	-2.193258	-1.475925	-4.468729	-2.289205	-1.565786	-4.345211	-1.664618	-2.030661	-4.341399
1	-2.689658	-2.08565	-5.221558	-2.818263	-2.195335	-5.058352	-2.084029	-2.821085	-4.957882
6	1.095662	2.412947	1.514955	1.118914	2.425263	1.513917	1.214137	2.390535	1.435732
6	1.140199	3.763396	1.880277	1.190775	3.782244	1.851893	1.163101	3.738457	1.80957
6	1.322988	1.435392	2.491965	1.324828	1.473245	2.521023	1.495507	1.432183	2.417576
6	1.392325	4.128874	3.195825	1.446913	4.177424	3.158362	1.378959	4.119179	3.127867
1	0.97769	4.529815	1.128215	1.055124	4.534005	1.080044	0.962943	4.494123	1.056044
6	1.593097	1.792307	3.8052	1.585006	1.855988	3.830208	1.716138	1.8	3.738097
1	1.316527	0.382343	2.21549	1.306466	0.41393	2.26982	1.565877	0.382344	2.137467
6	1.615657	3.140252	4.147025	1.6365	3.210051	4.137169	1.649995	3.144897	4.080446
1	1.412635	5.180382	3.472476	1.494174	5.235395	3.406143	1.333741	5.169892	3.405057
1	1.782874	1.024924	4.551973	1.752168	1.10283	4.596954	1.941982	1.044175	4.486737
7	1.257757	2.058767	-3.301716	1.248431	1.990033	-3.334408	1.44761	2.088153	-3.402412
6	2.222748	2.912295	-3.553762	2.222675	2.877074	-3.576055	2.376735	3.032169	-3.596056
6	2.660026	3.288506	-4.854919	2.656629	3.262963	-4.855325	2.717541	3.535652	-4.858344
6	3.611552	4.26239	-4.656874	3.608566	4.265294	-4.650457	3.641738	4.555774	-4.630553
6	3.752697	4.478463	-3.250799	3.758883	4.46868	-3.271925	3.86961	4.649081	-3.247956
6	2.112594	2.678771	-6.072822	2.124415	2.676002	-6.087691	1.93473	3.055043	-6.002721
6	2.837025	1.680798	-6.712337	2.908893	1.863687	-6.87364	2.139006	1.770204	-6.453622
6	0.830261	3.011117	-6.530036	0.779368	2.883454	-6.502372	0.800498	3.741229	-6.485592
6	2.2868	0.987641	-7.793183	2.390835	1.224819	-8.023459	1.220749	1.131232	-7.333305
1	3.836456	1.418243	-6.369601	3.948402	1.684765	-6.608912	2.974005	1.18551	-6.078718
6	0.259719	2.285443	-7.57345	0.227524	2.182041	-7.608243	-0.128535	3.099709	-7.38205
6	0.988145	1.274166	-8.203941	1.039835	1.362215	-8.370823	0.088006	1.792528	-7.800061
1	0.500634	0.746719	-9.020076	0.593996	0.857703	-9.223014	-0.621982	1.297242	-8.451507
6	4.624786	5.442879	-2.584728	4.627282	5.424261	-2.580495	4.785192	5.537156	-2.531473
6	4.649795	6.771025	-3.029263	4.639816	6.766829	-2.976547	4.865414	6.891523	-2.877493
6	5.441209	5.068752	-1.510985	5.467204	5.02804	-1.533467	5.604921	5.062426	-1.500255
6	5.462705	7.71124	-2.412182	5.467163	7.693183	-2.354856	5.745639	7.749057	-2.230457
1	4.001204	7.080988	-3.846877	3.972788	7.098451	-3.770966	4.208073	7.290509	-3.648461
6	6.271108	5.998966	-0.900415	6.298619	5.94461	-0.902243	6.487037	5.910484	-0.842544
1	5.423804	4.044583	-1.150338	5.457271	3.994391	-1.200908	5.535704	4.020817	-1.198278
6	6.273263	7.31265	-1.354606	6.293417	7.268781	-1.321731	6.554091	7.245997	-1.219139
1	5.457614	8.744391	-2.751604	5.45548	8.735044	-2.667294	5.787631	8.800446	-2.506096
1	6.906812	5.696982	-0.071518	6.943692	5.621715	-0.08822	7.11573	5.524811	-0.042873
7	2.921378	3.639759	-2.596007	2.91677	3.592815	-2.627966	3.078938	3.705486	-2.628431
8	-3.697823	0.303384	-4.922576	-3.665608	0.272641	-4.947568	-2.712443	-0.269758	-5.607247
8	-0.733099	-3.251155	-4.107845	-0.95731	-3.399343	-3.825141	-0.68016	-3.731041	-3.100235
8	3.078654	0.047911	-8.356869	3.262752	0.483278	-8.696911	1.536926	-0.116831	-7.63548
8	-1.001212	2.538636	-8.015209	-1.061104	2.331011	-7.969307	-1.180953	3.815809	-7.738986
6	-4.961601	-0.140848	-4.465301	-4.962452	-0.019481	-4.454868	-3.492762	-1.233072	-6.270416
1	-5.125228	0.15135	-3.41705	-5.115493	0.425775	-3.460005	-4.10307	-1.81342	-5.564031
1	-5.713926	0.33939	-5.096531	-5.676204	0.415922	-5.159587	-4.152767	-0.681193	-6.945927
1	-5.05608	-1.234011	-4.551678	-5.126303	-1.10529	-4.391552	-2.877041	-1.930664	-6.860065
6	0.388605	-3.803862	-3.461334	0.089589	-3.988875	-3.087354	0.064448	-4.158919	-1.982973
1	0.506596	-4.813664	-3.861878	0.145975	-5.029568	-3.415235	0.041358	-5.251323	-1.999226
1	1.299863	-3.224172	-3.670414	1.050539	-3.492491	-3.285958	1.108885	-3.818527	-2.039283
1	0.2395	-3.862333	-2.372966	-0.114282	-3.959234	-2.007411	-0.378494	-3.798768	-1.042322
6	2.571778	-0.661521	-9.460962	2.839608	-0.206734	-9.862211	0.645852	-0.890214	-8.424902
1	1.685081	-1.253828	-9.188676	2.059858	-0.939955	-9.619984	-0.329047	-0.970587	-7.928053
1	2.310446	0.014518	-10.288631	2.469991	0.496984	-10.618833	0.527931	-0.447449	-9.422222
1	3.368036	-1.336145	-9.785101	3.723194	-0.722395	-10.240946	1.101393	-1.877199	-8.511241
6	-1.999989	1.821663	-7.302154	-1.991273	1.503067	-7.265297	-2.244161	3.180742	-8.435983
1	-2.024548	2.105673	-6.23921	-2.064344	1.783093	-6.206633	-2.621147	2.329911	-7.852839
1	-2.9589	2.075229	-7.761313	-2.961583	1.655822	-7.741442	-3.022449	3.937469	-8.541075
1	-1.831337	0.735866	-7.376254	-1.700632	0.445546	-7.339005	-1.914604	2.850646	-9.429543
5	2.577263	3.573133	-1.047009	2.549141	3.557	-1.095808	2.773286	3.507835	-1.090577
9	2.186021	4.823146	-0.647178	2.106036	4.818006	-0.745829	2.467931	4.737665	-0.555019
9	3.627881	3.076151	-0.321219	3.607652	3.146155	-0.320169	3.826552	2.904538	-0.438552
53	4.70134	5.167575	-6.209095	4.703755	5.196155	-6.198484	4.656334	5.564566	-6.1878
53	-1.518253	-0.027062	0.934424	-1.509983	-0.015237	0.973893	-1.313064	-0.095766	0.830047
53	7.533338	8.744436	-0.402033	7.568156	8.683139	-0.348815	7.909852	8.55973	-0.213785
53	2.001235	3.700587	6.16828	2.023848	3.815009	6.151444	1.979007	3.725583	6.11225
53	-0.21812	4.674545	-5.719375	-0.386174	4.315606	-5.572813	0.371841	5.65919	-5.827279
53	-2.751047	2.54153	-2.827984	-2.628802	2.560563	-2.95205	-1.973471	2.314638	-4.052583

	T_1			T_2		
Atomic Number	X	Y	Z	X	Y	Z
7	0.864245	1.876017	-2.092041	0.868748	1.828029	-2.07907
6	-0.078752	0.872945	-1.665861	-0.110363	0.906594	-1.641398
6	0.742085	2.02195	0.124249	0.778506	2.010527	0.143023
6	-0.118415	0.96318	-0.295344	-0.140559	1.018634	-0.25677
7	1.312824	2.580971	-1.007353	1.377839	2.506257	-0.987576
6	-0.798249	-0.009784	-2.592056	-0.891399	0.057068	-2.547663
6	-1.899548	0.440732	-3.318908	-1.97884	0.546386	-3.277
6	-0.338766	-1.320015	-2.761967	-0.512035	-1.277393	-2.717661
6	-2.525961	-0.410279	-4.23668	-2.655391	-0.275162	-4.187417
6	-0.969364	-2.170078	-3.668647	-1.193092	-2.104081	-3.610744
1	0.523105	-1.640332	-2.181548	0.334871	-1.63889	-2.139625
6	-2.061018	-1.70617	-4.404349	-2.260747	-1.593816	-4.351717
1	-2.541097	-2.364643	-5.12591	-2.779859	-2.234079	-5.06269
6	1.003836	2.484319	1.473515	1.080986	2.457418	1.501566
6	1.057224	3.853493	1.77838	1.158515	3.815988	1.831556
6	1.18354	1.554672	2.511077	1.27564	1.510414	2.515696
6	1.267733	4.280123	3.08106	1.41067	4.217967	3.136692
1	0.926191	4.586459	0.988834	1.029514	4.563839	1.054941
6	1.410662	1.973818	3.812581	1.531911	1.899965	3.823649
1	1.184648	0.489633	2.2877	1.252236	0.44965	2.271138
6	1.44321	3.337399	4.08874	1.590521	3.255624	4.122276
1	1.292814	5.343675	3.306032	1.462714	5.277162	3.378088
1	1.567303	1.242105	4.60158	1.691198	1.150617	4.595787
7	1.244786	2.045432	-3.350559	1.250179	1.990325	-3.341791
6	2.214462	2.929985	-3.565988	2.234136	2.867254	-3.57831
6	2.64861	3.336546	-4.879093	2.680157	3.245512	-4.855229
6	3.642457	4.25945	-4.669292	3.641782	4.238715	-4.647067
6	3.817797	4.441134	-3.262605	3.784109	4.444557	-3.268281
6	2.066911	2.76837	-6.099802	2.134402	2.672762	-6.087004
6	2.761287	1.790091	-6.799926	2.902378	1.856414	-6.883531
6	0.775875	3.129429	-6.507974	0.787999	2.899051	-6.490575
6	2.171214	1.147245	-7.891058	2.364889	1.224185	-8.031128
1	3.766669	1.502849	-6.496835	3.943247	1.666787	-6.631927
6	0.166646	2.459455	-7.565647	0.214758	2.195291	-7.5893
6	0.866197	1.466201	-8.255188	1.010096	1.370154	-8.362055
1	0.353492	0.978386	-9.080629	0.550397	0.866147	-9.206989
6	4.706696	5.357364	-2.575089	4.657589	5.392375	-2.572312
6	4.884235	6.662859	-3.064111	4.684324	6.734572	-2.968569
6	5.401412	4.972236	-1.417052	5.486594	4.989	-1.519485
6	5.725079	7.557741	-2.420657	5.515049	7.653899	-2.340994
1	4.319531	6.996203	-3.932155	4.025653	7.07156	-3.767708
6	6.256948	5.856368	-0.778448	6.321299	5.898501	-0.88228
1	5.264798	3.973129	-1.014122	5.465598	3.955506	-1.1869
6	6.411786	7.143617	-1.283373	6.330137	7.222646	-1.301819
1	5.833474	8.57166	-2.798985	5.514258	8.695845	-2.65335
1	6.796829	5.540842	0.11134	6.957802	5.570229	-0.063646
7	2.947497	3.57713	-2.611454	2.928279	3.579877	-2.627731
8	-3.571339	0.024205	-4.995712	-3.677824	0.213174	-4.951546
8	-0.596467	-3.445937	-3.911033	-0.884908	-3.398522	-3.840687
8	2.933653	0.220998	-8.515257	3.22273	0.479626	-8.714883
8	-1.098395	2.752515	-7.968872	-1.074876	2.354588	-7.933517
6	-4.840833	-0.325791	-4.475492	-4.966105	-0.08824	-4.442854
1	-4.996086	0.11922	-3.480586	-5.112494	0.361516	-3.449158
1	-5.587575	0.070636	-5.168827	-5.69179	0.336014	-5.142287
1	-4.952672	-1.418265	-4.402385	-5.118631	-1.175362	-4.371419
6	0.52014	-3.95092	-3.217978	0.178454	-3.963384	-3.10812
1	0.652942	-4.980178	-3.560056	0.256066	-5.003271	-3.434509
1	1.429274	-3.374593	-3.444947	1.127477	-3.44659	-3.312722
1	0.354633	-3.950357	-2.130402	-0.019364	-3.936455	-2.026893
6	2.385194	-0.43163	-9.633985	2.783982	-0.203363	-9.880299
1	1.491623	-1.014851	-9.364796	2.007207	-0.936923	-9.631013
1	2.121006	0.28328	-10.427463	2.405209	0.506483	-10.62621
1	3.157414	-1.110604	-10.004276	3.662607	-0.71666	-10.273018
6	-2.096228	2.031347	-7.258512	-2.009791	1.550516	-7.204642
1	-2.093703	2.284741	-6.187565	-2.051012	1.832911	-6.144624
1	-3.058786	2.317086	-7.690731	-2.985797	1.726802	-7.66002
1	-1.951825	0.945512	-7.367728	-1.745266	0.487182	-7.287258
5	2.576801	3.525272	-1.076527	2.544079	3.559257	-1.0995
9	2.293845	4.802744	-0.661427	2.112598	4.827782	-0.76312
9	3.573476	2.938692	-0.329064	3.590099	3.141982	-0.310289
53	4.752916	5.118151	-6.233641	4.751755	5.159368	-6.190218
53	-1.48728	-0.107442	0.889697	-1.556574	0.02608	0.952943
53	7.701501	8.511965	-0.28218	7.609399	8.626892	-0.320304
53	1.780095	3.987688	6.089716	1.974328	3.870421	6.134137
53	-0.210986	4.773618	-5.58698	-0.340415	4.372652	-5.583344
53	-2.653294	2.406664	-3.024264	-2.675858	2.533319	-2.968615

Figure S2

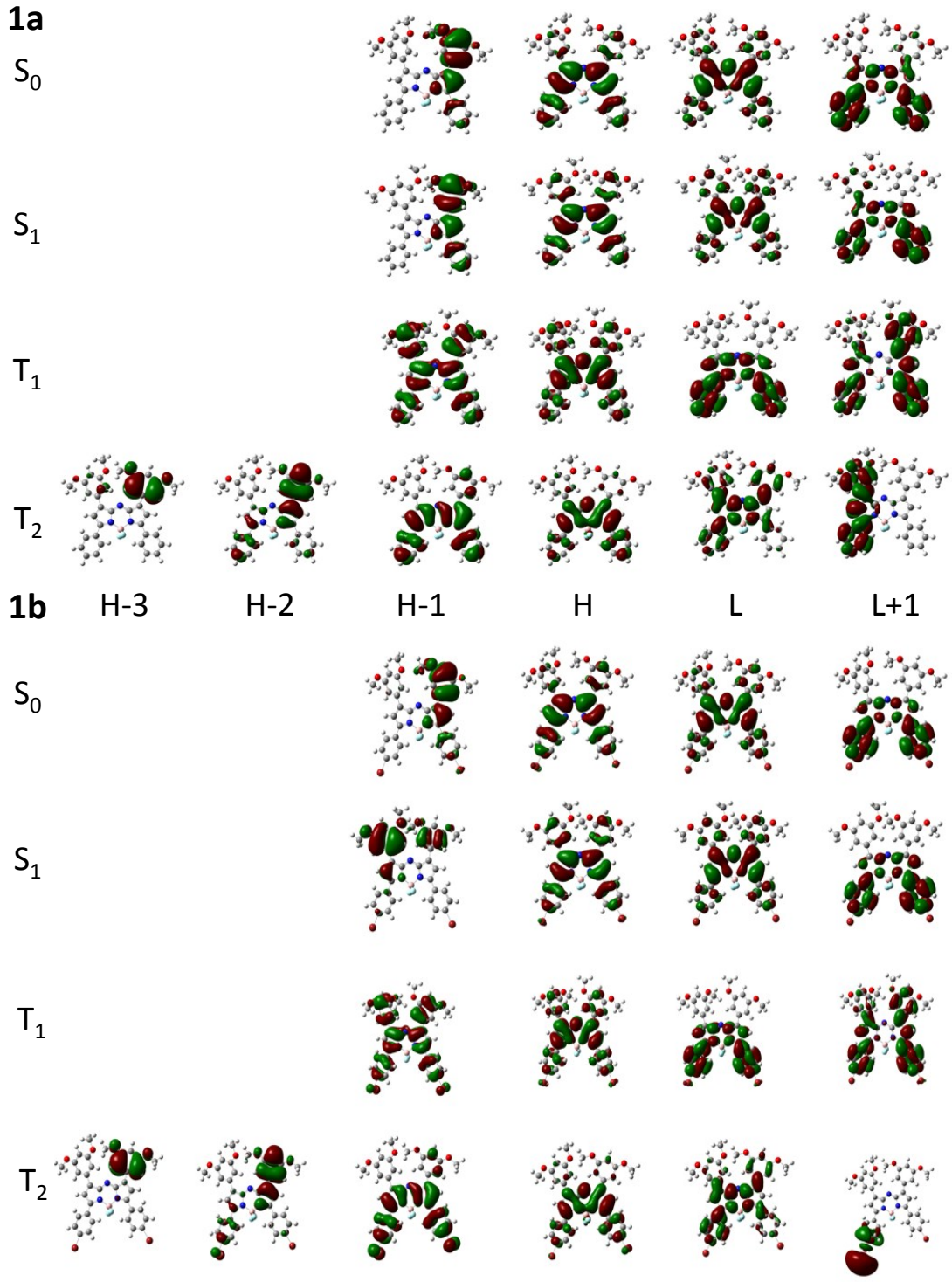

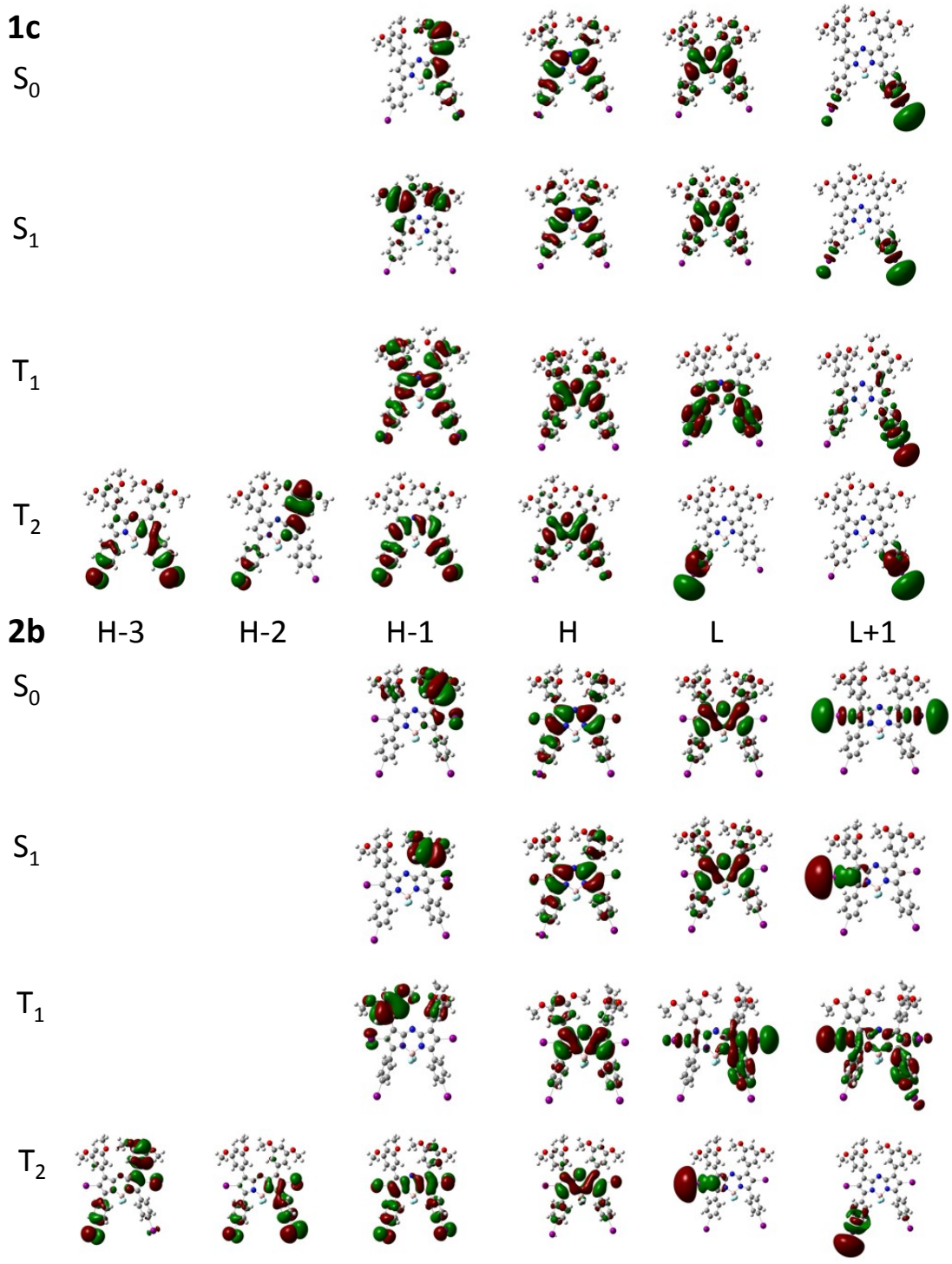
1c
S0
S1
T1
T2
2b
H-3
H-2
H-1
H
L
L+1
S0
S1
T1
T2

➢ MANUSCRIPT

Theoretical Insights on the switch off/on Photosensitization in Chemicontrolled Photodynamic Therapy

Jenny Pirillo, Gloria Mazzone*, Nino Russo.

Theoretical Insights on the switch off/on Photosensitization in Chemicontrolled Photodynamic Therapy

Jenny Pirillo, Gloria Mazzone and Nino Russo*

Dipartimento di Chimica e Tecnologie Chimiche, Università della Calabria, Via P. Bucci, 87036 Rende, Italy

ABSTRACT

We report herein DFT and TDDFT calculations on recently synthesized BODIPY-based compounds. The absorption wavelengths, singlet-triplet energy gaps and spin-orbit matrix elements for the radiationless $S_n \rightarrow T_m$ couplings, have been provided to verify the possible application of such compounds as type II photosensitizer (PS) in photodynamic therapy and to gain more insight in the ability of scavenger-containing BODIPY based compounds as Reactive Oxygen Species-activatable photosensitizer. The exploration of the photophysical properties have evidenced the potential applicability of all the investigated compounds in PDT. A TD-DFT qualitative analysis show how only a Br-substituted BODIPY derivative (**8**) could be involved in a photoinduced electron transfer (PeT) that causes the switch off of singlet oxygen photosensitization. Its oxidation with $^1O_2$ or cumyloxyl radical restores the ability of Br-substituted BODIPY derivative to act as type II photosensitizer and then to produce the cytotoxic $^1O_2$.

1. INTRODUCTION

Photodynamic Therapy (PDT) is an innovative treatment for different pathologies, cancer included,[1-3] using three key components: non-toxic light-activated drug (Photosensitizer), visible light, and oxygen. Their interaction triggers photochemical reactions leading to Reactive Oxygen Species (ROS) generation, that mediate cytotoxicity and cell death.

In PDT, a photosensitizer (PS) is excited by an appropriate light source from its ground state S_0 to the excited one S_n that, through a radiationless intersystem crossing transition (ISC), generates the triplet electronic state (T_1). The activated sensitizer can undergo two kinds of photoreactions: i) reacting directly, either with the substrate such as the cell membrane or a molecule, transferring an electron or a hydrogen atom to yield radical ions and free radicals that are subsequently scavenged by oxygen to produce oxygenated products (type I reaction); ii) the T_1 excited sensitizer can transfer its energy to the ground state of molecular oxygen ($^3\Sigma_g$) to yield the excited singlet oxygen agent ($^1\Delta_g$), which requires 0.98 eV to take place. The highly cytotoxic $^1O_2$ reacts with biological molecules, including lipids, proteins and nucleic acids, compromising the normal functions of the targeted cells. In order to minimize light scattering, favor light absorption of the tissues and allow the use of minimal doses of PS, the used radiation should fall in the so-called therapeutic window (from 500 to 850 nm). Therefore, the PS have to absorb within this range, to possess the first excited triplet state with energy higher than 0.98 eV, the energy required to excite the molecular oxygen, and to ensure an efficient intersystem crossing, then a high singlet oxygen quantum yield, Φ_Δ.

Though most of PSs currently used or under advanced clinical trials have a tetrapyrrolic unit, several classes of compounds appeared to be promising drugs for PDT.[4] Among PSs currently under evaluation, 4,4-difluoro-4-bora-3a,4a-diaza-s-indacene (BODIPY) and its aza (aza-BODIPY) derivatives, are taking a prominent place.[5-8] They possess several advantages over other dyes, such as large absorption extinction coefficients, sharp emissions, and quantum fluorescence yields as well as high redox and thermodynamic stability and relatively simple synthesis.[9-13] However, they present some limitations, such as the wavelength for their maximum absorption, that does not fall in the therapeutic window, and the ISC as they are highly fluorescent, therefore their use in PDT can be achieved by particular structural modifications aimed at modulating their photophysical properties.[14-16]

As known, PDT is emerged in the last years as promising cancer therapy for its efficiency in cell death induction and high selectivity for tumor cells. However, it can be possible to further minimize undesired side effects controlling at different levels the photosensitization of $^1O_2$. In this field, the

chemical activation of a sensitizer selectively in the targeted tissues has recently emerged as effective control of highly reactive species production demanded to achieve the cells death.[17-23]

In the last year, Cosa and co-workers synthesized a dormant singlet oxygen photosensitizer by combining the free radical scavenging action of the chromanol ring of α-tocopherol[24-29] with the photosensitization ability of a Br-substituted BODIPY dye (compound **8** in Scheme 1).[23]

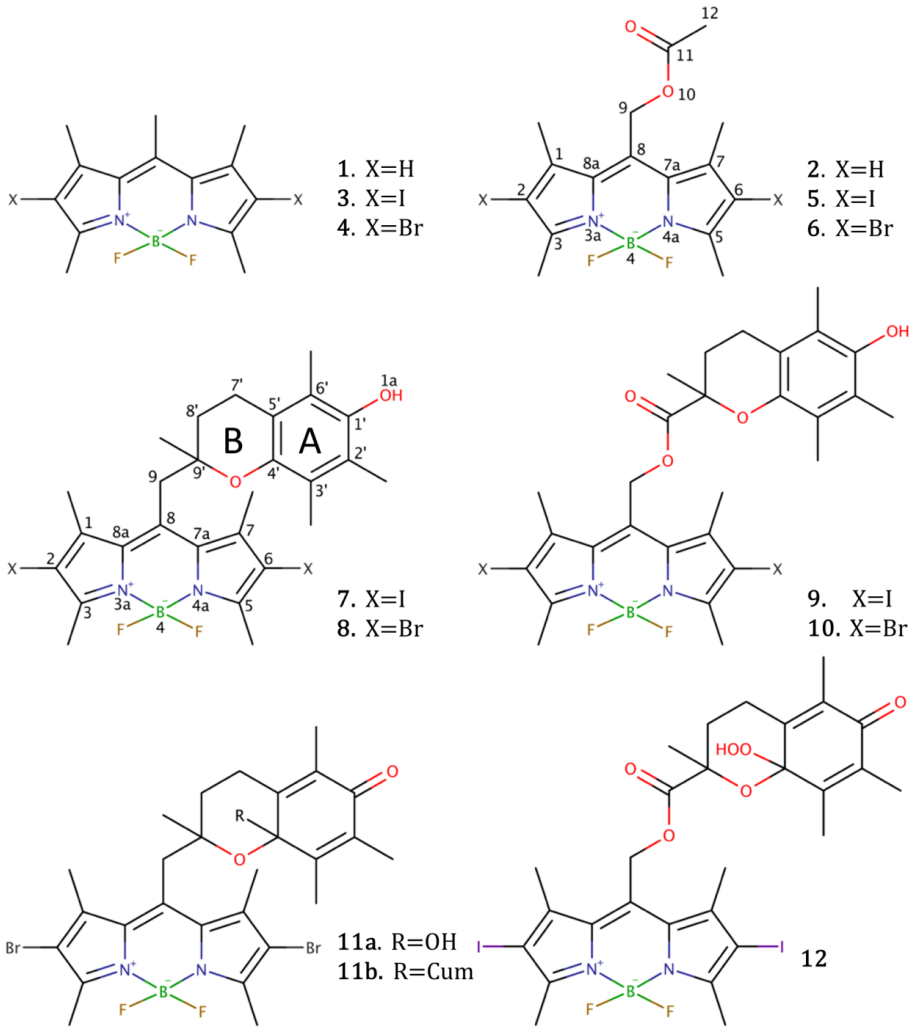

Scheme 1. Schematic representation of the investigated compounds **1**-**12**.

The first step in the design of this new photosensitizer was the substitution with halogens, both bromine and iodine atoms (compounds **3**-**6**), at position C2 and C6 of the BODIPY **1** and **2**, that ensure rapid ISC to the triplet excited state, allowing the $^1O_2$ production. The second step was based on the insertion of a chromanol moiety of α-tocopherol bound to the BODIPY segment by two different

linkers, a methylene (compounds **7** and **8**) and an ester group (compounds **9** and **10**). Although, they have taken into account only the bromine and iodine derivatives of **4** and **5**, respectively, leading to compounds **8** and **9**, we have considered also the correspondent iodine and bromine derivatives of **3** and **6**, respectively in order to rationalize the effects that play the major role in the switch off/on photosensitization. They supposed that in compounds **8** and **9** a photo-induced electron transfer (PeT) from the trap segment to the photosensitizer one competes with intersystem crossing reducing the yield of triplet state and inhibiting the $^1O_2$ photosensitization. They have shown that the subsequent treatment of the molecule with strong oxidants, such as $^1O_2$ itself and cumyloxyl radical, leading to **11a** and **11b**, respectively, activates the compound for the $^1O_2$ production.

In order to get more insight into the processes that could take part in the deactivation/activation of the $^1O_2$ photosensitization, a systematic theoretical study of the photophysical properties has been undertaken. For this purpose, DFT and TD-DFT[30] methods have been used to characterize ground and excited states properties. Our outcomes show how effectively, the presence of the scavenger in compounds **7**-**10**, promotes the photo-induced electron transfer (PeT) from the trap segment to the BODIPY portion. Moreover, our study show how the nature of the linker play the major role in the switch off the $^1O_2$ photosensitization in the presence of the free radical scavenger.

With the aim to evaluate the different levels of control in $^1O_2$ photosensitization proposed,[23] redox potentials and Gibbs free energy for photoinduced electron transfer of compounds **7**, **8**, **9**, **10** and **11a** have been calculated, considering the possibility that the PeT could take place from all the possible excited states (e.g S_1, S_2 and T_1).

In addition, the oxidation mechanism of the chromanol ring, by the two mentioned oxidants ($^1O_2$ and cumyloxyl radical), has been reported for the key compound **8** in order to estimate the energies come into play in the switch on photosensitization.

2. COMPUTATIONAL DETAILS

All the calculations have been done by using Gaussian 09 software package[31] at DFT levels of theory. The ground state structures have been optimized without any constrains in acetonitrile solution by using the M06[32] exchange and correlation functional. The standard 6-31+G** basis set of Pople has been used for all the atoms with the exception of iodine, for which the SDD pseudopotential[33,34] has been employed with its valence basis set. Absorption spectra (in acetonitrile) have been obtained as vertical electronic excitations from the minima of the ground-state structures by using time-dependent density functional response theory (TD-DFT).[30]

The solvent environments used to simulate the absorption spectra, acetonitrile (ε=36.64), and the oxidation reactions, water (ε=78.35), have been considered by means of the conductor-polarizable continuum models (CPCM),[35,36] in the linear response formalism in its equilibrium model[37] when excited state structural optimizations were performed, while the non-equilibrium model[38] have been applied in all other cases.

Local minima and transition states along the oxidation pathways have been identified by harmonic vibrational frequency calculations: real frequencies for local minima and a single imaginary frequency, which corresponds to the expected motion along the reaction coordinate, for transition states. All the intercepted transition states were checked by IRC (intrinsic reaction coordinate) analysis.[39,40]

Spin-orbit matrix elements have been computed using the quadratic-response TD-DFT approach,[41,42] as implemented in the Dalton code,[43] on the involved excited state optimized geometries, that are S_1 and S_2. The TD-B3LYP/cc-pVDZ//TD-M06/6-31+G** level of theory has been used in the framework of atomic-mean field approximation,[44] for **1**, **2**, **4**, **6**, **8, 10** and **11a**, **b**, while the spin–orbit coupling operators for effective core potentials with the effective nuclear charge has been employed in conjunction with the ECP for Iodine-substituted BODIPYs, **3**, **5**, **7** and **9**.[45]

This protocol has been successfully applied to study the photophysical properties of several photosensitizers.[46-57]

The standard redox potential in solution have been calculated in acetonitrile by using the most popular method based on Born-Haber cycle to derive the standard Gibbs free energy for the reaction.[58] Gibbs free energy of redox half reaction $\Delta G_{(sol)}$ consists of the free energy change in the gas phase ($\Delta G_{(gas)}$) and the solvation free energies of the oxidized and reduced species.

Using the Born-Haber thermodynamic cycle $\mathbf{\Delta G_{(sol)}}$ is defined as:

$$\mathbf{\Delta G_{(sol)} = \Delta G_{(gas)} + \Delta G_{(solv,ox)} - \Delta G_{(solv,red)}}$$

where $\mathbf{\Delta G_{(solv,ox)}}$ and $\mathbf{\Delta G_{(solv,red)}}$ are standard solvation energies of oxidized and reduced species, respectively. It is related to standard redox potential through the following thermodynamic relation:

$$\mathbf{E_{ox} = -\frac{\Delta G_{(sol)}}{nF}}$$

where *n* is the number of transferred electrons in the reaction, *F* is the Faraday constant (23.06 Kcal mol^{-1} V^{-1}).

The Gibbs free energy for photoinduced electron transfer ΔG_{PeT} has been calculated by using the following equation[59]:

$$\mathbf{\Delta G_{PeT} = E_{ox} - E_{red} - E_{00} - C}$$

where Eox and Ered are, respectively, the oxidation potential and reduction potential of the investigated compounds, estimated with respect to the SCE potential (4.60 eV in acetonitrile),[60] E_{00} is

the energy of the considered excited state and C is the Coulombic interaction term, estimated in acetonitrile as $e^2/\varepsilon a \approx 0.06$ eV.[61]

3. RESULTS

3.1 Ground state properties

Selected geometrical parameters of M06/6-31+G** optimized structures for all the investigated compounds sketched in Scheme 1 are collected in Table 1, while Cartesian coordinates are reported in the Supporting Information.

Both starting compounds, **1** and **2**, are characterized by the typical planar structure of BODIPY, in which the *meso* position is occupied by a methyl and a methyl acetate groups, respectively. A preliminary conformational analysis on compound **2** has been done in order to find the most stable orientation of methyl acetate group with respect to the BODIPY plane, which it has been taken as starting conformation for its derivatives. The intercepted geometry evidences a dihedral angle (φ_1) of 61.7 degrees of such a group with respect to the core unit. The introduction of methyl acetate group entails a slight bending of the *meso* group out of the plane (see φ_2 in Table 1) with respect to compound **1**.

Table 1. Main Bond Lengths (Å), Valence and Dihedral Angles (deg) for all the investigated BODIPYs, **1**-**12**, obtained at M06/6-31+G** Level of Theory in acetonitrile.

	1	**2**	**3**	**4**	**5**	**6**	**7**	**8**	**9**	**10**	**11a**	**11b**	**12**
	Bond Lengths												
B-N3a	1.542	1.546	1.560	1.546	1.549	1.550	1.549	1.549	1.550	1.549	1.545	1.548	1.548
B-N4a	1.543	1.543	1.560	1.547	1.546	1.547	1.547	1.546	1.546	1.546	1.547	1.546	1.546
C8-C9	1.494	1.505	1.496	1.493	1.505	1.505	1.498	1.498	1.507	1.507	1.495	1.495	1.506
C2-X[a]	1.085	1.085	2.111	1.874	2.108	1.874	2.107	1.873	2.105	1.871	1.872	1.872	2.106
	Valence Angles[b]												
θ_1	120.0	118.3	119.8	120.1	118.2	118.3	119.8	119.7	118.1	118.0	119.9	119.1	118.4
θ_2	-	-	-	-	-	-	109.3	109.2	108.7	108.7	111.6	111.8	110.2
	Dihedral Angles[c]												
φ_1	-	61.7	-	-	62.0	61.2	82.0	81.3	62.1	61.3	81.7	77.5	59.6
φ_2	177.0	-173.9	175.4	175.7	-173.0	-172.9	-159.7	-159.3	-171.3	-171.4	-164.2	-163.7	-173.4
φ_3	-	85.5	-	-	85.0	83.3	-	-	77.4	76.4	-	-	72.7
φ_4	-	-	-	-	-	-	-170.7	-170.0	154.8	154.1	-173.8	-172.5	148.5

a. X=H for **1** and **2**, I for **3**, **5**, **7**, **9** and **12**, Br for **4**, **6**, **8**, **10, 11a**, **11b**; b. θ_1=C7a-C8-C9, θ_2=C8'-C9'-O; c. φ_1= C7a-C8-C9-O10(C9'), φ_2=N4a-C7a-C8-C9, φ_3= C8-C9-O10-C11, φ_4=C3'-C4'-O-C9'.

Halogenation of precursors **1** and **2** in positions 2 and 6 leads to iodine derivatives **3** and **5**, and bromine derivatives **4** and **6**, starting from compounds **1** and **2**, respectively. The inclusion of halogen atoms does not imply significant changes in the optimized structures, which remain approximately planar for **1** derivatives, **3** and **4**, and with *meso* group slightly out of the plane for **2** derivatives, **5** and **6**.

As shown in Scheme 1, the addition of the chromanol ring of α-tocopherol to form compounds **7**, **8**, **9** and **10** implies a different connection of the antioxidant to the BODIPY, that is through a methylene linker in the former cases (**7** and **8**) and an ester group in the latter ones (**9** and **10**). The presence of scavenger definitely distorts out of the BODIPY plane the *meso* group, especially when methylene connects chromanol ring to the BODIPY (see φ_2 in Table 1) because of steric effects.

The chromanol ring presents a stereocentre C9', with configuration S, in **7** and **8**, and R in compounds **9**, **10**. In all cases, the most stable enantiomer is characterized by the orientation of the chromanol ring in order to maximize the π-π interaction between its ring A and BODIPY moiety. However, the other enantiomer, in which the chromanol adopts an orientation approximately orthogonal to the BODIPY plane, results to be less stable of no more than 0.2 eV in all cases.

On the basis of the photophysical properties described below and following the experimental findings, only for compound **8** the oxidation process has been investigated by using two oxidants, that are $^1O_2$ and cumiloxyl radical, resulted in compounds **11a** and **11b**. The oxidation of OH in position C1' takes place with the consequent formation of C9'-O bond. A detailed description of such a mechanism it will be presented in the next sections. However, they are characterized by slightly greater valence angle θ_2 and dihedral angle φ_2 as direct consequence of the oxidation of the chromanol ring. For compound **12**, deriving from the oxidation of **9** with $^1O_2$, a slight variation has been observed for geometrical parameters not involved in the oxidation process, as only φ_1, φ_2 and φ_4 decrease with respect to those found in **9**.

3.2 UV-Vis spectra

In Table 2 are collected the excitation energies for the main excited states computed at M06/6-31+G** level of theory for all the compounds. Therefore, together with absorption states, singlets, also the triplet states that could be populated through non-radiative processes described below have been included. As can be seen, all the investigated BODIPYs absorb within the low region of the therapeutic region. From data reported, a reasonable agreement between theory and experiment can be observed, keeping in mind that the inherent limits of TD-DFT, which within the vertical approximation does not take into account double excitations, and the linear response solvent effects it is known that entail a deviation between theory and experiment for this type of systems.[62]

Looking at data reported for precursor compounds **1** and **2**, due to the stabilizing effect that electron withdrawing groups in *meso* position have on BODIPY, methyl and methyl acetate groups in **1** and **2**, respectively, a red-shift of the first excited singlet state has been found. The most intense absorption at 430 and 452 nm has been computed for **1** and **2**, respectively, against 491 and 530 nm experimentally found, which correspond to the maximum deviation from the experimental data.

Table 2. Vertical absorption, ΔE (eV) and wavelengths (nm), Transition (%) and oscillator strengths (*f*) from the low-lying singlet state of **1** and its derivatives, **3**, **4**, **7** ,**8**, **11a** and **11b**, calculated at TD-M06/6-31+G** level of theory in acetonitrile.

	State[a]	Transition	ΔE	*f*	λ_{abs}[b]	State[a]	Transition	ΔE	*f*	λ_{abs}[b]
Precursors	**1**					**2**				
	T1	H→L (100%)	1.64, 754	0.000		T1	H→L (100%)	1.41, 880	0.000	
	S1	H→L (99%)	2.88, 430	0.636	491	S1	H→L (99%)	2.74, 452	0.605	530
	S2	H-1→L (98%)	3.65, 340	0.055		S2	H-1→L (98%)	3.45, 359	0.037	
	S3	H-2→L (99%)	3.92, 316	0.061		S3	H-2→L (99%)	3.72, 333	0.059	
Iodine derivatives	**3**					**5**				
	T1	H→>L (94%)	1.62, 766	0.000		T1	H→L (96%)	1.39, 893	0.000	
	T2	H-2→L (86%)	2.69, 460	0.000		T2	H-2→L (44%), H-1→L (43%)	2.52, 493	0.000	
	S1	H→L (98%)	2.70, 459	0.689	521	S1	H→L (97%)	2.56, 485	0.658	550
	S2	H-2→L (97%)	3.38, 367	0.186		S2	H-1→L (96%)	3.26, 380	0.124	
	S3	H-1→L (97%)	3.43, 362	0.061		S3	H-2→L (97%)	3.40, 365	0.067	
Bromine derivatives	**4**					**6**				
	T1	H→L (97%)	1.65, 751	0.000		T1	H→L (99%)	1.40, 885	0.000	
	S1	H→L (98%)	2.77, 448	0.693	515	T2	H-1→L (87%)	2.57, 482	0.000	
	S2	H-1→L (97%)	3.49, 355	0.148		S1	H→L (98%)	2.61, 476	0.646	543
	S3	H-2→L (97%)	3.62, 342	0.076		S2	H-1→L (72%)	3.17, 391	0.163	
						S3	H-2→L (73%)	3.23, 384	0.059	
Iodine derivatives – trap molecule	**7**					**9**				
	T1	H-1→L (51%), H→L (44%)	1.44, 861	0.000		T1	H-1→L (94%)	1.37, 906	0.000	
	S1	H→L (99%)	2.00, 621	0.046		T2	H→L (97%)	2.18, 568	0.000	
	T2	H-1→L (44%), H→L (54%)	2.08, 596	0.000		S1	H→L (100%)	2.19, 565	0.014	
	T3	H-3→L (64%)	2.62, 474	0.000		T3	H-4→L (37%), H-3→L (45%)	2.52, 493	0.000	
	S2	H-1→L (96%)	2.65, 468	0.512		S2	H-1→L (97%)	2.56, 485	0.615	552
bromine derivatives – trap molecule	**8**					**10**				
	T1	H-1→L (48%), H→L (47%)	1.44, 860	0.000		T1	H-1→L (97%)	1.39, 894	0.000	
	S1	H→L (99%)	1.98, 625	0.049		T2	H→L (98%)	2.17, 571	0.000	
	T2	H-1→L (47%), H→L (50%)	2.08, 595	0.000		S1	H→L (100%)	2.18, 568	0.013	
	T3	H-3→L (89%)	2.67, 464	0.000		T3	H-3→L (83%)	2.57, 482	0.000	
	S2	H-1→L (94%)	2.69, 462	0.432	532	S2	H-1→L (98%)	2.60, 476	0.602	
	S3	H-2→L (96%)	2.87, 433	0.120						
$^1O_2$ Oxidized derivatives	**11a**					**12**				
	T1	H→L (97%)	1.54,804	0.000		T1	H→L (96%)	1.39, 891	0.000	
	T2	H-2→L+1 (24%), H-1→L+1 (59%)	2.50,496	0.000		T2	H-2→L (83%)	2.53, 490	0.000	
	T3	H-2→L (51%), H-1→L (32%)	2.65, 467	0.000		S1	H→L (98%)	2.57, 483	0.646	
	S1	H→L (98%)	2.67, 464	0.612		S2	H-2→L (92%)	3.20, 387	0.144	
	S2	H-1→L (86%)	3.30, 376	0.039						
	S3	H→L+1 (97%)	3.31, 374	0.013						
	11b									
	T1	H→L (98%)	1.50, 827	0.000						
	T2	H-1→L+1 (66%)	2.42, 511	0.000						
	S1	H→L (98%)	2.63, 472	0.559						
	S2	H-1→L (92%)	3.14, 394	0.059						

a. only selected excited states are reported; b. experimental data are taken from ref. 23.

Starting from the simplest compound **1**, the inclusion of halogen atoms, resulted in compounds **3** and **4**, entails a bathochromic shift of the most intense band of no more than 30 nm, similarly to what has been experimentally found.[23] The same findings can be observed for compound **2** derivatives, that are **5** and **6**, whose band result red-shifted of 24 and 33 nm, respectively (see Table 2). The main electronic transition associated to the first singlet excited state is H→L in nature, with an oscillator strength

greater than 0.6 in all cases. The plot of molecular orbitals reported in Supporting Information clearly reveals that the transition occurs from π to π* orbitals.

The subsequent excited states appear to be very low in intensity than the first excited one, as the computed oscillator strength is no greater than 0.2. They are characterized by transitions starting from inner orbitals (H-1 and H-2) to the LUMO one. The associated wavelengths, similarly to what has been shown for the most intense absorption band, result red-shifted in going from precursors, **1** and **2**, to iodine (**3** and **5**) and bromine derivatives (**4** and **6**).

Starting from the just described derivatives, four dual-action PSs have been obtained by including a free radical scavenger attached to the last carbon atom of the *meso*-group, that is C9 in **3** and **4** and C12 in **5** and **6**, respectively, leading to compounds **7**, **8** and **9**, **10**, respectively. The insertion of the chromanol ring of α-tocopherol returns the second singlet state as the bright one, with oscillator strengths in the range 0.4-0.6. Such a state is originated by a H-1→L transition that is π-π* in nature.

However, looking at the plot of molecular orbitals (SI) it can be noted that only for **8**, and in a less pronounced manner for **7**, HOMO-1 orbital explicitly involves the just included free radical scavenger, being delocalized on the two portion of the molecule, contrariwise to compounds **9** and **10**, for which only HOMO is almost completely localized on the chromanol ring.

While the S_1 state, which remains originated by H→L transition, becomes a dark state and, though the oscillator strength is slightly different from 0 (between 0.01 and 0.05), it cannot be taken into consideration in evaluating the absorption band useful for PDT application. However, similarly to what has been experimentally found,[23] in all cases the presence of the chromanol ring does not significantly influence the region for the most intense absorption.

In the oxidized forms, **11a**, **11b** and **12**, the first singlet state turns to be the bright one, with oscillator strength very similar to those computed for the precursor compounds, **4** and **5**. Such a state arises from the H-L transition that, as usual, occurs from π to π* orbitals. They are all characterized by at least two triplet states lying below the first singlet excited one.

3.3 Spin-Orbit coupling Constants

From Table 2 it emerges that all the investigated compounds possess a triplet state T_1 with energy greater than that required to excite the molecular oxygen (0.90 eV),[51] then in principle all should be able to produce the highly cytotoxic singlet molecular oxygen ($^1\Delta_g$). Also looking at the adiabatic S_0-T_1 energy gaps reported in the Supporting Information.

However, once a singlet excited state is populated, the production of the cytotoxic singlet oxygen is possible only if an efficient intersystem crossing $S_n \rightarrow T_m$ occurs. As postulated by the Fermi Golden

Rule the rate of the intersystem crossing depends on the amplitude of the spin–orbit coupling matrix elements.

Table 3. SOC (cm^{-1}) computed between singlet and low-lying triplet excited states at B3LYP/cc-pVDZ//M06/6-31+G** level of theory, for **1**, **2**, **4**, **6**, **8**, **10**, **11a** and **11b** obtained in the framework of atomic mean field method, on the optimized geometry of the involved singlet excited state. For **3**, **5**, **7** and **9** the correspondent data obtained by using the effective core one electron Hamiltonian in conjunction with the ECP for I atom are reported.

	1	**2**	**3**	**4**	**5**	**6**	**7**	**8**	**9**	**10**	**11a**	**11b**
$\lvert\langle\Psi_{S_1}\lvert\hat{H}_{so}\rvert\Psi_{T_1}\rangle\rvert$	0.3	0.3	21.5	5.4	20.0	19.2	6.6	0.2	6.1	0.5	0.6	5.3
$\lvert\langle\Psi_{S_1}\lvert\hat{H}_{so}\rvert\Psi_{T_2}\rangle\rvert$	-	-	8.1	-	20.3	6.4	11.1	0.6	3.4	1.2	11.1	5.4
$\lvert\langle\Psi_{S_1}\lvert\hat{H}_{so}\rvert\Psi_{T_3}\rangle\rvert$	-	-	-	-	-	-	-	-	-	-	8.3	5.7
$\lvert\langle\Psi_{S_2}\lvert\hat{H}_{so}\rvert\Psi_{T_2}\rangle\rvert$	-	-	-	-	-	-	9.8	4.0	2.1	0.6	-	-
$\lvert\langle\Psi_{S_2}\lvert\hat{H}_{so}\rvert\Psi_{T_3}\rangle\rvert$	-	-	-	-	-	-	10.9	4.1	0.8	0.2	-	-

We have taken into consideration all the possibility for the radiationless transition from the populated singlet states to the triplets lying below. For compounds **1** and **2**, for which the S_1 is populated upon irradiation, the only feasible way to populate the triplet state is through an ISC $S_1 \rightarrow T_1$. As can be seen in Table 3, as expected, the nature of the *meso* substituent does not have any influence on the spin-orbit coupling, hence even on ISC efficiency. While the introduction of halogen atoms on the BODIPY core (**3** and **4**) entails an increase of one order of magnitude of the SOC, especially for compound containing iodine atoms (**4**).

For compounds **3**, **5** and **6**, because of two triplet states lying below the lowest singlet excited one, different scenarios may occur, as $S_1 \rightarrow T_n$ (n=1, 2) are, in principle, both possible. Especially for iodine-derivative **5**, the computed SOC in the two cases are essentially equal, while for **3** and **6** the $S_1 \rightarrow T_1$ seems to be the most probable one, despite the energy difference between the singlet and the two triplet states is 0.01 and 0.8 eV for T_2 and T_1, respectively.

Passing to the dormant singlet oxygen sensitizers, as mentioned above the S_2 is the bright state, so the occurrence of ISC from S_2 to triplet states T_2 and T_3 and from S_1 to T_1 state has been taken into consideration. As expected from experimental observations,[23] the presence of the free radical scavenger bound to BODIPY causes a decrease of the SOC amplitude quenching the ISC process. Among these derivatives, those containing iodine atoms present the highest SOC value. Comparing **7** and **8** compounds it appears that for iodine-derivate (**7**) the computed spin-orbit matrix elements are higher than those of **8** and are of the same magnitude considering the crossing from S_2 or S_1 excited states, while in the bromine-derivate the ISC seems to be more probable from the S_2 state. Contrariwise, the SOCs computed for compounds containing the ester linker, **9** and **10**, suggest a most probable crossing

from the S_1 state. Though all these compounds should turn off the sensitization, the SOC values of iodine-containing compounds are fairly significant, suggesting that such action is not played.

For the last analyzed compounds, **11a** and **11b**, it can be seen that the presence of three triplet states below the bright one (S_1) ensures a consistent coupling.

3.4 Intramolecular Photoinduced Electron Transfer

Preliminarily, in order to get further insights in the change of the electron density upon electronic transition, the electron density difference between the second singlet excited state (the bright state) and the ground state have been plotted for all the chromanol-containing compounds (**7**-**10**) and reported in Figure 1a-d. The electron density difference maps (EDDMs) clearly show that, while in **7** and **8** a decrease of the electron density (light blue in Figure 1a) on the chromanol ring can be observed from the ground to the second excited states, in **9** and **10** an electronic rearrangement upon the electronic transition can be ascribable only to the BODIPY portion of the molecule, suggesting that in the latter cases the inclusion of the chromanol ring does not considerably influence their ability to photosensitize $^1O_2$.

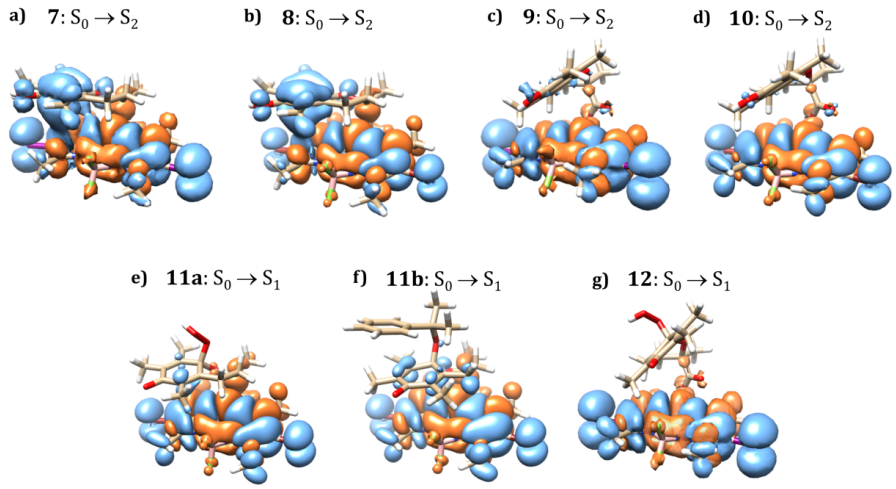

Figure 1. electron density difference maps (EDDMs) between the S_2 and S_0 states for compounds a) **7**, b) **8**, c) **9** and d) **10** and between the S_1 and S_0 states for the oxidized forms e) **11a**, f) **11b** and g) **12**. Light blue stands for a decrease in charge density, while orange an increase. All major components and their relative weight were taken into consideration for each transition.

In order to establish the occurrence of the intramolecular PeT from the electron rich chromanol ring to the BODIPY core that can be responsible of the switch off of $^1O_2$ sensitization, a preliminary qualitative analysis recently applied on several systems to explain the quench of fluorescence,[63-65] has

been performed. The computational approach consists of characterizing the potential energy profiles (PESs) of the low-lying excited state with TD-DFT method. For this purpose, the photodeactivation pathways for **7**, **8**, **9**, **10**, **11a** and **11b** are reported in Figure 2.

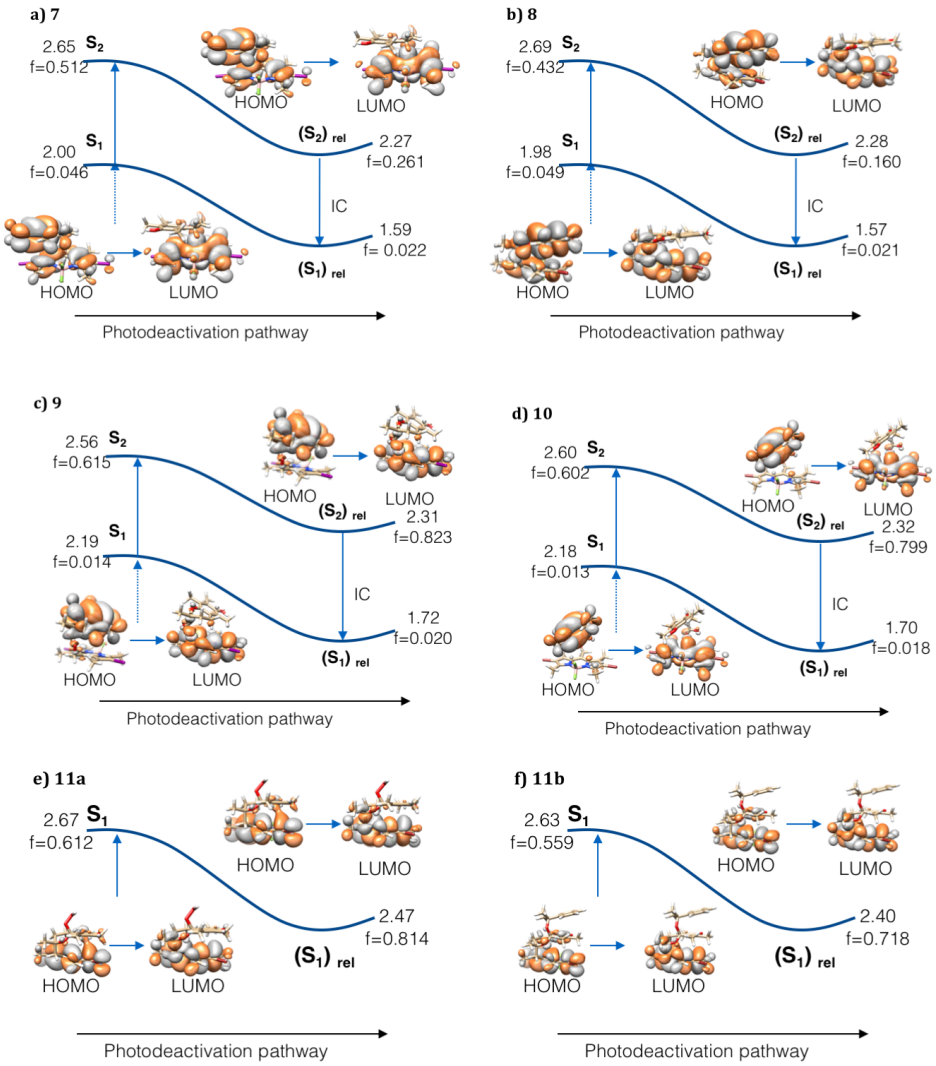

Figure 2. Schematic potential energy profiles for the photodeactivation pathway computed at TD-M06/6-31+G** for compounds a) **7**, b) **8, c) 9, d) 10, e) 11a** and f) **11b**.

By analyzing the behavior of compounds containing methylene linker, **7** and **8** (Figure 2a,b), initial excitation to the S_2 state is followed by an internal conversion (IC) $S_2 \rightarrow S_1$, which leads to the population of the lowest singlet state with intramolecular charge transfer (ICT) character. The

relaxation of S_1 ($\pi\pi^*$) potential energy surface (PES) leads to the twist of methyl groups in position 3 and 5, $(S_1)_{rel}$. Anyhow, as it can be noticed in Figure 2, in HOMO decreases the delocalization over the two portions of the molecule, which becomes essentially localized on the chromanol ring, while the LUMO is insensitive to the structural rearrangement occurring along the relaxation, and remains always of the same nature (localized on the BODIPY unit). It is noteworthy that in both compounds **7** and **8** a decrease of the oscillator strength is observed, which allow to hypothesize a turn off of the photosensitization. While, looking at PES computed for ester linker-containing compounds, the character of both HOMO and LUMO in the S_1 relaxed structure remain the same as those found on the ground state optimized geometry, together with an increase of the oscillator strength. This evidence supports the inability of compounds **9** and **10** to deactivate the photosensitizer before the oxidation process. Moreover, looking at Figure 2e, it can be seen that for oxidized forms of **8**, compounds **11a and 11b**, an increase of the oscillator strength has been observed after the relaxation of the S_1 excited states structure, switching on the $^1O_2$ photosensitization.

Cosa and co-workers reported that the deactivation on $^1O_2$ production, realized by addition of chromanol ring to compounds **4** and **5**, forming compounds **8** and **9**, is observed essentially for compound **8**, as only a 2-fold drop in Φ_f was recorded for **9** with respect to **5**, against the 25-fold drop in Φ_f recorded for **8** compared with the reference compound **4**.[23] To evaluate the thermodynamic feasibility of PeT from the chromanol portion, the authors[23] calculated the Gibbs free energy for photoinduced electron transfer[57] from the redox potentials of the two segments constituting the molecule. They found a ΔG_{eT} exergonic for both the examined compounds **8** and **9**, but, on the basis of the singlet oxygen quantum yield measurements and the intramolecular PeT quenching of the triplet state, only compound **8** has been proposed as dormant singlet oxygen photosensitizer, in perfect agreement with the considerations above reported.

In order to discriminate on the ability of all the possible dormant singlet oxygen generators reported here, the ΔG_{PeT} from each plausible excited states has been calculated for all the derivatives **7**-**10**. Preliminarily, this quantity has been computed for two precursor compounds, **4** and **5**, in order to compare the quantities experimentally determined, that are oxidation potentials and the excited states energy, and used to calculate the ΔG_{PeT}, with those come out from calculations to assess the reliability of the protocol used. The same quantity has been computed also for the oxidized form **11a** from T_1 and S_1 excited states to assess the inability of the oxidized compounds to promote the PeT. Data are all collected in the Table 4.

To evaluate the three possible PeT processes, the ΔG_{PeT} for **7**, **8**, **9** and **10** has been calculated from the excited states S_2, S_1 and T_1. Among them only the PeT from S_2 state results exergonic in all cases, while the highest value has been found from the T_1 states, suggesting that such a state cannot be involved in

PeT processes, in accordance with the experimental findings.[23] A similar behavior it can be noted for the first singlet excited state, therefore only from S_2 a PeT process can be predicted. On the basis of exoergonic ΔG_{PeT} calculated from S_2 state, all the compounds should promote a PeT. However, keeping in mind the high SOC values (see Table 3) computed for **7** and **9** a good probability that ISC occur can be hypothesized. While for compound **10**, as previously underlined, the EDDM between the S_2 and S_0 states(see Figure 1d) evidences that the charge transfer does not involve MOs the chromanol ring. Therefore only compound **8** can be considered a good dormant $^1O_2$ sensitizer.

Table 4. Calculated redox potentials at 298 K *vs* SCE in acetonitrile, the adiabatic energy gaps for the excited states (eV) computed in acetonitrile, and ΔG_{PeT} (eV).

	4	5	7	8	9	10	11a
$\mathbf{E_{red}}$	-1.43	-1.19 (-1.14)[b]	-1.41	-1.41	-1.19	-1.18	-1.33
$\mathbf{E_{ox}}$	0.73 (0.48)[a]	0.73 (0.48)[a]	0.81	0.81	1.08	1.09	1.31
$\mathbf{E\ (T_1)}$	1.61 (1.71)[b]	1.35 (1.54)[b]	1.34	1.33	1.32	1.35	1.51
$\mathbf{E\ (S_1)}$	2.53 (2.37)[b]	2.32 (2.21)[b]	1.59	1.57	1.72	1.70	2.46
$\mathbf{E\ (S_2)}$	-	-	2.27	2.28	2.31	2.33	-
$\mathbf{\Delta G_{PeT}\ (T_1)}$	0.50 (0.28)[b]	0.51 (0.27)[b]	0.82	0.83	0.89	0.86	1.07
$\mathbf{\Delta G_{PeT}\ (S_1)}$	-0.42 (-0.38)[b]	-0.45 (-0.40)[b]	0.56	0.59	0.49	0.51	0.11
$\mathbf{\Delta G_{PeT}\ (S_2)}$	-	-	-0.12	-0.13	-0.11	-0.12	-

a. ref. 66; b. catodic peak potential taken from ref. 23.

Looking at data computed for the oxidized form of **8**, compound **11a**, it can be noted that a PeT from S_1 excited state (the bright one) cannot occur, being endothermic the calculated ΔG_{PeT}, confirming the ISC as the most probable non-radiative process.

3.4 The oxidation mechanism of 8 by $^1O_2$ and Cumyloxyl radical

The oxidation reaction on compound **8** has been investigated by considering the action of two oxidants, singlet oxygen ($^1O_2$) and cumyloxyl radical (CumO·), which leads to the aforementioned **11a** and **11b** compounds, respectively. The action of the two reactive species on PS follow two different mechanisms that are schematically reported in Scheme 2, a) for $^1O_2$ and b) CumO·, respectively. The computed potential energy surfaces are both reported in Figure 3.

A recent DFT study on the local reactivity of the α-tocopherol by the calculation of the Fukui function[67] has evidenced that the most reactive sites for accepting electrons are associated with the leaving of the hydrogen atom in the extension of the phenolic OH bond on the α-tocopherol chromanol ring plane, in the place where the formation of H-bond of the precursor complex between approaching reactive oxygen species and phenolic OH group of α-tocopherol could be expected; while

the preferred sites for donating electron in a reaction with radical or oxidizing molecule are associated mostly with π electrons above and below the aromatic part of the α-tocopherol chromanol ring.

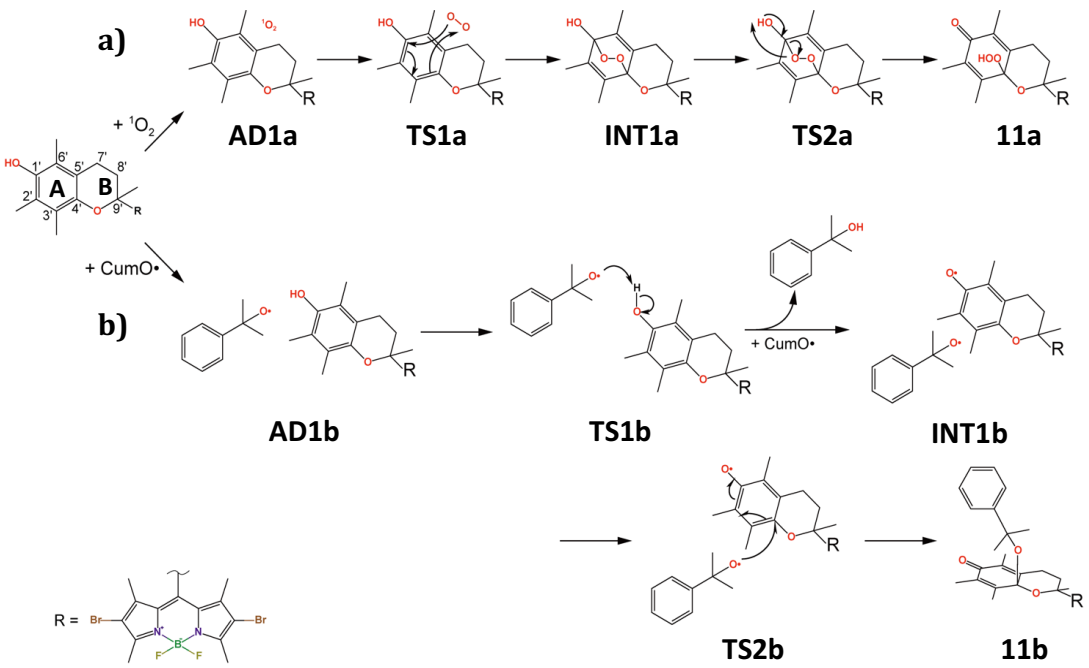

Scheme 2. M06/6-31+G** oxidation mechanism in water of **8** with a) $^1O_2$ and b) cumyloxyl radical.

As reported in literature for other phenolic compounds, the oxidation reaction with $^1O_2$ provides a 1,4-cycloaddition via endoperoxide formation.[68,69] According to the experimental evidences for the quenching mechanism of singlet oxygen by trolox and α-tocopherol, the first step of the reaction is the attach of the oxygen molecule to the aromatic ring A.[70,71] All the attempts to locate a transition state for the H-abstraction from phenolic group before the oxygen attack to the aromatic ring failed.

In the first adduct, **AD1a**, the molecular oxygen weakly interacts with π system of the aromatic ring A. Indeed, lying the two oxygen atoms at 2.438 and 2.390 Å from the C1' and C4', respectively, the planarity of the aromatic ring remain approximately unchanged. The adduct lies 10.6 kcal mol^{-1} lower in energy with respect to the reference, which is the sum of reactants' energies. The attack of the oxygen molecule to the ring A is realized through **TS1a**, overcoming an energy barrier of 7.8 kcal mol^{-1}. It is characterized by an asymmetric attack of oxygen molecule, as while the O2-C4' bond distance decrease until 1.672 Å, the O1-C1' one becomes 2.466 Å. However, the IRC calculation confirms that the subsequent minimum, **INT1a**, is that in which the two oxygen atoms are bound to C1' and C4' at approximately 1.5 Å. In this intermediate, which is more stable than the previous one of 6.7 kcal mol^{-1},

the ring assumes a like-boat conformation, with C1' and C4' atoms coming out of the ring plane. The structure of the **INT1a**, characterized by oxygen bridge, agrees with a previous experimental study.[69] The subsequent step provides an intramolecular H-abstraction to generate the hydroperoxide **11a**, in which the carbonyl C=O bond is formed. The intercepted transition state, **TS2a**, lies 28.9 kcal mol^{-1} above the reference energy. In order to form the O1-H bond, in **TS2a**, the O1-C1' bond is definitely broken. The high energy required to realize this step of the reaction can be proper ascribable to the arrangement of the OH group. The formation of the oxidized product, **11a**, is accomplished with a net energy gain of 40.3 kcal mol^{-1}. The planarity of ring A is thus restored, while the formation of the O2-C4' bond entail a reibridization of C4' from sp^2 to sp^3 and a consequent rearrangement of ring B.

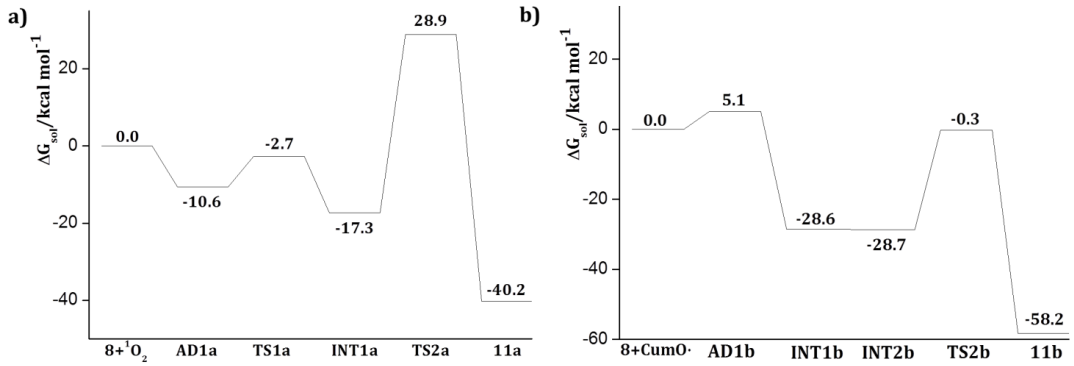

Figure 3. Potential free energy surfaces in water for the oxidation reaction of **8** by a) $^1O_2$ and b) CumO·.

The rate determining step of the oxidation reaction by $^1O_2$ is the second step, the HAT, as it requires the greater amount of energy to take place.

All the attempts to search for the most probable reaction mechanism has been initially carried out by considering only the chromanol portion of the molecule. The comparison between the model system and the real compound **8** has evidenced negligible differences from both energetic and geometrical point of views. Therefore, the reaction mechanism for the oxidation of **8** by the cumyloxyl radical reported below is referred to the simplest model system, in which the sensitizer segment is omitted.

With respect to the action of $^1O_2$, a different mechanism has been found for the oxidation reaction of **8** with cumyloxyl radical (Scheme 2b and Figure 3b). Contrariwise to the just described reaction, in this pathway the first step provides the H-abstraction by a radical molecule from phenolic group. The primary interaction of radical with the sensitizer **8** results to be slightly higher in energy than the sum of reactant's energies. In the adduct, **AD1b**, the radical is already directed to the H atom of hydroxyl

group so that H-abstraction occurs without any barrier and with an energy gain of 28.6 kcal mol^{-1}, **INT1b**. In order to continue the reaction an addition radical molecule is needed. This is realized in **INT2b**, that has approximately the same energy as **INT1b**. The attack of the radical to the chromanol ring occurs through the **TS2b**. It lies 0.3 kcal mol^{-1} below the reference energy and requires 28.4 kcal mol^{-1} to take place. In the transition state the partial formation of the C4-O (1.826 Å) bond does not affect the planarity of the cycle, even if it is evident the change of carbon atom hybridization. The formation of the final product **11b**, is achieved with an energy gain of 58.2 kcal mol^{-1}. The step limiting the reaction rate is the C4'-O bond formation, which is associated to the only transition state located along the reaction pathways.

CONCLUSIONS

DFT and its time-dependent extension (TDDFT) have been used herein to explore the photophysical properties of a series of recently synthetized BODIPY-based photosensitizers in order to gain more insight into the ability of a Br-substituted BODIPY derivative as ROS-activatable photosensitizer. The reaction mechanism of the oxidation process by $^1O_2$ and cumyloxyl radical has been elucidated.

The absorption wavelengths, singlet-triplet energy gaps and the spin-orbit matrix elements for the radiationless $S_n \rightarrow T_m$ couplings, have been provided to verify the possible use of such compounds as type II photosensitizer in photodynamic therapy. From the analysis of the photophysical properties the following conclusion can be outlined:

- all the investigated systems have the lowest triplet excited state (T_1) with energy higher than that required to activate the molecular oxygen;
- the EDDMs computed on the proposed dormant singlet oxygen photosensitizers, **7**-**10**, and their oxidized derivatives, **11a**, **11b** and **12**, evidence a decrease of the electron density, from the ground to the bright excited states, on the chromanol ring only for compound **8**, and in a less pronounced manner in compounds **7**, suggesting that the linker play the major role in promoting the PeT.
- the amplitude of the spin−orbit coupling matrix elements strongly depends on the heavy atoms included in the BODIPY core, while is less influenced by the *meso* substituent. As expected, iodine derivatives, **3** and **5**, show the highest values of SOC. The presence of trolox moiety in compound **9** and **10** entails a decrease of SOC, but they remain large enough to give an efficient intersystem crossing, implying the inability in deactivating the $^1O_2$ photosensitization. While the chromanol ring in compound **8** ensures a substantial decrease of the SOC values, which become consistent after the oxidation reaction realized in **11a** and **11b**, confirming the ability of this compound to switch off

the photosensitization until it reaches the cell in which, thanks to the overproduction of ROS, switch on the singlet oxygen photosensitization (**11a**).

- from the investigation of the oxidation mechanism of **8**, the reaction appears to be favored with cumyloxyl radical rather than the $^1O_2$ from both kinetic and thermodynamic point of views.

The computational analyses reported here support the use of compound **8** in chemicontrolled photodynamic therapy and could be of help in future design of new photosensitizers able to control the $^1O_2$ photosensitization.

AUTHOR INFORMATION

Corresponding Author

*(Gloria Mazzone) E-mail: gloria.mazzone@unical.it.

Author Contributions

The manuscript was written through contributions of all authors. All authors have given approval to the final version of the manuscript.

ACKNOWLEDGMENT

Università della Calabria is gratefully acknowledged.

REFERENCES

1. Juzeniene A, Peng Q, Moan J. *Photochem Photobiol Sci* **2007**, *6*, 1234-45.
2. MacDonald I J, Dougherty T J *J Porphyr Phthalocyanines* **2001**, *5*, 105-29.
3. Agostinis P, Berg K, Cengel KA, Foster TH, Girotti AW, Gollnick SO, et al. *CA Cancer J Clin* **2011**, *61*, 250-81.
4. Abrahamse H, Hamblin M. R. *Biochem J* **2016**, *473*(4), 347–364.
5. Kamkaew A, Lim SH, Lee HB, Kiew LV, Chung LY, Burgess K. *Chem Soc Rev* **2013**, *42*, 77-88.
6. Turan IS, Cakmak FP, Yildirim DC, Cetin-Atalay R, Akkaya EU. *Chem Eur J* **2014**, *20*, 16088-92.
7. Awuah SG, You Y. *RSC Adv* **2012**, *2*, 11169-83.
8. Lakshmi V, Rajeswara Rao M, Ravikanth M. *Org Biomol Chem* **2015**, *13*, 2501-17.
9. Loudet A, Burgess K. *Chem Rev* **2007**, *107*, 4891-932.
10. Ulrich G, Ziessel R, Harriman A. *Angew Chem Int Ed* **2008**, *47*, 1184-201.

11. Boens N, Leen V, Dehaen W. *Chem Soc Rev* **2012**, *41*, 1130-72.
12. Killoran J, Allen L, Gallagher JF, Gallagher WM, O'Shea DF. *Chem Commun* **2002**, 1862-3.
13. Gorman A, Killoran J, O'Shea C, Kenna T, Gallagher WM, O'Shea FD. *J Am Chem Soc* **2004**, *126*, 10619-31.
14. Turan IS, Cakmak FP, Yildirim DC, Cetin-Atalay R, Akkaya EU. *Chem Eur J* **2014**, *20*, 16088-92.
15. Loudet A, Burgess K. *Chem Rev* **2007**, *107*, 4891-932.
16. Boens N, Leen V, Dehaen W. *Chem Soc Rev* **2012**, *41*, 1130-72.
17. Zheng G, Chen J, Stefflova K, Jarvi M, Li H, Wilson BC. *Proc. Natl. Acad. Sci. U. S. A.* **2007**, *104*, 8989.
18. Lovell JF, Liu TW, Chen J, Zheng G. *Chem. Rev.* **2010**, *110*, 2839.
19. Kamkaew A, Lim SH, Lee HB, Kiew LV, Chung LY, Burgess K. *Chem. Soc. Rev.* **2013**, *42*, 77.
20. Huang L, Yang W, Zhao J. *J. Org. Chem.* **2014**, *79*, 10240.
21. Yogo T, Urano Y, Mizushima A, Sunahara H, Inoue T, Hirose K, Iino M, Kikuchi K, Nagano T. *Proc. Natl. Acad. Sci. U. S. A.* **2008**, *105*, 28.
22. Chen J, Stefflova K, Niedre MJ, Wilson BC, Chance B, Glickson JD, Zheng G. *J. Am. Chem. Soc.* **2004**, *126*, 11450
23. Durantini A. M., Greene L. E., Lincoln R., Martínez S. R., Cosa G. *J. Am. Chem. Soc.* **2016**, *138*, 1215–1225.
24. Alberto M. E., Russo N., Grand A., Galano A. *Phys. Chem. Chem. Phys.* **2013**, *15*, 4642-4650.
25. Stefek M., Kyselova Z., Rackova L., Krizanova L. *Biochim. Biophys. Acta* **2005**, *1741*, 183–190.
26. Friaa O., Brault D. *Org. Biomol. Chem.* **2006**, *4*, 2417–2423.
27. Mitarai K., Ouchi A., Mukai K., Tokunaga A., Mukai K., Abe K. *J. Agric. Food Chem.* **2008**, *56*, 84–91.
28. Lúcio M., Nunes C., Gaspar D., Ferreira H., Lima J. L. F. C., Reis S. *Food Biophys.* **2009**, *4*, 312–320.
29. Hall N. K., Chapman T. M., Kim H. J., Min D. B. *Food Chem.* **2010**, *118*, 534–539.
30. Casida ME. In: Seminario JM, editor. Recent developments and applications indensity-functional theory. Amsterdam, The Netherlands: Elsevier; **1996**. p. 155-92.
31. Gaussian 09, Revision D.01, Frisch, M. J. Trucks, G. W.; Schlegel, H. B.; Scuseria, G. E.; Robb, M. A.; Cheeseman, J. R.; Scalmani, G.; Barone, V.; Mennucci, B.; Petersson, G. A.; Nakatsuji, H.; Caricato, M.; Li, X.; Hratchian, H. P.; Izmaylov, A. F.; Bloino, J.; Zheng, G.; Sonnenberg, J. L.; Hada, M.; Ehara, M.; Toyota, K.; Fukuda, R.; Hasegawa, J.; Ishida, M.; Nakajima, T.; Honda, Y.; Kitao, O.; Nakai, H.; Vreven, T.; Montgomery, Jr., J. A.; Peralta, J. E.; Ogliaro, F.; Bearpark, M.; Heyd, J. J.; Brothers, E.; Kudin, K. N.; Staroverov, V. N.; Kobayashi, R.; Normand, J.; Raghavachari, K.; Rendell, A.; Burant, J. C.; Iyengar, S. S.; Tomasi, J.; Cossi, M.; Rega, N.; Millam, J. M.; Klene, M.; Knox, J. E.; Cross, J. B.; Bakken, V.; Adamo, C.; Jaramillo, J.; Gomperts, R.; Stratmann, R. E.; Yazyev, O.; Austin, A. J.; Cammi, R.; Pomelli, C.; Ochterski, J. W.; Martin, R. L.; Morokuma, K.; Zakrzewski, V. G.; Voth, G. A.; Salvador, P.; Dannenberg, J. J.; Dapprich, S.; Daniels, A. D.; Farkas, Ö.; Foresman, J. B.; Ortiz, J. V.; Cioslowski, J.; Fox, D. J. Gaussian, Inc., Wallingford CT, 2009.
32. Zhao Y, Truhlar DG. *Theor Chem Acc* **2008**, *120*, 215-41.

33. Dolg M., Wedig U., Stoll H., Preuss H. *J. Chem. Phys.* **1987**, *86*, 866.
34. Andrae D., Haussermann U., Dolg M., Stoll H., Preuss H. *Theor. Chim. Acta* **1990**, *77*, 123.
35. Scalmani G., Frisch M. J., Mennucci B., Tomasi J., Cammi R., Barone V. *J. Chem. Phys.* **2006**, *124*, 094107.
36. Corni S., Cammi R., Mennucci B., Tomasi J. *Phys. Chem. Chem. Phys.* **2005**, *123*, 134512.
37. Cossi M., Barone V. *J. Chem. Phys.* **2001**, *115*, 4708.
38. Cossi M, Barone V. *J Chem Phys* **2000**, *112*, 2427-35.
39. Fukui, K. J. *Phys. Chem.* **1970**, *74*, 4161−4163.
40. Gonzalez C., Schlegel H. B. J. *Chem. Phys.* **1989**, *90*, 2154−2161.
41. Rinkevicius Z., Tunell I., Sałek P, Vahtras O, Ågren H. *J. Chem. Phys.* **2003**, *119*, 34–46.
42. Ågren H, Vahtras O., Minaev B. *Adv. Quantum Chem.* **1996**, *27*, 71–162.
43. DALTON. A Molecular Electronic Structure Program. Release Dalton 2011. Available online: http://daltonprogram.org/.
44. Ruud K., Schimmelpfennig B., Ågren H. *Chem. Phys. Lett.* **1999**, *310*, 215–221.
45. Koseki S., Schmidt M. W., Gordon M. S. *J. Phys. Chem. A* **1998**, *102*, 10430.
46. Alberto M. E., Mazzone G., Quartarolo A.D., Sousa F. F. R., Sicilia E., Russo N. *J. Comput. Chem.* **2014**, *35*, 2107-2113.
47. Alberto M. E., De Simone B. C., Mazzone G., Quartarolo A.D., Russo N. *J. Chem. Theory Comput.* **2014**, *10*, 4006-4013.
48. Alberto M. E., De Simone B. C., Mazzone G., Marino T., Russo N. *Dyes Pigm.* **2015**, *120*, 335-339.
49. Alberto M. E., De Simone B. C., Mazzone G., Sicilia E., Russo N. *Phys. Chem. Chem. Phys.* **2015**, *17*, 23595-601.
50. Mazzone G., Quartarolo A.D., Russo N. *Dyes Pigm.* **2016**, *130*, 9-15.
51. Mazzone G., Alberto M. E., De Simone B. C., Marino T., Russo N. *Molecules* **2016**, *21*, 288.
52. Pirillo J., De Simone B. C., Russo N. *Theor. Chem. Acc.* **2016**, *135*, 8.
53. Pirillo J., Mazzone G., Russo N., Bertini L. *J. Chem. Inf. Model.* **2017**, *57*, 234−242.
54. De Simone B. C., Pirillo J., Mazzone G., Russo N., Sicilia E. *Phys. Chem. Chem. Phys.* **2017**, *19*, 2530-2536.
55. Alberto M. E., Russo N., Adamo C. *Chem. Eur. J.* **2016**, *22*, 9162-9168 .
56. Alberto M. E., Pirillo J., Russo N., Adamo C. *Inorg Chem* **2016**, *55*, 11185–11192.
57. Alberto M. E., Marino T., Quartarolo A.D., Russo N. *Phys. Chem. Chem. Phys.* **2013**, *15*, 16167-16171.
58. Roy, L.; Jakubikova, E.; Guthrie, G.; Batista, E. *J Phys Chem* **2009**, *113*, 6745-6750
59. Rehm D., Weller A. H. *Isr. J. Chem.* **1970**, *8*, 259-271.
60. Castro, L. Calculations of one-electron redox potentials of oxoiron(IV) porphyrin complexes. J. Chem. Theory Comput. 2013, 10, 243–251.
61. Lakowicz, J. R. Principles of Fluorescence Spectroscopy; Springer: Boston, MA, **2006**.
62. Le Guennic B, Jacquemin D. *Acc Chem Res* **2015**, *48*, 530.

63. Savarese M., Raucci U., Adamo C., Netti P. A., Ciofini I., Rega N. *Phys. Chem. Chem. Phys.* **2014**, *16*, 20681-20688,
64. Dondaine L., Escudero D., Ali M., Richard P., Denat F., Bettaieb A., Le Gendre P., Paul C., Jacquemin D., Goze C., Bodio E., *Eur. J. Inorg. Chem.* **2016**, 545–553,
65. Escudero D. *Acc. Chem. Res.* **2016**, *49*, 1816 – 1824.
66. **Phys. Chem. Chem. Phys., 2004, 6, 836–842**
67. Fabijanić I., Brala C., Pilepić V. *J Mol Model* **2015**, *21*, 99.
68. Mazzone G., Alberto M. E., Russo N., Sicilia E. *Phys. Chem. Chem. Phys.* **2014**, *16*, 12773-12781,
69. Li C., Hoffman M. *J Phys Chem* **2000**, *104*, 5998–6002.
70. Bisby RH, Morgan CG, Hamblett I, Gorman AA. *J Phys Chem* **1999**, *103,* 7459.
71. Dad S., Bisby R., Clark I., Parker A. *Free Radical Res* **2009**, *40***,** 333–338.

Supporting Information

Theoretical Insights on the switch off/on Photosensitization in Chemicontrolled Photodynamic Therapy

Jenny Pirillo, Gloria Mazzone and Nino Russo*

Dipartimento di Chimica e Tecnologie Chimiche, Università della Calabria, Via P. Bucci, 87036 Rende, Italy

Table of contents

Cartesian coordinates

1	S_0			S_1		
	x	y	z	x	y	z
C	-6.38002300	6.02649700	0.91499800	-6.386958	6.027828	0.913029
C	-5.67927000	7.24205500	0.96145800	-5.661503	7.241504	1.017656
C	-6.37425900	8.46181600	0.92765400	-6.379215	8.460841	0.926917
C	-8.19415400	4.72972400	0.83732000	-8.203460	4.723645	0.832249
C	-7.07521900	3.88892600	0.78323400	-7.076861	3.882862	0.751032
C	-5.93021900	4.67651600	0.83185200	-5.931805	4.664690	0.788180
H	-7.10819600	2.80737900	0.70789800	-7.117521	2.802285	0.659930
C	-5.91421600	9.80860700	0.86215800	-5.915166	9.822573	0.819671
C	-7.05340900	10.60542900	0.81633300	-7.055232	10.611897	0.788797
H	-7.07824500	11.68792300	0.75251300	-7.088928	11.693695	0.710352
C	-8.17824400	9.77216000	0.85629400	-8.187235	9.777336	0.857301
C	-9.60428900	10.18209400	0.83808100	-9.608288	10.178056	0.853084
H	-10.10625700	9.82516300	-0.06820500	-10.126763	9.803824	-0.040307
H	-10.15115400	9.76622700	1.69167800	-10.146665	9.764061	1.716271
H	-9.67973100	11.27187000	0.87220400	-9.691842	11.267504	0.874671
C	-4.52421800	10.34485000	0.81125100	-4.519334	10.330045	0.715062
H	-3.99194300	10.21044200	1.76154600	-3.982042	10.296810	1.672981
H	-3.91987300	9.86961800	0.03091000	-3.920485	9.763276	-0.007612
H	-4.55317600	11.41930100	0.60575500	-4.533294	11.376167	0.392148
C	-4.18721000	7.24272200	1.03873000	-4.180440	7.235914	1.210932
H	-3.74130000	7.30956300	0.03696300	-3.621513	7.242672	0.263373
H	-3.82047500	8.09085200	1.61780200	-3.856376	8.108373	1.783254
H	-3.80738400	6.33694600	1.50950600	-3.860731	6.352492	1.768572
C	-4.54590800	4.12639400	0.76389400	-4.539411	4.149971	0.673416
H	-3.94564400	4.59721600	-0.02247000	-3.938311	4.723524	-0.042010
H	-4.00158600	4.25025400	1.70866800	-4.000093	4.165798	1.630652
H	-4.58916200	3.05315000	0.55447900	-4.560595	3.108816	0.335211
C	-9.62278700	4.32887000	0.82115200	-9.627066	4.332001	0.827215
H	-10.16505400	4.74461700	1.67766500	-10.161681	4.743671	1.693822
H	-10.12474900	4.69220800	-0.08256800	-10.144435	4.715106	-0.063053
H	-9.70477800	3.23944600	0.85092700	-9.717471	3.242971	0.841423
N	-7.77364800	8.48717000	0.91254500	-7.774143	8.481096	0.926209
N	-7.78036600	6.01077500	0.90525500	-7.781979	6.016339	0.915317
B	-8.68928400	7.25155000	1.02763700	-8.689122	7.251085	1.051149
F	-9.35065100	7.25003000	2.26689500	-9.348184	7.248042	2.293713
F	-9.64864600	7.25670800	0.00869100	-9.660580	7.258296	0.040093

2	S_0			S_1		
	x	y	z	x	y	z
C	-6.083058	6.109435	1.034016	-6.066891	6.101554	1.117058
C	-5.490043	7.381851	1.044633	-5.432123	7.374041	1.100874
C	-6.262161	8.544007	0.931256	-6.231962	8.536505	0.973469
C	-7.772853	4.663984	0.859094	-7.754556	4.654595	0.8841
C	-6.620539	3.926573	1.162316	-6.610336	3.91248	1.234107
C	-5.55125	4.806761	1.278732	-5.545136	4.784331	1.397213
H	-6.581722	2.850154	1.289257	-6.585954	2.835321	1.361749
C	-5.940724	9.936775	1.027703	-5.913913	9.942177	1.099829
C	-7.137228	10.619767	0.865428	-7.097026	10.622674	0.864928
H	-7.268255	11.696094	0.888821	-7.232412	11.699157	0.87618
C	-8.164388	9.68376	0.673814	-8.119468	9.686047	0.619719
C	-9.602823	9.964545	0.449102	-9.538929	9.952886	0.316624
H	-9.964956	9.483708	-0.466406	-9.843761	9.478065	-0.625982
H	-10.211344	9.579547	1.275107	-10.196244	9.539597	1.09358
H	-9.764939	11.042071	0.367489	-9.712988	11.029047	0.242192
C	-4.642221	10.620609	1.289147	-4.618746	10.584461	1.444901
H	-4.195925	10.315319	2.243193	-4.199383	10.200658	2.385041
H	-3.911362	10.423699	0.496375	-3.864233	10.434337	0.660644
H	-4.804455	11.701675	1.337567	-4.764206	11.66259	1.56638
C	-3.993166	7.47109	1.169742	-3.944264	7.44117	1.153158
H	-3.648486	8.499473	1.240313	-3.57708	8.462432	1.22956
H	-3.643865	6.926969	2.050811	-3.528029	6.862047	1.980436
C	-4.171545	4.385883	1.653821	-4.179026	4.389995	1.833653
H	-3.423903	4.689302	0.914881	-3.400926	4.708474	1.129275
H	-3.867549	4.808158	2.620548	-3.923274	4.812798	2.815133
H	-4.134896	3.296869	1.752083	-4.12418	3.30091	1.927176
C	-9.144883	4.143575	0.645339	-9.114739	4.149967	0.614967
H	-9.815681	4.45957	1.452234	-9.82957	4.51096	1.367026
H	-9.573281	4.514432	-0.292231	-9.489886	4.497919	-0.356707
H	-9.129279	3.051225	0.616212	-9.120049	3.057347	0.625282
N	-7.645155	8.442928	0.726304	-7.59481	8.432114	0.701659
N	-7.453602	5.972195	0.79324	-7.420983	5.974191	0.828285

B	-8.430726	7.130031	0.502281	-8.37414	7.126224	0.459404
F	-9.525156	7.070291	1.370835	-9.517811	7.084999	1.266362
F	-8.895989	7.060677	-0.818765	-8.772716	7.03001	-0.883276
O	-3.347368	6.829716	0.057056	-3.346695	6.827594	-0.02361
C	-3.15921	7.551941	-1.064435	-3.32004	7.5674	-1.14401
C	-2.505407	6.726525	-2.122682	-2.700783	6.81344	-2.275458
H	-1.570392	6.302367	-1.745053	-1.705195	6.459174	-1.99275
H	-3.157292	5.889573	-2.392089	-3.306734	5.931701	-2.506844
H	-2.309341	7.338968	-3.003076	-2.633846	7.453163	-3.155962
O	-3.485776	8.714186	-1.170214	-3.749154	8.701723	-1.201569

3	**S_0**			**S_1**		
	x	**y**	**z**	**x**	**y**	**z**
C	-6.38273500	6.02604500	0.92336700	-6.381232	6.026876	0.906000
C	-5.67924200	7.24181800	0.98843800	-5.659422	7.241383	1.033870
C	-6.37487900	8.46277300	0.93659000	-6.373318	8.461834	0.919687
C	-8.20647200	4.73701600	0.83244900	-8.216993	4.735506	0.828635
C	-7.07589100	3.90444200	0.76173900	-7.074026	3.905502	0.737859
C	-5.92040100	4.68277800	0.81514800	-5.916191	4.685492	0.763944
C	-5.90374700	9.80423800	0.84495800	-5.899500	9.801900	0.794154
C	-7.05413900	10.59062400	0.79970500	-7.052290	10.589487	0.776121
C	-8.19008200	9.76462700	0.85949600	-8.200611	9.765907	0.855921
C	-9.62215800	10.14468000	0.84149700	-9.625908	10.150462	0.864646
H	-10.08887300	9.84333000	-0.10332300	-10.137776	9.783899	-0.034772
H	-10.17456200	9.64644000	1.64467300	-10.150591	9.712955	1.723313
H	-9.73583300	11.22538500	0.95511800	-9.733031	11.237091	0.905388
C	-4.50531100	10.30554800	0.75701100	-4.497652	10.280544	0.649495
H	-3.99387400	10.26541200	1.72757400	-3.992531	10.406375	1.617336
H	-3.90397000	9.73370500	0.04350900	-3.890161	9.598384	0.047401
H	-4.50053600	11.35129200	0.43500000	-4.481194	11.257091	0.153206
C	-4.19199700	7.23631800	1.12446900	-4.193660	7.234871	1.324713
H	-3.70047800	7.24055000	0.14186500	-3.565477	7.235090	0.421758
H	-3.84105500	8.10987100	1.67344600	-3.911731	8.111506	1.914359
H	-3.84642100	6.35450000	1.66348600	-3.918527	6.352858	1.909615
C	-4.52536800	4.17339700	0.71920500	-4.517449	4.200048	0.611792
H	-3.92124900	4.74959300	0.01156600	-3.906966	4.885488	0.016449
H	-4.01215900	4.19862200	1.68931000	-4.011476	4.060603	1.577282
H	-4.52798300	3.13157900	0.38468000	-4.507521	3.229039	0.104592
C	-9.64080600	4.36587700	0.81014300	-9.644674	4.359896	0.834539
H	-10.19243800	4.86422800	1.61364800	-10.165403	4.788973	1.699847
H	-10.10351300	4.67283100	-0.13487200	-10.155752	4.741339	-0.059065
H	-9.76101500	3.28541400	0.91951600	-9.758410	3.273503	0.860966
N	-7.77148700	8.48718500	0.92774900	-7.778000	8.482090	0.924355
N	-7.77952200	6.01075300	0.91577200	-7.785979	6.015613	0.911873
B	-8.68856500	7.25122700	1.08066800	-8.694636	7.251123	1.063517
F	-9.28771600	7.24773900	2.34677600	-9.330010	7.247183	2.315525
F	-9.67985800	7.25859700	0.09992000	-9.675318	7.258954	0.065066
I	-7.15400400	1.80389800	0.59424600	-7.144331	1.816728	0.600187
I	-7.11845300	12.69339400	0.65588400	-7.109046	12.680135	0.660854

4	**S_0**			**S_1**		
	x	**y**	**z**	**x**	**y**	**z**
C	-6.381920	6.026523	0.891983	-6.379099	6.027696	0.882463
C	-5.680547	7.242495	0.934311	-5.655517	7.242357	0.975795
C	-6.377161	8.462210	0.907745	-6.372766	8.461982	0.898664
C	-8.203476	4.732380	0.871177	-8.214933	4.735753	0.857608
C	-7.070867	3.906480	0.825450	-7.071739	3.90755	0.795222
C	-5.917355	4.681837	0.835717	-5.914427	4.680503	0.793993
C	-5.903762	9.803819	0.872055	-5.900719	9.80766	0.827433
C	-7.052382	10.586988	0.866357	-7.053654	10.586927	0.842001
C	-8.190127	9.767970	0.896383	-8.201344	9.764402	0.895374
C	-9.610722	10.185372	0.889037	-9.620581	10.165322	0.905541
H	-9.985556	10.261528	-0.139721	-10.053994	10.102752	-0.103377
H	-10.242746	9.473490	1.424228	-10.213257	9.506416	1.548334
H	-9.716480	11.171885	1.349856	-9.725646	11.198421	1.248484
C	-4.514525	10.331103	0.805564	-4.508129	10.315922	0.702588
H	-3.984119	10.215573	1.759144	-3.991805	10.371495	1.670648
H	-3.919648	9.833811	0.033276	-3.899442	9.692384	0.040499
H	-4.536532	11.400992	0.576444	-4.518857	11.330434	0.289747
C	-4.190154	7.243421	1.019853	-4.179017	7.237162	1.199834
H	-3.738239	7.307437	0.020623	-3.598335	7.239534	0.265737
H	-3.827821	8.092178	1.599774	-3.869359	8.111864	1.776583
H	-3.813843	6.340098	1.496873	-3.874321	6.355927	1.769253
C	-4.532886	4.143565	0.751423	-4.524208	4.166222	0.666851
H	-3.941265	4.642770	-0.022321	-3.910618	4.793357	0.012719

H	-3.992716	4.244042	1.701152	-4.010534	4.097861	1.635518
H	-4.566616	3.076246	0.511881	-4.539178	3.15619	0.243324
C	-9.626155	4.322330	0.864575	-9.636232	4.341974	0.85824
H	-10.254553	5.035700	1.401840	-10.229876	5.000947	1.499863
H	-10.001741	4.249815	-0.164159	-10.063118	4.409596	-0.153168
H	-9.736074	3.335186	1.323079	-9.748118	3.308015	1.196566
N	-7.775081	8.488764	0.912117	-7.778065	8.480618	0.914745
N	-7.780675	6.008309	0.901239	-7.784591	6.016661	0.895837
B	-8.701709	7.250928	0.934136	-8.70232	7.25063	0.964861
F	-9.480310	7.247623	2.095448	-9.451637	7.243357	2.150799
F	-9.538580	7.257585	-0.183396	-9.587682	7.261471	-0.119971
Br	-7.145873	2.036069	0.744350	-7.145674	2.049131	0.697976
Br	-7.112964	12.459081	0.809823	-7.116388	12.447104	0.770733

5		**S_0**			**S_1**	
	x	**y**	**z**	**x**	**y**	**z**
C	-6.073742	6.109158	1.034157	-6.049664	6.10494	1.114632
C	-5.478277	7.383062	1.039332	-5.419134	7.380464	1.089951
C	-6.252765	8.546574	0.928097	-6.221405	8.543458	0.971254
C	-7.779037	4.673931	0.86819	-7.761503	4.673228	0.87625
C	-6.622974	3.945	1.201184	-6.610687	3.943299	1.263024
C	-5.538641	4.813536	1.309514	-5.529516	4.812816	1.426347
C	-5.927231	9.936669	1.049588	-5.904703	9.929707	1.12559
C	-7.136455	10.60652	0.890741	-7.109138	10.599998	0.90835
C	-8.168723	9.672843	0.673192	-8.139637	9.666464	0.638924
C	-9.610495	9.920309	0.443286	-9.565418	9.909335	0.343864
H	-9.977212	9.357784	-0.421004	-9.889018	9.353642	-0.544385
H	-10.198595	9.598795	1.3105	-10.200159	9.571245	1.173724
H	-9.79663	10.983365	0.272775	-9.750776	10.973707	0.178754
C	-4.618132	10.586522	1.329998	-4.602282	10.553508	1.479649
H	-4.179394	10.238022	2.272151	-4.172359	10.122405	2.392712
H	-3.898335	10.397786	0.525056	-3.865756	10.441159	0.672518
H	-4.74602	11.6693	1.416348	-4.732423	11.625347	1.659013
C	-3.979735	7.466423	1.153659	-3.929398	7.451645	1.12275
H	-3.627966	8.491396	1.223631	-3.565332	8.475059	1.169927
H	-3.625461	6.920637	2.031348	-3.497903	6.894577	1.957024
C	-4.15683	4.425629	1.702403	-4.16475	4.445147	1.890639
H	-3.407088	4.778174	0.988986	-3.386208	4.744206	1.179746
H	-3.896303	4.827337	2.690382	-3.927001	4.903328	2.859697
H	-4.076849	3.336936	1.769034	-4.092946	3.361328	2.023865
C	-9.158014	4.181656	0.648004	-9.126208	4.187859	0.594156
H	-9.796764	4.427329	1.50452	-9.817342	4.476663	1.397498
H	-9.6097	4.643402	-0.235189	-9.521149	4.624841	-0.330381
H	-9.161979	3.096684	0.517471	-9.140137	3.098809	0.504565
N	-7.631254	8.442394	0.712637	-7.594274	8.431403	0.694813
N	-7.44002	5.973167	0.784277	-7.411279	5.976073	0.806039
B	-8.401529	7.129284	0.424296	-8.349392	7.124341	0.383805
F	-9.549571	7.062324	1.210166	-9.540374	7.064925	1.11082
F	-8.755063	7.064626	-0.92773	-8.648211	7.040166	-0.984258
O	-3.352424	6.825489	0.032014	-3.350457	6.819075	-0.050792
C	-3.18479	7.55192	-1.091875	-3.318576	7.553163	-1.175412
C	-2.548927	6.73118	-2.164268	-2.726256	6.780829	-2.309104
H	-1.617184	6.289197	-1.799246	-1.744458	6.388722	-2.027899
H	-3.215144	5.906958	-2.438628	-3.365031	5.92288	-2.542646
H	-2.352418	7.351533	-3.039141	-2.636836	7.42	-3.188159
O	-3.518046	8.713394	-1.185846	-3.725546	8.695971	-1.233858
I	-7.434425	12.690892	0.983237	-7.400277	12.672025	0.980917
I	-6.588396	1.859146	1.507302	-6.585617	1.868527	1.540624

6		**S_0**			**S_1**	
	x	**y**	**z**	**x**	**y**	**z**
C	-6.075043	6.114731	1.055718	-6.049664	6.10494	1.114632
C	-5.48271	7.388094	1.069652	-5.419134	7.380464	1.089951
C	-6.256611	8.549401	0.955989	-6.221405	8.543458	0.971254
C	-7.767038	4.670647	0.846286	-7.761503	4.673228	0.87625
C	-6.602196	3.949154	1.151814	-6.610687	3.943299	1.263024
C	-5.527633	4.819638	1.293501	-5.529516	4.812816	1.426347
C	-5.92111	9.937036	1.042827	-5.904703	9.929707	1.12559
C	-7.124372	10.60499	0.861854	-7.109138	10.599998	0.90835
C	-8.164792	9.679215	0.670741	-8.139637	9.666464	0.638924
C	-9.599221	9.951795	0.431416	-9.565418	9.909335	0.343864
H	-9.945834	9.466556	-0.487147	-9.889018	9.353642	-0.544385
H	-10.209909	9.563777	1.253897	-10.200159	9.571245	1.173724
H	-9.769116	11.02729	0.344687	-9.750776	10.973707	0.178754
C	-4.621386	10.608731	1.310122	-4.602282	10.553508	1.479649

H	-4.181166	10.289939	2.261725	-4.172359	10.122405	2.392712
H	-3.89656	10.411434	0.512394	-3.865756	10.441159	0.672518
H	-4.771783	11.690513	1.366876	-4.732423	11.625347	1.659013
C	-3.984872	7.475921	1.18514	-3.929398	7.451645	1.12275
H	-3.637444	8.502834	1.250187	-3.565332	8.475059	1.169927
H	-3.631082	6.936694	2.067112	-3.497903	6.894577	1.957024
C	-4.151347	4.413258	1.683918	-4.16475	4.445147	1.890639
H	-3.399585	4.742632	0.961442	-3.386208	4.744206	1.179746
H	-3.877444	4.825101	2.663581	-3.927001	4.903328	2.859697
H	-4.096677	3.324032	1.765024	-4.092946	3.361328	2.023865
C	-9.133717	4.152743	0.615166	-9.126208	4.187859	0.594156
H	-9.801205	4.439703	1.435336	-9.817342	4.476663	1.397498
H	-9.560883	4.555855	-0.308655	-9.521149	4.624841	-0.330381
H	-9.11794	3.062267	0.54843	-9.140137	3.098809	0.504565
N	-7.636134	8.446889	0.741869	-7.594274	8.431403	0.694813
N	-7.440998	5.974925	0.801725	-7.411279	5.976073	0.806039
B	-8.421658	7.132244	0.499624	-8.349392	7.124341	0.383805
F	-9.521493	7.067384	1.352294	-9.540374	7.064925	1.11082
F	-8.855265	7.069187	-0.827151	-8.648211	7.040166	-0.984258
O	-3.351192	6.829729	0.070582	-3.350457	6.819075	-0.050792
C	-3.213241	7.537507	-1.069475	-3.318576	7.553163	-1.175412
C	-2.575432	6.707513	-2.133024	-2.726256	6.780829	-2.309104
H	-1.645403	6.266326	-1.763513	-1.744458	6.388722	-2.027899
H	-3.243463	5.882749	-2.401333	-3.365031	5.92288	-2.542646
H	-2.378054	7.319651	-3.013312	-2.636836	7.42	-3.188159
O	-3.571919	8.689141	-1.181504	-3.725546	8.695971	-1.233858
Br	-7.368851	12.462499	0.884287	-7.400277	12.672025	0.980917
Br	-6.540602	2.086566	1.348114	-6.585617	1.868527	1.540624

7	**S_0**			**S_1**		
	x	**y**	**z**	**x**	**y**	**z**
C	-5.320441	9.102985	-1.891992	-5.308218	9.032688	-2.008631
C	-6.105878	8.230198	-1.123975	-6.102828	8.177386	-1.196754
C	-6.645783	8.656588	0.107716	-6.570738	8.647517	0.06578
C	-3.95537	10.842724	-2.192295	-3.931679	10.774596	-2.413185
C	-3.970539	10.086079	-3.37831	-4.021228	10.005799	-3.565243
C	-4.824216	8.999965	-3.227202	-4.893296	8.916969	-3.360227
C	-7.553658	8.03607	1.018247	-7.456884	8.082903	1.015192
C	-7.728712	8.963489	2.044632	-7.521864	9.030004	2.061482
C	-6.959813	10.108143	1.782603	-6.721972	10.123967	1.770148
C	-6.823734	11.319869	2.624595	-6.458205	11.348491	2.568374
H	-6.261639	11.087077	3.538381	-5.504989	11.285475	3.110307
H	-6.31132	12.127037	2.100312	-6.409452	12.236712	1.930558
H	-7.811276	11.676175	2.939629	-7.249861	11.496876	3.309505
C	-8.26129	6.726991	0.932476	-8.265402	6.829214	0.941556
H	-8.856714	6.640697	0.016441	-8.88086	6.782013	0.034096
H	-7.578198	5.870329	0.969814	-7.661044	5.911607	0.974489
H	-8.951266	6.621522	1.774837	-8.953102	6.77823	1.792317
C	-6.274895	6.805834	-1.556544	-6.295534	6.74185	-1.576603
H	-7.193363	6.402402	-1.130432	-7.195341	6.340991	-1.103315
H	-6.399548	6.737063	-2.639946	-6.463787	6.620762	-2.652037
C	-5.211655	8.041568	-4.298262	-5.366349	7.955691	-4.398294
H	-4.860753	7.024252	-4.097992	-5.007453	6.928821	-4.244806
H	-6.301285	8.002337	-4.416507	-6.462435	7.911265	-4.437305
H	-4.78799	8.357848	-5.256924	-5.022551	8.269506	-5.390621
C	-3.15972	12.057475	-1.901181	-3.163464	12.018583	-2.156424
H	-3.231603	12.348757	-0.852198	-2.716754	12.010345	-1.156629
H	-2.104125	11.879444	-2.143459	-2.361253	12.12723	-2.89363
H	-3.492505	12.898455	-2.523117	-3.794481	12.915127	-2.223251
N	-6.321743	9.920806	0.612294	-6.145415	9.884955	0.550094
N	-4.804391	10.271876	-1.32081	-4.744241	10.189653	-1.473903
B	-5.2736	10.893104	0.015747	-5.186656	10.850279	-0.161158
F	-5.851044	12.142459	-0.23064	-5.839133	12.075897	-0.438166
F	-4.207638	11.048201	0.908304	-4.080999	11.147128	0.666527
C	-5.133139	5.799146	-1.186959	-5.175422	5.732541	-1.206654
C	-4.499951	5.979009	0.187871	-4.587304	5.837104	0.191603
C	-3.574592	7.184472	0.300967	-3.686244	7.044684	0.420856
H	-3.920379	5.064591	0.379836	-4.007492	4.919185	0.36237
H	-5.280819	6.016527	0.958219	-5.405192	5.829221	0.921346
H	-2.910197	7.03121	1.1631	-3.027369	6.837093	1.274874
H	-4.138329	8.096124	0.543689	-4.266542	7.931001	0.713172
C	-2.746379	7.390709	-0.934588	-2.840009	7.368384	-0.768679
C	-3.015754	6.654856	-2.089506	-3.063302	6.689988	-1.999181
C	-2.188365	6.726626	-3.22172	-2.183022	6.825527	-3.127571
C	-1.690134	8.315614	-0.936717	-1.832149	8.308275	-0.70211
C	-0.904554	8.432317	-2.084029	-1.037545	8.522548	-1.860137

C	-1.115249	7.629339	-3.213563	-1.172249	7.756152	-3.054184
O	-4.103493	5.815866	-2.189367	-4.08512	5.880261	-2.180994
O	0.118724	9.350451	-2.052091	-0.104874	9.465132	-1.764148
H	0.57726	9.370275	-2.900536	0.413987	9.546783	-2.578721
C	-2.441869	5.844071	-4.412672	-2.393703	5.979786	-4.343984
H	-3.274352	5.162192	-4.229649	-3.18413	5.243886	-4.192511
H	-2.681077	6.428398	-5.31246	-2.66783	6.598277	-5.209102
H	-1.561518	5.235047	-4.653265	-1.476385	5.441582	-4.606154
C	-0.171608	7.7525	-4.375747	-0.190621	7.981895	-4.162084
H	0.852056	7.458353	-4.102578	0.821623	7.676366	-3.865471
H	-0.46949	7.126327	-5.219033	-0.451464	7.416125	-5.057263
H	-0.128466	8.782193	-4.760983	-0.155621	9.035879	-4.469188
C	-1.413252	9.150972	0.277331	-1.568484	9.076366	0.55051
H	-1.173095	8.527128	1.149417	-1.415364	8.397888	1.398406
H	-0.573176	9.828911	0.112572	-0.685691	9.710936	0.461768
H	-2.289832	9.754175	0.549619	-2.427979	9.714876	0.792876
C	-5.732731	4.405812	-1.311882	-5.687326	4.329673	-1.472759
H	-6.499554	4.238449	-0.546611	-6.476363	4.080005	-0.754515
H	-6.192647	4.271631	-2.298241	-6.103161	4.254379	-2.484038
H	-4.948229	3.651656	-1.188997	-4.880137	3.597208	-1.367475
I	-2.856792	10.596724	-5.089029	-2.985501	10.430657	-5.359062
I	-8.936128	8.746122	3.757113	-8.667366	8.837416	3.831714

	T_1			S_2		
	x	**y**	**z**	**x**	**y**	**z**
C	-5.22206	9.028031	-1.90659	-5.403935	8.83582	-2.272179
C	-6.066841	8.160054	-1.139906	-6.089186	8.069336	-1.285789
C	-6.585206	8.648474	0.081023	-6.338231	8.654661	-0.014746
C	-3.844935	10.75648	-2.280579	-4.033185	10.479249	-2.983924
C	-3.935159	10.016092	-3.464518	-4.326673	9.632661	-4.061966
C	-4.79571	8.93663	-3.284839	-5.209434	8.610727	-3.651173
C	-7.524822	8.07785	1.007179	-7.134707	8.221983	1.083498
C	-7.660966	9.030059	2.022612	-6.937918	9.192577	2.08032
C	-6.858569	10.141034	1.749621	-6.074625	10.185858	1.621027
C	-6.659014	11.378108	2.539229	-5.555819	11.383363	2.324135
H	-5.724083	11.33712	3.113962	-4.612815	11.164409	2.846784
H	-6.601251	12.256993	1.889653	-5.356388	12.197685	1.622061
H	-7.480774	11.516686	3.247518	-6.272378	11.73018	3.075941
C	-8.28708	6.800741	0.912235	-8.073549	7.066448	1.168942
H	-8.874721	6.738714	-0.01249	-8.752497	7.022833	0.308544
H	-7.645944	5.90993	0.955283	-7.565703	6.093856	1.234858
H	-8.992876	6.725133	1.745441	-8.695784	7.155643	2.065855
C	-6.248393	6.727046	-1.544291	-6.38725	6.623484	-1.544192
H	-7.159693	6.334011	-1.090187	-7.1875	6.269961	-0.888094
H	-6.409004	6.625637	-2.622726	-6.766635	6.485591	-2.561829
C	-5.292478	8.00243	-4.328838	-5.833908	7.588423	-4.538329
H	-4.991924	6.962652	-4.148111	-5.480728	6.570396	-4.330165
H	-6.388678	8.019694	-4.386387	-6.927037	7.58391	-4.444107
H	-4.904705	8.2926	-5.311238	-5.603069	7.806197	-5.58699
C	-3.037719	11.961832	-1.991929	-3.22751	11.724228	-2.968108
H	-2.937601	12.125209	-0.916414	-2.847467	11.944121	-1.967103
H	-2.035167	11.853453	-2.424709	-2.378843	11.645718	-3.657282
H	-3.488557	12.861393	-2.434368	-3.82424	12.589472	-3.292135
N	-6.209398	9.896688	0.568609	-5.719949	9.856683	0.344393
N	-4.676683	10.16039	-1.352836	-4.705575	10.000475	-1.906902
B	-5.187595	10.849511	-0.068217	-4.83673	10.730417	-0.560159
F	-5.791166	12.073075	-0.414648	-5.440729	11.992435	-0.762864
F	-4.141	11.124719	0.825861	-3.579754	10.951107	0.026413
C	-5.131328	5.70906	-1.18124	-5.229032	5.597627	-1.372768
C	-4.524007	5.857373	0.207453	-4.69677	5.455797	0.048837
C	-3.622561	7.075776	0.376073	-3.917772	6.667824	0.53239
H	-3.938206	4.945962	0.393367	-4.03521	4.577699	0.056844
H	-5.327483	5.868917	0.955153	-5.525195	5.227931	0.730617
H	-2.931619	6.891081	1.210493	-3.301718	6.393331	1.400205
H	-4.204847	7.957439	0.681603	-4.602617	7.449177	0.908114
C	-2.827336	7.385309	-0.856885	-3.054041	7.242631	-0.534481
C	-3.070115	6.678332	-2.05017	-3.174858	6.811098	-1.852122
C	-2.233788	6.820013	-3.1864	-2.287417	7.263984	-2.840906
C	-1.809603	8.343486	-0.826584	-2.08199	8.235118	-0.197484
C	-1.038671	8.539811	-1.979794	-1.245816	8.736996	-1.197961
C	-1.208068	7.757838	-3.144481	-1.323953	8.265309	-2.508124
O	-4.071279	5.776013	-2.167717	-4.124999	5.918638	-2.250364
O	-0.06502	9.486228	-1.917152	-0.333791	9.682102	-0.825548
H	0.414936	9.541401	-2.753733	0.136765	10.030003	-1.592821
C	-2.454214	5.961739	-4.398641	-2.30995	6.66061	-4.203615
H	-3.254054	5.237706	-4.23405	-3.050902	5.862771	-4.269627
H	-2.723991	6.567252	-5.27532	-2.547538	7.408898	-4.975974
H	-1.547748	5.402341	-4.659187	-1.326993	6.247437	-4.463612
C	-0.249532	7.946178	-4.28305	-0.3732	8.797406	-3.53179

H	0.765693	7.625929	-4.0091	0.666812	8.54641	-3.279498
H	-0.541643	7.373922	-5.16541	-0.568032	8.406257	-4.531594
H	-0.193056	8.995141	-4.60696	-0.432583	9.893293	-3.607114
C	-1.527069	9.118216	0.423129	-1.964726	8.70614	1.209239
H	-1.266715	8.448937	1.254118	-1.538512	7.921199	1.850045
H	-0.699535	9.816496	0.283277	-1.330297	9.589953	1.283163
H	-2.407228	9.693438	0.734481	-2.951806	8.958805	1.616019
C	-5.702318	4.31354	-1.361914	-5.728135	4.252866	-1.870478
H	-6.480007	4.122185	-0.61302	-6.590429	3.926986	-1.27682
H	-6.1468	4.203178	-2.358273	-6.036565	4.318479	-2.92062
H	-4.914954	3.561178	-1.244936	-4.940909	3.495895	-1.785397
I	-2.942855	10.546319	-5.24211	-3.626046	9.961002	-6.01142
I	-8.878026	8.849408	3.736334	-7.784843	9.176025	4.013688

8	**S_0**			**S_1**		
	x	**y**	**z**	**x**	**y**	**z**
C	-5.314487	9.087452	-1.894369	-5.323703	9.022561	-2.024991
C	-6.105514	8.224918	-1.124364	-6.119312	8.17519	-1.208636
C	-6.63949	8.658815	0.105404	-6.576413	8.650826	0.053407
C	-3.912746	10.797688	-2.189388	-3.91659	10.738139	-2.430918
C	-3.916761	10.017611	-3.356971	-3.99646	9.948169	-3.565719
C	-4.805964	8.963915	-3.220652	-4.897751	8.887103	-3.368638
C	-7.544138	8.044988	1.020447	-7.448885	8.08822	1.013663
C	-7.708141	8.978302	2.038448	-7.490622	9.032641	2.059119
C	-6.943989	10.121396	1.771347	-6.698303	10.126859	1.759043
C	-6.830854	11.33478	2.612328	-6.442383	11.351744	2.556185
H	-6.374967	11.085711	3.578633	-5.417167	11.377997	2.944721
H	-6.237139	12.114612	2.135338	-6.582446	12.258422	1.957533
H	-7.828632	11.735403	2.827928	-7.126744	11.391189	3.408695
C	-8.261901	6.740766	0.962391	-8.265207	6.839277	0.970123
H	-8.874061	6.648004	0.058211	-8.896779	6.784652	0.074507
H	-7.584327	5.880063	0.998549	-7.666027	5.918588	1.004387
H	-8.934786	6.65566	1.821001	-8.935068	6.808216	1.836109
C	-6.281084	6.799922	-1.551511	-6.307895	6.73693	-1.578008
H	-7.195799	6.399374	-1.113728	-7.203224	6.33544	-1.095675
H	-6.417469	6.730179	-2.633809	-6.481479	6.608592	-2.651804
C	-5.197741	8.021084	-4.30241	-5.36232	7.928592	-4.411607
H	-4.875673	6.994594	-4.102734	-5.025572	6.896558	-4.245708
H	-6.285359	8.011442	-4.440252	-6.457351	7.904191	-4.478253
H	-4.744773	8.336297	-5.24784	-4.983327	8.235702	-5.392941
C	-3.095447	12.000345	-1.915006	-3.109622	11.957361	-2.180973
H	-3.170434	12.313266	-0.872496	-2.595035	11.902321	-1.214909
H	-2.043571	11.792819	-2.149259	-2.357718	12.077996	-2.96732
H	-3.407362	12.835253	-2.555675	-3.724009	12.867142	-2.168676
N	-6.30984	9.925965	0.60177	-6.14078	9.887804	0.531596
N	-4.785072	10.253203	-1.326646	-4.750172	10.178398	-1.49661
B	-5.251469	10.886704	0.004541	-5.191918	10.853123	-0.191811
F	-5.81414	12.139724	-0.249561	-5.854395	12.070101	-0.481173
F	-4.187945	11.034109	0.899916	-4.087791	11.166965	0.62911
Br	-2.917467	10.445592	-4.880249	-3.071083	10.297102	-5.166529
Br	-8.80355	8.804484	3.54811	-8.520484	8.868998	3.627323
C	-5.138451	5.790709	-1.190487	-5.181132	5.733878	-1.205344
C	-4.507649	5.95838	0.186818	-4.599861	5.841222	0.195591
C	-3.575757	7.157798	0.311899	-3.70126	7.049583	0.42856
H	-3.934408	5.03929	0.374374	-4.019969	4.924263	0.370227
H	-5.290627	5.995669	0.954881	-5.421369	5.833171	0.921035
H	-2.910456	6.990757	1.170642	-3.046278	6.843688	1.285829
H	-4.135551	8.068526	0.567835	-4.284119	7.935461	0.717641
C	-2.750191	7.379752	-0.923024	-2.850464	7.374854	-0.757111
C	-3.019688	6.654677	-2.084532	-3.068209	6.6986	-1.989219
C	-2.196279	6.742896	-3.21849	-2.188906	6.845727	-3.116913
C	-1.706648	8.318973	-0.922891	-1.84446	8.315754	-0.68436
C	-0.945036	8.471081	-2.081715	-1.050312	8.539998	-1.840269
C	-1.138552	7.662807	-3.209456	-1.189906	7.788519	-3.042578
O	-4.104967	5.812661	-2.190021	-4.086748	5.88511	-2.17513
O	0.042497	9.428774	-2.064133	-0.115167	9.478914	-1.734995
H	0.402902	9.548215	-2.95116	0.400007	9.570062	-2.551078
C	-2.444159	5.868684	-4.416478	-2.39179	6.006272	-4.338598
H	-3.280388	5.188486	-4.245444	-3.175886	5.262329	-4.19441
H	-2.67122	6.460967	-5.313929	-2.667592	6.630532	-5.198679
H	-1.564884	5.256329	-4.652616	-1.468703	5.479211	-4.60273
C	-0.208092	7.818294	-4.378407	-0.223468	8.041148	-4.157698
H	0.844006	7.741838	-4.071067	0.794415	7.73527	-3.881968
H	-0.370796	7.053809	-5.140514	-0.493321	7.493078	-5.061029
H	-0.336577	8.790708	-4.878815	-0.198294	9.101869	-4.441375
C	-1.417699	9.130358	0.304166	-1.585955	9.073341	0.575244

H	-1.19766	8.485183	1.165537	-1.398283	8.387111	1.409933
H	-0.560703	9.790326	0.154981	-0.726618	9.738602	0.483698
H	-2.28109	9.748979	0.583506	-2.462435	9.678725	0.838783
C	-5.739646	4.39957	-1.328407	-5.685208	4.328562	-1.472894
H	-6.508585	4.227603	-0.566661	-6.476023	4.075278	-0.758152
H	-6.197139	4.274441	-2.316912	-6.09601	4.250781	-2.485874
H	-4.956734	3.643385	-1.209793	-4.874961	3.600342	-1.36363
		T_1			**S_2**	
	x	**y**	**z**	**x**	**y**	**z**
C	-5.211663	9.02692	-1.876987	-5.383253	8.85106	-2.266111
C	-6.084641	8.165137	-1.135276	-6.088836	8.086652	-1.295507
C	-6.61743	8.647255	0.079829	-6.347898	8.66126	-0.022695
C	-3.7696	10.713072	-2.185519	-3.988535	10.491439	-2.942879
C	-3.836661	9.971673	-3.366595	-4.219063	9.616892	-4.005631
C	-4.750652	8.933418	-3.236399	-5.128378	8.60725	-3.629622
C	-7.558662	8.070851	0.99436	-7.135079	8.210828	1.070089
C	-7.70565	9.022686	2.005009	-6.937495	9.170615	2.075921
C	-6.914595	10.139782	1.743774	-6.090691	10.177147	1.630098
C	-6.752539	11.368037	2.555554	-5.597671	11.378866	2.343434
H	-5.975024	11.240415	3.321099	-4.573487	11.234661	2.714867
H	-6.471435	12.222979	1.936119	-5.578728	12.250805	1.681341
H	-7.686131	11.601247	3.077888	-6.236766	11.600897	3.203181
C	-8.310326	6.78694	0.918316	-8.069641	7.052621	1.165298
H	-8.908012	6.709443	0.00139	-8.782258	7.027851	0.331752
H	-7.659399	5.903564	0.963571	-7.56118	6.078794	1.188993
H	-9.00319	6.717352	1.763302	-8.652913	7.125301	2.089567
C	-6.251346	6.732301	-1.543431	-6.387722	6.642987	-1.566253
H	-7.163578	6.332677	-1.095792	-7.22	6.298633	-0.945329
H	-6.401684	6.629563	-2.623792	-6.72469	6.509968	-2.599313
C	-5.2355	8.033705	-4.315346	-5.69179	7.575788	-4.546541
H	-4.972659	6.982138	-4.146873	-5.328075	6.563482	-4.324783
H	-6.327231	8.085363	-4.414413	-6.787443	7.551885	-4.508034
H	-4.797865	8.333558	-5.273421	-5.40963	7.805988	-5.580025
C	-2.923549	11.885948	-1.878018	-3.197601	11.745835	-2.933767
H	-3.000671	12.170772	-0.827123	-2.979004	12.073209	-1.915248
H	-1.872435	11.650976	-2.100344	-2.250145	11.612223	-3.470381
H	-3.198237	12.750759	-2.496899	-3.738138	12.557676	-3.441063
N	-6.252198	9.89991	0.571513	-5.735124	9.862735	0.349192
N	-4.65187	10.140616	-1.294756	-4.706309	10.025675	-1.889867
B	-5.183131	10.828462	-0.019379	-4.856445	10.74933	-0.543194
F	-5.733754	12.076236	-0.366377	-5.467377	12.008546	-0.740194
F	-4.15864	11.055073	0.91348	-3.600634	10.97659	0.045863
Br	-2.901344	10.440075	-4.918757	-3.512254	9.881164	-5.715258
Br	-8.827519	8.872839	3.501268	-7.73472	9.146498	3.777363
C	-5.128456	5.72373	-1.167278	-5.250252	5.602579	-1.351106
C	-4.511737	5.900826	0.213779	-4.728166	5.484684	0.076377
C	-3.606755	7.121171	0.351729	-3.922316	6.688125	0.536086
H	-3.92763	4.992134	0.416203	-4.08937	4.590842	0.109083
H	-5.311553	5.930688	0.964766	-5.563327	5.294621	0.760994
H	-2.903051	6.94878	1.178108	-3.303123	6.416675	1.40263
H	-4.183339	8.008478	0.650962	-4.588841	7.487185	0.906158
C	-2.828193	7.414809	-0.896105	-3.060063	7.240484	-0.540493
C	-3.075201	6.679408	-2.072159	-3.182107	6.782836	-1.849418
C	-2.245576	6.796975	-3.219131	-2.298075	7.223868	-2.842012
C	-1.832162	8.392971	-0.903046	-2.099415	8.257053	-0.224119
C	-1.0876	8.581112	-2.07671	-1.281254	8.764016	-1.23679
C	-1.238256	7.752429	-3.213212	-1.331749	8.238149	-2.527394
O	-4.072111	5.774594	-2.162792	-4.128062	5.879612	-2.22594
O	-0.164311	9.574961	-2.06583	-0.414229	9.756264	-0.884258
H	0.279216	9.643329	-2.922139	-0.019182	10.16324	-1.664592
C	-2.4659	5.903742	-4.405158	-2.32102	6.619836	-4.201927
H	-3.280469	5.199916	-4.229035	-3.136331	5.903512	-4.305556
H	-2.711066	6.484094	-5.305137	-2.433117	7.391265	-4.978189
H	-1.566275	5.319868	-4.634114	-1.377051	6.099591	-4.412118
C	-0.293396	7.93303	-4.363595	-0.403565	8.725382	-3.588483
H	0.753908	7.876833	-4.036373	0.540002	9.105997	-3.184526
H	-0.426716	7.164658	-5.126737	-0.146207	7.933253	-4.295439
H	-0.438542	8.902452	-4.863476	-0.86807	9.532987	-4.176863
C	-1.524603	9.178148	0.333844	-1.979509	8.742259	1.175945
H	-1.105861	8.527067	1.113451	-1.54844	7.961337	1.818246
H	-0.799505	9.970773	0.138214	-1.347808	9.627926	1.240233
H	-2.429488	9.638428	0.744799	-2.964883	8.992343	1.588088
C	-5.694227	4.323461	-1.321647	-5.765494	4.254309	-1.820896
H	-6.464509	4.140511	-0.563478	-6.629819	3.950444	-1.218704
H	-6.147126	4.197126	-2.312126	-6.075796	4.301912	-2.871233
H	-4.903008	3.576119	-1.200421	-4.98671	3.490627	-1.721917

9	S_0			S_1		
	x	y	z	x	y	z
C	1.851631	8.126171	-3.203508	1.826582	8.173407	-3.238921
C	1.997079	7.225408	-2.13188	1.933346	7.251025	-2.156253
C	2.614384	5.981433	-2.308078	2.496571	5.962895	-2.368836
C	1.959484	8.76061	-5.343617	1.995399	8.834882	-5.389778
C	1.446929	9.832785	-4.59294	1.508644	9.893021	-4.639339
C	1.379165	9.473023	-3.249149	1.397751	9.522479	-3.282336
C	2.980838	4.946301	-1.385145	2.841211	4.913462	-1.476445
C	3.582464	3.965771	-2.162626	3.353975	3.890999	-2.298533
C	3.589003	4.370011	-3.512637	3.344603	4.289848	-3.627995
C	4.131517	3.630587	-4.674369	3.809963	3.565185	-4.837368
H	3.723336	3.993564	-5.618699	3.171446	3.776359	-5.70038
H	5.224101	3.734394	-4.711355	4.833346	3.852823	-5.113788
H	3.91282	2.562202	-4.57656	3.806135	2.485359	-4.659135
C	2.821823	4.888689	0.092602	2.764305	4.868053	0.012195
H	3.294925	5.742314	0.591225	3.272398	5.720901	0.480712
H	1.763727	4.86442	0.379196	1.728324	4.85261	0.374903
H	3.294316	3.983506	0.485093	3.256748	3.964226	0.38688
C	1.415382	7.612064	-0.79656	1.403408	7.648768	-0.823928
H	1.641275	6.887973	-0.019218	1.642927	6.933873	-0.040802
H	1.777823	8.590012	-0.473122	1.732233	8.640358	-0.506847
C	0.954406	10.368762	-2.139194	0.965438	10.422517	-2.173119
H	0.127004	9.951404	-1.559219	0.149949	9.999656	-1.575608
H	1.781917	10.567836	-1.446481	1.787736	10.660198	-1.484706
H	0.629957	11.334075	-2.538492	0.609921	11.375395	-2.579775
C	2.222334	8.714085	-6.80058	2.288401	8.772167	-6.845103
H	3.157195	9.23959	-7.036506	3.281142	9.182303	-7.075675
H	2.306389	7.690124	-7.169837	2.265012	7.745012	-7.218207
H	1.420521	9.224815	-7.346146	1.5545	9.361249	-7.40824
N	3.022105	5.583914	-3.587851	2.833723	5.559717	-3.661867
N	2.208244	7.743914	-4.499062	2.187053	7.787561	-4.529066
B	2.843155	6.391645	-4.898288	2.711746	6.405968	-4.93233
F	4.087303	6.607293	-5.494966	3.963061	6.523113	-5.572216
F	2.012781	5.703549	-5.786344	1.825087	5.788264	-5.857361
O	-0.014924	7.762843	-0.902829	-0.066445	7.797954	-0.847668
C	-0.747295	6.638718	-0.935844	-0.778419	6.683812	-0.86387
O	-0.284715	5.530587	-0.79949	-0.34054	5.563149	-0.723084
I	4.411623	2.14773	-1.499404	4.071039	2.011571	-1.639723
I	0.841001	11.659204	-5.443499	0.954273	11.753783	-5.472595
C	-2.245544	6.937907	-1.096571	-2.279436	6.960762	-1.051489
C	-2.549309	8.175859	-1.927422	-2.612676	8.174532	-1.894625
C	-1.983369	8.053754	-3.335938	-1.992967	8.077112	-3.281694
H	-3.644958	8.249022	-1.957735	-3.707773	8.218484	-1.957551
H	-2.181881	9.078899	-1.427329	-2.281691	9.083146	-1.382184
H	-2.537048	8.72097	-4.010713	-2.555487	8.703619	-3.985056
H	-0.944474	8.414227	-3.355513	-0.969301	8.477647	-3.273421
O	-2.843484	5.813573	-1.721771	-2.7943	5.78382	-1.731579
C	-2.032856	6.638538	-3.855381	-1.947959	6.666377	-3.797895
C	-2.475394	5.597628	-3.036081	-2.412765	5.59232	-2.987705
C	-2.583752	4.276525	-3.48821	-2.500784	4.240543	-3.445043
C	-1.760613	5.021315	-5.627665	-1.490804	5.006104	-5.485412
C	-1.640955	6.337543	-5.17118	-1.476396	6.368972	-5.058289
C	-2.23389	3.982316	-4.811907	-2.027949	3.939745	-4.702724
C	-1.108024	7.392314	-6.099744	-0.977586	7.408426	-6.0068
H	-0.868988	8.32298	-5.57574	-0.898932	8.391979	-5.537876
H	-0.172882	7.065998	-6.578886	0.032411	7.15762	-6.357787
H	-1.821175	7.64643	-6.897219	-1.63989	7.5028	-6.8775
C	-2.344105	2.586887	-5.357691	-2.032757	2.545546	-5.247161
H	-1.670087	1.895866	-4.834911	-1.379412	1.893174	-4.655837
H	-3.360039	2.189156	-5.244674	-3.039989	2.117208	-5.210267
H	-2.089923	2.55647	-6.418815	-1.689812	2.513897	-6.281538
C	-3.077678	3.227092	-2.537534	-3.043807	3.218175	-2.504256
H	-2.496522	3.237257	-1.608045	-2.441272	3.184072	-1.588917
H	-4.121508	3.409216	-2.250294	-4.063997	3.474212	-2.19657
H	-3.018251	2.223614	-2.964459	-3.056215	2.221876	-2.947073
C	-2.840342	7.025554	0.298184	-2.946957	6.981786	0.306062
H	-2.670411	6.091677	0.844802	-2.747881	6.0515	0.847591
H	-2.390861	7.854099	0.856063	-2.564184	7.823794	0.892036
H	-3.918964	7.198458	0.219625	-4.028368	7.10219	0.184586
O	-1.414372	4.688184	-6.913187	-1.008969	4.671808	-6.670887
H	-1.146496	5.474741	-7.403102	-0.611222	5.428231	-7.131352
	T_1			S_2		
	x	y	z	x	y	z
C	1.88303	8.147087	-3.180841	1.894429	8.146432	-3.147304
C	2.019284	7.275609	-2.069985	2.026156	7.249237	-2.051638
C	2.610344	6.000497	-2.28237	2.648133	5.990567	-2.254158
C	1.931781	8.760392	-5.337436	1.938882	8.739473	-5.311997

C	1.43108	9.845841	-4.590815	1.45237	9.830545	-4.552577
C	1.403378	9.518924	-3.244881	1.436104	9.497052	-3.195732
C	2.997821	4.96291	-1.336865	3.038439	4.969466	-1.333579
C	3.526284	3.946575	-2.113677	3.600078	3.966432	-2.125434
C	3.499592	4.318572	-3.472453	3.578215	4.356025	-3.48595
C	3.981331	3.569161	-4.649629	4.084057	3.628741	-4.667311
H	3.416478	3.824606	-5.549357	3.457669	3.811131	-5.545819
H	5.039325	3.794021	-4.845678	5.101742	3.958626	-4.923035
H	3.905232	2.492103	-4.472913	4.124992	2.553542	-4.471415
C	2.906217	4.981048	0.144894	2.915464	4.951614	0.14821
H	3.383491	5.871193	0.573034	3.365569	5.839169	0.610218
H	1.862805	4.95731	0.484195	1.865941	4.897474	0.467807
H	3.413763	4.106752	0.563495	3.431565	4.078643	0.559958
C	1.428341	7.664593	-0.757412	1.421251	7.626756	-0.742117
H	1.666821	6.958176	0.033495	1.633094	6.903891	0.041561
H	1.734883	8.657985	-0.425769	1.743467	8.611483	-0.396884
C	1.015799	10.417489	-2.126867	1.060615	10.403341	-2.076576
H	0.19715	10.006716	-1.525431	0.236642	10.007422	-1.471847
H	1.860545	10.610831	-1.453233	1.907269	10.592095	-1.403739
H	0.688737	11.384418	-2.520855	0.744088	11.374092	-2.470605
C	2.197883	8.677286	-6.787861	2.168859	8.662598	-6.768895
H	3.184894	9.102207	-7.019776	3.151525	9.084269	-7.028222
H	2.189605	7.644062	-7.142583	2.149789	7.630122	-7.127227
H	1.455019	9.25618	-7.347351	1.415486	9.245469	-7.310436
N	2.949882	5.577002	-3.547137	3.012726	5.581729	-3.549
N	2.203	7.742423	-4.457287	2.210007	7.73445	-4.452357
B	2.793918	6.376536	-4.856281	2.809643	6.372928	-4.855263
F	4.03904	6.551542	-5.470795	4.034922	6.559426	-5.506572
F	1.941968	5.709712	-5.744958	1.942404	5.688707	-5.718088
O	-0.024823	7.778665	-0.847608	-0.025319	7.769318	-0.862068
C	-0.71516	6.640637	-0.94425	-0.733702	6.641016	-0.960692
O	-0.220891	5.537543	-0.861121	-0.256974	5.531329	-0.872313
I	4.306175	2.11903	-1.428922	4.395601	2.151198	-1.456061
I	0.798001	11.649857	-5.456994	0.812757	11.628373	-5.402436
C	-2.220271	6.902581	-1.108687	-2.233851	6.925844	-1.129005
C	-2.539212	8.14055	-1.934269	-2.538163	8.163695	-1.96019
C	-1.948236	8.035582	-3.333203	-1.964701	8.04449	-3.365749
H	-3.635495	8.195071	-1.982154	-3.633874	8.236003	-1.996715
H	-2.191779	9.046088	-1.424971	-2.170939	9.066208	-1.459392
H	-2.477349	8.723359	-4.006772	-2.50326	8.728853	-4.035206
H	-0.903393	8.383736	-3.321648	-0.918772	8.38939	-3.372338
O	-2.794714	5.770908	-1.744265	-2.823265	5.798036	-1.75762
C	-2.008726	6.629008	-3.875342	-2.038174	6.634105	-3.897831
C	-2.438787	5.576378	-3.063617	-2.469124	5.589442	-3.075081
C	-2.548811	4.261074	-3.532581	-2.584767	4.269608	-3.530347
C	-1.764313	5.037281	-5.67541	-1.797768	5.020866	-5.679888
C	-1.641569	6.347404	-5.202696	-1.682033	6.338272	-5.224692
C	-2.217476	3.985282	-4.865052	-2.251421	3.977785	-4.8588
C	-1.128731	7.417126	-6.125347	-1.183776	7.393672	-6.170905
H	-0.893608	8.344131	-5.593093	-1.055478	8.364032	-5.683242
H	-0.196698	7.105064	-6.619952	-0.202098	7.123391	-6.588683
H	-1.853351	7.67434	-6.911396	-1.871311	7.552191	-7.014383
C	-2.32978	2.596358	-5.426887	-2.361198	2.582412	-5.404622
H	-1.657191	1.898161	-4.911995	-1.68718	1.891615	-4.881595
H	-3.346367	2.19876	-5.318334	-3.377016	2.184253	-5.291573
H	-2.075896	2.577927	-6.488379	-2.1072	2.55196	-6.465801
C	-3.026252	3.19754	-2.589128	-3.067987	3.217914	-2.57665
H	-2.4367	3.201262	-1.664718	-2.478233	3.226078	-1.652525
H	-4.068501	3.369342	-2.289843	-4.109018	3.399228	-2.278841
H	-2.964643	2.199354	-3.028066	-3.013139	2.215365	-3.006375
C	-2.827155	6.968983	0.281826	-2.839924	7.008353	0.261257
H	-2.637387	6.037269	0.826026	-2.661478	6.077988	0.811497
H	-2.402249	7.805626	0.846513	-2.405417	7.843638	0.820564
H	-3.909435	7.114763	0.19725	-3.920351	7.166288	0.175085
O	-1.439812	4.722726	-6.971588	-1.465043	4.692493	-6.969898
H	-1.185267	5.51687	-7.456368	-1.185124	5.477742	-7.455285

10	**S_0**			**S_1**		
	x	**y**	**z**	**x**	**y**	**z**
C	1.866937	8.115467	-3.192778	1.865128	8.19079	-3.150902
C	2.02352	7.220065	-2.120553	2.003119	7.277173	-2.067757
C	2.645878	5.980214	-2.296016	2.560522	5.990484	-2.288083
C	1.931381	8.731767	-5.339285	1.902142	8.815124	-5.317297
C	1.376767	9.780475	-4.591367	1.430237	9.869968	-4.556043
C	1.347672	9.442588	-3.244163	1.417312	9.531109	-3.190349
C	2.992804	4.939081	-1.376277	2.90357	4.940538	-1.401252

C	3.58695	3.960711	-2.156222	3.404903	3.920738	-2.228299
C	3.613836	4.366622	-3.50246	3.392884	4.317503	-3.556098
C	4.164041	3.616034	-4.652013	3.818571	3.572484	-4.765704
H	3.791431	3.992879	-5.605333	3.009499	3.505341	-5.503144
H	5.25964	3.686804	-4.657405	4.666666	4.057341	-5.263372
H	3.912755	2.554057	-4.562131	4.117427	2.556642	-4.491338
C	2.819454	4.851035	0.097486	2.821144	4.870622	0.084996
H	3.299648	5.685683	0.620364	3.338839	5.70664	0.572518
H	1.75866	4.834141	0.373452	1.782597	4.863739	0.441026
H	3.276339	3.928308	0.467098	3.296192	3.949511	0.439555
C	1.438926	7.604988	-0.786479	1.449485	7.662545	-0.742504
H	1.663805	6.880132	-0.009209	1.680639	6.94493	0.041159
H	1.802957	8.582369	-0.462434	1.762688	8.655124	-0.413225
C	0.906173	10.35147	-2.15255	1.034037	10.454616	-2.083714
H	0.068501	9.941794	-1.581211	0.210487	10.067355	-1.471692
H	1.720818	10.556868	-1.447407	1.873518	10.665265	-1.408323
H	0.591347	11.310103	-2.574877	0.71099	11.415315	-2.49885
C	2.182804	8.700071	-6.79713	2.126113	8.747573	-6.783001
H	3.089885	9.269678	-7.038321	3.134223	9.088673	-7.054282
H	2.310958	7.682334	-7.170555	2.019954	7.728066	-7.165022
H	1.353825	9.177879	-7.331432	1.410085	9.39194	-7.305315
N	3.060089	5.585464	-3.575896	2.888813	5.589301	-3.584743
N	2.227339	7.735072	-4.488307	2.167024	7.79018	-4.450789
B	2.877298	6.39045	-4.887197	2.611207	6.38291	-4.863299
F	4.117339	6.616987	-5.485508	3.75997	6.449719	-5.673078
F	2.05137	5.695249	-5.77276	1.591855	5.746623	-5.625661
O	0.00932	7.760196	-0.893014	-0.020487	7.80275	-0.799552
C	-0.727595	6.639916	-0.948494	-0.721512	6.684758	-0.894248
O	-0.270138	5.527905	-0.833915	-0.279177	5.562454	-0.791852
C	-2.224026	6.951852	-1.100895	-2.217387	6.961965	-1.113548
C	-2.523495	8.196378	-1.923407	-2.531679	8.172737	-1.967862
C	-1.983049	8.07498	-3.342111	-1.888677	8.064715	-3.341917
H	-3.618129	8.285229	-1.935409	-3.625293	8.223663	-2.049696
H	-2.13511	9.092507	-1.426445	-2.202379	9.081134	-1.454282
H	-2.550473	8.743149	-4.004226	-2.400628	8.733242	-4.044517
H	-0.945173	8.435278	-3.381488	-0.846072	8.410446	-3.296713
O	-2.836498	5.835611	-1.726857	-2.722799	5.782365	-1.7939
C	-2.040292	6.661538	-3.864804	-1.905094	6.660286	-3.876877
C	-2.476627	5.619859	-3.043779	-2.364807	5.59172	-3.056652
C	-2.586647	4.299042	-3.495119	-2.483525	4.241853	-3.513581
C	-1.768739	5.043283	-5.635158	-1.551898	5.001039	-5.590792
C	-1.655834	6.360872	-5.18231	-1.502863	6.362337	-5.160766
C	-2.239935	4.004448	-4.819234	-2.058255	3.937299	-4.786548
C	-1.126033	7.409277	-6.119005	-1.040507	7.394751	-6.13457
H	-0.981088	8.376033	-5.629188	-0.925629	8.379113	-5.676274
H	-0.145712	7.117445	-6.525339	-0.052679	7.131186	-6.535128
H	-1.799472	7.584294	-6.970527	-1.744896	7.494041	-6.970844
C	-2.345651	2.608331	-5.363505	-2.084421	2.541335	-5.325322
H	-1.668506	1.920272	-4.841194	-1.457064	1.878964	-4.718206
H	-3.359963	2.207396	-5.248753	-3.101577	2.135115	-5.305672
H	-2.092746	2.578064	-6.424769	-1.72384	2.497152	-6.353042
C	-3.073182	3.248351	-2.542361	-3.003458	3.222334	-2.557131
H	-2.492948	3.265684	-1.612721	-2.302323	3.088237	-1.724064
H	-4.118719	3.422523	-2.25684	-3.952118	3.547562	-2.117748
H	-3.005091	2.244466	-2.966693	-3.154974	2.254375	-3.035667
C	-2.810243	7.038337	0.297611	-2.910306	6.992177	0.231461
H	-2.642551	6.101848	0.840163	-2.720448	6.066033	0.783205
H	-2.353343	7.862618	0.855416	-2.539079	7.838675	0.817859
H	-3.888195	7.216976	0.225412	-3.989254	7.110044	0.088739
O	-1.413302	4.708918	-6.917914	-1.132509	4.667996	-6.800102
H	-1.129157	5.493051	-7.402832	-0.737462	5.42171	-7.267948
Br	0.76513	11.379102	-5.347393	0.867358	11.512911	-5.279063
Br	4.293831	2.333909	-1.561608	4.037639	2.251424	-1.630883

	T_1			S_2		
	x	**y**	**z**	**x**	**y**	**z**
C	1.883788	8.159971	-3.193214	1.909042	8.131948	-3.145892
C	2.015113	7.281206	-2.089848	2.045657	7.244963	-2.04481
C	2.578288	5.997494	-2.315918	2.669523	5.988447	-2.24124
C	1.937845	8.78862	-5.344515	1.926658	8.706148	-5.315233
C	1.404136	9.849564	-4.590371	1.397003	9.777889	-4.560008
C	1.386435	9.523399	-3.247723	1.414305	9.470163	-3.202637
C	2.929525	4.938952	-1.382832	3.038285	4.96175	-1.316537
C	3.419683	3.91857	-2.173969	3.600704	3.962747	-2.104033
C	3.41594	4.304201	-3.526761	3.605479	4.35169	-3.463361
C	3.87335	3.550299	-4.708854	4.11062	3.613902	-4.634977
H	3.189531	3.683959	-5.552701	3.355155	3.575792	-5.428814
H	4.864044	3.894916	-5.034795	4.990901	4.113011	-5.062375

H	3.950564	2.485764	-4.472857	4.390153	2.594503	-4.357555
C	2.846434	4.91884	0.098701	2.898316	4.920489	0.161842
H	3.359633	5.777215	0.549185	3.376133	5.781124	0.646507
H	1.805607	4.921788	0.444592	1.844556	4.898793	0.468978
H	3.324206	4.011771	0.481178	3.377736	4.017908	0.553513
C	1.43423	7.669162	-0.772853	1.434787	7.627373	-0.73947
H	1.679295	6.961849	0.015575	1.648258	6.906143	0.045874
H	1.746109	8.662324	-0.445497	1.75725	8.613572	-0.398468
C	0.984287	10.427428	-2.140091	1.030006	10.393716	-2.102862
H	0.170003	10.012643	-1.53636	0.214512	9.999478	-1.48608
H	1.824748	10.638944	-1.466968	1.87633	10.606572	-1.437158
H	0.646669	11.383863	-2.550491	0.701252	11.348981	-2.523468
C	2.221103	8.740587	-6.79185	2.150864	8.637493	-6.77125
H	3.201946	9.189637	-7.002901	3.137898	9.049801	-7.02927
H	2.237766	7.714814	-7.167003	2.123612	7.606851	-7.136206
H	1.472197	9.317972	-7.344297	1.401454	9.233306	-7.30278
N	2.910017	5.580691	-3.585716	3.049495	5.580822	-3.532412
N	2.219595	7.770312	-4.471405	2.236544	7.719466	-4.448139
B	2.794145	6.402131	-4.884365	2.83633	6.35661	-4.846191
F	4.051249	6.565752	-5.475211	4.053103	6.538407	-5.509465
F	1.947083	5.765678	-5.79924	1.961265	5.662146	-5.690132
O	-0.019738	7.787894	-0.851427	-0.009172	7.770097	-0.864879
C	-0.717311	6.652356	-0.93237	-0.719646	6.642775	-0.971533
O	-0.229729	5.54822	-0.838372	-0.243176	5.533195	-0.893671
C	-2.221772	6.919477	-1.09562	-2.220389	6.930699	-1.12926
C	-2.538306	8.153644	-1.926872	-2.531915	8.173739	-1.949022
C	-1.94886	8.041373	-3.325612	-1.973889	8.065326	-3.361857
H	-3.634388	8.209528	-1.974574	-3.627643	8.247372	-1.973422
H	-2.190646	9.061259	-1.421703	-2.160662	9.072336	-1.444885
H	-2.488487	8.716959	-4.002936	-2.52984	8.744134	-4.022716
H	-0.907443	8.398573	-3.321961	-0.93287	8.42284	-3.38086
O	-2.800491	5.787233	-1.727378	-2.816026	5.808253	-1.761765
C	-1.993141	6.629848	-3.855402	-2.039413	6.656794	-3.899457
C	-2.428102	5.581598	-3.041227	-2.466432	5.607048	-3.081961
C	-2.521245	4.261373	-3.498372	-2.58138	4.289772	-3.5433
C	-1.68149	5.01785	-5.625552	-1.806701	5.054931	-5.691614
C	-1.595771	6.336919	-5.170548	-1.684202	6.368204	-5.227906
C	-2.151872	3.972525	-4.817627	-2.256011	4.006717	-4.875172
C	-1.075175	7.395183	-6.100684	-1.175712	7.424821	-6.166688
H	-1.025077	8.380198	-5.628498	-1.023977	8.38805	-5.671829
H	-0.055436	7.153011	-6.434898	-0.203684	7.137974	-6.59596
H	-1.703599	7.506685	-6.995825	-1.866723	7.605606	-7.002668
C	-2.232621	2.575716	-5.364689	-2.365859	2.614512	-5.428506
H	-1.573708	1.89	-4.81692	-1.695537	1.920155	-4.905948
H	-3.249425	2.171551	-5.287938	-3.382866	2.217782	-5.321873
H	-1.940784	2.545685	-6.415916	-2.107425	2.589141	-6.488546
C	-3.011817	3.205087	-2.553817	-3.056109	3.231574	-2.592883
H	-2.428448	3.209194	-1.625646	-2.463043	3.238777	-1.67106
H	-4.054673	3.385172	-2.262538	-4.096817	3.406259	-2.290651
H	-2.953354	2.204676	-2.987655	-2.997688	2.231458	-3.027407
C	-2.828002	6.993705	0.294299	-2.816305	7.003499	0.266057
H	-2.640342	6.064263	0.842733	-2.634626	6.069283	0.808271
H	-2.401	7.832197	0.854494	-2.377172	7.834524	0.827918
H	-3.909827	7.141555	0.209241	-3.897028	7.162669	0.188723
O	-1.303775	4.689594	-6.903622	-1.480142	4.733783	-6.98528
H	-0.964182	5.467414	-7.362342	-1.203992	5.521913	-7.468449
Br	0.81634	11.45113	-5.347106	0.762859	11.352877	-5.31835
Br	4.050895	2.266819	-1.573329	4.289795	2.344887	-1.495063

11a	**S_0**			**S_1**			**T_1**		
	x	**y**	**z**	**x**	**y**	**z**	**x**	**y**	**z**
C	-5.235295	9.159484	-1.854244	-5.24677	9.13853	-1.846191	-5.225752	9.161513	-1.824799
C	-6.050071	8.286026	-1.112663	-6.063526	8.240854	-1.100863	-6.054327	8.259033	-1.10361
C	-6.58393	8.686571	0.126472	-6.617924	8.691215	0.12398	-6.599	8.708571	0.124684
C	-3.920999	10.946323	-2.128944	-3.898047	10.911954	-2.115042	-3.898973	10.94415	-2.131838
C	-3.881521	10.179004	-3.302068	-3.894556	10.148327	-3.303412	-3.881164	10.1786	-3.309883
C	-4.726088	9.082604	-3.185352	-4.773093	9.075635	-3.193241	-4.734144	9.098016	-3.1941
C	-7.486851	8.043765	1.028654	-7.559085	8.081502	1.016864	-7.550007	8.082251	1.02636
C	-7.648196	8.945329	2.073283	-7.711898	9.000435	2.050762	-7.693471	8.979853	2.0692
C	-6.892234	10.101386	1.832517	-6.924678	10.147189	1.811858	-6.910553	10.124475	1.842849
C	-6.799099	11.303358	2.691033	-6.782497	11.345226	2.661003	-6.775912	11.317916	2.702008
H	-6.376928	11.040081	3.668601	-6.0107	11.188647	3.429364	-6.23121	11.066135	3.622255

H	-6.183208	12.08262	2.241859	-6.491895	12.220441	2.075596	-6.245552	12.126644	2.198271
H	-7.801337	11.707221	2.878527	-7.720063	11.553761	3.186544	-7.764678	11.677811	3.010315
C	-8.202249	6.740118	0.940319	-8.305442	6.797977	0.908325	-8.302306	6.805904	0.893844
H	-8.834611	6.679193	0.047241	-8.916049	6.750378	-0.001975	-8.904364	6.778226	-0.022467
H	-7.524615	5.878804	0.930306	-7.653932	5.914483	0.916596	-7.655047	5.919844	0.89218
H	-8.855681	6.623892	1.81	-8.98645	6.70051	1.759691	-8.98979	6.700952	1.738871
C	-6.274203	6.887992	-1.592409	-6.26241	6.831291	-1.555074	-6.254841	6.846572	-1.56664
H	-7.204059	6.49639	-1.179464	-7.172816	6.424639	-1.112434	-7.171721	6.443528	-1.133616
H	-6.395959	6.86195	-2.678608	-6.421804	6.780803	-2.637632	-6.413996	6.797288	-2.649053
C	-5.068716	8.158997	-4.300729	-5.162387	8.156044	-4.294421	-5.134109	8.179854	-4.289025
H	-4.698246	7.144518	-4.132377	-4.807328	7.132451	-4.130755	-4.795931	7.152892	-4.114854
H	-6.153691	8.101913	-4.447952	-6.252186	8.116762	-4.415996	-6.224886	8.156371	-4.406471
H	-4.628456	8.530649	-5.231595	-4.737175	8.512954	-5.238555	-4.703114	8.525366	-5.234283
C	-3.217871	12.221797	-1.867223	-3.188591	12.176537	-1.846437	-3.212764	12.220212	-1.854578
H	-3.160783	12.447591	-0.800803	-3.040466	12.338156	-0.77543	-3.060734	12.373143	-0.783241
H	-2.204333	12.181592	-2.281196	-2.217731	12.182916	-2.354276	-2.245643	12.247926	-2.36755
H	-3.735835	13.049911	-2.369051	-3.762068	13.031642	-2.235898	-3.805765	13.065447	-2.232645
N	-6.258526	9.938977	0.660047	-6.268152	9.950371	0.648338	-6.253122	9.939028	0.656997
N	-4.752196	10.33728	-1.266952	-4.73068	10.302078	-1.244609	-4.740353	10.313811	-1.244708
B	-5.288359	10.969057	0.039193	-5.266345	10.951281	0.046173	-5.267044	10.952109	0.055039
F	-5.964453	12.154597	-0.260288	-5.898947	12.162692	-0.266911	-5.911759	12.15965	-0.246233
F	-4.252935	11.247262	0.933995	-4.238445	11.214642	0.958261	-4.233605	11.218726	0.960312
Br	-2.949096	10.708714	-4.836778	-2.968061	10.662631	-4.833799	-2.975688	10.706632	-4.855793
Br	-8.733522	8.729086	3.583471	-8.803821	8.807688	3.546776	-8.786274	8.776794	3.570263
C	-5.153827	5.859165	-1.256834	-5.126991	5.818654	-1.247188	-5.130519	5.829637	-1.252645
C	-4.570413	5.948659	0.154145	-4.534068	5.911967	0.158033	-4.541501	5.921424	0.155931
C	-3.511586	7.033859	0.359834	-3.500296	7.020553	0.358507	-3.490122	7.014177	0.360497
H	-4.132525	4.971373	0.384134	-4.071746	4.944656	0.383978	-4.096066	4.948254	0.390077
H	-5.390034	6.092811	0.868211	-5.354081	6.034453	0.876784	-5.362733	6.059959	0.870383
H	-2.86199	6.735688	1.197516	-2.844382	6.74355	1.198642	-2.835803	6.722674	1.197057
H	-3.966465	7.982415	0.678283	-3.975821	7.961434	0.670044	-3.951397	7.960742	0.676052
C	-2.665522	7.286729	-0.84963	-2.658978	7.286586	-0.851661	-2.648007	7.273451	-0.850607
C	-2.070563	6.545242	-3.228609	-2.071045	6.58159	-3.242655	-2.049432	6.542043	-3.232069
C	-1.82081	8.328301	-0.951349	-1.811478	8.328272	-0.939665	-1.818378	8.327145	-0.956478
C	-1.056222	8.533749	-2.20097	-1.042738	8.54683	-2.184365	-1.079737	8.558275	-2.217771
C	-1.23249	7.593083	-3.333523	-1.223606	7.624236	-3.329774	-1.226474	7.601817	-3.340573
O	-4.130047	6.028917	-2.269273	-4.116418	6.021421	-2.271632	-4.110865	6.027991	-2.273954
O	-0.275666	9.480822	-2.312385	-0.254263	9.489997	-2.280842	-0.352028	9.544646	-2.346424
C	-2.284238	5.546013	-4.325627	-2.277742	5.591874	-4.349202	-2.237196	5.5285	-4.320308
H	-3.010075	4.783829	-4.03617	-3.112406	4.92162	-4.133465	-3.01892	4.810361	-4.064916
H	-2.649884	6.035467	-5.23718	-2.48108	6.097786	-5.300129	-2.511184	6.009893	-5.266592
H	-1.347064	5.03891	-4.588476	-1.38079	4.975301	-4.498422	-1.310207	4.967872	-4.501484
C	-0.419665	7.881528	-4.55418	-0.395245	7.916989	-4.538971	-0.412161	7.889948	-4.56091
H	0.632215	8.032342	-4.287982	0.654875	8.053072	-4.258426	0.61642	8.14455	-4.285206
H	-0.481824	7.078043	-5.291078	-0.455921	7.120337	-5.283191	-0.388273	7.041861	-5.248528
H	-0.757088	8.81183	-5.029403	-0.71493	8.855824	-5.010117	-0.814631	8.757703	-5.100391
C	-1.61357	9.301975	0.165503	-1.602359	9.284627	0.190946	-1.615871	9.300172	0.16087
H	-1.416086	8.783595	1.111844	-1.387915	8.751005	1.125331	-1.397056	8.78021	1.101702
H	-0.766737	9.957564	-0.050914	-0.765524	9.953685	-0.023389	-0.785888	9.974647	-0.062711
H	-2.498305	9.932794	0.32402	-2.492959	9.901255	0.371477	-2.510378	9.912445	0.33521
C	-5.735488	4.473427	-1.497038	-5.681607	4.423174	-1.489906	-5.686368	4.434997	-1.496965
H	-6.510867	4.244741	-0.756143	-6.445952	4.178864	-0.741711	-6.453963	4.193021	-0.751121
H	-6.181502	4.411381	-2.496377	-6.137755	4.35853	-2.484863	-6.14076	4.371788	-2.492926
H	-4.94649	3.718352	-1.418828	-4.880239	3.679978	-1.423336	-4.888532	3.68818	-1.42832
C	-2.805477	6.272363	-1.942171	-2.795702	6.283822	-1.95584	-2.787256	6.263709	-1.948198
O	-2.347935	4.968013	-1.436202	-2.308724	4.979241	-1.471307	-2.325673	4.957969	-1.449598
O	-1.012593	5.081389	-0.959918	-0.969087	5.105865	-1.010497	-0.986941	5.072467	-0.981834
H	-0.491834	4.752104	-1.712618	-0.453828	4.790837	-1.772934	-0.471327	4.742751	-1.737881

11b	**S0**			**S1**		
	x	**y**	**z**	**x**	**y**	**z**
C	-5.050734	6.733196	-1.968659	-5.010857	6.760048	-1.957295
C	-5.139703	6.574888	-0.576978	-5.11702	6.562182	-0.551719
C	-5.222853	7.702782	0.263806	-5.216358	7.705862	0.28014
C	-4.699773	7.876719	-3.856281	-4.516668	7.919447	-3.817009
C	-4.890301	6.525083	-4.182841	-4.747493	6.570041	-4.16385
C	-5.12942	5.785454	-3.034328	-5.111755	5.835142	-3.038993
C	-5.43963	7.824248	1.666152	-5.498102	7.831271	1.67849
C	-5.306237	9.18379	1.929686	-5.367174	9.191038	1.946534
C	-5.047693	9.880737	0.741863	-5.062042	9.89649	0.764391
C	-4.837464	11.336807	0.57644	-4.854974	11.344518	0.574101
H	-3.880128	11.634421	1.02404	-3.823975	11.557271	0.260472
H	-4.834313	11.630723	-0.47356	-5.508572	11.735437	-0.215665
H	-5.621686	11.894573	1.100713	-5.055234	11.884656	1.502594
C	-5.82258	6.807802	2.685822	-5.924728	6.798882	2.661089
H	-6.663264	6.190543	2.351844	-6.761523	6.198236	2.285048

H	-4.999289	6.135763	2.954096	-5.119747	6.105572	2.939929
H	-6.129869	7.31364	3.606436	-6.257517	7.285983	3.583171
C	-5.012914	5.204336	0.007561	-4.995325	5.183307	0.015671
H	-5.431455	5.156699	1.01401	-5.421999	5.125099	1.019563
H	-5.585095	4.493739	-0.593771	-5.572831	4.477864	-0.589367
C	-5.467924	4.337256	-3.01871	-5.54145	4.411583	-3.036493
H	-4.662889	3.739967	-2.576941	-4.791581	3.753637	-2.578559
H	-6.389264	4.139553	-2.459236	-6.487448	4.272569	-2.499638
H	-5.625921	3.984418	-4.042739	-5.698865	4.071203	-4.065444
C	-4.420189	8.994194	-4.785792	-4.134368	9.050975	-4.682358
H	-4.035023	9.871409	-4.263949	-3.110985	9.385787	-4.454224
H	-3.690481	8.677965	-5.540502	-4.178289	8.760313	-5.735328
H	-5.33198	9.281299	-5.325743	-4.79128	9.914671	-4.523192
N	-5.014718	8.983979	-0.259186	-4.979898	8.991536	-0.236945
N	-4.824393	7.997077	-2.52551	-4.700901	8.026759	-2.483409
B	-4.826482	9.33732	-1.754898	-4.784909	9.35965	-1.721587
F	-5.893305	10.129171	-2.195639	-5.889871	10.103586	-2.174513
F	-3.634135	10.030407	-1.949589	-3.635455	10.1235	-1.908293
Br	-4.8976	5.884688	-5.944708	-4.646258	5.920019	-5.907561
Br	-5.480318	10.021279	3.595314	-5.602483	10.00817	3.606611
C	-3.550019	4.651312	0.092452	-3.551049	4.606245	0.106665
C	-2.677838	5.329203	1.151554	-2.67517	5.285896	1.158563
C	-2.094546	6.669099	0.727624	-2.114632	6.631542	0.724629
H	-1.857261	4.639734	1.384946	-1.845981	4.605844	1.389436
H	-3.255568	5.435425	2.07651	-3.253691	5.391636	2.084732
H	-1.269482	6.938871	1.403079	-1.282285	6.918061	1.384466
H	-2.83039	7.477063	0.849361	-2.859341	7.430635	0.860921
C	-1.631814	6.673599	-0.697898	-1.679999	6.644758	-0.708231
C	-1.722418	5.358474	-1.427869	-1.738305	5.323704	-1.429172
C	-1.60043	5.459315	-2.93393	-1.616928	5.403274	-2.938674
C	-1.204888	7.800695	-1.299018	-1.298168	7.781725	-1.322786
C	-0.915501	7.808235	-2.750127	-1.030018	7.781534	-2.77657
C	-1.223293	6.599672	-3.544227	-1.298551	6.558076	-3.559959
O	-2.983687	4.773436	-1.222189	-2.983695	4.714514	-1.215612
O	-0.468658	8.822376	-3.292379	-0.622804	8.799802	-3.3432
C	-1.914375	4.219459	-3.70668	-1.867257	4.120361	-3.667606
H	-2.896413	4.319658	-4.192287	-2.85359	4.145096	-4.152858
H	-1.182016	4.052208	-4.504889	-1.123994	3.950128	-4.453617
H	-1.946188	3.334682	-3.065584	-1.853727	3.266531	-2.985837
C	-1.059532	6.682398	-5.031076	-1.105238	6.68086	-5.038912
H	-0.299411	5.972715	-5.385693	-0.038623	6.799595	-5.274739
H	-1.994984	6.438382	-5.552239	-1.483023	5.810702	-5.581038
H	-0.749553	7.687015	-5.328141	-1.610602	7.573562	-5.426169
C	-1.030477	9.075856	-0.536429	-1.134479	9.062064	-0.568068
H	-0.287004	8.958519	0.264708	-0.352363	8.966445	0.199106
H	-0.699859	9.878039	-1.199351	-0.861469	9.875874	-1.242309
H	-1.969464	9.39413	-0.063427	-2.061226	9.345775	-0.052573
C	-3.654679	3.164684	0.408409	-3.662097	3.122171	0.423293
H	-4.139798	3.012203	1.380951	-4.151189	2.974044	1.394657
H	-4.241612	2.64295	-0.355996	-4.251764	2.60451	-0.342418
H	-2.654107	2.720401	0.442441	-2.664935	2.670035	0.460002
C	2.616575	5.698967	-4.419665	2.572082	5.644033	-4.485543
C	2.653433	6.548708	-3.319473	2.561103	6.550304	-3.430223
C	2.022758	6.187503	-2.128723	1.946004	6.218032	-2.223665
C	1.340375	4.973933	-2.013992	1.326418	4.978014	-2.046698
C	1.319996	4.126041	-3.127937	1.352877	4.075221	-3.116226
C	1.94439	4.481666	-4.317933	1.963355	4.401017	-4.32232
H	3.105051	5.981244	-5.349387	3.049556	5.902899	-5.427761
H	3.172443	7.502735	-3.382502	3.029276	7.525885	-3.541801
H	2.066156	6.878694	-1.289947	1.950181	6.952684	-1.421564
H	0.796272	3.173642	-3.072042	0.875258	3.102921	-3.014563
H	1.90433	3.806096	-5.17006	1.961561	3.68126	-5.138254
C	0.634544	4.547829	-0.727938	0.64431	4.582584	-0.737992
C	1.056087	3.134342	-0.334013	1.099228	3.193086	-0.297177
H	2.13901	3.092472	-0.172194	2.185954	3.176371	-0.156998
H	0.547617	2.849642	0.595367	0.616541	2.936966	0.654014
H	0.78834	2.4056	-1.104493	0.828333	2.427988	-1.030547
C	0.951746	5.460078	0.451772	0.959575	5.540962	0.40524
H	0.685333	6.506214	0.280884	0.668326	6.575589	0.20822
H	0.420314	5.102825	1.340764	0.450623	5.202384	1.314275
H	2.025824	5.418425	0.6674	2.037878	5.528799	0.602843
O	-0.798538	4.385817	-0.917364	-0.786546	4.383901	-0.90639

12	**S_0**		
	x	**y**	**z**
C	1.934048	8.088132	-3.300438

C	2.081031	7.163091	-2.25051
C	2.795119	5.970271	-2.427121
C	2.088821	8.783386	-5.418286
C	1.464282	9.795303	-4.669555
C	1.370887	9.40169	-3.337303
C	3.146971	4.9112	-1.526436
C	3.902936	4.026397	-2.285457
C	4.002434	4.503352	-3.607332
C	4.706648	3.877073	-4.748911
H	4.2964	4.199162	-5.707406
H	5.771801	4.143396	-4.730015
H	4.643044	2.786677	-4.681802
C	2.812796	4.728511	-0.088046
H	3.204785	5.537643	0.538861
H	1.728153	4.669127	0.061288
H	3.248958	3.796359	0.282422
C	1.45363	7.484199	-0.919513
H	1.660312	6.723589	-0.172603
H	1.823112	8.440205	-0.539604
C	0.879638	10.25991	-2.22498
H	0.029142	9.825303	-1.694104
H	1.669496	10.440343	-1.485003
H	0.570799	11.235	-2.612271
C	2.379261	8.777936	-6.870308
H	3.024811	9.624298	-7.135181
H	2.866479	7.854505	-7.185103
H	1.449536	8.898531	-7.442329
N	3.345911	5.671674	-3.67917
N	2.380658	7.76955	-4.585498
B	3.14497	6.484891	-4.981192
F	4.381538	6.816691	-5.536849
F	2.404606	5.740268	-5.90364
O	0.026999	7.656838	-1.009228
C	-0.712786	6.555482	-1.196366
O	-0.250532	5.447351	-1.334345
I	4.815494	2.246777	-1.625912
I	0.721048	11.56743	-5.524415
C	-2.210357	6.885064	-1.119278
C	-2.591614	8.17705	-1.824237
C	-2.239633	8.116768	-3.310676
H	-3.671178	8.302013	-1.679855
H	-2.10359	9.027232	-1.336631
H	-2.930602	8.750675	-3.886147
H	-1.240067	8.539915	-3.481936
O	-2.924737	5.787065	-1.684646
C	-2.270216	6.705621	-3.835965
C	-3.152671	5.765192	-3.062308
C	-3.166284	4.31372	-3.476676
C	-1.707059	4.873853	-5.361081
C	-1.637695	6.298025	-4.95088
C	-2.454369	3.895916	-4.541616
C	-0.845027	7.18852	-5.849642
H	-0.815083	8.224588	-5.500137
H	0.182572	6.818208	-5.948122
H	-1.272738	7.18234	-6.859619
C	-2.36842	2.479191	-5.014201
H	-2.830246	1.775541	-4.319647
H	-2.845297	2.364575	-5.995358
H	-1.320365	2.188367	-5.146693
C	-4.024003	3.442586	-2.619362
H	-3.53082	3.232659	-1.662006
H	-4.963266	3.954863	-2.38326
H	-4.261216	2.491576	-3.098974
C	-2.588509	6.90663	0.353917
H	-2.361054	5.942781	0.821793
H	-2.044433	7.697193	0.880427
H	-3.663208	7.09641	0.443226
O	-1.133728	4.508071	-6.387913
O	-4.518326	6.299565	-3.138336
O	-5.006721	6.142761	-4.464033
H	-4.888708	7.031013	-4.841818

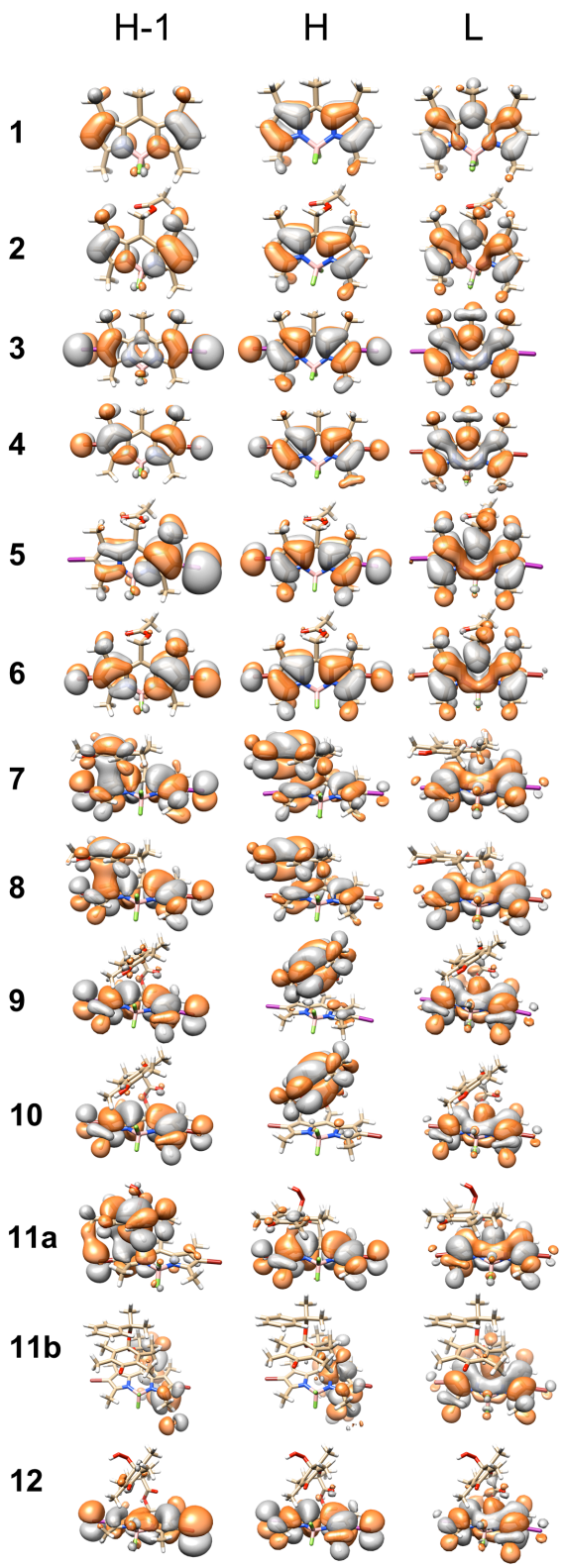
H-1
H
L
1
2
3
4
5
6
7
8
9
10
11a
11b
12